

**Autoxidation Behaviour of Hydrocarbons  
in the Context of  
Conventional and Alternative Aviation Fuels**

Detlev Conrad Mielczarek

Submitted in accordance with the requirements for the degree of  
Doctor of Philosophy.

The University of Leeds,  
The School of Chemical and Process Engineering

July 2015

The candidate confirms that the work submitted is his own, except where work which has formed part of jointly authored publications has been included. The contribution of the candidate and the other authors to this work has been explicitly indicated below. The candidate confirms that appropriate credit has been given within the thesis where reference has been made to the work of others.

Some of the work in Chapter 5 was presented at IASH 2013.

D. C. Mielczarek, S. Blakey, K. J. Hughes, D. B. Ingham, M. Pourkashanian, C. W. Wilson, Experimental and Theoretical Investigation of Pathways to Deposit Formation in Thermally Stressed Aviation Fuel in the Presence of Nitrogenous Additives, *the 13th International Conference on Stability, Handling and Use of Liquid Fuels*, Rhodes, Greece, 2013.

The work presented in the presentation and included in the thesis is attributable to the author of this thesis. The co-authors provided experimental data and observations that formed the basis for the work as well as contributed to the discussion of the work carried out.

This copy has been supplied on the understanding that it is copyright material and that no quotation from the thesis may be published without proper acknowledgement.

The right of Detlev Conrad Mielczarek to be identified as Author of this work has been asserted by him in accordance with the Copyright, Designs and Patents Act 1988.

©2015 The University of Leeds and Detlev Conrad Mielczarek.

# Acknowledgements

My thanks go to Dr. Kevin Hughes whose patience as well as help and support in chemistry were invaluable for the completion of this PhD.

This PhD would not have been possible without the help from the University of Sheffield and the Low Carbon Combustion Centre. My thanks go to Dr. Simon Blakey whose help was invaluable in obtaining experimental data as well as Dr. Ehsan Alborzi who offered valuable suggestions and the opportunity for interesting discussions and further collaboration. Work for this PhD also depended on the support team at the LCCC.

My thanks also go to Simon Thorpe at the University of Sheffield for introducing me to a gas chromatograph and making his analytical lab available to me.

Further thanks belong Professor Pourkashanian and Professor Ingham who arranged the position and funding at the University of Leeds for my PhD.



# Abstract

This PhD aspired to develop greater insight into the fundamentals of hydrocarbon autoxidation processes in the context of thermal stability of aviation fuels. A number of approaches to develop a better understanding of the observed processes have been considered. This covers establishing the suitability of an automated reaction mechanism generator to develop autoxidation reaction mechanism as well as manipulating the resultant schemes, for example by lumping species and their associated reactions as well as reaction rate based mechanism reduction. Further a number of postulated interactions between contaminants in fuel and oxidised products in thermally stressed hydrocarbons employing ab initio quantum chemistry methods were examined. Finally a set of systematic experiments was carried out to obtain quantitative data of the effect of a number of additives on the stability of thermally stressed hydrocarbons. These tests employed a small scale test device, the PetroOxy which provides reliable and reproducible experimental data under well defined test conditions. The PetroOxy enabled the collection of samples of the deposition products on metal foils for further analysis under a scanning electron microscope with x-ray dispersive spectroscopy for elemental analysis. This provided both the morphology as well as the elemental distribution of the deposits formed on the foils, offering a first hand look at the differences between deposits formed from different additives.

This thesis shows that automated mechanism generation is a suitable method when describing the initial steps of autoxidation processes without any additives. It further shows that the PetroOxy is a very useful tool for obtaining systematic, reliable, experimental data for further analysis.



# Contents

<b>Abstract</b>	<b>vi</b>
<b>Table of Contents</b>	<b>xi</b>
<b>List of Figures</b>	<b>xvii</b>
<b>List of Tables</b>	<b>xxi</b>
<b>Nomenclature</b>	<b>xxviii</b>
<b>1 Introduction</b>	<b>1</b>
1.1 Energy - A Historic Perspective . . . . .	1
1.2 Aviation Fuel . . . . .	2
1.3 Objective of this Thesis . . . . .	4
1.4 Outline of this Thesis . . . . .	6
1.4.1 Chapter 1 . . . . .	6
1.4.2 Chapter 2 . . . . .	6
1.4.3 Chapter 3 . . . . .	6
1.4.4 Chapter 4 . . . . .	6
1.4.5 Chapter 5 . . . . .	6
1.4.6 Chapter 6 . . . . .	7
1.4.7 Chapter 7 . . . . .	7
<b>2 Background and Literature Review</b>	<b>9</b>
2.1 Background Details on Aviation Fuel . . . . .	9
2.1.1 Aviation Fuel Properties and Requirements . . . . .	9
2.1.2 Synthetic Fuels - Fischer Tropsch Fuels . . . . .	12
2.2 Development of Stability and Deposition Research . . . . .	13
2.2.1 Deposit Modelling Methodology . . . . .	13
2.2.2 Theoretical Approaches to Stability . . . . .	20
2.2.2.1 Pseudo-Detailed Reaction Schemes . . . . .	21
2.2.2.2 Reduced Detailed Reaction Schemes . . . . .	23

2.2.2.3	Combined Pseudo-Detailed as well as Detailed Reaction Schemes . . . . .	23
2.2.2.4	Surrogate Models . . . . .	24
2.2.3	Experimental Investigations into Thermal Stability . . . . .	27
2.3	Additives . . . . .	31
2.4	Stability Limits . . . . .	35
2.5	Thermal Stability Conclusion . . . . .	35
<b>3</b>	<b>Software Tools and Theory</b>	<b>39</b>
3.1	Chemical Kinetics . . . . .	39
3.1.1	Description of Chemical Kinetics . . . . .	39
3.1.2	Stoichiometric Equations . . . . .	39
3.1.3	Elementary Reactions and Reaction Rates . . . . .	40
3.1.3.1	Elementary Reactions . . . . .	40
3.1.3.2	Reaction Rates . . . . .	40
3.1.4	Arrhenius Equation . . . . .	41
3.1.5	Thermodynamics . . . . .	42
3.1.6	Ideal Gas Law . . . . .	43
3.2	Employing and Handling Kinetics . . . . .	44
3.2.1	Background for Employing Time Dependent Chemical Kinetics . . . . .	44
3.2.1.1	Basic Introduction to Differencing Schemes . . . . .	44
3.2.1.2	Translating Chemical Reactions to Differential Equations . . . . .	46
3.2.2	Existing Software for Time Dependent Chemical Kinetics . . . . .	47
3.2.2.1	Chemkin . . . . .	47
3.2.2.2	SPRINT . . . . .	51
3.2.3	A New Chemical Kinetics Solver . . . . .	54
3.2.3.1	Basic Use . . . . .	55
3.2.3.2	Mechanism Reduction . . . . .	55
3.2.3.3	PetroOxy Pressure Drop . . . . .	62
3.2.3.4	Creating an Analytical Jacobian . . . . .	66
3.3	RMG Usage and Findings . . . . .	67
3.3.1	Initial Settings . . . . .	67
3.3.1.1	Temperature and Pressure . . . . .	69
3.3.1.2	Liquid Phase Kinetics in RMG . . . . .	69
3.3.1.3	Reactants and Concentrations . . . . .	70
3.3.1.4	Error Tolerance, Pruning - Controlling Mechanism Size . . . . .	71
3.3.1.5	Termination Criteria - Species Conversion or Reaction Time . . . . .	72
3.3.1.6	Databases . . . . .	73
3.3.2	Influencing Models - Observations . . . . .	74
3.3.2.1	Effects of the Error Tolerance . . . . .	74



3.3.2.2	Effects of the RMG Database . . . . .	74
3.3.3	Computational Requirements . . . . .	75
3.3.4	Potential Difficulties . . . . .	75
3.4	Computational Chemistry . . . . .	76
3.4.1	Choosing Appropriate Methods . . . . .	76
3.4.1.1	Basis Sets . . . . .	77
3.4.1.2	Computational Method - Level of Theory . . . . .	77
3.4.2	Geometry - Creating Structures . . . . .	77
3.4.3	Searching For Transition States . . . . .	78
3.4.3.1	Finding Transition State - QST2 . . . . .	78
3.4.3.2	Finding Transition State - QST3 . . . . .	78
3.4.3.3	Finding Transition State - Opt=TS . . . . .	79
3.4.3.4	Verifying The Transition State . . . . .	79
3.4.3.5	Solvation . . . . .	79
<b>4</b>	<b>Reaction Mechanism Generation</b>	<b>81</b>
4.1	Initial Evaluation of RMG Models . . . . .	81
4.1.1	Criteria for RMG Evaluation . . . . .	81
4.1.2	Heptane Autoignition Delay Times . . . . .	81
4.1.2.1	Comparison of Product Species after Combustion . . . . .	83
4.1.3	Initial Conclusion on the Validity of RMG Models . . . . .	85
4.2	Developing a Good RMG Scheme . . . . .	85
4.2.1	RMG Sensitivity . . . . .	85
4.2.1.1	Termination Criteria - Reaction Time . . . . .	86
4.2.1.2	Single Reaction Temperature . . . . .	88
4.2.1.3	Single or Multiple Temperatures . . . . .	89
4.2.1.4	Solvation - Solvent Type and Viscosity . . . . .	89
4.2.2	Chosen Models to Describe Autoxidation Behaviour with RMG . . . . .	95
4.3	Mechanism Reduction . . . . .	99
4.4	Modelling the PetroOxy with RMG . . . . .	102
4.5	Antioxidant Speculation . . . . .	106
4.6	Closer Scheme Inspection . . . . .	109
4.6.1	Difference Between Iso and Normal Paraffinic Scheme . . . . .	109
4.6.2	Hydroperoxide Decomposition Speculation . . . . .	110
4.7	RMG Conclusions . . . . .	115
<b>5</b>	<b>Deposits and Precursors in the HiReTS</b>	<b>119</b>
5.1	The HiReTS . . . . .	120
5.1.1	Specifications . . . . .	120
5.1.2	Test Methodology . . . . .	121
5.1.3	Known Issues . . . . .	123

5.2	Precursor Concentration and Deposit Formation in HiReTS . . . . .	124
5.3	Application - Electrophilic Aromatic Substitution . . . . .	125
5.4	Amine Alkene Reaction . . . . .	130
5.5	Surface Effects . . . . .	130
5.6	Deposition Process - Initial Conclusion . . . . .	133
5.7	HiReTS Experimental Work . . . . .	134
5.8	HiReTS Conclusion . . . . .	134
<b>6</b>	<b>Assessing Thermal Stability with the PetroOxy</b>	<b>137</b>
6.1	The PetroOxy - A Look at the Device . . . . .	137
6.2	Experimental Methodology . . . . .	137
6.2.1	Sample Preparation . . . . .	137
6.2.2	PetroOxy Usage . . . . .	138
6.3	Test Series . . . . .	139
6.4	Experimental Results and Observations . . . . .	141
6.4.1	Repeatability of the PetroOxy . . . . .	141
6.4.2	Neat Fuels . . . . .	142
6.4.3	Addition of Amines . . . . .	142
6.4.4	Addition of Aromatic Species . . . . .	146
6.4.5	Addition of Aromatic Species and Butylamine . . . . .	147
6.4.6	Addition of Sulphurous Species . . . . .	148
6.5	Gas Chromatography . . . . .	149
6.6	SEM EDX . . . . .	157
6.6.1	Clean Foil . . . . .	158
6.6.2	Banner Solvent Only Foil . . . . .	159
6.6.3	Banner Solvent with 50:1 Butylamine . . . . .	160
6.6.4	Banner Solvent with 50:1:1 Butylamine and p-Xylene . . . . .	161
6.6.5	Banner Solvent with 50:1 m-Toluidine . . . . .	162
6.6.6	20% GTL 80% Jet-A . . . . .	163
6.6.7	Filtered Unstressed Blend 20% GTL 80% Jet-A with 50:1 m-Tol	164
6.6.8	Filtered 120 min Stressed Blend 20% GTL 80% Jet with 50:1 m-Tol	166
6.6.9	Addition of Sulfides and Disulfides . . . . .	167
6.6.9.1	Trimethylpentane with 500:1 Dibutylsulfide . . . . .	167
6.6.9.2	2,2,4-Trimethylpentane with 500:1:10 Dibutylsulfide and p-Xylene . . . . .	169
6.6.9.3	Trimethylpentane with 500:1 Dibutyldisulfide . . . . .	171
6.6.9.4	Trimethylpentane with 500:1:10 Dibutyldisulfide and p- Xylene . . . . .	172
6.6.9.5	Dodecane with 500:1 Dibutyldisulfide . . . . .	173
6.6.9.6	Dodecane with 500:1:10 Dibutyldisulfide and p-Xylene .	175
6.6.9.7	Sulfide species Summary . . . . .	176

<i>CONTENTS</i>	xi
6.6.10 SEM EDX Summary . . . . .	176
6.7 PetroOxy Conclusion . . . . .	177
<b>7 Conclusion and Future Work</b>	<b>181</b>
7.1 Conclusion . . . . .	181
7.2 Suggestions for Future Work . . . . .	185
<b>A Full List of Options “initial.inp”</b>	<b>189</b>
<b>B Excel VBA Code</b>	<b>191</b>
B.1 The VBA Menu Addition . . . . .	191
B.2 The VBA Data handling Module . . . . .	192
<b>C Automated Ignition Time Plot in R</b>	<b>195</b>
<b>Bibliography</b>	<b>211</b>



# List of Figures

1.1	The world's energy consumption by fuel type. . . . .	2
2.1	Generalized outline of the proposed autoxidation behaviour of aviation fuel, RH, according to West, including the influence of sulfur species SH and antioxidants AH. . . . .	16
2.2	Gas chromatography chromatogram of a 20% GTL with 80% Jet-A fuel blend, showing a significant number of peaks corresponding to a complex multicomponent mixture. . . . .	25
2.3	Proposed behaviour of THNone as an antioxidant by Beaver et al. . . . .	33
3.1	Drawing of a parabola with 3 points, to illustrate the principle of differencing in Equations (3.2.2), (3.2.4) and (3.2.6). . . . .	44
3.2	Accuracy comparison of the solver developed in this thesis with the established solver SPRINT in an early high temperature autoxidation scheme. . . . .	56
3.3	Schematic layout of the solver written and used in this thesis. . . . .	57
3.4	Example of a typical Chemkin input file, consisting of a species list, species thermodynamic data in the form of NASA-7 polynomials and lastly the mechanism itself in the form of a list chemical reactions with appropriate Arrhenius parameters. . . . .	58
3.5	Example of a minimal input file. . . . .	58
3.6	Outline of the species mapping algorithm implemented in the solver. . . . .	60
3.7	Example of the input for the species lumping algorithm. . . . .	61
3.8	Outline of the rates based reduction algorithm implemented in the solver. . . . .	63
3.9	Sample Input to activate PetroOxy-Module in the solver in the main input file, "initial.inp". . . . .	64
3.10	Structs employed to retain the data for the analytical Jacobian. . . . .	67
3.11	Applying correct signs when evaluating the analytical Jacobian. . . . .	67
3.12	Evaluation of the analytical Jacobian during code execution. . . . .	68
4.1	Autoignition times from experimental data by Westbrook et al. as well as RMG models for Heptane over a temperature range of 625 K to 1400 K. . . . .	82

4.2	Development of the oxygen fraction over time for undecane at 458K for several reaction time termination criteria in the RMG 3.3 model. . . . .	87
4.3	Plots of the development of the oxygen concentration in RMG schemes run for varying reaction time termination criteria in RMG4. . . . .	87
4.4	Plots of the development of the oxygen concentration in RMG schemes run for varying reaction time termination criteria in RMG4. . . . .	88
4.5	Plots displaying the impact of reaction time on an RMG4 scheme generated and solved at a temperature of 500 K. . . . .	90
4.6	Comparative plot of the behaviour of a 1000 minute reaction times 500 K RMG scheme at 500 K and 423 K. . . . .	91
4.7	Comparing a single temperature RMG scheme vs. a multi-temperature RMG scheme. . . . .	92
4.8	Plots of the development of the oxygen concentration in RMG schemes run for dodecane in different solvent types where the initial oxygen concentration is 0.002 mol/L. . . . .	94
4.9	Plots of the development of the oxygen concentration in RMG schemes run for dodecane in different solvent types where the initial oxygen concentration is 0.2 mol/L. . . . .	94
4.10	Plots of the development of the oxygen concentration in RMG schemes run for dodecane with different viscosity values in Pas. . . . .	95
4.11	Development of a number of initial species in different hydrocarbons in a scheme generated with an O <sub>2</sub> concentration of 0.020 00 mol/L. . . . .	97
4.12	Radical Position Identifiers, where positions are left blank, these are covered by symmetry or not included in the final RMG scheme. . . . .	98
4.13	Example of species grouping input employed by the chemical kinetics solver presented in this thesis. . . . .	101
4.14	Different yet similar dodecane based radical species which can be represented as a single species in a lumped reaction scheme. . . . .	101
4.15	Impact of different species grouping on an RMG4 scheme for autoxidation conditions representative of the PetroOxy, 7.14 atm, 423 K . . . . .	102
4.16	Comparison plot for an RMG model of dodecane with Henry's Law applied and PetroOxy data. . . . .	103
4.17	Comparison plot for an RMG model of decane with Henry's Law applied and PetroOxy data. . . . .	104
4.18	Comparison plot for RMG models of Banner Solvent np1014 with Henry's Law applied and PetroOxy data for Banner Solvent in the PTFE dish. . . . .	105
4.19	Comparison plot for an RMG model of Banner Solvent np1014 and its components under identical conditions. . . . .	106
4.20	Consumption of R· in a dodecane mechanism, first by a removal reaction then with an additive. . . . .	107

4.21	Consumption of ROO· in a dodecane mechanism, first by a removal reaction then with an additive. . . . .	108
4.22	Consumption of ROO· and HOO· in a dodecane mechanism, first by a removal reaction then with an additive. . . . .	108
4.23	Rate Reduced and then Species Lumped RMG Scheme. Minimal irreversible scheme to describe oxygen consumption behaviour in the PetroOxy when solved with the addition of Henry's Law. . . . .	110
4.24	Reduced chemical reaction scheme from RMG for 2,8-dimethyldecane. . .	111
4.25	Reduced chemical reaction scheme from RMG for 2-methylundecane. . .	112
4.26	Illustration of points picked for a closer inspection of the O <sub>2</sub> consumption rates. For the iso-schemes points at similar locations were chosen. . . . .	113
4.27	Plots of hydroperoxide decomposition in an elevated temperature RMG scheme, solved at 423K. . . . .	115
4.28	Modified reduced mechanism with added hydroperoxide decomposition. . .	116
4.29	Plots of artificially added hydroperoxide decomposition in an RMG scheme, solved at 423K. . . . .	117
5.1	Photograph of the HiReTS Thermal Stability Test Rig. . . . .	120
5.2	Schematic Outline of the key elements of the HiReTS thermal stability tester. . . . .	122
5.3	Schematic sketch of the capillary pipe test section in a HiReTS test device. . .	122
5.4	Original plots for both a Jet-A and GTL blend showing a peak in Figure 5.4a as well as Banner Solvent showing a flat surface in Figure 5.4b, as generated by the HiReTS interface during a run. . . . .	122
5.5	Electrophilic addition reaction between m-toluidine and propionaldehyde. . .	125
5.6	Two step Electrophilic addition reaction between m-toluidine and propanoic acid in which water is released. . . . .	126
5.7	Numbering scheme to identify the position at which an aromatic substitution reaction takes place in connection with Table 5.1 . . . . .	127
5.8	Logarithmic plot of the concentration development over time for the reaction m-toluidine + aldehyde → product . . . . .	129
5.9	Schematic polymerisation between m-toluidine and an alkene. . . . .	130
5.10	Plot of the effect of estimated ideal case limits for the pre-exponential factor <i>A</i> given an activation energy of zero. . . . .	133
6.1	The PetroOxy, in operation and ready for use. . . . .	138
6.2	Schematic side view of the PetroOxy. . . . .	139
6.3	Pressure development in the PetroOxy using a gold dish for neat fuels. . .	143
6.4	Pressure development in the PetroOxy with the addition of aromatic amines. . .	144
6.5	Pressure development in the PetroOxy with the addition of butylamine. . . .	144
6.6	Photos of the different look of two samples post stressing in the PetroOxy. . .	145

6.7	Macro photographs of deposits formed on a metal foil during a PetroOxy thermal exposure test with Banner Solvent np1014 doped with m-toluidine.	145
6.8	Macro photographs of 0.2 $\mu\text{m}$ pore size filters through which stressed and unstressed 20% GTL with 80% Jet-A with a 50:1 addition on m-toluidine were passed. . . . .	146
6.9	Macro photographs of a metal foil placed in a 50:1:1 blend of Banner Solvent np1014 with both butylamine and p-xylene. . . . .	147
6.10	Deposits from a sulfur test; post test and during the cleaning phase. . .	149
6.11	Macro photographs of deposits formed on metal foils during PetroOxy thermal exposure tests. . . . .	150
6.12	Macro photographs of deposits formed on metal foils during PetroOxy thermal exposure tests. . . . .	151
6.13	Chromatograms of samples of Banner Solvent, Shellsol T and 20% GTL with Jet-A. . . . .	154
6.14	Chromatograms of undiluted samples of Dodecane and GTL. . . . .	156
6.15	SEM EDX equipment. . . . .	157
6.16	SEM image of a clean foil which had been stored in heptane after cutting to clean it. . . . .	158
6.17	Selected element distributions from a clean 316 stainless steel metal foil.	158
6.18	SEM image of a foil with deposits from a test in neat Banner Solvent. .	159
6.19	Selected element distributions from a 316 stainless steel metal foil placed in Banner Solvent. . . . .	159
6.20	SEM image of a foil with deposits from a test Banner Solvent with 50:1 butylamine added. . . . .	160
6.21	Selected element distributions from a 316 stainless steel metal foil placed in Banner Solvent with 50:1 butylamine added. . . . .	160
6.22	SEM image of deposits from Banner Solvent with butylamine and p-xylene.	161
6.23	Elemental maps of the deposits from Banner Solvent with butylamine and p-xylene. . . . .	162
6.24	Elemental maps of the spherical particle deposits from Banner Solvent with butylamine and p-xylene. . . . .	162
6.25	SEM image of a foil with deposits from a test in Banner Solvent with 50:1 m-toluidine. . . . .	163
6.26	Selected element distributions from a 316 stainless steel metal foil placed in Banner Solvent with a 50:1 additive ratio of m-toluidine for the duration of thermal stressing. . . . .	163
6.27	SEM image of a foil with deposits from a test in 20% GTL 80% Jet-A. .	164
6.28	Selected element distributions from a 316 stainless steel metal foil placed in a 20% GTL with 80% Jet-A fuel mixture for the duration of thermal stressing. . . . .	164



6.29 SEM image of filter through which an unstressed 20% GTL with 80% Jet-A blend doped with m-toluidine was passed. . . . .	165
6.30 Elemental analysis of a polycarbonate filter through which 10 mL of an unstressed blend of 20% GTL with 80% Jet-A doped with 50:1 m-toluidine was passed. . . . .	165
6.31 SEM image of filter through which a stressed 20% GTL with 80% Jet-A blend doped with m-toluidine was passed. . . . .	166
6.32 Elemental analysis of a polycarbonate filter through which approximately 5 mL of a stressed blend of 20% GTL with 80% Jet-A doped with 50:1 m-toluidine was passed. . . . .	166
6.33 SEM image of part of a foil placed in trimethylpentane with dibutylsulfide.	167
6.34 Elemental analysis of the surface and detected particle. . . . .	167
6.35 EDX analysis of the site shown in Figure 6.33b. . . . .	168
6.36 SEM images of the surface of a foil placed in trimethylpentane with 500:1:10 dibutylsulfide and p-xylene. . . . .	169
6.37 EDX analysis of the surface area shown in Figure 6.36a . . . . .	169
6.38 EDX analysis of the surface area shown in Figure 6.36b . . . . .	170
6.39 SEM image of the surface of a foil placed in trimethylpentane with dibutyldisulfide. . . . .	171
6.40 EDX analysis of the surface area shown in Figure 6.39 . . . . .	171
6.40 EDX analysis of the surface area shown in Figure 6.39 . . . . .	172
6.41 SEM image . . . . .	172
6.42 EDX analysis of the area shown in the image Figure 6.41. . . . .	173
6.43 SEM image of one of the “arms” reaching outwards from a bubble, such as was shown in Figure 6.12c. . . . .	173
6.44 EDX analysis of the area shown in the image Figure 6.43. . . . .	174
6.45 SEM image of a particle found on the foil placed in Dodecane with dibutyldisulfide and p-xylene. . . . .	175
6.46 EDX analysis of the area shown in the image Figure 6.45. . . . .	175



# List of Tables

2.1	Pseudo Detailed Reaction Mechanism as published by Kuprowicz et al. .	14
2.2	Suggested reactions in pseudo-detailed reaction schemes that lead to particles and deposits in thermally stressed aviation fuel according to West, where AH denote antioxidants and SH denote sulfur containing species. . . . .	17
2.3	Proposed surrogate component candidates according to Dooley et al. . .	26
2.4	Proposed surrogate component candidates according to Huber et al. . .	26
2.5	Proposed best fit surrogate compositions for two jet fuels, according to Huber et al. . . . .	26
3.1	List of orders of reactions with the appropriate units for the rate constant.	41
3.2	Commands from a sample input file for Senkin as well as PSR. Reactant amounts given under “REAC” are normalised internally by the solver and employed to calculate and output concentrations appropriate for the given temperature and pressure. . . . .	50
4.1	Table showing autoignition times and key species from Westbrook and RMG . . . . .	84
4.2	Typical Values of viscosity of some solvents. . . . .	95
4.3	Reaction parameters for different radical positions on dodecane and trimethylpentane. The location of the free radical electron can be determined from Figure 4.12. Values are presented for an RMG scheme created with an initial O <sub>2</sub> concentration of 0.020 mol/L. . . . .	99
4.4	Reaction parameters for different radical positions on a number of branched C <sub>12</sub> molecules. The location of the free radical electron can be determined from Figure 4.12. Values are presented for an RMG scheme created with an initial O <sub>2</sub> concentration of 0.020 mol/L. . . . .	100
4.5	Reaction and Species counts for original and grouped species chemical kinetics schemes. The class count is included in the species when the scheme is solved. . . . .	102
4.6	Species and reaction counts in a number of RMG generated autoxidation schemes. . . . .	104

4.7	Overview of O <sub>2</sub> consumption rates, in mol L s <sup>-1</sup> in a normal paraffinic as well as iso paraffinic RMG scheme. . . . .	113
4.8	Tabulated overview of modifications of the Arrhenius Parameters for Figure 4.29. . . . .	116
5.1	Energy gaps between reactants and the transition state as calculated by Gaussian 09 for a number of reactant combinations. Steps one and two denote a reaction with a predicted relatively stable intermediary step. The number denotes the position in the aromatic ring at which the substitution takes place based on the numbering in Figure 5.7. . . . .	128
5.2	Activation energies for the polymerisation/addition of an amine and an alkene as well as an aromatic ring. Calculation were carried out to consider various positions and hence varying accessibility of the carbon-carbon double bond. . . . .	131
5.3	Results of HiReTS runs for various solvent and fuel combinations. . . .	135
6.1	Specification for fuel/solvents employed in the test series. . . . .	139
6.2	Specification for additives employed in the test series. . . . .	140
6.3	Overview of tests carried out in the PetroOxy. . . . .	140
6.4	Repeatability of tests in the PetroOxy using Dodecane - test 4 suffered from a contaminated dish from the previous test. . . . .	141
6.5	Sampling from different locations in the bottle of Shellsol T, a commercial solvent. . . . .	141
6.6	Residence time in the PetroOxy in minutes. . . . .	142
6.7	Residence time in minutes in the PetroOxy with amine species additives at a ratio of 50:1. . . . .	142
6.8	Residence in the PetroOxy with diamine species additives at a ratio of 50:1. . . . .	144
6.9	Residence times in minutes in the PetroOxy with aromatic species additives at a volume based ratio of 50:1. The different ShellSol times are a result of ShellSol behaviour changing during the test period. . . . .	146
6.10	Residence times for additive combinations from two test series. . . . .	147
6.11	Residence times in the PetroOxy for a blend of dodecane or 2,2,4-trimethylpentane (Isooctane) with additives consisting of p-xylene as well as dibutylsulfide and dibutyldisulfide. A metal foil was also added to retain potential deposits. One test, as indicated was carried out with a larger sample. . . . .	148
6.12	Output of automated identification of compounds in 0.1% diluted Banner solvent. . . . .	153
6.13	Output of automated identification of compounds in 0.1% diluted 20% GTL with 80% Jet-A solvent. . . . .	153

6.14 Output of automated identification of compounds in 0.1% diluted ShellSol T solvent. . . . .	155
---	-----



# Nomenclature

## Roman Variables

$A$	Arrhenius pre-exponential parameter, has units of $k$ , details in Section 3.1.3
$a_1$	coefficient used to calculate thermodynamic data J
$a_2$	coefficient used to calculate thermodynamic data JK <sup>-1</sup>
$a_3$	coefficient used to calculate thermodynamic data JK <sup>-2</sup>
$a_4$	coefficient used to calculate thermodynamic data JK <sup>-3</sup>
$a_5$	coefficient used to calculate thermodynamic data JK <sup>-4</sup>
$a_6$	coefficient used to calculate thermodynamic data JK
$a_7$	coefficient used to calculate thermodynamic data J
$c_p, C_p$	heat capacity at constant pressure, JK <sup>-1</sup> g <sup>-1</sup>
$c_v$	heat capacity at constant Volume, JK <sup>-1</sup> g <sup>-1</sup>
$c_{adjust}$	amount by which the concentration in the Henry's Law module is adjusted
$c_{current}$	current concentration in the Henry's Law module
$c_{new}$	adjusted new concentration in the Henry's Law module
$D$	the diffusion coefficient
$D_{AB}^0$	the diffusion coefficient for dilute solute A in solvent B
$E$	total energy (in DFT description)
$e$	internal energy per mass, Jg <sup>-1</sup>
$E^J$	electron-electron repulsion (in DFT description)
$E^T$	kinetic energy (in DFT description)

$E^V$	potential energy of the nuclear-electron attraction and repulsion between nuclei (in DFT description)
$E^{XC}$	“remaining part of electron electron interactions” (in DFT description)
$E_a$	chemical activation energy, $\text{Jmol}^{-1}$
$e_k$	internal energy of the $k$ th species $\text{Jg}^{-1}$
$\Delta G^\ddagger$	Gibbs energy of activations
$\hbar$	reduced Planck Constant in the Schrödinger Equation
$H$	enthalpy, $\text{Jmol}^{-1}$
$h$	enthalpy, $\text{Jg}^{-1}$
$h_k$	heat capacity of the $k$ th species
$H_T$	enthalpy, $\text{Jmol}^{-1}$ at temperature $T$
$k_H$	Henry’s constant
$\bar{K}^\ddagger$	“gas solvent partition” in RMG, employed as equilibrium constant
$k$	rate constant, details in Section 3.1.3
$k_{eff}$	“effective $k$ ”, rate constant limited by diffusion in RMG
$k_{int}$	“intrinsic $k$ ”, rate constant as predicted by kinetic theory in RMG
$m$	mass, kg
$M_B$	molecular weight of solvent B g/mol
$n$	integer counter, used to describe the number of mol in the ideal gas law
$N_A$	Avogadro’s number, $6.022141 \times 10^{23} \text{ mol}^{-1}$
$n_{current}$	amount of moles of gas in the headspace in the Henry’s Law module
$n_{new}$	adjusted new amount of moles of gas in the headspace in the Henry’s Law module
$p$	pressure, Pa sometimes also atm
$p_{new}$	adjusted new pressure in the headspace in the Henry’s Law module
$Q$	reactor heat loss, W
$R$	gas constant, $8.3145 \text{ Jmol}^{-1}\text{K}^{-1}$
$r$	reaction rate, $\text{moll}^{-1}\text{s}^{-1}$



$r$	sum of the radii of the reactants in RMG
$R_{Char}$	species flux in the model core in RMG
$R_{min}$	minimum species flux for the inclusion of edge species in core in RMG
$S$	entropy, $\text{JK}^{-1}\text{mol}^{-1}$
$T$	temperature, K
$t$	time, s
$T_{final}$	maximum outer wall temperature of heated HiReTS pipe
$T_{min}$	minimum outer wall temperature of heated HiReTS pipe
$T_{ref}$	reference temperature for Modified Arrhenius Equation
$V$	potential in the Schrödinger Equation
$V$	volume, $\text{m}^3$ , $\text{cm}^3$ , or l
$v$	volume per unit mass, $\text{cm}^3\text{g}^{-1}$
$V_A$	molar volume of solute A at its normal boiling temperature $\text{cm}^2/\text{mol}$
$V_{gas}$	volume of gas in the headspace for the Henry's Law module
$V_{sample}$	volume of the sample for the Henry's Law module
$W_k$	molecular weight of the $k$ th species, $\text{gmol}^{-1}$
$Y_k$	$Y_k = \frac{m_k}{m}$ mass fraction of the $k$ th species

### Greek Variables

$\eta_B$	viscosity of solvent B, cP
$\rho$	density, $\text{g cm}^{-3}$
$\tau$	nominal residence time in a perfectly stirred reactor, s
$\tau_0$	friction stress
$\phi$	association factor of solvent B, 1 if unassociated
$\psi$	time-dependent wavefunction in the Schrödinger Equation
$\dot{\omega}_k, \dot{\omega}_i$	molar production rate of the $k$ th species, $\text{mol s}^{-1} \text{cm}^{-3}$

### Abbreviations

ADC	Advanced Distillation Curve
-----	-----------------------------

CAS	Chemical Abstracts Service
CFD	Computational Fluid Dynamics
CTL	Coal To Liquid, type of synthetic fuel
DFT	density functional theory
EDX	electron dispersive x-ray spectroscopy
ESI-MS	ElectroSpray Ionisation Mass Spectrometry
ETII	Energy Technology Innovation Initiative (Leeds University Department)
GC	Gas Chromatography
GC-MS	Gas Chromatography Mass Spectrometry
GPU	Graphics Processing Uni
GRI	Gas Research Institute
GTL	Gas To Liquid, type of synthetic fuel
GUI	General User Interface
HiReTS	High Reynolds Number Thermal Stability (Tester/Test Rig)
IRC	Intrinsic Reaction Coordinates, Gaussian method
JP-7	Jet Propellant 7, a type of aviation fuel
JP-8	Jet Propellant 8, US Military aviation fuel
LSODA	Lawrence Solver for Ordinary Differentials equations with Automatic method switching
MIT	Massachusetts Institute of Technology
NASA	National Aeronautics and Space Administration
NIFTR	Near-Isothermal Flowing Tube Reactor
NIST	National Institute of STandards
ODE	Ordinary Differential Equation, plural ODEs
OPEC	Organization of the Petroleum Exporting Countries
PC	Personal Computer
PCAF	Principal Component Analysis of matrix F, KinalC routine

PCAS	Principal Component Analysis of matrix S, KinalC routine
PSR	Perfectly Stirred Reactor, a Chemkin II solver
QCM	Quarz-Crystal Microbalance
RAM	Random Access Memory
RIMP	Reaction IMPortance, KinalC function
RMG	Reaction Mechanism Generator - Open Source software for generating chemical reaction schemes, developed at MIT
RP-3	Rocket Propellant 3
SEM	scanning electron microscope
SMORS	Soluble Macromolecular Oxidatively Reactive Species
SPE	Solid Phase Extraction
SPRINT	Software for PRoblems IN Time
VBA	Visual Basic for Applications
<b>Chemicals</b>	
BHT	butylated hydroxy toluene
DCP	dicyclohexylphenylphosphine
DHB	1,4-dihydrobenzene
di-EGME	di-ethylene-glycol-monomethyl-ether
FAME	fatty acid methyl ester
m-tol	meta-toluidine, m-toluidine
NP	1-nitropropane
PTFE	polytetrafluoroethylene
TEA	triethylamine
TEMPO	3,6,9-triethyl-3,6,9-trimethyl-1,4,7-triperoxonane
THN	1,2,3,4-terhydronaphthalene also called tetralin
THNol	$\alpha$ -tetralol
THNone	$\alpha$ -tetralone

THQ            1,2,3,4-tetrahydroquinoline

**Short Notation**

AH            generic term for an antioxidant species

I              generic term for a radical initiator species

RH            generic term for an alkane in chemical reaction, R· for a radical

ROO·        generic term for an alkyl hydroperoxyl radical

ROOH        generic term for an alkyl hydroperoxide, also RO<sub>2</sub>H

SH            generic term for an sulfur containing species

**Non-Standard Units**

Å              $1 \times 10^{-10}$  m

cP             $10^{-2}$  Pa s

nmi          nautical mile, equivalent to 1.852 km

ppm         parts per million

torr         133.3 Pa

# Chapter 1

## Introduction

### 1.1 Energy - A Historic Perspective

Energy has been the driving factor of human development, evolution and technological innovation. It started with a simple energy source, firewood to cook food, to coal that transformed to coke was used to melt iron and power the industrial revolution in the 19th century. This was followed by, gas, electricity, oil and nuclear power which powered the 20<sup>th</sup> century.

As a result, our modern world has become very dependent on a steady and reliable energy supply, organising our lives and economies around an abundance of energy. Take away our energy sources, and our current life would come to an immediate standstill. Communication, transportation as well as production all rely on a continuous energy supply, our modern just-in-time economies even more so than the economies of previous decades. It was the availability of high density energy sources that enabled much of human development, from steam trains to diesel trains, from the first propeller aircraft that barely carried their own weight to the modern jumbo jets of today. After the rapid rise in the 20<sup>th</sup> century, this continues in the 21<sup>st</sup> century with an annual increase of 0.5% to 2% in global energy consumption per year<sup>1</sup>.

Our energy is primarily produced from crude oil, natural gas and coal, constituting finite fossil resources<sup>2</sup>. Nuclear power, also a finite resource as well as hydroelectric power constitute only a small amount of the global energy production and consumption. An overview over the current breakdown of energy sources is shown in Figure 1.1. Of our current energy resources, crude oil is the only major resource used directly for the transportation of people and goods, and in total we invest roughly one quarter of our world's energy consumption into transportation<sup>3</sup>. The mobility of people, goods and services has become vital to us, thus it is important that we investigate how we can ensure the sustainability and reliability of the transport sector. At the moment, oil dominates all modes of transportation with only electric passenger trains and trams

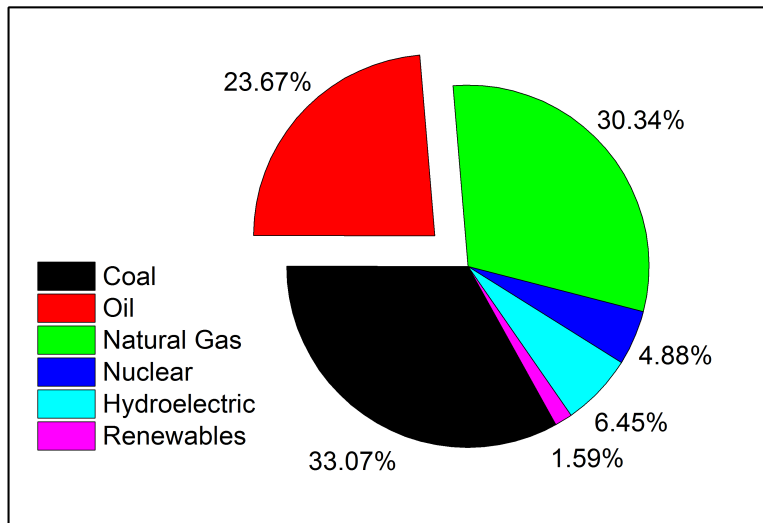


Figure 1.1: The world's energy consumption by fuel type<sup>2</sup>.

capable of utilizing non-fossil fuel based sources of electrical energy such as for example renewable energy sources. In some regions, natural gas is also used for transportation in cars or buses in addition to crude oil based fuel. However, currently, no alternative exists that can offer the same mobility as crude oil based fuel. Two reasons for this are ease of handling and storage as well the energy density of such fuels, i.e. the amount of energy contained in a set amount of fuel<sup>4</sup>.

Air transport and travel constitute one of the industries currently dependent on crude oil based fossil fuel, which is in search of a sustainable alternative for their energy demands. Because air travel and transport is one of the fastest growing transportation sectors worldwide, it is important that our understanding of fuel is improved, to enable us to use our resources more efficiently and to aid in the investigation of alternative fuels, to sustain our current economies and mode of life, as well as to reduce the detrimental effects on the environment<sup>4,5</sup>. Provided that growth continues at current levels, air transport will grow by roughly 30-35% every decade.

## 1.2 Aviation Fuel

In the last decades, aviation fuel has developed from gasoline in the first engines to aviation gasoline and then to kerosene, a by-product of petrol production. With the introduction of gas turbines as the preferred engine worldwide, kerosene has become the global aircraft fuel of choice. With the rapid rise in air travel towards the end of the 20th century, kerosene consumption, the main fuel for aircraft jet engines, has risen in parallel. In 1997 the industry required approximately 670 million tonnes of aviation fuel

per day, rising to 715 million tonnes of fuel per day in 2001<sup>6,7</sup>. With the realization that resources of crude oil are limited and added concern about global pollution, focus has been drawn to more efficient and cleaner engines as a first step of limiting the global impact of aviation and ensuring its sustainability.

Traditionally, engineers have sought to raise the efficiency as a part of designing higher performance engines and aircraft with the added benefit of reducing operational costs. These improvements in engine efficiency also offer the positive side effect of reducing the impact aviation has on the environment through improved fuel economy. Because gas turbines are expected to operate reliably over a long period of time, with long service intervals to reduce operating costs, their design, as well as the composition of the fuel pose an engineering challenge. Especially given that as a result of improving engine efficiency, the temperature in the engine has been raised, to obtaining a more complete combustion, but also as a result of higher compression ratios<sup>8</sup>. A side effect of this development is the production of nitrous oxides which are prevented or at least reduced through the use of elaborate cooling and air mixing in the engine after the combustion chamber<sup>8</sup>.

In current aircraft designs, fuels are employed as the primary coolant for aircraft engines and systems. Especially in a military application, the high speeds of aircraft prohibit the use of air for cooling purposes. With less fuel combusted per pound of thrust in a modern engine compared to older engine models, the suitability of aviation fuel as a heat sink, requiring high thermal stability, has thus received significant research attention<sup>9</sup>. Two main issues are related to the thermal stability of fuels, which is the formation of particles in the fuel and gums or varnishes on pipe surfaces. Depositions in fuel systems reduce their efficiency, leading to higher maintenance costs, while particles can, in a worst case scenario, clog fuel injectors, leading to engine failure. Methods to mitigate these effects have been developed through an improvement in the understanding of the fuel's chemistry as well as its behaviour in the engine and fuel system, which have enabled engineers to place higher demands on the fuel used worldwide. These demands were met by employing stricter criteria for the refining process as well as adding additives to the fuel, which are primarily selected based on experience and experimental evidence<sup>6,10,11</sup>. An example for fuel with improved characteristics is the military fuel JP-8+100 (standard Jet-A1 with additives), with enhanced thermal stability, which was created by evaluating over 300 additive combinations to obtain the desired results<sup>6</sup>.

In view of the scale of global air travel operations, several studies have argued that the only viable alternative for the currently used petroleum based fuel in the near and foreseeable future will be a "drop-in" alternative<sup>11-13</sup>. This is mainly because implementing a different fuel supply systems at airports globally for alternatively fuelled engines, or alternatively refitting aircraft engines globally, would be cost prohibitive, if

at all possible<sup>14</sup>. Phasing out of older engines may also be excluded as an alternative approach due to the long life, of often 30 years or more, of most aircraft<sup>15</sup>.

This same restriction further applies to any improvements to conventional fuel in areas such as thermal stability. Hence any improvement to conventional fuel, such as a drop-in fuel or additives must conform to at least the same specifications as current Jet-A1 and be compatible with aircraft engines and fuel systems designed over a 30 to 40 year period<sup>7</sup>.

However, because aviation fuels from crude oil are essentially a natural product, their composition differs across the world. The exact composition of aviation fuel is not known, but it is estimated to contain about 1000 different components<sup>7</sup>. This complexity creates a challenge in multiple ways. On the one hand, some compounds might add to the beneficial properties of the fuel, such as the swelling of seals caused by aromatics, while another might have a negative effect, for example increasing the rate of autoxidation, affecting thermal stability or leading to inefficient combustion and thus not releasing as much energy as would theoretically be possible. Hence any method to improve thermal stability needs to be evaluated and tested thoroughly to ensure it is safe to use.

One solution to improve thermal stability and mitigate deposits would be to use synthetic fuels, which have been shown to improve thermal stability, either as neat fuel or as a blend with conventional Jet-A1 fuel<sup>16</sup>. A 50/50 mix of conventional Jet-A1 with synthetic fuel produced from coal has been in use in South Africa under the name of SASOL since the 1970s<sup>11,13,17-19</sup>.

### 1.3 Objective of this Thesis

The aim of this thesis is to develop an improved understanding of the autoxidation behaviour exhibited by aviation fuel, especially in the context of deposit formation. While the topic of autoxidation of aviation fuel has been studied extensively in the past, published work is limited to primarily simple descriptions of the observed results, with seemingly arbitrary assumptions in published mechanisms. Experimental work in published studies used to verify these mechanisms generally employs real fuels, which thus require fitting of the mechanism and also suffers from repeatability problems due to the differences in fuels, based on the type of crude oil, transport conditions as well as storage conditions.

Solvents avoid some of the reproducibility issues induced by the complexity of fuel, however are only seldom employed in published work due to cost. In this work, a number of components representative of fuel constituent have been selected for further in depth investigation from both a modelling perspective as well as an experimental



perspective. Use of a comparatively simpler mixture of compounds leads to a drastically simplified chemistry under more controlled conditions which benefits the repeatability of experiments. In addition, to further simplify the test setup, a small scale static test is employed to further reduce the number of outside influences on the chemical reactions taking place and allow the collection of more robust data. Samples are doped with compounds expected to impact the autoxidation behaviour as well as deposition behaviour to collect well controlled data on the impact of individual species classes.

Automatic reaction mechanism generation software is employed to produce reaction mechanisms that describe the behaviour of the hydrocarbon components in detail. This mechanism is then compared to the collected data in an attempt to validate the proposed reaction mechanism for autoxidation processes. In addition, the proposed mechanisms can be extended to incorporate proposed interactions between doping compounds and reaction products to reproduce the observed behaviour and extend the mechanism to incorporate species which are not supported by the mechanism generation tool.

The novelty in this work lies in the combination of the systematic collection of reproducible data through the use of solvents as well as the application of a systematic method for the generation of a reaction scheme to obtain justifiable parameters.

The work carried out for this thesis covers the following major points:

- i) A comprehensive reaction scheme for the autoxidation of various alkane types as well as alkane combinations, constituting fuel surrogates, has been drawn up using an automatic reaction mechanism generator. For convenience, the comprehensive chemical reaction scheme describing the autoxidation of a surrogate fuel was reduced to offer a human accessible description of the process. A positive side effect of model reduction is that species whose structure is unrealistic, but have been included in the model as a part of the brute force model generation approach, can be removed from the model.
- ii) Postulated reactions describing the deposition process in the HiReTS test rig were investigated using quantum chemical methods as well as theory based parameter estimation. These reactions were then incorporated into a comprehensive reaction scheme and their viability assessed using available experimental data.
- iii) Experiments were carried out by means of an small scale static test rig to assess both the impact of different additives as well as the impact of a stainless steel metal foil on the autoxidation process. The closely controlled environment also enabled an attempt at validating any proposed reaction models. Where foils were employed, these were then analysed using a scanning electron microscope with energy dispersive x-ray spectroscopy to obtain a better understanding of the elemental composition

as well as the morphology of the deposits.

## 1.4 Outline of this Thesis

### 1.4.1 Chapter 1

Chapter 1 introduces the reader to this thesis by providing a general introduction as well as the aims and outline of this thesis.

### 1.4.2 Chapter 2

Chapter 2 provides the reader with background information that is required to understand this thesis. Details on aviation fuel and its testing as well as the key concepts of the underlying chemistry. This chapter further provides the reader with a literature review presenting the current state of research in the area of thermal stability of aviation fuel as well as a review of available software tools.

### 1.4.3 Chapter 3

Chapter 3 introduces the software selected for this thesis as well as relevant aspects of specialist theory required for the theoretical aspects in this thesis. Some of the software employed are MIT's Reaction Mechanism Generator (RMG) which is designed to produce chemical reaction schemes from a basic library of kinetics and properties as well as Gaussian which is used to carry out an ab initio study into the interaction of molecules. Lastly, the topic of handling chemical kinetics is addressed, covering Chemkin II, one in house solver named Sprint as well as the rationale for developing a new solver.

### 1.4.4 Chapter 4

Chapter 4 presents results from using an automated reaction mechanism generator (RMG) which has been employed to carry out an investigation into the behaviour of thermally stressed hydrocarbon compounds. We use a validated combustion scheme to obtain an initial estimate of the suitability of RMG for the generation of chemical reaction schemes. Following, we investigated and compared RMG under autoxidation conditions to experimental data from a small scale experimental oxidation test device. Lastly, we employed a reduction algorithm to obtain reduced mechanisms enabling a better understanding of the underlying chemical reactions predicted by RMG.

### 1.4.5 Chapter 5

Chapter 5 presents the investigation of intermolecular reactions using quantum chemistry software Gaussian. We assessed a number of reaction paths, primarily electrophilic aromatic substitution reactions but also speculate about interactions with amines in an RMG generated reaction mechanism. We compared our models to historic data from a

HiReTS and later obtained new additional experimental data from the HiReTS which proved inconclusive.

#### **1.4.6 Chapter 6**

Chapter 6 presents a comprehensive experimental investigation of thermal stability employing a small scale oxidation test device which enables us to obtain systematic experimental data on the behaviour of a number of hydrocarbon compounds with varying additives as well as in the presence of metal foils. Where metal foils were employed, further analysis comprising of SEM imaging and EDX elemental analysis to visualise the differences between the deposits formed on the foils.

#### **1.4.7 Chapter 7**

Chapter 7 concludes this thesis with the conclusions and suggestions for further work.



## Chapter 2

# Background and Literature Review

### 2.1 Background Details on Aviation Fuel

#### 2.1.1 Aviation Fuel Properties and Requirements

Aviation fuel is in some ways a natural refined product, being produced from crude oil, whose properties vary depending on the source of oil employed in the production process. It is estimated that crude oil based aviation fuel consists of at least one thousand different components<sup>7</sup>. These are predominantly hydrocarbons consisting of carbon and hydrogen only, however species that contain oxygen or nitrogen as well as other elements may be present at trace levels. Due to the complexity of aviation fuels, it is not defined by its composition but through a set of verifiable properties. The comprehensive review from the Chevron Corporation<sup>7</sup> introduces the reader to all the key general points with respect to fuel, its handling, storage and production. Amongst the information presented, are details on how customers or manufacturers can verify their fuel is being produced or delivered according to specifications. Different standards, with slight variations, exist in the world, but overall the specifications are very similar and mainly only adapt the fuel to the local climate. The main groups issuing aviation fuel specifications are the US, Europe (UK Ministry of Defence Standard), the former Soviet Union (now Russia) and China<sup>7,14</sup>.

The following is a very condensed overview of the test methods listed in the review from Chevron<sup>7</sup> on pages 20 to 23.

- i) Distillation - 100 mL sample used.
- ii) Thermal Stability - fuel is pumped across heated aluminium for 2.5 hours. Particles are collected with the help of a filter, the pressure drop is monitored during the experiment and the aluminium tube is inspected after the test.

- iii) Density - Either via a hydrometer or an oscillating tube, specification sheets provide a density value at 15.6 °C for comparison.
- iv) Viscosity - A sample is left to flow through a calibrated glass viscometer under gravity.
- v) Vapour Pressure - A chilled sample is heated to 37.8 °C and the pressure then measured.
- vi) Flash Point - A sample is heated in a lidded cup and an ignition source presented at various temperatures.
- vii) Net Heat of Combustion - Either estimated from the properties and composition of the fuel or determined via a calorimeter.
- viii) Freezing Point - Fuel is cooled until crystals appear, then reheated. The temperature at which the last crystals disappear is noted.
- ix) Naphthalenes Content - A sample is dissolved in iso-octane and the absorbance at a wavelength of 285 nm is measured to calculate the content.
- x) Luminometer Number - A sample is burned in a Luminometer Lamp.
- xi) Sulfur - Either via X-ray fluorescence, X-ray beam patterns or by combustion in a closed system, to capture sulphur dioxide, of which the amount can be determined. Alternatively, ultraviolet fluorescence of combustion gases may also be used.
- xii) Mercaptan Sulfur - A sample free of hydrogen sulfide is dissolved in sodium acetate and titrated.
- xiii) Copper Strip Corrosion - A polished copper strip is immersed in a sample for two hours at 100 °C, then washed and inspected.
- xiv) Acidity - A sample is dissolved in solvent and titrated.
- xv) Existent Gum - A known amount of fuel is evaporated under a flow of steam, the residue weighted.
- xvi) Aromatics Content - Activated silica gel which is treated with dye is placed in a glass adsorption column. Isopropyl alcohol is used to wash the sample along the column. Alternatively a refractive index detector may also be used.
- xvii) Smoke Point - A sample is burnt in a wick fed lamp, the maximum flame size without smoking is then determined.
- xviii) Electrical Conductivity - The current between two electrodes with a defined potential is measured to calculate the conductivity.

- xix) Water Reaction - Mixing with water and inspecting, this test method is being removed.
- xx) Water Separability - A semi-automatic Micro-Separometer is used.
- xxi) Lubricity - A non-rotating spherical ball is held against a rotating cylinder. The ball is then inspected for wear.
- xxii) Particulate Matter - Fuel fed through a membrane with 0.8 micrometer pores. Afterwards the colour is inspected. Alternatively, the fuel is fed through two membranes of equal mass, which are afterwards dried and the mass compared.

In some cases fuels may not meet the desired specifications and need to be enhanced through the addition of additives. Civilian aviation tends to not employ additives, however where required, five main types of additives are certified for use in aviation fuels today<sup>6,7</sup>.

These are as follows:

- i) A corrosion inhibitor which also improves fuel lubricity.
- ii) A fuel icing inhibitor, commonly referred to as antifreeze. The current permitted type being di-ethylene glycol monomethyl ether (di-EGME) at a maximum concentration of 0.15 % by volume. This additive also inhibits growth of microorganisms in the fuel as it acts as a biocide. (Russian TS-1 fuel may use ethylene glycol monoethyl ether.)
- iii) A static dissipator additive to improve conductivity of the fuel as it is capacitive. The only approved static dissipator is the proprietary Stadis® 450 at a maximum concentration of 0.2-0.5 mg L<sup>-1</sup>.
- iv) An antioxidant, consisting of a hindered phenol at a maximum concentration of 24 mg/L to help prevent the oxidative degradation of fuel during storage.
- v) A metal deactivator, as some metals such as copper catalyse oxidation in the fuel, at a concentration of up to 6 mg/L.

A property that is of interest when developing alternative fuels, or improving current fuels, is thermal stability. This is due to the fact that fuel is used as a heat sink, especially in military aircraft, as air can no longer provide adequate cooling at high, especially supersonic, speeds<sup>9</sup>. At the same time, other problems no longer occur with synthetic fuels, such as existing gums or potentially excessive aromatics content. Properties such as the vapour pressure, flash point, viscosity and density are also more controllable in synthetic fuel, where the fuel can be designed to fit specifications.

### 2.1.2 Synthetic Fuels - Fischer Tropsch Fuels

The Fischer Tropsch process was invented in Germany in the 1920s and continuously developed and improved, supplied a significant amount of fuel to Nazi Germany<sup>20,21</sup>. After World War 2 interest in the process initially continued under the impression that oil is scarce, until the discovery of the middle eastern oilfields lead to a price drop that made the technology too expensive for commercial use in most markets.

In a most basic explanation, the Fischer Tropsch process is a method for turning syngas consisting of carbon monoxide and hydrogen into hydrocarbons with the help of a catalyst<sup>21</sup>. Traditionally, coal as well as natural gas (methane) have been used as feedstock for the syngas, but technically any substance that contains carbon could be used, including biomass<sup>20,22</sup>. The syngas is reacted under the presence of either a cobalt or iron catalyst under high temperatures and elevated pressure to combine to form short alkanes. By recycling the product, longer alkane chains can be produced. The benefit of this process is, that it allows for the production of a specific group of alkanes, such as for example long or short carbon chain alkanes. Additionally, Fischer Tropsch alkanes are free of sulphur which needs to be removed from crude oil during refinement. As a result, Fischer Tropsch fuels are a very attractive candidate for a replacement of crude oil based fuels.

Dry<sup>21</sup> introduces the dominant reaction for a cobalt catalyst:



According to Dry, with an iron catalyst, the so-called “water gas shift” reaction:



also becomes important and at high temperatures produces carbon monoxide in a reverse reaction which can then be converted via the cobalt catalysed Fischer Tropsch reaction.

Both Dry<sup>21</sup> and Schulz<sup>20</sup> mention further catalysts in addition to cobalt and iron that can be used for the Fischer Tropsch process, namely nickel and ruthenium. However, according to Dry<sup>21</sup>, for financial reasons only cobalt and iron are currently used in commercial fuel production by the Fischer Tropsch process.

The only country using Fischer Tropsch fuels commercially is South Africa, where the 1970s oil embargo made producing hydrocarbon based fuel from local coal reserves important to national development<sup>22</sup>. As a result, only South Africa has been mass producing fuel with the Fischer Tropsch process and possibly has the most experience when it comes to producing Fischer Tropsch fuels at current. South Africa is also the



only country that regularly operates aircraft on a 50/50 blend of conventional Jet-A1 fuel with Fischer Tropsch fuel<sup>7,11,13,14</sup>. This blend of fuel, with 50% synthetic fuel and 50% conventional aviation fuel was shown to have no negative effects and has been used in South Africa for several decades<sup>7,11,13,14</sup>.

The use of synthetic fuel also offers a number of advantages. The ability to influence the types of hydrocarbons present in the fuel during production allows for a cleaner combustion with fewer particulate emissions. A 0% sulphur content prevents the formation of sulphur oxides during combustion which are seen as environmental contaminants. Synthetic fuel offers a higher thermal stability, due to the ability to select the exact composition of hydrocarbons depending on conditions/requirements placed on the fuel<sup>23</sup>. Because synthetic fuels can be produced from many different base materials, either gas, coal or biomass, supply issues are unlikely to occur with respect to the feedstock for the production of such fuels leading to improved security of supply<sup>11,13,24-26</sup>.

Currently Fischer-Tropsch fuels, which appear to be the best alternative or improvement to crude oil based Jet-A1 kerosene have one significant drawback. The production is energy intensive, and thus costly<sup>27,28</sup>. Operating aircraft on Fischer-Tropsch fuels is possible, as has been shown in South Africa with the 50/50 blend and it may be the best choice for the future. In addition, as currently synthetic fuels consist primarily of normal and iso alkanes as well as some cyclic alkanes depending on the supplier<sup>29</sup>, older or existing aircraft may depend on the addition of conventional jet fuel to efficiently include aromatic compounds which have been found to be important for seal swelling<sup>29</sup>. At the same time, it most likely will also lead to an increase in costs for air travel.

## 2.2 Development of Stability and Deposition Research

Research into thermal stability developed in parallel with aircraft engines with some of the earlier studies into the effect of metal surfaces on hydrocarbon deposition processes, carried out by Taylor<sup>30,31</sup>, dating back to the the 1960s. Experimental investigations were carried out to observe the effects of surface interactions on the rate of deposit formation. Hydrocarbons were thermally stressed, i.e. heated, in different metal tubes and the rate of deposit formation recorded to obtain correlations between metal types and the rate of deposit formation as well as the amount of deposits.

### 2.2.1 Deposit Modelling Methodology

The absence of a detailed understanding of the reactions in the field of fuel autoxidation has significant implications for the accuracy of any proposed models. Software to solve chemical kinetics problems, such as Chemkin, detailed in Section 3.2.2.1, relies on an accurate input of reactive species as well as reactions that occur. A reaction not

incorporated in the model can invalidate it, or have significant effects on the accuracy of the obtained results and predictions derived from these results. With an increased understanding of the topic, models have been extended from incorporating only a few reactions, to incorporating several hundred reactions when modelling the behaviour of regular or alternative aviation fuels. Because the detailed chemical reactions that occur in the oxidation of jet fuel are not known, a simplified surrogate model is used instead. Wade<sup>32</sup> developed a Genetic Algorithm approach to improve the modelling of autoxidation, progressing from published 3 or 5 step reaction models to a 17 step model presented in 1998 by Ervin and Zabarnick<sup>33</sup>. The latest published scheme is from Kuprowicz et al.<sup>34</sup> and is shown in Figure 2.1, featuring 18 steps.

Nr.		A (mol L s)	Ea (kJ mol <sup>-1</sup> )	Type
1	$I \longrightarrow R \cdot$	$1 \times 10^{-3}$	0	radical formation
2	$R \cdot + O_2 \longrightarrow RO_2 \cdot$	$3 \times 10^9$	0	reaction with O <sub>2</sub>
3	$RO_2 \cdot + RH \longrightarrow RO_2H + R \cdot$	$3 \times 10^9$	50.21	propagation
4	$RO_2 \cdot + RO_2 \cdot \longrightarrow$ termination	$3 \times 10^9$	0	termination
5	$RO_2 \cdot + AH \longrightarrow RO_2H + A \cdot$	$3 \times 10^9$	20.92	propagation
6	$A \cdot + RH \longrightarrow AH + R \cdot$	$1 \times 10^5$	50.21	propagation
7	$A \cdot + RO_2 \cdot \longrightarrow$ ProductsAH	$3 \times 10^9$	0	termination
8	$R \cdot + R \cdot \longrightarrow R_2$	$3 \times 10^9$	0	termination
9	$RO_2H \longrightarrow RO \cdot + \cdot OH$	$1 \times 10^{15}$	163.18	radical formation
10	$RO \cdot + RH \longrightarrow ROH + R \cdot$	$3 \times 10^9$	41.84	propagation
11	$RO \cdot \longrightarrow R_{\text{prime}} \cdot +$ carbonyl	$1 \times 10^{16}$	62.76	propagation
12	$\cdot OH + RH \longrightarrow H_2O + R \cdot$	$3 \times 10^9$	41.84	propagation
13	$RO \cdot + RO \cdot \longrightarrow RO_{\text{term}} \cdot$	$3 \times 10^9$	0	termination
14	$R_{\text{prime}} \cdot + RH \longrightarrow$ alkane + R $\cdot$	$3 \times 10^9$	41.84	propagation
15	$RO_2H + SH \longrightarrow$ ProductsSH	$3 \times 10^9$	75.31	
16	$RO_2 \cdot \longrightarrow R \cdot + O_2$	$1 \times 10^{16}$	79.50	propagation
17	$RO_2 \cdot + R \cdot \longrightarrow$ termination	$3 \times 10^9$	0	termination
18	$RO_2H + M \longrightarrow RO \cdot + \cdot OH + M$	$3 \times 10^{10}$	62.76	radical formation

Table 2.1: Pseudo Detailed Reaction Mechanism as published by Kuprowicz et al.<sup>34</sup>

The underlying assumptions made in these models are, that while hundreds of individual reactions occur, they can be grouped into certain types of reactions, such as free radical formation, reaction with oxygen, deposit formation, termination of reactions and similar. The exact type of hydrocarbon is not considered in such a model and instead replaced by a general placeholder “R”, denoting the hydrocarbons in the fuel. Besides simplifying the reaction model, this also simplifies validating the model, as it is easier to determine whether for example hydroxides in a specific concentration are present, rather than what hydroxides are present and in what concentration, as tests to determine certain species of chemicals exist and are comparatively easy to do, while detailed analysis with respect to the type of compound often require a combination of analysis methods including spectroscopy if little is known about the compound’s identity beforehand.

Reaction models for complex systems are generally chosen on the basis of empirical research. This enables the researchers to verify that some reactions occur, for example by analysing products of the reaction and also enables the empirical determination of the Arrhenius parameters, such as the pre-exponential factor  $A$ , the temperature dependency  $n$  and the activation energy  $E_a$ . If the activation energy and pre-exponential factor are known, the rate of the reactions can be estimated with the use of an Arrhenius equation. However, as Wade<sup>32</sup> points out, due to the large temperature range found in aircraft engines and fuel systems, non-Arrhenius behaviour can occur during the thermal degradation of aviation fuels. As such generalized models have led to reasonable results, the assumption is that they are suitable for modelling the behaviour of aviation fuels when thermally stressed.

Once a reaction mechanism has been proposed, it is possible to describe the rate of change in concentration of a species throughout the fuel using a system of differential equations, commonly referred to in mathematics as “dynamical systems”<sup>32</sup>. Such systems can either be solved analytically, or in cases where this would be too complex, such as aviation fuels, via iterative numerical methods that generally approximate the analytical results reasonably well with the appropriate parameters.

In-depth research into the nature of deposits is less extensive than more general investigations of thermal stability. The formation of deposits is more often a research focus in investigations testing additive candidates. One in-depth report that focusses exclusively on the formation of particulate matter and deposits during thermal stressing of aviation fuel was published in 1998 by Katta et al.<sup>35</sup> and presents the still generally accepted description of the deposition mechanism. In their work, the authors aimed to improve the prediction of deposits by combining pseudo-detailed chemical reaction mechanisms with CFD simulations. Their results, comparing a global two-step model to a nine-step model, clearly show that employing more detailed models will lead to a more accurate description of the oxygen consumption in fuel as well as the deposition behaviour in fuel. The latter mechanism was then modified by Katta et al.<sup>35</sup> to account for the suggested reaction of hydroperoxides with sulfur in the fuel. This was used to predict the formation of deposits, which proved reasonably accurate with respect to the general deposition behaviour in a flow reactor. Typical of pseudo-detailed models, the model parameters were fitted to the fuel under investigation, which is the same approach that is applied to all later models.

The same general approach to modelling deposits has been more recently reiterated by Kuprowicz et al.<sup>34</sup> and West<sup>36</sup>, implicating that hydroperoxides, denoted by ROOH or oxidized fuel radical species, namely  $\text{RO}_2\cdot$  react with either sulphur containing species or an antioxidant AH to produce deposits. A layout of the overall process is offered by West<sup>36</sup> in his 2011 PhD Thesis and is shown in Figure 2.1.

The reactions leading to deposit generation are denoted in a reaction mechanism by employing a set of pseudo reactions as shown in Figure 2.2 and taken from West<sup>36</sup>. As can be seen from Figure 2.2, West<sup>36</sup> suggests that the initiation of the chemistry stems from the presence of a metal, +M which leads to the formation of radical species  $R\cdot$  in connection with hydroperoxides, the radical decomposition products of hydroperoxides,  $RO\cdot$  and  $HO\cdot$  to be exact. Once the initial radicals have formed, alkyl radicals,  $R\cdot$  will exist in an unstable equilibrium with alkyl peroxy radicals  $ROO\cdot$  which abstract hydrogen from the main alkane species  $RH$  as and lead to the formation of hydroperoxides,  $ROOH$ . West further suggests that antioxidants will interact with the alkyl peroxy radicals,  $RO_2\cdot$  to form deposits, while sulfur species,  $SH$  will primarily react with hydroperoxides. The reason for the distinction is unclear as sulfur species should be equally vulnerable to attack by radical species such as by the alkyl peroxy. However, besides empirical data on deposit build-up, no data is available on the origin of these deposits and the resulting reactions are the result of speculation rather than scientific fact. As a result, these can only be fitted to fuels with known deposition behaviour and cannot be used to predict the behaviour of yet untested fuels.

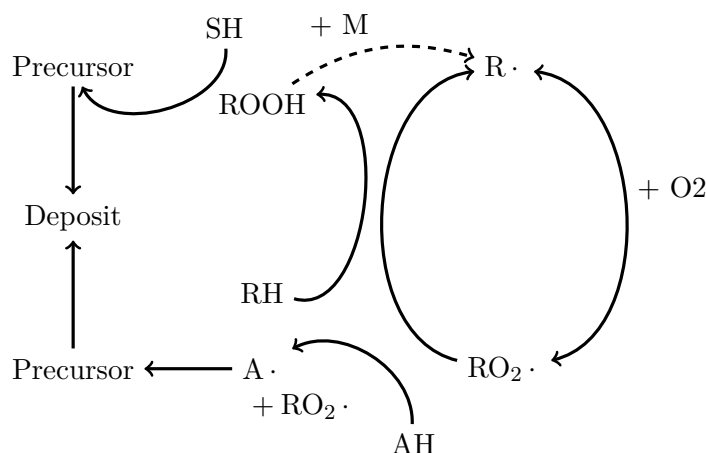


Figure 2.1: Generalized outline of the proposed autoxidation behaviour of aviation fuel,  $RH$ , according to West<sup>36</sup>, including the influence of sulfur species  $SH$  and antioxidants  $AH$ .

An attempt to classify some of the species responsible for the formation of deposits was undertaken by Sobkowiak et al.<sup>16,37,38</sup> in 2009 in an in-depth three article study into the degradation of aviation fuel. The authors carried out extensive experimental research, measuring various parameters during their experiments, such as the rate of oxygen consumption as well as various species class concentrations as well as deposition patterns.

The first study by Sobkowiak et al.<sup>16</sup> focussed on the role of phenol, indole, and carbazole derivatives on fuel degradation in a blend of petroleum based fuel with Fischer-Tropsch fuel. The authors suspected that polar compounds have an effect on the thermal stability

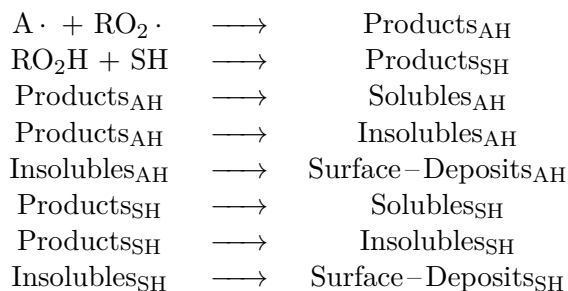


Table 2.2: Suggested reactions in pseudo-detailed reaction schemes that lead to particles or deposits in thermally stressed aviation fuel according to West<sup>36</sup>, where AH denote antioxidants and SH denote sulfur containing species.

of fuel, which is further suggested by studies by Zabarnick et al.<sup>39</sup> and Commodo et al.<sup>40,41</sup>. Initially Sobkowiak et al.<sup>16</sup> focussed on the soluble macromolecular oxidatively reactive species (SMORS) hypothesis, reiterating and expanding the SMORS hypothesis originally published by Beaver et al.<sup>42</sup> in 2005. The SMORS hypothesis is one of the few detailed suggestions for the chemical reactions that lead to the formation of deposits in aviation fuel and a speculation with regard to a proposed mechanism is laid out in greater detail by Sobkowiak et al.<sup>37</sup> in Part 3 of their study.

Sobkowiak et al.<sup>16</sup> initially pointed out that blending a petroleum based fuel with a Fischer-Tropsch fuel will lead to a reduction of polar species in the fuel suspected of being responsible for deposits. The authors further predicted that one fuel, with an unusually high concentration of indoles and carbazoles, would be a heavy depositor of residue, however during the experiments the fuel turned out to be only an intermediate depositor. On the other hand, the original expectation of increased thermal stability from added Fischer-Tropsch fuel was found to be true for temperatures below 550 °C. They produced linear relationships between the concentration of polar compounds and deposits for various fuel types with the correlation coefficient calculated and provided as a measure of the accuracy of the suggested model. They hence conclude that their results suggest that the concentration of phenol, indole and carbazole, as well as the total polar concentration, are related. The latter was also suggested by Commodo et al.<sup>40</sup> and Striebich et al.<sup>39</sup>.

In their first paper<sup>16</sup>, they provided evidence that a correlation exists between the concentration of polar compounds in aviation fuel and the amounts of deposits produced under thermal stress. The second study by Sobkowiak et al.<sup>38</sup> thus focused on the relationship between thermal stability, smoke point and small reactive species. During their investigation, they found that the deposition behaviour of aviation fuel correlated linearly to the concentration of polar species up to 100 ppm, except for one fuel where this correlation broke down for a concentration higher than 100 ppm of polar species. Therefore they conclude that a change in the deposition mechanism possibly occurs

between a 100 ppm to 200 ppm concentration of polar species. However it is not possible to say whether this behaviour is unique to the fuel tested, and thus further research is warranted. However, due to the complexity of jet fuel, the impact of trace compounds as co-oxidants results in a limited informative value of experimental studies employing jet fuels, as too many aspects of the chemical interactions remain unknown<sup>43</sup>.

The final study in the series by Sobkowiak et al.<sup>37</sup> investigated the use of a stabilizer in the form of an antioxidant, 1,4-Dihydrobenzene (DHB), as well as a proprietary stabilizer derived from DHB, in Jet-A and JP-8, fuel including blends of 50/50 Fischer-Tropsch fuel at different temperatures. This is accompanied by a 14 step generic peroxy-radical chain mechanism, along with a 4 step mechanism for DHB, to explain the interaction of DHB with aviation fuel. Adding the additive DHB leads to two distinct behaviours. At around 180 ppm, DHB was found to increase carbon deposits by about 16 %, which the authors state is an indicator of peroxy radical initiation. Increasing the concentration of DHB to 0.5 % by volume was shown to reduce the deposit formation significantly, especially at higher temperatures of up to 350 °C. For the authors, this is indicative of DHB reacting with peroxy radicals before these react with phenols in the fuel whose products are suspected of forming deposits. The soluble macromolecular oxidatively reactive species (SMORS) hypothesis presented by Sobkowiak et al.<sup>16,37</sup> suggests that a quinone, an oxygenated cyclic species, will react with an antioxidant to form deposits in the form of polyaromatic co-polymers which appears to be the only theory implicating a specific species in the formation of deposits, rather than a general species group. Unfortunately, neither the publication by Sobkowiak et al.<sup>37</sup> nor the older paper by Beaver et al.<sup>42</sup> offer parameters required for chemical kinetics simulations. No comparison between the model and the experimental data is supplied either. On the other hand, the suggested mechanism may be compared to a detailed scheme drawn up using for example an automated mechanism generation and would allow for the recognition of realistic deposition precursor candidates based on the behavioural pattern of the species in the detailed scheme when compared to the SMORS hypothesis. In addition, based on the presented data, it would be most interesting to observe the impact of the identified polar species in a “clean fuel” such as industrial solvent or even reagent grade solvents to ascertain whether correlation implies causality in this study.

A further interesting 2011 publication comes from DeWitt et al.<sup>44</sup> who investigated pyrolytic cracking, and the associated deposits, which occurs at temperatures higher than those considered for autoxidation, at the same time this study seems to be the first to have analysed the deposits which form during experiments offering a first experimentally validated opinion on the type of species responsible for deposition. In addition to the deposition products, species in the fuel have also received significant attention and were found to be smaller hydrocarbons as well as cyclic species. Besides extensive analytical data from their experiment, DeWitt et al.<sup>44</sup> also supply a simple 6-step supercritical

pyrolysis model which can be considered to be pseudo-detailed to describe some of the reactions occurring in the fuel, however it does not include any reaction parameters. In agreement with other studies, such as these by Sobkowiak et al.<sup>37</sup>, the abundance of cyclic species in stressed fuel as well as the deposits analysis supports the suggestions put forth in the SMORS hypothesis, that cyclic species are responsible for the formation of deposits. Once again, sulphur is also implicated in the formation of deposits during the thermal decomposition of aviation fuels.

The most comprehensive recent publication on thermal stability is a PhD by West<sup>36</sup> from 2011, parts of which were published in a paper by West et al.<sup>45</sup> as well. West<sup>36</sup> primarily focussed on catalytic hydroperoxide decomposition in thermally stressed aviation fuel, however he also investigated the deposition pattern for carbon and sulfur based deposits in high temperature flows, including a comparison of the prediction with experimental data.

West<sup>36</sup> suggests a more comprehensive 27 step reaction model, which attempts to establish different reaction paths leading to sulfur-based insolubles and solubles, antioxidant-based insolubles and solubles as well as an extended description of the behaviour of hydroperoxides in fuel, citing Kuprowicz et al.<sup>34</sup> as the initial source for his suggested mechanism. Besides distinguishing the type of (in-)solubles formed in fuel, West<sup>36</sup> further added reactions to describe the decomposition of hydroperoxides in fuel, which is the primary focus of his work. Typical of pseudo-detailed schemes, the reaction parameters have been fitted in the model by West<sup>36</sup> to the fuel it is compared against.

Overall, West<sup>36</sup> has shown that metals are important in accelerating, however not necessarily catalysing, hydroperoxide decomposition. As a result, significant effort of his work focused on the inclusion of metals and their effects on the decomposition of stressed fuel in models and experiments from a flow reactor. West<sup>36</sup> further investigated the accuracy of his model in a high temperature regime by comparing experimentally obtained data with CFD simulation predictions carried out in ANSYS Fluent<sup>46</sup> which enabled him to model the species transport as well as species chemistry, enabling a modelling of the predicted deposit build up. While he considers the model to be a reasonable first step towards the prediction of the behaviour of aviation fuel under a higher temperature regime, the presented graphs suggest a significant discrepancy between the predicted deposition behaviour and the measured deposition behaviour. Nevertheless, this work is useful for modelling alternative fuels as it suggests suitable model parameters such as mesh size as well as boundary conditions, which may be combined with the information from Kuprowicz et al.<sup>34</sup> for future CFD simulations.

Overall, one cannot avoid the impression that the primary focus of work into thermal stability as well as autoxidation has primarily focussed entirely on developing descrip-

tions of the process rather than developing an understand of it instead. Even where work focuses on fundamental aspects, such as the thesis by West<sup>36</sup>, the experimental assessment and validation of the model employs real fuels which introduce a multitude of unknown parameters through the complex composition and thus significant uncertainty as interactions between individual trace species cannot be ruled out in real fuels.

### 2.2.2 Theoretical Approaches to Stability

As experiments are time intensive, expensive and suffer repeatability issues due to the complexity of fuels, much attention has in recent years shifted to producing accurate models for the behaviour of aviation fuels. However, such models have their own limitations due to the complex nature of the reactions taking place in the aviation fuels. Often surrogate mixtures are used which behave in a similar manner to the actual aviation fuel, but consist of only a few known chemicals, as opposed to the hundreds present in regular aviation fuel<sup>7,19,25,47</sup>. While this increases the repeatability of experiments with such surrogate mixtures, it also introduces further assumptions as to the behaviour of the fuel, which may or may not be accurate.

A good theoretical model would shift the experimental focus from a trial approach, to a validation approach. Expectations can be set using theoretical results, and experiments would then confirm or reject the theoretical findings, significantly reducing research costs. Therefore, obtaining accurate theoretical models would have significant implications for further research into alternative aviation fuels.

However, this approach is still limited, as the complex reactions occurring in aviation fuel systems before combustion or during autoxidation are not yet well understood<sup>48,49</sup>. This is also the main reason why surrogates are used, as their less complex composition should make predicting their behaviour significantly easier compared to Jet-A1 fuels, which differ across the planet. In general, the combustion itself is better understood but consists of very complicated turbulent flows, that pose a significant challenge if they are to be modelled in detail.

Four approaches are available to generate models which describe the autoxidation behaviour of aviation fuel.

- i) The first method consists of drawing up a generalized pseudo-detailed scheme from general chemical theory. Such mechanisms are drawn up by manually analysing experimental data and evaluating the obtained results. These mechanisms can be accurate and have been proven to be accurate in the past, however their major drawback is that they need to be fitted to a given fuel for accurate results and do not help to further our understanding of the details of the underlying chemical reactions.



- ii) A second approach is to draw up detailed reaction schemes for the behaviour of alkanes or combinations of alkanes which may then be reduced using for example sensitivity analysis. Using an automated reaction mechanism generator which considers any possible reactions allows for the consideration of potentially unintuitive reactions. Such an approach is currently used in combustion modelling where detailed schemes are drawn up and then reduced for use in fluid dynamics simulations. A downside of this approach is, that to model a given combination of alkanes, it is potentially required to apply sensitivity analysis to the original scheme under various conditions to ensure that the effects of fuel composition are also fully reflected in the reduced model. Additionally, such a general approach will require a systematic comparison with experimental data to ensure that this approach results in a realistic model.
- iii) A third approach to generating an improved reaction scheme consist of extending existing theoretical pseudo-detailed models with detailed reaction schemes. Existing mechanisms that present established chemical reactions for the overall behaviour can be enhanced by extending these schemes through the addition of detailed mechanism steps for reactions that are of specific interest, such as for example the behaviour of antioxidant species or sulfur species. Such a scheme would then combine existing knowledge of the overall behaviour with existing knowledge with regards to the detailed behaviour of the species under investigation. Where existent detailed chemistry is employed to describe the reactions, some of the chemistry may be absorbed into the pseudo-detailed scheme where reaction steps exhibit no significant impact.
- iv) A fourth approach tries to simulate the behaviour of complex fuels using a smaller number of select surrogate alkanes which, because their identity is known, are easier to model. Surrogates have been used in experimental investigations into autoxidation, yet do not seem to have been used for the creation of mechanisms outside of combustion.

### 2.2.2.1 Pseudo-Detailed Reaction Schemes

Pseudo-detailed schemes tend to be reaction schemes derived from predictions about the possible behaviour of compounds in aviation fuel during thermal stressing. As a result, these schemes are fitted to data obtained using flow reactors and are thus in most cases accompanied by extensive data from an experimental investigation. A shared pattern amongst these pseudo-detailed mechanisms is that all unreacted hydrocarbons are combined into a single species, labelled RH and antioxidants are lumped together into AH. Otherwise, the detail provided by the mechanism is rather coarse providing no detailed kinetics besides distinguishing between key species classes such as alkanes, antioxidants, hydroxides or deposits.

The potentially most cited reaction mechanism for the autoxidation of aviation fuel is the 17-step pseudo-detailed reaction scheme by Ervin and Zabarnick<sup>33</sup> from 1998, which forms the basis of many newer pseudo-detailed reaction schemes. In their study, Ervin and Zabarnick<sup>33</sup> carried out an experimental investigation into the autoxidation behaviour of aviation fuel. On the basis of empirical measurements as well as assumptions, a pseudo-detailed model of the autoxidation behaviour and a comparison between predictions and measurements which appear to agree fairly well are presented in the paper. Since then, Zabarnick has contributed to two more recent studies, including a 19 step model for severely-hydrated fuel in a 2004 publication by Kuprowicz et al.<sup>50</sup>. Similar to the aforementioned study from 1998<sup>33</sup>, once again reactions are predicted to occur and the resulting model is again fitted to data and compared to experimental results.

The most recent study aiming to provide an improved pseudo-detailed reaction scheme for the autoxidation of aviation fuel was carried out by Kuprowicz et al.<sup>34</sup> in 2007, shown previously in Figure 2.1. The specific focus of the study lay on whether deposit formation may be estimated from the measurements of key species class concentrations, specifically phenols, reactive sulphur species, dissolved metals and hydroperoxides. Metals are of interest as they act as catalysts, with attention mainly given to copper and manganese during this study.

Experiments were conducted in two test rigs, one was the near-isothermal flow rig (NIFTR) at 185 °C for investigating laminar flow, under conditions of approximately constant temperature, while the other test rig employed was a “non-isothermal flowing reactor system referred to as the “ECAT” to model fuel degradation behaviour under non-isothermal turbulent flow. Tubes made from silcosteel were employed to reduce surface catalysis when running oxidation experiments, and tubes made from 316 stainless steel were employed when running deposition experiments. Seven fuel samples were used in the experiments with the NIFTR at a single temperature, while experiments employing the ECAT were performed at several temperatures but for just one selected fuel sample.

In a next step, the proposed model was compared to experimental data, using the ODE solver LSODA to model the chemical kinetics and ANSYS Fluent to model the fluid flow<sup>34</sup>. The predicted concentrations and measured concentrations for certain identified species are provided, showing good agreement. However the prediction of deposits and deposition peaks was less accurate. In their paper Kuprowicz et al.<sup>34</sup> concluded that under isothermal flow conditions the model was satisfactory, however was not able to accurately predict the magnitude of the deposits at elevated temperatures.

As a result of their investigation, Kuprowicz et al.<sup>34</sup> suggest that further research should focus on expanding the understanding of reactions occurring in fuel. Specifically, how

individual species behave at different temperatures, which metals catalyse autoxidation of fuels and which are inactive as well as more sophisticated analysis methods capable of detecting traces of metals in the parts per billion range. The study also highlights a potential problem with accurately predicting the behaviour of thermally stressed aviation fuels, namely variation between different fuels. A plot showing the oxygen consumption types for a variety of fuels by Kuprowicz et al.<sup>34</sup> nicely illustrates the point with oxygen consumption ranging from 1 minute to 8 minutes for various fuels under otherwise identical conditions.

A different pseudo-detailed model focuses on the idea of a “soluble macromolecular oxidatively reactive species”, SMORS, being produced as a part of the autoxidation process and eventually forming deposits. The theory was laid out by Beaver et. al.<sup>42</sup> in 2005 with a suggested mechanism published by Sobkowiak et al.<sup>37</sup> in 2009. Overall the scheme follows the same principle as the models suggested by Zabarnick et al.<sup>33</sup> and Kuprowicz et al.<sup>34,50</sup>, however it provides a more detailed speculative mechanism for the production of deposits during the autoxidation process from cyclic species. While this would be useful for zero dimensional chemical studies, the lack of Arrhenius parameters currently precludes the use and assessment of the proposed mechanism.

#### 2.2.2.2 Reduced Detailed Reaction Schemes

The advantage of using a detailed scheme as a starting point is, that the reaction parameters are experimentally or theoretically justified. Thus a scheme which is created by reducing a detailed scheme does not need to employ guesswork to describe the behaviour of certain species classes but can justify parameter choices based on for example the composition of fuel. To the author’s knowledge, no study has been published that presents a low temperature autoxidation scheme which employs a detailed kinetics model as a starting point.

However, this approach has been used successfully in combustion modelling, where a detailed reaction scheme describing the oxidation behaviour of alkanes was reduced to allow for a CFD simulation of the flow in an aircraft combustor, which incorporates the chemical reactions during the process. This approach was for example used by Shafagh<sup>51</sup> to improve an oxidation model for aviation fuel. Given that detailed combustion models can be successfully reduced to model the combustion behaviour for a specific fuel, it is not unreasonable to expect that it is possible to reduce a detailed autoxidation model provided such a detailed model has been created.

#### 2.2.2.3 Combined Pseudo-Detailed as well as Detailed Reaction Schemes

Combining a pseudo-detailed scheme with a detailed reaction scheme would allow the use of established mechanisms while expanding the scheme, with the help of scientifically

justified parameters. By not reducing the scheme, extra detail in the reactions may be retained in the resulting scheme to describe the behaviour of known compounds. In published journals, no study has been found that presented a low temperature autoxidation scheme which employed a combination of a detailed kinetics model and a pseudo model.

However, in combustion, You et al.<sup>52</sup> published a study on the oxidation of n-dodecane, creating a reaction scheme that uses a combination of pseudo-models as well as a detailed reaction scheme. As this study focussed on combustion, this model is only meant to be valid for temperatures of 850 K and above. The authors employed the following mechanisms for the creation of their complete scheme:

1. the USC-Mech II mechanism for C<sub>1</sub> to C<sub>4</sub> carbon oxidation,
2. a set of reactions for normal alkanes in the range C<sub>5</sub> to C<sub>12</sub> and
3. a “4 species lumped n-dodecane autoxidation model” to decompose the carbon chain.

While the result is not directly applicable to autoxidation, the study indicates that the method of combining detailed schemes with “artificial” pseudo models can be employed successfully to obtain a description of an oxidation process.

#### 2.2.2.4 Surrogate Models

Surrogate compounds can be selected to try and model the behaviour of a more complex mixture, such as aviation fuel, a typical gas chromatography chromatogram is shown in Figure 2.2, on the basis that certain groups of species or compounds will behave similarly under autoxidation or combustion conditions.

Surrogate model have been used successfully in combustion modelling by Catalanotti et al.<sup>47</sup> who used methyl butanoate as a surrogate for fatty acid methyl ester (FAME) biofuel combustion, which is itself a FAME. A later model was drawn up by Shafagh et al.<sup>51</sup> describing the behaviour of methyl tridecanoate as a more advanced surrogate. In both cases, the assumption is made that the behaviour of a single FAME models that of the overall composition of FAME based biofuels.

Two studies using a more advanced, methodically similar, approach to creating a surrogate model for aviation fuel were presented in 2010 by Dooley et al.<sup>53</sup> and Huber et al.<sup>54</sup>. The approach taken by both research groups is similar and consists of analysing fuel to identify as many constituents as possible and then representing these by a reduced number of chemical species based on shared characteristics of certain compounds. Examples of fuel characteristics are properties such as viscosity, cetane and octane number, thermal conductivity, the boiling point, hydrogen to carbon ratio and other

properties. The studies of Dooley et al.<sup>53</sup> and Huber et al.<sup>54</sup> differ with respect to the exact fuel properties used to select suitable surrogate compounds, however in both cases a multitude of properties are considered.

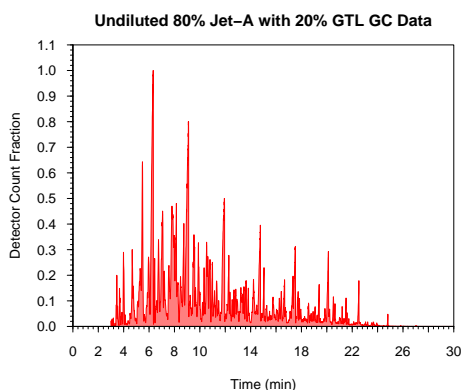


Figure 2.2: Gas chromatography chromatogram of a 20% GTL with 80% Jet-A fuel blend, showing a significant number of peaks corresponding to a complex multicomponent mixture.

Both Dooley et al.<sup>53</sup> and Huber et al.<sup>54</sup> list their suggested surrogate species, shown in Tables 2.3 and 2.4, offering valuable suggestions for suitable species in surrogate mechanisms, but only Huber et al.<sup>54</sup> offer two clearly defined surrogate models with respect to composition, shown in Table 2.5. Measurements and model predictions are supplied by Dooley et al.<sup>53</sup> for four key species that were chosen as indicators of the accuracy of the model. However, these species are typical combustion products and not autoxidation products. Huber et al.<sup>54</sup> offer plots of properties such as viscosity and density, offering a comparison between the model and the actual fuel. In both studies, the suggested surrogate models appear to agree very well with the behaviour of the actual fuel. Unfortunately however, the primary focus of the study by Dooley et al.<sup>53</sup> lay on combustion and not on autoxidation. As a result the suggested chemical kinetics model is based on combustion models, with autoxidation temperatures seemingly only considered for completion. In contrast, the data presented by Huber et al.<sup>54</sup> suggest that the temperatures of the autoxidation regime and below were the primary focus of their investigation, however no suggestion is offered on how a chemical kinetics model may be produced from the data. Another potential issues with such surrogate model is that they may fail to consider relevant trace species in aviation fuel which may have a potential impact on the thermal stability of aviation fuel. On the other hand, given that only a select number of species is considered, it should be easier to attempt to obtain a detailed understanding of the behaviour of these species under a variety of controlled conditions that are not subject to the variation of regular aviation fuel.


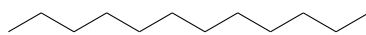
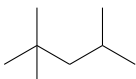
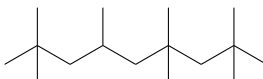
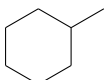
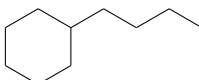
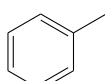
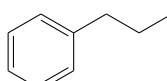
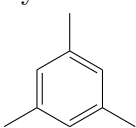
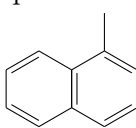
Component	Formula	Component	Formula
n-decane 	$C_{10}H_{22}$	n-dodecane 	$C_{12}H_{26}$
iso-octane 	$C_8H_{18}$	iso-cetane 	$C_{16}H_{34}$
methylcyclohexane 	$C_7H_{14}$	n-butylcyclohexane 	$C_{10}H_{20}$
toluene 	$C_7H_{14}$	n-propylbenzene 	$C_9H_{12}$
1,3,5-trimethylbenzene 	$C_9H_{12}$	1-methylnaphthalene 	$C_{11}H_{10}$

Table 2.3: Proposed surrogate components according to Dooley et al.<sup>53</sup>, reproduction of Figure given in their publication.

normal paraffinic	iso paraffinic	cyclic
n-heptane	5-methylnonane	n-propylcyclohexane
n-octane	2-methyldecane	n-hexylcyclohexane
n-nonane	2,4-dimethylnonane	n-heptylcyclohexane
n-decane	n-pentylcyclohexane	aromatics
n-undecane	3-methylundecane	toluene
n-dodecane	5-methyldodecane	ortho-xylene
n-tridecane	2-methyltridecane	tetralin
n-tetradecane		dicyclic paraffin
n-pentadecane		transdecalin
n-hexadecane		1-methyldecalin

Table 2.4: Proposed surrogate component candidates according to Huber et al.<sup>54</sup>.

compound	Jet-A-4658 surrogate	Jet-A-3638 surrogate
n-hexylcyclohexane	0%	26.8%
n-heptylcyclohexane	27.9%	0%
1-methyldecalin	1.3%	6.4%
5-methylnonane	16.5%	13.0%
2-methyldecane	15.4%	28.4%
n-tetradecane	5.7%	3.5%
n-hexadecane	3.3%	0%
ortho-xylene	7.1%	9.4%
tetralin	22.8%	12.5%

Table 2.5: Proposed best fit surrogate compositions for two jet fuels, according to Huber et al.<sup>54</sup>.

### 2.2.3 Experimental Investigations into Thermal Stability

Widegren and Bruno<sup>55,56</sup> published two papers, first investigating the thermal decomposition of Jet-A fuel in an ampoule reactor, followed by the decomposition of propylcyclohexane in an identical ampoule reactor. The compound was thermally stressed at about 35MPa in a stainless steel ampoule reactor at various temperatures for various amounts of time, with longer residence times for lower temperatures and shorter residence times for higher temperatures to ensure any reactions occurring can proceed to completion. After the thermal stressing, the liquid products were analysed using gas chromatography (GC) while the gaseous products were analysed by gas chromatography mass spectrometry (GC-MS). However a visual inspection of the reaction product was also carried out.

For their Jet-A investigation, Widegren and Bruno<sup>55</sup> employed a blend of five aviation fuels, under the name of POSF-4658 which they claim is representative of a typical aviation fuel. According to the authors, the rate constants of the blended fuel will be close to the average of the rate constants that would be obtained from testing the individual fuels the blend is composed of. Analysis of the fuel after stressing shows that high thermal stresses lead to the formation of small hydrocarbon gaseous products in aviation fuel but also produces some unidentified black particulate matter. From the composition of fuel after thermal stressing, Widegren and Bruno<sup>55</sup> conclude that aviation fuel has a thermal stability similar to that of C<sub>10</sub> to C<sub>14</sub> alkanes. The authors provide an Arrhenius plot, i.e. a plot of  $\ln(k)$  versus  $\frac{1}{T}$  (see Section 3.1.4 for details), for the decomposition of Jet-A. They conclude that that the strong linearity over a temperature range spanning 75 °C is indicative of the assumption of first-order kinetics in the decomposition reactions of fuel being reasonable.

However given that Widegren and Bruno<sup>55</sup> also state that the rate constants for the thermal decomposition of individual fuel batches of kerosene based fuel can vary by as much as a factor of 6, it is questionable whether blending fuels is an ideal method for creating a typical fuel. Especially if one considers that trace compounds are suspected of having a significant impact on the thermal stability of aviation fuel and may be present in one fuel while absent from another<sup>39-41</sup>. Running tests with different fuel types rather than a fuel blend would however be more time consuming and also more expensive, given that every individual fuel would have to be analysed before and after the experiment. Widegren and Bruno<sup>55</sup> additionally investigated thermally stressed fuel under static conditions in a stainless steel ampoule reactor, but the question arises whether such conditions are representative of the turbulent flow that can occur in fuel systems. A turbulent flow can lead to a better mixing of fuel and hence potentially accelerate any reactions. At the same time, the more controllable environment of a calorimetric bomb reactor allows for an easier control as well as modification of the parameters.

Widgren and Bruno<sup>56</sup> continued their work by investigating the thermal decomposition of propylcyclohexane, employing the same methodology they had used with Jet-A fuel. On the assumption of first-order kinetics in the reaction they again plotted an Arrhenius plot, which shows near perfect linearity that they once again state is indicative of the assumption of first-order kinetics being correct, also because neither a half or second order rate law could improve the fit of the curve.

Investigating the thermal degradation of individual compounds as done by Widgren and Bruno<sup>56</sup> may be an appealing approach to examine the details of thermal degradation, however excludes any “interspecies reactions” that may take place in aviation fuel which consists of thousands of compounds. The research into additives by Liu et al.<sup>57</sup>, introduced in Section 2.3, illustrates such a problem in the form of very different results being observed for the deposition behaviour induced by an additive in the fuel surrogate and in aviation fuel. Hence investigating individual compounds can only help to further our understanding of how this specific compound behaves and not how aviation fuel behaves.

In fact, Widgren and Bruno<sup>55,56</sup> specifically state that their experiments can only be considered valid for experimental conditions equivalent to those used in their investigation, namely a pressure of around 35 MPa and a pipe surface constructed from 300 series stainless steel.

Further experimental research into high thermal stability fuel was presented by Heyne et al. in 2009<sup>58</sup>. Their work focuses on autoignition of a high thermal stability fuel, so far running under the development name of JP-900. This relates to the wish of the US Air Force and Army to reduce operational costs by implementing a single battlefield fuel, which can be used in ground based vehicles as well as aircraft. For the experiments, a 50:50 blend of light cycle oil and chemical oil was used, the latter stated to be rich in cycloalkanes. Additionally an individual component, decalin, was chosen for the experiments, as according to the authors it occurs often when fuel is produced from heavy feedstock, such as oil sands. Thermal stability was not a key focus, but interesting information can be still obtained from their paper. For example, Heyne et al.<sup>58</sup> in 2009 state that the thermal stability of the two isomers of decalin is different, with trans-decalin being the more stable version. The authors further state that, cis-decalin will isomerise to trans-decalin under supercritical conditions, which explains why cis-decalin is of lesser interest and the study focussed on trans-decalin. According to the authors, decalin is one of the thermally most stable and endothermic components of fuel. This makes researching decalin very interesting, considering the expected higher heat sink capabilities required from future aviation fuel.

The question that arises from this paper is, what isomers of other hydrocarbon compounds can be found in aviation fuel, and if so, how their properties affect the thermal



stability of aviation fuel. The implication of the different behaviour of the decalin isomers is that a thorough understanding of aviation fuel would need to consider not only the type of alkanes in fuel but also the variation in the structure of isomers.

Corporan et al.<sup>29</sup> published a general overview for alternative aviation fuels. Thermal stability is one of the points considered, besides other concerns such as seal swell, chemical stability and emission profiles. The fuels investigated were six fuels from non-petroleum sources, namely coal, natural gas, camelina and animal fats. Thermal stability was analysed by two methods - Quartz crystal Microbalance (QCM) at 140 °C on 60ml of fuel, and single tube flow at 340 °C. The research shows that higher thermal stability occurred in the alternative fuels, compared to currently used JP-8 at temperatures below which cracking occurs. Pyrolytic cracking, that some researchers consider an option to increase heat sink capabilities was not investigated in this study and this is expected to occur at about 480 °C, with higher reactivity and larger amounts of deposits.

Some of the most recent investigations into thermal stability were carried out by a group of researchers around Mikaël Sicard<sup>59-66</sup> at ONERA. Sicard et al. carried out a systematic investigation into the behaviour of both Jet-A fuel, neat and doped as well as representative solvents in very controlled thermal stability experiments using a commercial small scale oxidation tester as well as a reflux condenser.

Sicard et al.<sup>64</sup> began their investigation by identifying a small number of compounds representative of regular aviation fuel. These consisted of a normal paraffinic hydrocarbon as well as cycloalkanes and aromatics. Their initial investigation was carried out through a flask oxidation study which enabled strict control of the experiment and offered the ability to sample both the products as well as current reactants during the test. Sicard et al.<sup>64</sup> do state that their test conditions are not representative of aircraft fuel systems, however their work and analysis confirmed that the employed test conditions are representative of autoxidation conditions and present accelerated conditions.

As a result, Sicard et al.<sup>60,61</sup> have continued to develop their technique, mainly employing more sophisticated analysis techniques to evaluate the underlying chemistry during the autoxidation process in greater detail. Gas chromatography mass spectrometry as well as Fourier transform infra-red adsorption analysis enabled Sicard et al.<sup>60,61,64</sup> to identify many of the products resulting from an autoxidation regime. These were found to be predominantly aldehydes, ketones as well as carboxylic acids, however no quantitative data has been collected. Besides sampling at different residence times, Sicard et al.<sup>60</sup> used their expertise to compare the products from three different fuels - which were found to be remarkably similar, except for the lack of deposits in a biomass derived fuel.

Finally, Sicard et al.<sup>61</sup> investigated a number of fuels in three very different test rigs.

Work was carried out using a reflux condenser, employed in the initial study<sup>64</sup> as well as a PetroOxy and a High Reynolds Thermal Stability (HiReTS) tester. This cross test rig investigation shows how the test regime can have a significant impact on the behaviour of the tested fuel. A fuel that appears fairly unstable in the PetroOxy due to a comparatively rapid oxidation, a naphththeno-aromatic cut, was shown to be the most stable fuel in the HiReTS test<sup>61</sup>. Thus this study shows how different thermal stability manifests itself in very distinctively different behaviour, dependent on the test method employed and even suggests that we should question the “literature assessment” of non-standard fuels, whose behaviour may not agree with the behaviour of conventional fuels under thermal stress. The difference in data obtained by Sicard et al.<sup>59</sup> very much suggest that the flask oxidation study is more sensitive to differences in the test fuel due to the longer test duration in comparison to the HiReTS. Fuels that would have passed the HiReTS showed a considerably different behaviour when studied in the long term static regime where a lack or presence of thermal stability became more pronounced over a longer time frame.

Following their comparative evaluation of different test methods<sup>61</sup>, Sicard et al.<sup>59–61,64</sup> continued their investigation of static thermal stability tests with the PetroOxy which offers both controlled conditions as well as uncontaminated samples after the test as no hard to clean fuel coolers are used. This enabled Sicard et al.<sup>61</sup> to establish that autoxidation behaviour in the PetroOxy consists of three distinct steps, the initial oxygen consumption, the production of volatile compounds immediately after oxygen has been consumed, identified by a pressure rise, followed by continued reactions in the solution consuming any volatile compounds, identified by a pressure drop. Besides identifying these reactions steps, Sicard et al.<sup>61,62</sup> also identified the relevant species during the individual reactions steps for dodecane. These initial products of autoxidation were again determined to include alcohols, carboxylic acids, aldehydes and ketones. According to Sicard<sup>61,62</sup>, the aldehydes occur in the second step and primarily smaller alkanes form first, which then combine to form heavy products such as esters and lactones as a result of the autoxidation process.

DeWitt et al.<sup>67</sup> investigated the effects of aromatics on synthetic paraffinic kerosene, offering some additional insights into the formation of deposits, especially with regards to deposit thickness. As opposed to standard visual ratings, DeWitt et al.<sup>67</sup> employed an ellipsometry method to quantify the thickness of deposits on the JFTOT tubes. The work shows that ellipsometry is an effective measurement of thermal stability as it allowed quantitative measurement of the thickness of deposit which is more informative than the usual colour rating. The at times large discrepancy between visual ratings and ellipsometry measurements shown in the work suggests that very different deposits were produced which unfortunately were not subject to further investigation. DeWitt’s<sup>67</sup> experiments further show a reduction of thermal stability in connection with the addition

of aromatic species which they describe as containing "negligible heteroatomic compounds". Given that such heteroatomic compounds are considered to be the primary source of deposit formation<sup>68,69</sup>, this assessment is questionable.

In many ways, the experimental investigation into the thermal stability of fuels or its autoxidation behaviour suffers from the same problems as work into the deposition behaviour of fuels. Work is predominantly carried out using real fuels which provide valuable observations, yet also are of very limited scientific research use. The inherent complexity of fuels precludes any reliability in the data as fuel to fuel variation is significant. In retrospect especially, many studies end up reinforcing accepted general observations while not providing any value when attempting to understand the underlying fundamental aspects of the process.

## 2.3 Additives

Additives are a vital component of today's military aviation fuels and are one of the few ways the performance of fuels, and hence engines, can currently be enhanced. Because additives can be added during refuelling, they do not need to be compatible with older engine and fuel system components such as seals, but only the current generation of engines and fuel systems. Additionally, additives can potentially allow the use of less ideal fuels in aircraft engines without significant drawbacks, such as for example deposit formation. Current research on additives focusses on military applications for high performance engines, stabilizing biofuel or improving the performance of rocket propellants.

Oxygen is considered to be the primary cause of autoxidation in aviation fuel, with fast oxidation rates observed in thermally stable fuels. Beaver et al.<sup>70</sup> tested the hypothesis that fuels that oxidise quickly are more stable by employing an oxygen scavenging compound in a thermally stressed fuel surrogate. In their experimental study, dodecane was thermally stressed in a static bomb reactor, with and without tetrahydronaphthalene (THN) added as a hydrogen donor. Dicyclohexylphenylphosphine (DCP) was employed as an oxygen scavenging stabilizer. Beaver et al.<sup>70</sup> show that DCP was able to reduce the amount of deposits formed during thermal stressing of dodecane with THN, consistent with the expectation that oxygen removal can reduce the amount of deposits in a bomb reactor. However, the authors also show that dodecane alone was thermally stable at 250 °C, while dodecane with DCP showed a yellow discolouration at 250 °C which may be attributed to the oxidation of DCP. As a part of their study, Beaver et al.<sup>70</sup> also suggest a reaction scheme to describe the behaviour of the oxygen scavenging species, however without any clear indication as to which species may be contributing to deposits. Common to all pseudo-detailed schemes, alkanes are described using a generic R while the oxygen scavenging process of DCP is described in greater detail. However unfortunately the suggested model lacks any parameters and thus cannot be easily tested using a

chemical kinetics solver.

Sobkowiak et al.<sup>71-73</sup> conducted research into high thermal stability jet fuels. The first focus was on developing an additive package that would enhance the thermal stability of the standard air force fuel JP-8 up to about 480 °C. In 2007 Sobkowiak et al.<sup>72,73</sup> continued their study by investigating products from light cycle oil. JP-8 fuel, specifically POSF-3804, was stabilized with  $\alpha$ -tetralone (THNone),  $\alpha$ -tetralol (THNol) and tetralin (THN). A sample of JP-8 fuel was tested in a flow reactor, without additives as well as with three additives. THN was also investigated by Bruno et al.<sup>74</sup>, however, while Bruno et al.<sup>74</sup> investigated THN as a stabiliser for biofuels, Sobkowiak et al.<sup>72,73</sup> focussed on stabilizing conventional fuel.

In the data presented by Sobkowiak et al.<sup>72</sup>, all three additives are added at a concentration of 1% by volume and result in a visible reduction in deposits when compared to neat fuels, especially in the high temperature region of the plot. The reduction in deposits is most impressive in the case of a 1:1 mixture of THN and  $\alpha$ -tetralone (THNone), which the authors also point out in their conclusion. However, while this is extremely encouraging, the Sobkowiak et al.<sup>72</sup> also point out that the fuel used in the experiment, POSF-3804, is already a very stable variation of fuel, which they speculate may come from the lack of polar aromatic compounds suspected of supporting deposit formation. As a result, this study cannot necessarily be considered valid for the currently available Jet-A1 products which do not feature such initial high thermal stability characteristics and must be considered as another specific case study valid only for a specific fuel. The experimental results with JP-8 fuel, prompted Sobkowiak et al.<sup>72,73</sup> to publish a third study in which they investigate the underlying mechanisms of the autoxidation involving polar compounds. Beaver et al.<sup>73</sup> suggest that the additives limit the oxidation of polar species in the fuel. The proposed antioxidant behaviour in the paper for THNone is illustrated in Figure 2.3.

A flask oxidation study was carried out to validate the hypothesis, in which oxygen was bubbled through a mixture involving decane as a solvent, butylated hydroxy toluene (BHT) to model a polar species, as well as the following additives:

- i) tetralin (THN),
- ii)  $\alpha$ -tetralone(THNone) ,
- iii)  $\alpha$ -tetralol (THNol).

The advantage of flask oxidation studies is the close control over reaction conditions. The amount of fuel used, the temperature as well as the oxygen flow rate in this case can be measured and controlled very accurately. At the same time, the reaction conditions in such a reactor are very different when compared to an aircraft's fuel system in which the fuel is non-static.

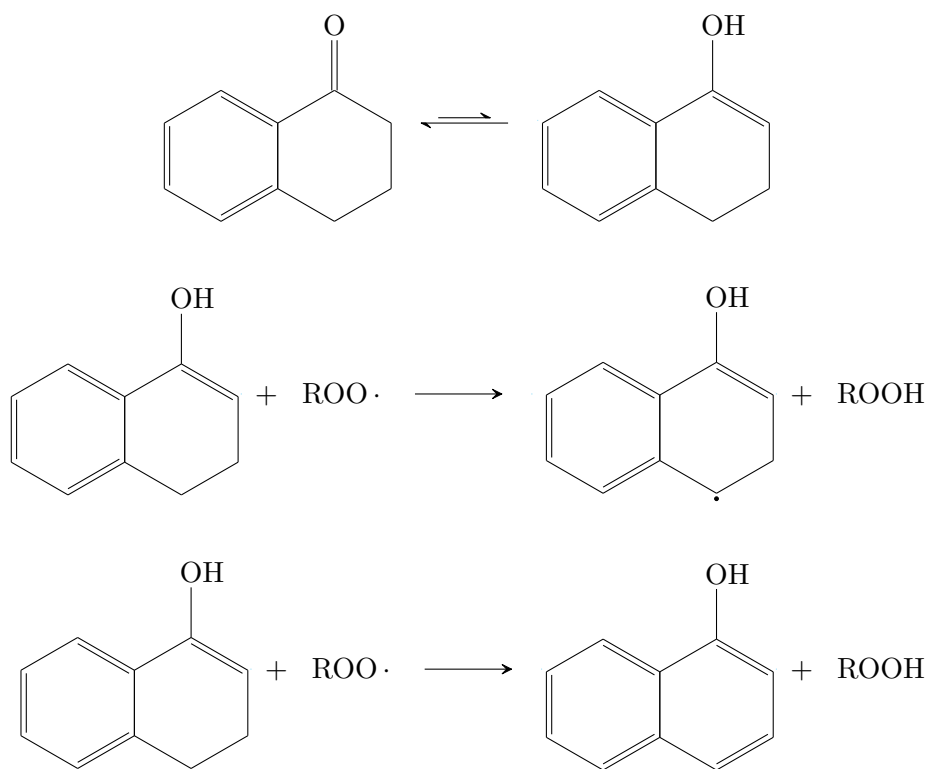


Figure 2.3: Proposed behaviour of THNone as an antioxidant by Beaver et al.<sup>73</sup>

Beaver et al.<sup>73</sup> found that adding a high concentration of additives as stabilizers can prevent the oxidation of BHT while a lower concentration of stabilizers leads to a reduced consumption of BHT. The authors therefore conclude that the additives can, as they state, concentrate the oxidisation of peroxy radicals in the fuel.

The other focus of the paper by Beaver et al.<sup>73</sup> was to explain the modification of the deposition behaviour exhibited by thermally stressed aviation fuel. The authors suggest that the fuel's "solvating" capacity with respect to the products of oxidised additives is responsible for the amount of deposits observed.

Additives can also be added to biofuels as investigated by Bruno et al.<sup>74</sup>. Their goal was to stabilise FAMEs (Fatty Acid Methyl Esters) by adding hydrogen donors and evaluating a self developed "advanced distillation curve (ADC) measurement" as a method to analyse thermal stability. A biofuel, B100, produced from soybeans, which is representative of other commercial fuels, was used to test the following three additives at concentrations of of 1% and 3% by volume of the fuel:

- i) 1,2,3,4-tetrahydroquinoline (THQ),
- ii) 1,2,3,4-tertrahydronaphthalene (THN) ,
- iii) trans-decahydronaphthalene.

It was found that hydrogen donors are effective at improving the thermal stability of biofuels in the lower temperature regime below approximately 365 °C, but as the temperature rises, their effectiveness is decreased because the additives themselves are predicted to start to decompose into reactive radicals.

These findings should not be treated as proving the general usability of FAME, but rather as a one off case study. Even more so considering that other researchers have voiced very negative opinions about the thermal stability and suitability of FAME fuels<sup>58,75,76</sup>.

A further investigation of additives involved rocket fuel and was conducted in the People's Republic of China. Liu et al.<sup>57</sup> focussed on additives that encourage pyrolytic cracking of fuel, which is endothermic and thus enhances the heat sink capabilities of modern fuels. They compared three additives,

- i) 1-nitropropane (NP),
- ii) triethylamine (TEA) ,
- iii) 3,6,9-triethyl-3,6,9-trimethyl-1,4,7-triperoxonane (TEMPO),

that would increase the rate of pyrolysis in the fuel and compared the resultant carbonaceous surface deposits.

Liu et al.<sup>57</sup> first used n-dodecane as a surrogate for aviation fuel, which they claim it is a major constituent of commercially available fuels, such as JP-8, JP-7, RP-3 and other aviation fuels. It was found that these additives increased the rate of pyrolytic cracking when n-dodecane is stressed and two of the three additives, TEA and TEMPO, also reduced the amount of surface fouling, which would be desirable in aviation fuels as deposits increase maintenance costs or could lead to engine failure by clogging fuel filters and fuel injectors.

Following the initial results with n-dodecane, Chinese RP-3 fuel was stressed with and without any additives and the deposits analysed. It was found that in the Chinese RP-3 fuel, the deposit rates are slightly increased with TEA and TEMPO over regular fuel, and significantly increased with the addition of NP. A question that arises from this experiment is how representative Chinese RP-3 fuel is for other globally used aviation fuels. Additionally, as Hughes<sup>77</sup> points out, the very different deposition behaviour of RP-3 fuel compared to the n-dodecane surrogate leads to questions about the suitability of surrogate models with respect to researching additives or potentially deposition behaviour in general.

## 2.4 Stability Limits

Currently research by Spadaccini<sup>78</sup> shows that deposition layers are mainly dependent on the oxygen in the fuel, as well as the temperature. Fuel is generally stable below about 177 °C and most reactive between the temperatures of about 177 °C and 371 °C. Oxygen can be present at concentrations of about 70 ppm or more, dropping as low as 5 ppm after any reactions in the fuel take place. It has been observed that the formation of deposits, which is an indicator of thermal stability, decreases with the oxygen concentration. Tests on aviation fuels in a flow reactor frequently show deposits only at the start of the pipe with no deposits further downstream in the pipe, or in an attached fuel filter if one is used<sup>9,78</sup>.

At temperatures above about 427 °C, autoxidation is replaced by endothermic pyrolysis in which larger molecules are broken up into smaller molecules, thus consuming energy but also leading to coke formation<sup>78</sup>. Some of the recent research is considering the use of endothermic reactions in the fuel system to, on the one hand, increase the energy content of the fuel and, on the other hand, improve the heat sink capability of the fuel. However, at this time, the coke formation during endothermic reactions is a reason for concern and prohibits such a design in aircraft engines<sup>6,9,79,80</sup>.

## 2.5 Thermal Stability Conclusion

Overall, research into the thermal stability of aviation fuel is very comprehensive and detailed. The understanding of fuel autoxidation, including the deposition behaviour has improved, with key species pinpointed as likely initiators by several studies, such as the research by Sobkowiak et al.<sup>16,37,38</sup> as well as Widegren and Bruno<sup>55</sup>. Detailed hypotheses as to the origin of deposits are presented by the authors, thus encouraging further work on the topic. At the same time, all these studies are limited to the very specific conditions at which they were carried out. The investigations by Sobkowiak et al.<sup>16,37,38</sup> are possibly the studies closest to offering a more general result, namely a generalized mechanism.

Nevertheless, even though there is such an extensive amount of knowledge about the behaviour of aviation fuel, many publications and suggestions still include a significant amount of educated guesswork as to the behaviour of fuel which also has not been resolved by using surrogate compounds to obtain a simplified understanding of the behaviour occurring during the thermal stressing of fuel. The mechanisms of Ervin and Zabarnick<sup>33</sup>, Kuprowicz et al.<sup>34</sup> or West<sup>36</sup> are all good examples of mechanisms that are created based on expectations derived from an understanding of how individual compounds behave, rather than derived from fundamental studies into the behaviour of compounds. Additionally, each of the studies only considered a small aspect of the many factors

influencing thermal stability, especially in real fuels. In the cases of Kuprowicz et al.<sup>34</sup> and West<sup>36</sup>, trace metals in fuel and their catalytic effect as well as polar species were covered, excluding the expected impact of other potential components or contaminants in the fuel. And while Kuprowicz et al.<sup>34</sup> and West<sup>36</sup> were able to accurately fit their models to the fuel when it came to oxygen consumption as well as species class concentrations, neither was able to accurately predict the deposition behaviour of a fuel using a CFD simulation, indicating that there are reactions participating in the formation or inhibition of deposits that have not been considered so far. It would not be unreasonable to expect a better agreement between models and test results in a more fundamental background study using more pure components such as solvents to obtain a better understanding of the fundamental processes, before the complexity of fuel is tackled as a whole.

While individual aspects of aviation fuel thermal stability thus seem to be understood quite well, such as for example that oxygen is vital in the degradation process as shown by Commodo et al.<sup>40,41,81,82</sup>, the overall process still poses many open questions. As a result we are sometimes faced with unpredicted and unexpected results, such as for example opposing behaviour between a surrogate and actual fuel in the work presented by Liu et al.<sup>57</sup>. An additive behaved completely different in the simplified single component fuel surrogate compared to actual aviation fuel. This casts doubt on the accuracy of surrogates for providing insight into the behaviour of more complex fuels and offers reasons to question whether Dooley et al.<sup>53</sup> and Huber et al.<sup>54</sup> are right in suggesting that surrogates can be used to accurately model the behaviour of fuels.

The final study by Sobkowiak et al.<sup>37</sup> points out that the predicted deposition behaviour was observed in a flow reactor, but not in a static calorimetric bomb test. A question that arises with respect to the studies by Widegren and Bruno<sup>55,56</sup> is hence how reliable or valuable their results are given the aforementioned observation by Sobkowiak et al.<sup>37</sup>. While a calorimetric bomb offers the ability to closely influence and control all the parameters in the experiment, such as pressure and temperature as well as the amount of fuel, the conditions in a calorimetric bomb reactor are not representative of the turbulent flow that occurs in an aircraft's fuel system. Additionally, testing individual compounds, as done by Widegren and Bruno<sup>56</sup>, ignores any interspecies reactions which may be key to the autoxidation behaviour of aviation fuel.

Despite the application of various analysis techniques that have proven successful in other areas of chemical research, it has also not yet been possible to identify all important species taking part in the autoxidation process. The studies by Commodo et al.<sup>40,41,81,82</sup>, DeWitt et al.<sup>44</sup> or Striebich et al.<sup>39</sup> had all achieved their aim by showing the presence of species or again validating the importance of oxygen in the autoxidation process. However neither study was able to offer any definite information on the identity of important species, with only DeWitt et al.<sup>44</sup> clearly identifying characteristic cyclic



species in the deposits that formed during thermal stressing.

While the overall chemistry is most likely correct given that it has proven effective and generally accurate so far, there is at present no foundation in a fuels' composition for parameters in published schemes other than expectation as to the nature of the reaction and the observation that the selected values lead to a general agreement in the behaviour of a specific fuel. Additionally, given the sometimes unexpected behaviour and the difficulty of predicting the behaviour of fuels in experimental studies, it is not unreasonable to suspect that many schemes are very incomplete. Interestingly, nobody has yet attempted to amalgamate the behaviour of individual species into a comprehensive model based on the behaviour of particular compounds. While such a model would include most likely require hundreds of species to capture most of the suggested reactions in aviation fuel, the availability of such a model should simplify the process of extending the knowledge of aviation fuel behaviour allowing researchers to more easily investigate the accumulated knowledge of the past decades.



## Chapter 3

# Software Tools and Theory

This work, focusses on three distinct research areas with respect to thermal stability. Experimental work, including analysis work, to obtain data as well as modelling work which is broken down into an investigation of chemical kinetics as well as quantum chemistry calculations to investigate postulated reactions and obtain realistic kinetics parameters for further investigation.

While experimental equipment is introduced where used, the available software and their theoretical background as well as any developed codes are discussed in greater detail in this chapter.

### 3.1 Chemical Kinetics

#### 3.1.1 Description of Chemical Kinetics

Chemical kinetics refers to the study of chemical systems and their development over time. Individual elementary reactions can be combined to form a complex mechanism and thus allow a more detailed analysis of chemical processes such as fuel autoxidation. In chemical kinetics, such mechanisms are integrated over time to track their development and to obtain a better understanding of the process but also to be able to validate predicted results with the assistance of experimental data.

#### 3.1.2 Stoichiometric Equations

Stoichiometric equations are a fundamental component of chemistry, frequently used to present reactions in a clear and concise manner. Stoichiometric equations are used to either describe basic elementary reactions or to describe overall reactions reduced in a concise way. In either case, a specific number of atoms of species A react with a specific number of atoms of species B. An example for such an overall reaction is the well known oxidation, also known as combustion, of hydrogen gas, e.g.  $2\text{H}_2 + \text{O}_2 \longrightarrow 2\text{H}_2\text{O}$ .

Besides listing the reactants,  $\text{H}_2$  and  $\text{O}_2$ , a stoichiometric equation also supplies the ratios of atoms required for a complete reaction. At this point, it may be worthwhile to mention that similar to mathematical reactions, stoichiometric equations need to balance. Thus, both sides of the equation are required to contain the same number of atoms, as atoms cannot be created or destroyed (although this is possible in a particle collider or during nuclear decay).

### 3.1.3 Elementary Reactions and Reaction Rates

#### 3.1.3.1 Elementary Reactions

Elementary reactions describe direct, single step, chemical reactions that take place in a single transition state. The oxidation of hydrogen,  $2\text{H}_2 + \text{O}_2 \longrightarrow 2\text{H}_2\text{O}$ , introduced in Section 3.1.2 is an overall reaction, which encompasses an elementary reaction while a reaction written as  $\text{O} + \text{H}_2 \longrightarrow \text{OH} + \text{H}$  describes an elementary reaction<sup>83</sup>.

#### 3.1.3.2 Reaction Rates

Reaction rates tend to be given as a number per volume per unit time<sup>84–86</sup>. Common units are moles or molecules per centimetre cubed, metre cubed or litre per second. In this thesis, reaction rates will generally be given in  $\text{moll}^{-1}\text{s}^{-1}$  unless indicated otherwise.

The rate of a reaction is mainly influenced by the concentration if all other conditions, such as temperature and pressure, are kept the same. Hence, in the case of a reaction featuring just one reactant, a first-order reaction, the reaction rate can be computed easily when the rate constant and concentration are known, as follows<sup>84–86</sup>:

$$r = k [A] \tag{3.1.1}$$

We define  $[A]$  to be the concentration in  $\text{moll}^{-1}$  of the chemical  $A$ , and  $k$  is the constant of proportionality, defined by the Arrhenius equation, which is elaborated on in Section 3.1.4.

However considering that most reactions feature more than one species, the notation in Equation (3.1.1) needs to be expanded for reactions featuring two or three species. The majority of reactions take the form of a second-order reaction in which the rate is described as follows, where  $A$  and  $B$  are generic placeholders:

$$r = k [\text{Reactant}_A] [\text{Reactant}_B] . \tag{3.1.2}$$

Because such elementary reactions are classed depending on the number of reactants, they are referred to as first, second or third order reactions. Depending on the order of the reaction, the units of the rate constant need to be adjusted to ensure the equation balances<sup>86</sup>, shown in Table 3.1.

			units of $k$
Reactant <sub>A</sub>	→	Product(s)	First-order $s^{-1}$
Reactant <sub>B</sub> + Reactant <sub>B</sub>	→	Product(s)	Second-order $l\text{mol}^{-1}\text{s}^{-1}$
Reactant <sub>A</sub> + Reactant <sub>B</sub> + Reactant <sub>C</sub>	→	Product(s)	Third-order $l^2\text{mol}^{-2}\text{s}^{-1}$

Table 3.1: List of orders of reactions with the appropriate units for the rate constant.

A more general form of the rate equation may also be used to account for nonlinearities<sup>84-86</sup>, namely:

$$r = k [\text{Reactant}_A]^a [\text{Reactant}_B]^b . \quad (3.1.3)$$

Third order reactions are most often third body reactions, in which the third reactant, Reactant<sub>C</sub>, is labelled M. This third body is employed to account for pressure dependencies or where an intermediate reaction product is considered to be stabilised by the presence of other species<sup>77,87,88</sup>.

### 3.1.4 Arrhenius Equation

Many experiments show a linear relationship between the natural log of the rate constant of a reaction and the inverse of the temperature at which the reaction occurs. Empirical observations found that the rate constants of most reactions adhere to the Arrhenius Equation, which takes the following form<sup>85,86,89-91</sup>:

$$k = Ae^{-\frac{E_a}{RT}} , \quad (3.1.4)$$

where  $A$  is the pre-exponential factor,  $E_a$  is the activation energy, i.e. the amount of energy required to trigger the reaction,  $R$  is the gas constant,  $8.314\,472\text{Jmol}^{-1}\text{K}^{-1}$  and  $T$  is the temperature in Kelvin<sup>92</sup>.

The Arrhenius Equation is interesting as the logarithm of the rate constant shows a linear relationship with the inverse temperature, i.e.

$$\ln(k) = \ln(A) - \frac{E_a}{RT} \quad (3.1.5)$$

and this results in a straight line plot when plotting  $\ln(k)$  against  $1/T$ .

Now  $\ln(A)$  is simply a constant, the same goes for the activation energy  $E_A$  which is specific to the reaction, as is the gas constant  $R$ . Hence, combining the aforementioned terms into two constants  $B$  and  $C$ , equation (3.1.5) becomes:

$$B = \ln(A) , \quad (3.1.6)$$

$$C = \frac{E_A}{R} , \quad (3.1.7)$$

$$\ln(k) = B - C \frac{1}{T} , \text{ and thus} \quad (3.1.8)$$

$$\ln(k) \propto -\frac{1}{T} . \quad (3.1.9)$$

These models have proven to be very reliable and accurate over smaller temperature ranges and this allows for an accurate prediction of the reaction rate. If such a linear reaction is found in a reaction, the reaction is said to display an Arrhenius behaviour. In the case of large temperature ranges, some reactions may deviate from Arrhenius behaviour over the entire temperature range, however over smaller temperature range subsets, it will also display Arrhenius behaviour.

To overcome the issue of large temperature ranges, a Modified Arrhenius Equation has been introduced<sup>77</sup>,

$$k = A \left( \frac{T}{T_{ref}} \right)^n e^{-\frac{E_A}{RT}} , \quad (3.1.10)$$

where  $\frac{T}{T_{ref}}$  is a dimensionless coefficient and for  $T_{ref} = 1\text{K}$  Equation (3.1.10) simplifies to

$$k = AT^n e^{-\frac{E_A}{RT}} . \quad (3.1.11)$$

### 3.1.5 Thermodynamics

To solve equations describing chemical rates under varying conditions, it is necessary to describe the behaviour of compounds in a reasonably general format over as wide a range of conditions as possible. Scientists have been attempting to amalgamate calorimetric data since the late 19<sup>th</sup> century<sup>93</sup>. Since the 1960's this has been done in the form of polynomials. The so-called NASA-7 polynomials are amongst the most widely used as they are also used by the Chemkin Suite and input format (for Chemkin see Section 3.2.2.1). NASA-7 polynomials contain thermodynamic data fitted at two temperatures which results in 14 coefficients<sup>93</sup>. As an example, the polynomial coefficient for elementary Carbon is given below, taken from the GRI-Mechanism 3<sup>94</sup>.

```

C          L11/88C   1          G   200.000  3500.000  1000.000   1
 2.49266888E+00  4.79889284E-05 -7.24335020E-08  3.74291029E-11 -4.87277893E-15  2
 8.54512953E+04  4.80150373E+00  2.55423955E+00 -3.21537724E-04  7.33792245E-07  3
-7.32234889E-10  2.66521446E-13  8.54438832E+04  4.53130848E+00  4

```

The polynomial coefficients define the thermal capacity at constant pressure ( $C_p$ ), enthalpy ( $H_T$ ) as well as entropy ( $S$ ) for a given temperature<sup>87,95</sup>, which are defined

as<sup>93,96–98</sup>:

$$\frac{C_p}{R} = a_1 + a_2T + a_3T^2 + a_4T^3 + a_5T^4, \quad (3.1.12)$$

$$\frac{H_T}{RT} = a_1 + a_2\frac{T}{2} + a_3\frac{T^2}{3} + a_4\frac{T^3}{4} + a_5\frac{T^4}{5} + \frac{a_6}{T}, \quad (3.1.13)$$

$$\frac{S_T}{R} = a_1\ln(T) + a_2T + a_3\frac{T^2}{2} + a_4\frac{T^3}{3} + a_5\frac{T^4}{4} + a_7. \quad (3.1.14)$$

The coefficients  $a_1$  to  $a_7$  are the coefficients given in the NASA-7 polynomial,  $R$  the gas constant and  $T$  is the temperature in Kelvin at which the user wishes to calculate the thermodynamic property of the chemical. In the thermodynamic data, values 1 to 7 apply to the upper temperature range, in the carbon example 1000-3500 K, while the values 8 to 14 cover the lower temperature range, in the carbon example 200-1000 K.

Thermodynamic data is used in chemical kinetics to obtain the equilibrium constant of a reaction, as well as to compute forward and backward reaction rates in a reversible reaction. Additionally, thermodynamic data allows us to model the enthalpy change during a reaction, which is important if reactions do not occur under constant temperature conditions<sup>77</sup>.

Exothermic reactions release energy which raises the heat and hence in a closed system raises the temperature and thus speeds up the reaction, as occurs for example during the autoignition of alkanes, used to test RMG and detailed in Section 4.1.2, while in contrast, an endothermic reaction will result in a temperature reduction which slows down the reactions so that it no longer has any significant effect. This can also be inferred from the Arrhenius Equation presented in Section 3.1.4.

### 3.1.6 Ideal Gas Law

The ideal gas law describes the relationship between a specified number of molecules, a specified pressure and temperature and thus the related volume<sup>99</sup>. The relationship is given as follows,

$$pV = nRT \quad (3.1.15)$$

where  $n$  denotes the number of moles of gas. This equation may be rearranged to give Equation (3.1.16)

$$p = \frac{n}{V} \times RT \quad (3.1.16)$$

Which relates the concentration of a gas, given by  $p/V$  to the pressure,  $p$ , in the system.

## 3.2 Employing and Handling Kinetics

Understanding the chemical kinetics introduced in Section 3.1 allows us to describe the development of a chemical reaction by translating the chemical reactions into a system of ordinary, time dependent, differential equations which may be solved using suitable software. On the basis of the chemical reaction scheme itself or the time development of the chemical reaction scheme we may also attempt to modify the scheme, by for example removing or combining reactions.

### 3.2.1 Background for Employing Time Dependent Chemical Kinetics

#### 3.2.1.1 Basic Introduction to Differencing Schemes

Differential equations are used to express a rate of change. Many problems in nature may be described with the help of time dependent systems of ordinary differential equations, referred to as a dynamical system. In the context of chemical kinetics, this is a rate of change over time in the concentration of different species during a chemical reaction. Differential equations or dynamical systems may be solved either analytically, or, as this is not feasible in many real life problems, numerically. Methods to solve ordinary differential equations are based on the assumption that it is possible to predict the next step based on the rate of change. These prediction methods for the rate of change can be sorted into three types namely<sup>100–104</sup>:

- i) Forward Differencing
- ii) Backward Differencing
- iii) Central Differencing

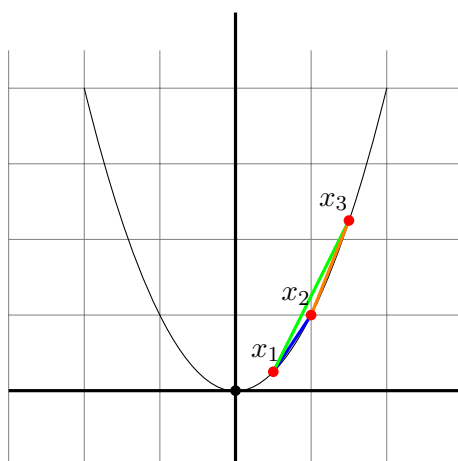


Figure 3.1: Drawing of a parabola with 3 points, to illustrate the principle of differencing in Equations (3.2.2), (3.2.4) and (3.2.6).

The prediction of the gradient of a curve is illustrated in Figure 3.1. A differencing scheme will allow us to obtain an approximation for the gradient of the curve at a given



point, given the coordinates or values of two other points.

In a forward differencing scheme we aim to predict the following value based on two previous values, and hence solve:

$$f'_{(x)} = \frac{f_{(x+\delta x)} - f_{(x)}}{\delta x} \quad (3.2.1)$$

Which in the context of our plot in Figure 3.1 translates to

$$f'_{(x_1)} = \frac{f_{(x_2)} - f_{(x_1)}}{\delta x} \text{ where } \delta x = x_2 - x_1 \quad (3.2.2)$$

which is illustrated by the blue line and predicts the gradient at point  $x_1$ .

In contrast, in a backward differencing scheme we predict the current gradient based on the previous value and thus solve:

$$f'_{(x)} = \frac{f_{(x)} - f_{(x-\delta x)}}{\delta x} \quad (3.2.3)$$

Which in the context of our plot in Figure 3.1 translates to

$$f'_{(x_3)} = \frac{f_{(x_3)} - f_{(x_2)}}{\delta x} \text{ where } \delta x = x_3 - x_2 \quad (3.2.4)$$

which is illustrated by the orange line and predicts the gradient at point  $x_3$ .

In a central differencing scheme we approximate the gradient between two points and thus solve:

$$f'_{(x)} = \frac{f_{(x+\delta x)} - f_{(x-\delta x)}}{2\delta x} \quad (3.2.5)$$

Which in the context of our plot in Figure 3.1 translates to

$$f'_{(x_2)} = \frac{f_{(x_3)} - f_{(x_1)}}{2\delta x} \text{ where } 2\delta x = x_3 - x_1 \quad (3.2.6)$$

which is illustrated by the green line and predicts the gradient at point  $x_2$ .

Of these three methods for numerically approximating the rate of change, two methods are commonly employed to solve a system of ordinary differential equations numerically, the forward and backward differencing schemes. In these numerical schemes, we generally have an expression for the rate of change,  $f'_{(x)}$  as well as the value of  $x$ . The primary difference between the forward and backward scheme lies in the efficiency for predicting the behaviour of functions which contain rapid changes in the rate of change of the order of several magnitudes. While forward schemes can solve such systems, an accurate prediction for the behaviour of the system may only be obtained if the stepsize is

continuously reduced to respond to rapid changes, which eventually makes forward schemes too computationally intensive. Such systems of ordinary differential equations are referred to as stiff. Backwards schemes in contrast are more efficient in systems with rapid rate changes, as the scheme works backwards from the current step and hence does not suffer from severe over-prediction or under-prediction at the next step. The downside of such backwards schemes is however that they generally require a solution of a non-linear equation often using an iterative process to approach an accurate estimate for the current step.

Hence backward schemes are less efficient for non-stiff systems with gradual rate changes that can be solved using forward schemes as they will under otherwise identical conditions require more computational steps. As problems in chemical kinetics often involve rapid changes and very different rates of change, an algorithm suitable for stiff ordinary differential equations is required.

Shampine and Gear<sup>105</sup> realized that if a system of ODEs, describing an initial value problem, can be described using the expression in Equation (3.2.7),

$$F(t, y, y') = 0 \quad (3.2.7)$$

it is possible to replace the differential with a backward differencing scheme. Hence one would no longer solve a system described by Equation (3.2.7), but instead a system described by Equation (3.2.8)

$$F\left(t, y, \frac{y_n - y_{n-1}}{\delta t}\right) = 0 \quad (3.2.8)$$

which may be solved using iterative methods. Gear's method is employed in SPRINT<sup>106</sup>, but is also available in DASSL<sup>107</sup>.

### 3.2.1.2 Translating Chemical Reactions to Differential Equations

When we have a chemical reaction mechanism, the next step is to solve the mechanism over time and compare the results obtained to experimental data. Chemical reactions can be translated into a set of differential equations by a straightforward process. If for example we take the first two reactions from the reaction scheme proposed by Ervin and Zabarnick in 1998<sup>33</sup>:

1.  $\text{I} \longrightarrow \text{R} \cdot$
2.  $\text{R} \cdot + \text{O}_2 \longrightarrow \text{RO}_2 \cdot$

These translate to the following set of ordinary differential equations (ODEs), based on the rate equations discussed in Section 3.1.3 and hence are as follows:

1.  $\frac{d}{dt} [I] = -k_1 [I]$
2.  $\frac{d}{dt} [R \cdot] = k_1 [I] - k_2 [R \cdot] [O_2]$
3.  $\frac{d}{dt} [O_2] = -k_2 [R \cdot] [O_2]$
4.  $\frac{d}{dt} [RO_2 \cdot] = k_2 [R \cdot] [O_2]$

where  $k_1$  and  $k_2$  are rate constants for the two reactions and  $[I], [R \cdot], [O_2]$  and  $[RO_2 \cdot]$  are the species concentrations. A fuel reaction scheme normally comprises of significantly more reactions and hence ODEs, leading to a more difficult problem to solve. As the rate constants often cover several orders of magnitude, such ODEs are said to be stiff<sup>108</sup>.

### 3.2.2 Existing Software for Time Dependent Chemical Kinetics

A number of products are available to investigate the time dependent development of chemical kinetics schemes. Available to us are Chemkin II as well as an in house solver named SPRINT. In addition, software we use incorporates DASSL as a pure numerical solver. However, for increased flexibility with regards to adding research specific functionality, it was decided to develop a new in house code as well.

#### 3.2.2.1 Chemkin

The Chemkin II package consists of a suite of several tools of which three are required for this thesis.

**Chemkin Mechanism Interpreter** The Chemkin Mechanism Interpreter is a key component to using the Chemkin Suite. It is required to check an existing Chemkin input file for errors which are reported to the user, as well as to create a binary data file that can be used by the solvers in the package.

**Senkin** Senkin is one of the solvers supplied in the Chemkin package used for time dependent closed systems<sup>109,110</sup>.

Lutz et al.<sup>109,110</sup> state that Senkin is written to solve six different types of problems, given the assumption that the total mass remains constant throughout the reaction. The first three cases Senkin is designed to model, are an adiabatic system with either constant pressure, constant volume or with volume a specified function of time. This would describe for example autoignition in a shock tube and requires the program to keep track of the energy changes in the system to be able to model changes in temperature.

Alternatively, Senkin can solve a system with constant temperature in which either the pressure or volume are constant. To solve these two types of systems, Senkin uses the approach outlined in Section 3.2.1.2, but works with mass fractions rather than

concentrations. Because the temperature is assumed to be constant, the program does not need to keep track of energy in the system. This condition is most appropriate for fuel autoxidation, which is often modelled under isothermal conditions.

The last option for the Senkin solver is a system in which the pressure and temperature are specified functions of time.

For any system, Chemkin solves an equation describing the species in terms of mass fractions, following the principle introduced in Section 3.2.1.2. The Chemkin manual<sup>110</sup> gives this as

$$\frac{dY_k}{dt} = v\dot{\omega}_k W_k \quad (3.2.9)$$

where  $\frac{dY_k}{dt}$  is the mass fraction change over time of the  $k$ th species,  $\dot{\omega}_k$  is the molar production rate of the  $k$ th species while  $v$  is the specific volume and  $W_k$  the molecular weight of the  $k$ th species.

Lutz et al.<sup>110</sup> state that for the adiabatic cases, Senkin applies the first law of thermodynamics:

$$de + pdv = 0 . \quad (3.2.10)$$

Where  $e$  is the internal energy per mass,  $p$  the pressure and  $v$  the volume per mass. Lutz et al.<sup>110</sup> show that from this it can be worked out, that in addition to equation (3.2.9), Senkin needs to solve an additional equation, in the case of the constant volume:

$$c_v \frac{dT}{dt} + v \sum_{k=1}^K e_k \dot{\omega}_k W_k = 0 \quad (3.2.11)$$

and in the case of constant pressure:

$$c_p \frac{dT}{dt} + v \sum_{k=1}^K h_k \dot{\omega}_k W_k = 0 \quad (3.2.12)$$

where  $c_p$  is the heat capacity at constant pressure,  $c_v$  the heat capacity at constant volume,  $h_k$  the species enthalpy of the  $k$ th species and  $T$  is the temperature.

To compare autoignition models in Senkin, a constant volume adiabatic model is best, which requires integrating Equation (3.2.9) and Equation (3.2.11). For isothermal flow conditions the temperature is kept constant which means that only Equation (3.2.9) needs to be solved.

**Perfectly Stirred Reactor - PSR** A perfectly stirred reactor describes a reactor vessel which is considered to be perfectly stirred and hence contains a homogeneous

mixture of species<sup>77,111</sup>. The outflow from the reactor is assumed to have the same composition as the contents in the reactor.

Problems solved using a perfectly stirred reactor are time independent problems, in which a steady state solution is sought. As the residence time, determined by the mass flow rate, in the reactor vessel is limited, the steady state solution may be different from the equilibrium solution. PSR can model a constant temperature system, a system which is subject to heat loss or alternatively an adiabatic system.

Glarborg et al.<sup>111</sup> derive and then state the equation that PSR integrates as follows:

$$c_p \frac{dT}{dt} = \frac{1}{\tau} \sum_{k=1}^K Y_k^* (h_k^* - h_k) - \sum_{k=1}^K \frac{h_k \dot{\omega}_k W_k}{\rho} - \frac{Q}{\rho V} \quad (3.2.13)$$

where  $c_p$  is the heat capacity at constant pressure,  $\tau$  the residence time in the reactor,  $Y_k^*$  the  $k$ th species mass inflow,  $Y_k$  the  $k$ th species mass fraction outflow.  $h_k^*$  and  $h_k$  describes the  $k$ th species enthalpy at the inflow and outflow.  $\rho$  describes the mass density based on the ideal gas equation of state,  $V$  the volume and  $Q$  the reactor heat loss.

**Sensitivity Analysis** Sensitivity Analysis is a key feature of Chemkin II and available in both Senkin and PSR<sup>110,111</sup>. Sensitivity analysis enables the user to judge the importance of a species or reaction by investigating the mass fraction with respect to the reaction rate. This approach allows for the identification of species that are not of great importance to the overall mechanism, and hence provide a clear starting point for a mechanism reduction approach by removing the least important species or reactions. Additionally, sensitivity analysis allows the user to determine which species are of greatest importance in a mechanism and hence warrant further investigation,

**Running Chemkin** Running Chemkin to solve models generated by RMG is very straightforward. RMG supplies a “chem.inp” file, which is a text file containing a list of species, thermodynamic data as well as the mechanism. To run Chemkin, this file needs to be first interpreted by the Chemkin Mechanism Interpreter which is called from a command line and requires no further input. Provided the file contains no error, a binary file which can be read by either Senkin or PSR is created.

Senkin and PSR are both called in a similar manner from a command line. Both programs will automatically pick up the binary file created by the Chemkin Mechanism interpreter and require an input file. The user may chose whether he wishes the output to be on screen or in a file. Senkin will also write a “tign.out” file which contains the species concentration at roughly every chosen timestep. To run the Senkin executable “senkin” with input from “senk.inp” and output dumped to a file, “senk.out”, the following command is used:

```
senkin < senk.inp > senk.out
```

For PSR, the user would just need to replace the name of the executable with “psr”. For the sake of clarity it is also recommended to call the input file “psr.inp” and output file “psr.out”.

The input file for Senkin and PSR contain the model choice as well as the initial conditions to model. Table 3.2 contains a sample input for Senkin and PSR to model the autoxidation of heptane. First a keyword is supplied to chose the type of model used to obtain a solution. In this case, Senkin uses a constant volume “CONV” while PSR is set to solve for a given temperature, “TGIV”. This entry is then followed by further keywords defining the initial conditions.

Senkin		PSR		
CONV		TGIV		model type
PRES	24.48E+00	PRES	24.48e+00	initial pressure (atm)
TEMP	448.	TEMP	700	initial temperature (K)
TIME	1.E+3			end time (s)
DELT	1.E-5			output timestep (s)
ATOL	1E-18	ATOL	1.00e-20	absolute tolerance
RTOL	1E-8	RTOL	1.00e-10	relative tolerance
		VOL	10	reactor volume
		TAU	100	residence time (s)
		PRNT	2	controls output
REAC	O2 0.0018	REAC	O2 0.0018	reactant, “amount”
REAC	C7H16 4.7	REAC	C7H16 4.7	reactant, “amount”

Table 3.2: Commands from a sample input file for Senkin as well as PSR. Reactant amounts given under “REAC” are normalised internally by the solver and employed to calculate and output concentrations appropriate for the given temperature and pressure.

The reactants input in both Senkin and PSR is in mole fractions. The manuals<sup>110,111</sup> suggest that in an ideal case these should add up to 1, however if they do not, both Senkin and PSR will normalize the total mole fraction to 1.

In a final step, the “senk.out” and “tign.out” files may be inspected by the user to check the development of the reaction in the Senkin simulation at the output timesteps. For PSR, the “psr.out” file will contain the development of iterative solutions or alternatively, if “PRNT” is set to 1 will only contain the final output.

An advantage of the Senkin solver is the code’s stability which is greater than that of SPRINT which is dependant on the size of the initial time step. PSR while more appropriate to the flow conditions expected in a fuel system or modelled in a NIFTR sometimes obtains a steady state concentration featuring negative concentrations which invalidates the result.

**Expanding Chemkin Output** Without extensive knowledge of Fortran and extensive analysis of the code, beyond an expansion of allocated memory, it is suggested not to modify Chemkin. However, some simple code may be added to Senkin to allow the program to produce a concentration profile over time. Adding the following lines to the output function in Senkin will result in the creation of a number of files that contain first the time and temperature and then, ordered as in the mechanism file, the species concentrations. As this only prints calculated values without modifying them, the calculation itself will be unaffected. This modification works for schemes of up to around 400 species, as a file ending of more than 99 will result in an error from Senkin.

```
c trying a loop, time and temp in another file to avoid error
      write(11,*) ,TIM,Z(1)
      DO 40 J = 1, NPRINT * 3 / 4 + 1
        write(J+11,*) XMOL(4*J-3) ,XMOL(4*J-2) ,XMOL(4*J-1) ,XMOL(4*J)
40      CONTINUE
```

A dedicated written code may then be used to recombine the data to obtain analysis friendly output from Senkin, such as for example the VBA macro for Excel included in Appendix B.

### 3.2.2.2 SPRINT

A package called “SPRINT”, Software for PRoblems IN Time, which has been developed at Shell Research Ltd. and the University of Leeds, is available, which implements Gear’s Method for solving stiff ordinary differential equations<sup>105,106,112</sup>. This package is interfaced to a Chemkin mechanism interpreter written, written by Hughes<sup>77</sup>, at the University of Leeds and available internally. The program has an advantage over Chemkin, see Section 3.2.2.1, as the output is more analysis friendly due to its significantly better structure over the unmodified Chemkin output.

**The SPRINT Interface** The interface for SPRINT was written in C, which is a powerful and versatile programming language. This makes SPRINT an ideal choice if additional processing of the mechanism or output is desired by the user.

After compilation of SPRINT into an executable, in its default configuration, the interface is designed to accept a Chemkin style mechanism and initial conditions in a separate input file. The requirements for these files are that the initial concentration is given as a pressure in Torr and that the mechanism is provided with rate parameters in molecules cm<sup>3</sup> s units and activation energies in K.

When run, the interface converts the pressures to a concentration given in molecules cm s units by applying the ideal gas law introduced in Section 3.1.6. Next the interface translates the input into a set of ordinary differential equations, which in conjunction with the current concentrations and the time interval, are solved as an initial value

problem by the Gear's Method solver in SPRINT. The interface loops over the user selected time step by calling SPRINT in a loop and thus obtains output at the user defined time steps. At every time step calculated out by the solver, the interface further evaluates the reaction rates as well as the temperature change in the system. In this case, due to the nature of the reactions considered, the equations used for the species production and hence concentration are straightforward rate equations as presented in Section 3.1.3.

Additionally, a modified version of the interface exists, that allows the use of two specific routines from KinalC to automatically reduce a chemical reaction mechanism based on sensitivity analysis of the reaction mechanism to identify redundant species and reactions.

**Running SPRINT via the Interface** Running SPRINT via the interface is similar to Chemkin, detailed in Section 3.2.2.1, however excludes the Chemkin Mechanism Interpreter step. The mechanism is supplied in a plain text file, called "mechanism\_data" while the initial conditions are supplied in a file called "input\_data". To ensure that the reaction mechanism is compatible with SPRINT, it is recommended to run Mechmod<sup>113</sup> on the mechanism first. The SPRINT input file contains similar information to the Senkin input file, such as initial temperature as well as the concentrations of species expressed as a pressure. However, the Sprint Interface can be modified to work with alternative expressions of concentrations, such as for example  $\text{mol}^{-1}$ . An example of the input file is provided below:

```
3   output control, (1=t,T,P, 2 = +species, 3 = +rates, 4 =
   everything)
0   sensitivity output control (1 = yes, 0 = no)
438  initial temperature/K
1500
1.0e-6   1.0e-15   1   RTOL, ATOL, ITOL (sprint tolerances)
1.0e-8 1.e3 1.0e-7 1.0e-2  TINC1, TMAX, TCHANGE, TINC2 (ensure
   TMAX>TCHANGE)
0 0 0 0   HEAT TRANSFER COEF.
0.0 20.0   0.49   1.3   COMP T/S, V M/S, L/M, GAMMA (rapid
   compression)
O2X2X      4.91844E+01
C10H22X1X  1.28426E+05
```

The first line requests the desired output, either just the time, temperature or pressure or additionally species as well as rates. Next is an option related to sensitivity which has no effect in regular SPRINT. This is followed by the initial temperature in Kelvin, here 438 K and then the cut-off temperature at which the simulation is aborted. Next come the tolerances for SPRINT as well as the chosen time step at which the user wishes to be presented with output. The program will switch from TINC1 to TINC2 at



time TCHANGE, therefore if TMAX is greater than TCHANGE the time step is held constant. The next line contains heat loss parameters followed by rapid compression machine parameters which were required for the original application of SPRINT. Finally the user supplies the initial concentrations of all non-zero species.

**Flexibility and Extendibility of SPRINT** As SPRINT itself is just an ODE solver, the interface is vital for interpreting the reaction mechanism. As the interface is written in C the user is provided with the opportunity to revise the code to carry out additional tasks. The simplest modification of the code would require only a modification of the the main routine to carry out additional tasks. An example for such a modification in the interface would for example be a systematic change in the reaction parameters. Alternatively, SPRINT could also be modified to work with liquid phase kinetics in  $\text{mol}^{-1}$  units through a suitable adaption of the internal calculations. Another potential modification of the interfaces focuses around the output format. It is possible to request additional output or alternatively modify the existing output by for example requesting more or less precision in the output. The user is only limited by his/her ability to write C code when working with the SPRINT interface.

**Known Limitations and Issues of SPRINT** Despite all the advantages of SPRINT, the program offers some known limitations and issues. A major issue with SPRINT is the lack of stability when it comes to solving reaction mechanisms. For some reason, SPRINT will fail if the initial time step is either too large or too small. To some extent this problem can be overcome by employing an adaptive time step, however this approach is tedious and time consuming. Especially in the case of applying automatic mechanism reduction procedures, having to modify time steps to ensure a stable operation is a bit unfortunate. This problem is generally characterised by SPRINT setting some variable to “not a number” or not achieving a tolerance, after which an error will be output. It is not clear if the source of the error stems from the interface or the SPRINT solver itself, resulting in the following error.

```
INITAL- NONLINEAR EQUATIONS SOLVER FAILED TO CONVERGE ON
        THE INITIAL VALUES USING FUNCTIONAL ITERATION A
        NEWTON METHOD WILL BE TRIED NOW
INITAL- NONLINEAR SOLVER FAILED TO CONVERGE USING A DAMPED
        NEWTON METHOD (DAMPING FACTOR =R1) TO SOLVE FOR
        INITIAL VALUES. CONVERGENCE RATE WAS (=R2).
IN ABOVE,  R1 =  0.10000000000000D+01  R2 =
           0.11468800000000D-09
SPRINT- ATTEMPT TO INITIALIZE DY/DT AND Y FAILED IN THE
        ROUTINE INITAL.
SPRINT- RUN ABORTED.
SPRINT- THE INPUT VALUE OF INFORM(1) (CALLED ISTATE IN
        SPRINT) HAS ILLEGAL VALUE (=I1)
```

```
IN ABOVE MESSAGE I1 =          -8
SPRINT- RUN ABORTED BECAUSE OF ILLEGAL INPUT
```

Other limitations in `SPRINT` are less problematic and could be overcome by modifying the interface. For example `SPRINT` is limited to the units mentioned in Section 3.2.2.2, specifically reaction parameters in molecules cm s units and K as well as initial concentrations supplied as pressures in torr. Further known limitations affect species naming as well as species coefficients in reactions. No species may contain an “M” in its species name and species with a coefficient other than “1” may only have a whole number coefficient of either “2” or “3”. However, all of these limitations can be removed by appropriate modification or extension of the `SPRINT` interface.

Finally, `SPRINT` does not have the ability to adapt the output time step dynamically. While the solver is able to dynamically change the time step, `SPRINT` will return output at the user selected time steps. For reactions taking place over a long time span, this can lead to extremely large output files or alternatively requires the user to run `SPRINT` multiple times for multiple time steps over different time spans. In contrast, `Senkin` will increase the time steps at which information is reported to the user if the reactions start to slow down.

**Closing Comments Regarding `SPRINT`** Despite the limitations, an advantage of `SPRINT` is the availability of a version that contains an implementation of `KINALC`<sup>114</sup> to apply sensitivity analysis to the model. In combination with available shell scripts and `Chemkin`, `SPRINT` can be used to automatically reduce a reaction mechanism, by employing the functions `PCAF` and `CONNECT` implemented in `KINALC`.

To employ this version of `SPRINT`, the user is required to supply a number of input files that contain a variety of appropriate conditions and `SPRINT` will simulate the mechanism’s behaviour for every specified condition, applying the `CONNECT` routine according to a predefined patterns implemented in the modified interface. The resulting data is then interpreted to produce a reduced mechanism which the user may compare to the original mechanism.

This version of `SPRINT` has been used successfully in combustion research, however it is not yet clear whether it can be used for autoxidation models. Initial tests with an autoxidation scheme have not been successful, leading only to a reduced non-functional and thus inaccurate mechanism.

### 3.2.3 A New Chemical Kinetics Solver

As the `SPRINT` interface uses a significant amount of global variables, a more modular software to investigate the time dependent development of a chemical reaction scheme

was written in C++, taking large inspiration from the original SPRINT interface<sup>115</sup>. Additionally, the SPRINT solver<sup>105,106,112</sup> was replaced by the Intel ODE solver<sup>116</sup> to improve the stability of the program. The primary advantage of the new solver over SPRINT lies in the improved stability and the modular structure built around function calls, which allows easier modification and extension of the code. A known drawback of the new solver is its lower speed when compared to SPRINT.

To ensure that the new solver produces accurate results, it was compared to SPRINT, which has been used in previously published work, in a chemical reaction test scheme which includes stiffness. The scheme was automatically generated under high temperature autoxidation conditions in which oxygen is rapidly consumed in reactions with a hydrocarbon, leading to the eventual formation of water as one of the products. Hence a comparison with SPRINT looking at oxygen and water enables the assessment of the accuracy of the new code on both the short as well as long time scale. Figure 3.2a shows the concentration of water developing over a time span of 1000s, comparing the long term behaviour of the new solver on an irreversible as well as reversible version of a reaction mechanism to SPRINT. Figure 3.2b shows the development of the oxygen concentration, which nears zero within about 1 second, and can therefore be used to assess the performance of the new solver when the differential equations to solve the chemical kinetics scheme exhibit very large stiffness.

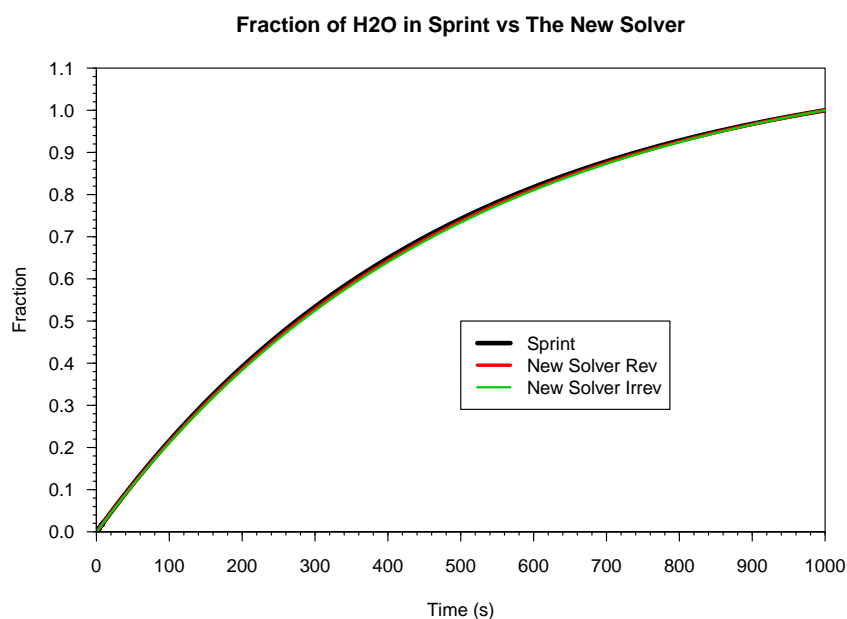
### 3.2.3.1 Basic Use

The most basic input for the Chemical Kinetics Solver comprises of a chemical reaction mechanism in the Chemkin format as well as an input file which specifies as a minimum temperature, time, output timestep and initial concentrations. An example of a chemkin mechanism input file is provided in Figure 3.4 while an example of a minimal input file is provided in Figure 3.5.

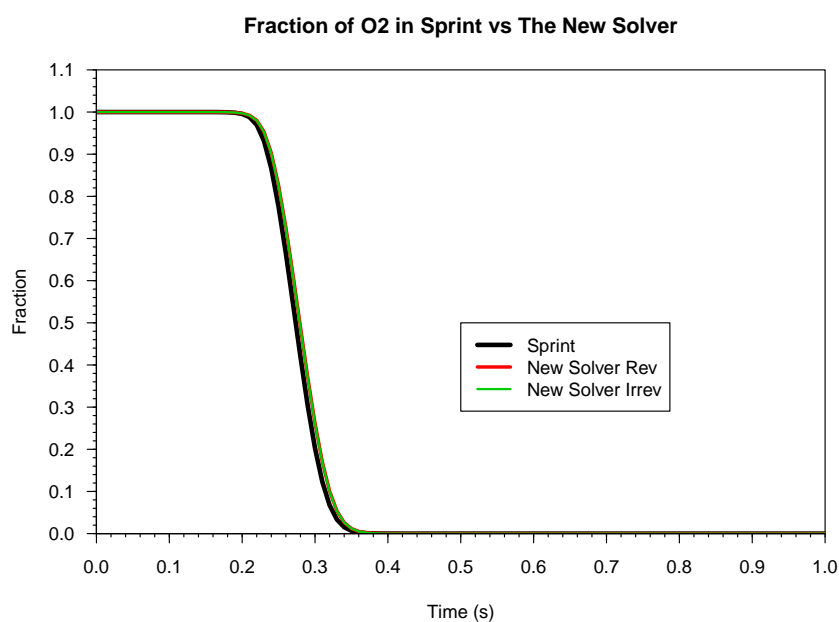
### 3.2.3.2 Mechanism Reduction

Because RMG is prone to producing large mechanisms containing over one hundred species and hundreds or even thousands of reactions, a mechanism reduction technique that can reduce the scheme to sizes appropriate for analysis and simulations other than time based kinetics was required. This reduction approach needs to consist of a series of steps. Identifying species that can be represented by an overall species class and merging these to represent groups such as alkanes or alcohols, dealing with the mathematical implications of such grouping as well as the identification of reactions that do not contribute significantly to the development of the scheme and hence can be removed.

During the development of the code<sup>115</sup>, it has transpired that it is required for the



(a) H<sub>2</sub>O forms gradually as a final autoxidation product in a high temperature scheme enabling the assessment of the performance of the solver over a larger time scale.



(b) O<sub>2</sub> is rapidly consumed at the start of the mechanism which allows the assessment of the solver's performance over short time scales with very large rates, specifically with a stiff system of ODEs.

Figure 3.2: Accuracy comparison of the solver developed in this thesis with the established solver SPRINT<sup>106,112</sup> in an early high temperature autoxidation scheme.

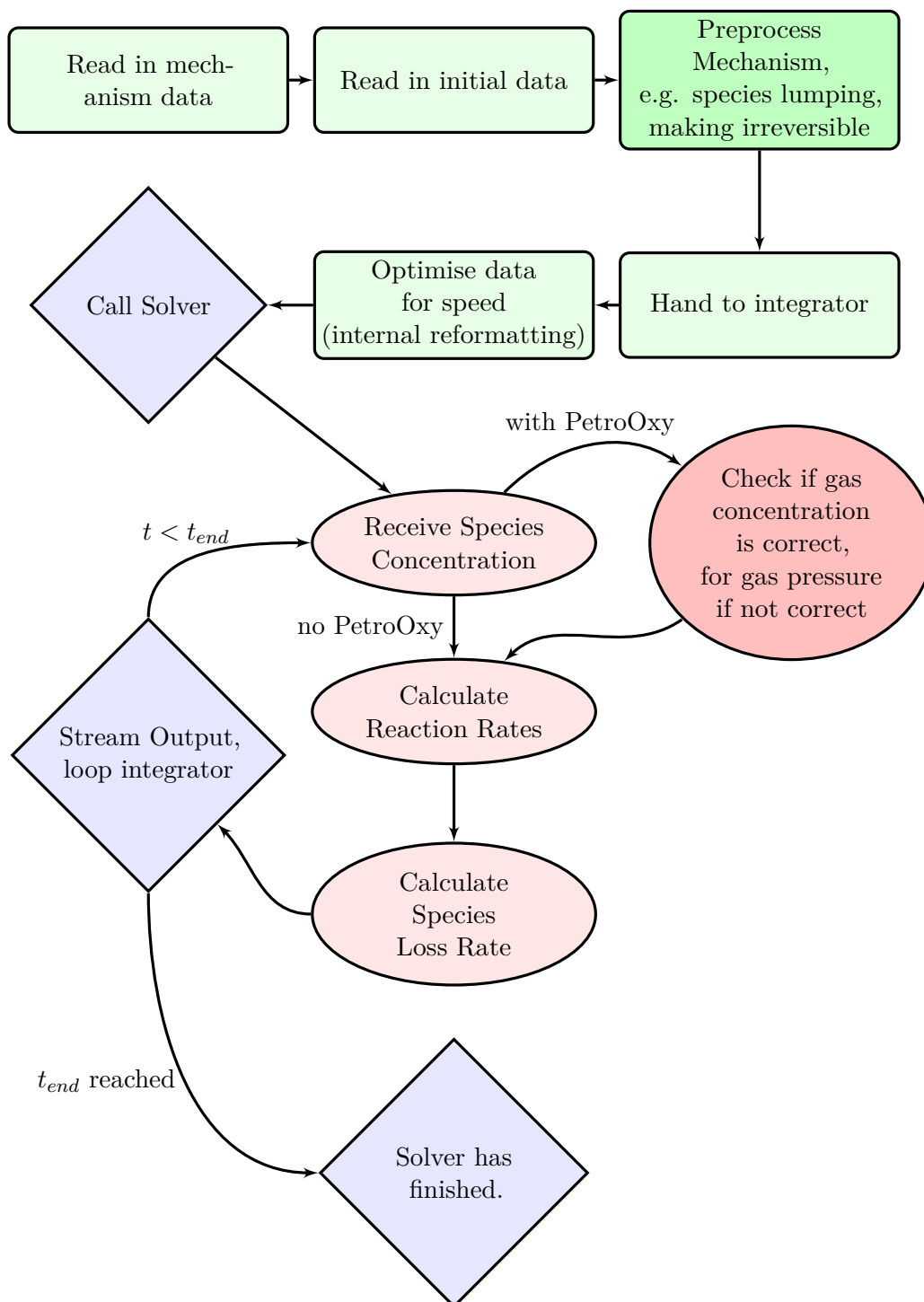


Figure 3.3: Schematic layout of the solver written and used in this thesis.

```

SPECIES
  C10H22(1)
  O2(2)
  H02J(4)
  C10H21J(5)
  C10H21J(6)
END

THERMO ALL
  300.000 1000.000 5000.000

!Estimated by RMG using Group Additivity
C10H22(1)      C  10H  22      G  250.000  5000.000  995.043   1
  2.36565478E+01  5.83495331E-02-2.08220419E-05  3.35977291E-09-2.01655849E-13   2
-4.13652648E+04-7.81638433E+01  2.91914784E+00  7.80112927E-02  4.55660519E-05   3
-1.05456827E-07  4.33024980E-11-3.40847902E+04  3.76253959E+01   4

!Primary Thermo Library: GRIMech3.0 (Species ID: s00010295)
O2(2)          C   OH   00   2      G  250.000  5000.000  995.043   1
  3.27573492E+00  1.37750101E-03-5.55093355E-07  9.57662136E-11-5.98886255E-15   2
-1.12388014E+03  4.23675379E+00  3.54869986E+00-1.28797020E-03  5.82700881E-06   3
-5.76400113E-09  1.86418279E-12-1.10056936E+03  3.31131179E+00   4

!Primary Thermo Library: GRIMech3.0 (Species ID: s00010103)
H02J(4)        C   OH   10   2      G  250.000  5000.000  995.043   1
  3.93891938E+00  2.49134217E-03-7.86894875E-07  1.15425499E-10-6.44483776E-15   2
  3.07592852E+02  8.52368841E+00  3.95968629E+00-2.13114054E-03  1.30237937E-05   3
-1.37219091E-08  4.62191757E-12  5.28165613E+02  9.55272836E+00   4

!Estimated by RMG using Group Additivity
C10H21J(5)     C  10H  21      G  250.000  5000.000  995.043   1
  2.08593815E+01  5.91475827E-02-2.12650252E-05  3.44662632E-09-2.07505170E-13   2
-1.68254502E+04-5.82011682E+01  3.19095398E+00  7.83245097E-02  2.79870483E-05   3
-8.19184436E-08  3.43969981E-11-1.07424772E+04  3.98489390E+01   4

!Estimated by RMG using Group Additivity
C10H21J(6)     C  10H  21      G  250.000  5000.000  995.043   1
  2.02650323E+01  5.98920487E-02-2.16722704E-05  3.52863225E-09-2.13111726E-13   2
-1.66010486E+04-5.49535291E+01  3.31734291E+00  7.81832480E-02  2.58826003E-05   3
-7.86676518E-08  3.30847979E-11-1.07610933E+04  3.91226111E+01   4
END

REACTIONS KCAL/MOL  MOLES
C10H21J(5)+H02J(4)=C10H22(1)+O2(2)          4.955e+08    1.18    15.56
C10H21J(6)+H02J(4)=C10H22(1)+O2(2)          4.955e+08    1.18    15.56
END

```

Figure 3.4: Example of a typical Chemkin input file, consisting of a species list, species thermodynamic data in the form of NASA-7 polynomials and lastly the mechanism itself in the form of a list chemical reactions with appropriate Arrhenius parameters.

```

Temperature 423    ! initial temperature/K
EndTime 5e4 1.0e0! second entry is time step
O2(2)      0.02 ! concentrations of initial species, mol/L
C12H26(1)  4.7

```

Figure 3.5: Example of a minimal input file.

scheme to be irreversible for the methods to function correctly. To ensure a scheme consists only of irreversible reactions, the code has been extended with the relevant algorithm to convert a reversible scheme into an irreversible scheme, based on work by Rolland and Simmie<sup>117</sup>.

**Species Lumping** One approach to reducing the size of RMG generated mechanisms would be to combined some of the individual species produced as an artefact of the mechanism generation process employed in RMG. For example, if the autoxidation of a C<sub>10</sub> hydrocarbon is modelled, a hydrogen can be abstracted from five different positions, considering that the molecule is symmetric, resulting in five distinct product species from the initial hydrogen abstraction. Inspection of kinetic parameters in which these species participate will show that these are generally very similar if not identical in their behaviour, especially for simple normal alkanes, while differences are typically small on iso-paraffinic alkanes. If these species are thus combined into a single expression, such as the R· employed to describe an alkyl radical in pseudo detailed schemes, the complexity of the automatically generated scheme may be reduced significantly. As the automatic identification of similar species is a subject beyond the scope of this work, it was decided that the user should manually identify species that can be grouped together based on their overall structure or behaviour. This is achieved by providing the solver with a text file that contains a list of species with the species class number next to it, beginning with 1. The program will then automatically create classes for the grouped species and treat every ungrouped species as a class of its own or, leaving it “as is”. Internally, this is achieved by remapping species IDs which correspond to vector positions. An outline of the species mapping algorithm is shown in Figure 3.6, while Figure 3.7 shows a sample of a user defined species lumping pattern. The file uses a Chemkin<sup>118</sup> style input pattern, beginning with a keyword, MAPPING, and ending with a keyword END. Between those two keywords, the user supplies a list of species, which may consist of only the species to be mapped or all species. In Figure 3.7, an example is given where 2 classes of species are grouped together into Class(1) and Class(2) while the species here at the beginning of the list are left ungrouped. The group numbers, 1 and 2 in the given examples can be separated either by white-spaces or tabs.

When remapping species and grouping them into classes it has to be taken into account that duplicate reactions will be formed and that the classes will have a direct influence on the concentrations of the species in the solver which affects the calculated rates for a given reaction. It is therefore necessary to account for these changes in the calculation of time based development of the scheme and to correct for these factors to obtain an accurate result.

The first correction is achieved by identifying duplicate reactions in the reaction mechanism and combining them to a single reaction. The code makes no distinction between duplicate reactions and reactions that are duplicates as a result of species being grouped

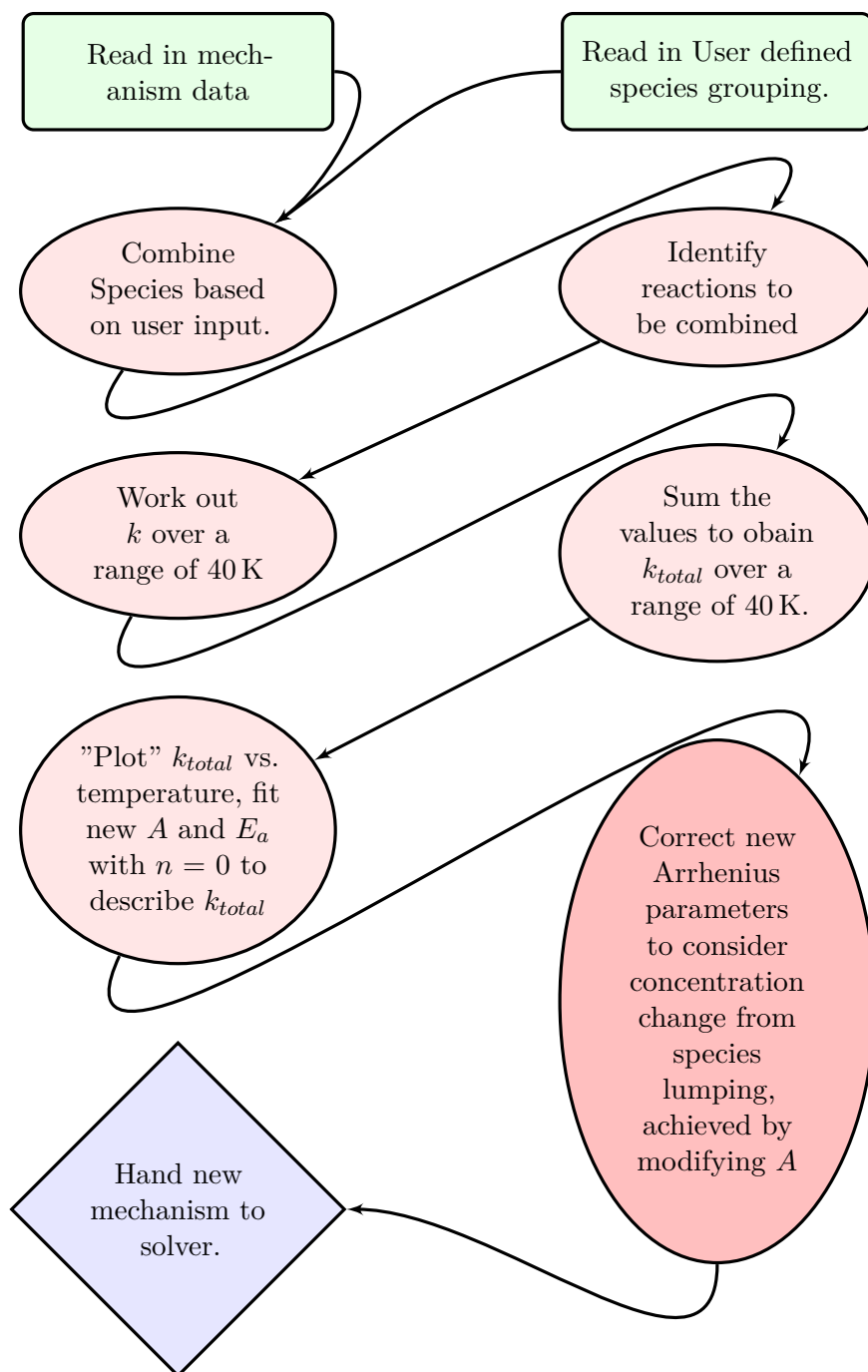


Figure 3.6: Outline of the species mapping algorithm implemented in the solver.



```
MAPPING
N2
C10H22 (1)
TOLUENE (2)
O2 (3)
H2O2 (5)
C10H21J (6) 1
C10H21J (7) 1
C10H21J (8) 1
C10H21J (9) 1
SPC (40) 2
SPC (81) 2
SPC (61) 2
SPC (100) 2
C10H21J (4) 1
SPC (460) 2
END
%\end{verbatim}
```

Figure 3.7: Example of the input for the species lumping algorithm.

together. Because similar compounds are expected to behave similarly, the decision has been taken to initially use a simple averaging approach for combining the reaction parameters of duplicate reactions that exist as a result of combining species into a single species class. The assumption that is made in this approach is that the reaction parameters do not differ significantly and that the production and consumption rates of the species in a class are similar leading to comparable concentrations. If the parameters between reactions differ significantly, especially the activation energy as well as the parameter  $n$ , this approach can result in a large numerical error. However for similar reactions, the results have been found to show good agreement with the original scheme. Upon the recommendation of Hughes<sup>77</sup> the code was later adjusted to combine reactions based on the rate constant  $k$  instead and fit new Arrhenius parameters with  $n = 0$  based on the total rate constant which has led to an improvement in the reduction capabilities of the code, enabling a more reliable mechanism reduction. The value of  $k$  is calculated over a range of  $\pm 20$  K and then summed over the grouped reactions to obtain an overall rate constant. An Arrhenius plot of the total rate constant of  $k$  versus  $1/T$  is employed to obtain fitted values for  $A$  and  $E_a$ , where  $\ln(A)$  is given by the intercept,  $n$  is assumed to be zero and  $E_a$  is defined by the gradient of the Arrhenius plot.

In a second step, the increase in concentration resulting from the lumping of species has to be accounted for. Grouping for example two species into a single class would double the concentration which can have a significant effect on the reaction rate, given that for a reaction between species A and B, with stoichiometric coefficients  $a$  and  $b$ , the rate is given by

$$r = k \times [A]^a \times [B]^b \quad (3.2.14)$$

Because the rate constant  $k$  is defined by

$$k = Ae^{\frac{-E_a}{RT}} \quad (3.2.15)$$

the change in species concentration as a result of grouping multiple species can be accounted for by modifying the pre-exponential coefficient in the Arrhenius parameters. However, as not only the concentration but also the stoichiometric coefficients are of relevance in working out the reaction rate, these also need to be considered and accounted for. Hence the pre-exponential coefficient  $A$  is scaled by the number of species in a species class raised to the power of the stoichiometric coefficient to account for the concentration change.

**Rates Based Reaction Reduction** To help us analyse RMG generated schemes, a simple rates based reduction mechanism has been implemented in the solver developed in this thesis which removes reactions based on the order of magnitude of their contribution at different timesteps. If the user selects the mechanism reduction option, it must be accompanied by an integer value which describes the number of orders of magnitude difference relative to the maximum rate at which a reaction is deemed insignificant. When the solver is run, the scheme will first be converted to an irreversible reaction scheme. At every output time point, the maximum reaction rate is identified, following, all reactions whose order of magnitude are not less than the chosen orders of magnitude below the maximum rate are marked for retention. When the solver runs for a suitable amount of time, different parts of the reaction mechanism will dominate during different phases. Analysing reaction rates over the entire time frame ensures that all behaviour of a reaction scheme is considered.

When the first run with a full scheme has been completed, reactions that were not marked for retention at any time are removed, after which the reduced scheme is both printed and solved over the same time frame again. After the reduced scheme has been run, the code then compares the concentration output from the full scheme against the reduced scheme and reports the average percentage difference per species as well as the minimum and maximum percentage difference between the two schemes. The outline of the rates based reduction algorithm is shown in Figure 3.8.

### 3.2.3.3 PetroOxy Pressure Drop

Employing the in house solver enables us to extend the code to include a simplified simulation of the conditions found in the PetroOxy. The side module is shown in the schematic code layout in Figure 3.3. This requires us to take the volume of the sample into account as well as the headspace which acts as a pressurized oxygen reservoir. In a

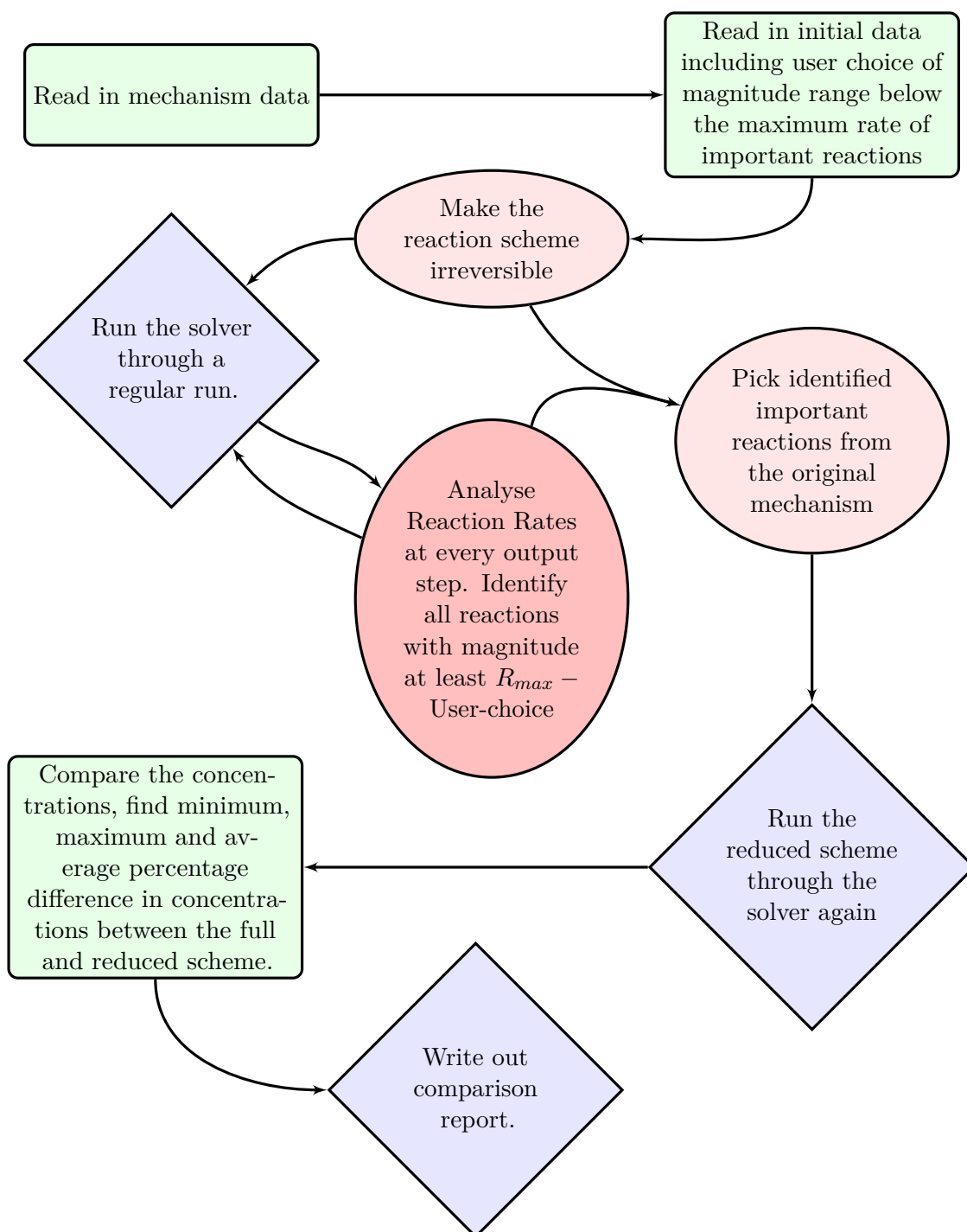


Figure 3.8: Outline of the rates based reduction algorithm implemented in the solver.

```
PetroOxy Solvent Sample=5
PetroOxy Initial Pressure=700
PetroOxy Maximum Pressure=1015
PetroOxy Gas Species=O2(2)
PetroOxy Gas Solubility=0.002
```

Figure 3.9: Sample Input to activate PetroOxy-Module in the solver in the main input file, "initial.inp".

most simple model, the liquid phase concentration of oxygen has to be adjusted and will vary as oxygen is consumed, manifested in the pressure drop recorded by the PetroOxy. The relationship between the gas saturation of liquids and pressure is described by Henry's Law<sup>88</sup> at "low pressures", which has been implemented in the solver as an add-on function. Further simplifications in this implementation are the assumption that gas to liquid phase transfer is fast due to the comparatively large surface area of the liquid sample as well as the assumption that there is no major contribution to the gas phase from the liquid sample.

A correction routine has been developed which adjusts the gas concentration in the liquid phase during execution of the solver, which is called before any rates are calculated. This is achieved by including a hardcoded estimate of 22.5 ml for the total volume of the PetroOxy dish which can only be obtained approximately from the dimensions of the dish. This does ignore the volume of the gas inlet pipe as well as the minor differences in volume due to different lid tightening. The user is then required to supply the solver with the volume of liquid used, the initial pressure as well as the maximum pressure recorded by the PetroOxy as well as the name of the gas species. The temperature is implicitly included in the initial temperature provided to the solver in a standard input file. With this data it is now possible to calculate the following:

- the oxygen concentration in the liquid phase, which will be the saturation limit defined by Henry's Law
- the amount of oxygen in moles in the headspace of the PetroOxy
- the oxygen component of the total pressure
- the vapour pressure component at the start of the test of the total pressure which is assumed to be constant

If the user desires to use the PetroOxy module, the "initial.inp" file requires additional keywords, shown in Figure 3.9. The PetroOxy module will only work when all parameters have been set by the user. Should any parameter be omitted, the module will not be called.

**Implementation And Theory** Henry's law states that for any solution one can obtain Henry's Constant,  $k_H$ , described by the pressure  $p$  and the concentration of the gas in liquid  $c$ , shown in equation (3.2.16). Henry's Constants are published for some compounds under normal conditions and can be used to estimate the value at higher pressures and temperature.

$$k_H = p/c \quad (3.2.16)$$

Henry's law does not consider any changes due to temperature, which is appropriate for modelling the PetroOxy as it tests compounds under isothermal conditions and temperature changes only occur during the initial heating and final cooling phase.

In this implementation, the solver must therefore check, every time it is called, whether the concentration of oxygen in the liquid phase is appropriate for the oxygen pressure in the headspace and correct it appropriately. Only then can the solver calculate the appropriate reaction rate. The concentration in the liquid  $c_{new}$  can be estimated from the oxygen in the headspace using Henry's Law, shown in Equation (3.2.17).

$$c_{new} = \frac{p_{new}}{k_H} \quad (3.2.17)$$

Pressure,  $p_{new}$ , can be calculated with the help of the ideal gas law, which requires the atom count,  $n_{new}$ , in the headspace of the PetroOxy, shown in Equation (3.2.18)

$$p_{new} = n_{new}RT/V_{gas} \quad (3.2.18)$$

The corrected concentration in the liquid phase  $c_{new}$  can also be described as being the current concentration  $c_{current}$  plus a correction of  $c_{adjust}$ , shown in Equation (3.2.19).

$$c_{new} = c_{current} + c_{adjust} \quad (3.2.19)$$

In this case, a known number of moles transfer from the headspace to the sample, which results in Equation (3.2.20), which describes the updated number of moles of gas as the current value minus the amount of oxygen transferred to the liquid phase from Equation (3.2.19).

$$n_{new} = n_{current} - c_{adjust} \times v_{sample} \quad (3.2.20)$$

Returning to Henry's Law, in Equation (3.2.17), it is possible to substitute in Equation (3.2.18) for the pressure giving us the following, shown in Equation (3.2.21).

$$c_{new} = \frac{n_{new}RT}{k_H V_{gas}} \quad (3.2.21)$$

Next, the atom count  $n_{new}$  can be substituted into Equation (3.2.21) from Equation (3.2.20), giving us the expression shown in Equation (3.2.22).

$$c_{new} = \frac{(n_{current} - c_{adjust} \times v_{sample}) RT}{k_H V_{gas}} \quad (3.2.22)$$

Rearranging Equation (3.2.19) for  $c_{adjust}$ , it can be substituted into Equation (3.2.22) to obtain Equation (3.2.23).

$$c_{new} = \frac{[n_{current} - (c_{new} - c_{current}) \times v_{sample}] RT}{k_H V_{gas}} \quad (3.2.23)$$

Rearrangement of Equation (3.2.23) yields a compact expression for the corrected concentration of oxygen in the solution, shown in Equation (3.2.24).

$$c_{new} = \frac{(n_{current} + c_{current} V_{sample}) RT}{k_H V_{gas} + V_{sample} RT} \quad (3.2.24)$$

By applying this formula in a correction routine before the reaction rates are calculated, it is possible to incorporate the consumption of oxygen in the headspace of the PetroOxy using Henry's Law. Keeping track of the oxygen in the headspace and its depletion enables us therefore to assess the quality or accuracy of chemical reactions schemes using PetroOxy data which consists of the headspace pressure.

### 3.2.3.4 Creating an Analytical Jacobian

The Intel ODE solver<sup>116</sup> provides a number of different solvers, which offer the choice between a numerical or analytical Jacobian matrix, the later which must be supplied by the user. The code was extended to employ an analytical Jacobian for chemical kinetics involving reactions expressed through regular Arrhenius Equations. This requires us to develop a method to calculate  $\frac{\partial Rate(Species_i)}{\partial Species_j}$ .

For regular Arrhenius expressions, a manual differentiation can be employed, i.e. it must be identified whether the species which is differentiated with respect to is present, and if it is present the power needs to be modified in the rate term and the appropriate coefficient must be added. The most efficient way identified was to employ a vector with a custom data type in the form of a struct, shown in Figure 3.10, that would retain one differentiation each per vector position for the Jacobian. The numerical values are then calculated on the fly using current concentrations while the rate constant is updated for the current temperature. One of the difficulties with calculating the Jacobian in an efficient manner is to differentiate between species production and loss while including the differentiation. This was solved by employing two boolean variables to determine if species are gained or lost and whether the reaction is a forward reaction or reverse reaction. With these two parameters set, the code can pick the correct forward or reverse rate constant when evaluating the analytical Jacobian with the sign arrangement shown in Figure 3.11.

Once the signs have been worked out correctly, one can traverse the data vector to

```

struct JacobianSpecies{
    int SpeciesID;
    double power;
};

struct JacobianData {
    int ColumnWiseArrayPosition;
    bool IsForward;
    bool IsProduction;
    int ReactionID;
    double coefficient;
    vector< JacobianSpecies > Species;
};

```

Figure 3.10: Structs employed to retain the data for the analytical Jacobian.

	Species Production	Species Loss
Forward	Kf	-Kf
Reverse	Kr	-Kr

Figure 3.11: Applying correct signs when evaluating the analytical Jacobian.

evaluate the correct value at every position in the Jacobian matrix, which for the Intel ODE solver is supplied in a column wise order. While this may seem computationally intensive, this provides the user with a significant speed up over employing the automated numerical Jacobian approximation contained in the Intel ODE Library<sup>116</sup>. The evaluation function is shown in Figure 3.12.

### 3.3 RMG Usage and Findings

RMG is an open source automated Reaction Mechanism Generator developed at MIT by Green et al.<sup>119</sup> for hydrocarbon chemistry, with a primary focus on combustion. Later releases have been extended to also include liquid phase chemistry, making it a suitable candidate for the generation of autoxidation schemes.

#### 3.3.1 Initial Settings

RMG works on the basis of initial conditions being supplied to the program by the user. As a result attention should be given to the selection of these parameters on the basis of the conditions that one wishes to model. The following pieces of information need to be provided by the user for RMG to use.

- i) pressure(s)
- ii) temperature(s)
- iii) reactants and their concentrations

```

for(i=0;i<(int) JacobianMatrix.size();i++)
{
    double temp;

    if(JacobianMatrix[i].IsForward) // Forward
    {
        if(JacobianMatrix[i].IsProduction) // species are gained
        {
            temp = Kf[JacobianMatrix[i].ReactionID]*JacobianMatrix[i]
                ].coefficient;
        }
        if(!JacobianMatrix[i].IsProduction) // species are lost
        {
            temp = -Kf[JacobianMatrix[i].ReactionID]*JacobianMatrix[i]
                ].coefficient;
        }
    }

    if(!JacobianMatrix[i].IsForward) // Reverse
    {
        if(JacobianMatrix[i].IsProduction) // species are gained
        {
            temp = Kr[JacobianMatrix[i].ReactionID]*JacobianMatrix[i]
                ].coefficient;
        }
        if(!JacobianMatrix[i].IsProduction) // species are lost
        {
            temp = -Kr[JacobianMatrix[i].ReactionID]*JacobianMatrix[i]
                ].coefficient;
        }
    }

    for(j=0;j<(int) JacobianMatrix[i].Species.size();j++)
    {
        if(JacobianMatrix[i].Species[j].power != 0) // power 0 = *1
        {
            if(JacobianMatrix[i].Species[j].power == 1) // power 1 is
                simple multiplication
            {
                temp = temp * Concentration[JacobianMatrix[i].Species[j]
                    ].SpeciesID];
            }
            else
            {
                temp = temp *
                    pow(Concentration[JacobianMatrix[i].Species[j].
                        SpeciesID],
                        JacobianMatrix[i].Species[j].power);
            }
        }
    }

    JacobeanColumnWise[JacobianMatrix[i].ColumnWiseArrayPosition]
        =
        JacobeanColumnWise[JacobianMatrix[i].
            ColumnWiseArrayPosition] + temp;
}

```

Figure 3.12: Evalaution of the analytical Jacobian during code execution.



- iv) error tolerance, pruning criteria
- v) termination criteria
- vi) databases

This information is supplied by a text file, which the developers suggest to name “condition.txt” but can have any name. Future references to this file will call it the condition text file.

### 3.3.1.1 Temperature and Pressure

By default, RMG will only attempt to simulate the reactions under isothermal conditions. Therefore, for reactions occurring under non-isothermal conditions it is essential to provide a range of temperatures that cover the temperature range for which the model is expected to be valid. In our test case, RMG has been set up for temperatures ranging from 1000 K to 2000 K, 650 K to 2200 K as well as 400 K to 800 K to capture the low temperature as well as the high temperature chemistry of the species under investigation. In the case of an autoxidation mechanism, it is not unreasonable to also use a single temperature during the mechanism generation process if the expected temperature range is going to be small. The next setting is the pressure where RMG will again only try to simulate constant pressure conditions, thus requiring a range of values for an environment which experiences pressure changes. Experimental investigations into aviation fuels tend to use constant pressures even though the pressure will differ across an aircraft’s fuel system, thus our models are created for just one constant pressure.

### 3.3.1.2 Liquid Phase Kinetics in RMG

While liquid phase chemical kinetics schemes are solved analogously to gas phase scheme using standard Arrhenius expressions, with a fixed volume and pressure irrespective of any stoichiometric changes, the mechanism generation process needs to take care to consider the impact of chemical kinetics in the liquid phase<sup>119</sup>. When using the liquid phase condition in RMG, three adjustments are employed by the code<sup>119,120</sup>.

- i) The concentrations from the input file are used as is and not “corrected” via the ideal gas law. Additionally the pressure and volume are fixed, irrespective of stoichiometry changes.
- ii) The thermodynamic data is adjusted to include solvation effects. The authors of RMG define  $\bar{K}^\ddagger$  as the gas solvent partition and estimate it using Abraham LSER, employing predefined, not further defined, parameters for the solvent and solute<sup>120</sup>.  $\bar{K}^\ddagger$  in this case is employed as an equilibrium constant<sup>121</sup>.

$$\log \bar{K}^\ddagger = c + eE + sS + aA + bB + lL \quad (3.3.1)$$

This allows us to calculate the Gibbs energy of activation  $\Delta G^\ddagger$ <sup>120,121</sup>.

$$\Delta G^\ddagger = -RT \ln \bar{K}^\ddagger \quad (3.3.2)$$

To simulate temperatures other than 298 K, the enthalpy of activation is also estimated from the solvent and solute parameters<sup>120</sup>.

$$\Delta H_{298K} = c' + a'A + b'B + e'E + s'S + l'L \quad (3.3.3)$$

This data thus enables RMG to estimate solvent corrected parameters for the Arrhenius expression based on transition state theory<sup>120,121</sup>.

- iii) The rate constants are further adjusted so that reactions are not able to exceed the diffusion limit set by the solvents, which the authors of RMG named  $k_{eff}$ <sup>120</sup>. This is defined by  $r$ , the sum of the radii of the reactants,  $D$ , the sum of the speed at which the reactants diffuse through the solvent and  $k_{int}$ , the rate constant calculated from transition state theory<sup>120</sup>.

$$k_{eff} = \frac{4\pi r D k_{int}}{4\pi r D + k_{int}} \quad (3.3.4)$$

### 3.3.1.3 Reactants and Concentrations

RMG requires that the user supplies the initial reactants that take place in a reaction. These are provided straightforwardly as concentrations and can be present at an initial concentration or at a constant concentration. The reactants need to be given a name by the user which may not start with a number and is otherwise arbitrary, followed by the concentration including units and then the molecular structure. More information on the allowed units is available in the RMG manual<sup>122</sup>. It is sufficient to supply RMG with just the carbon structure as the program will by itself add the appropriate number of hydrogen atoms to the structure.

An example for a cyclic species is given below, featuring single and double bonds.

```
C11CYC (mol/l) 4.7
1 C 0 {6,S} {2,D} {7,S}
2 C 0 {1,D} {3,S}
3 C 0 {2,S} {4,D}
4 C 0 {3,D} {5,S}
5 C 0 {4,S} {6,D}
6 C 0 {5,D} {1,S}
7 C 0 {1,S} {8,S}
8 C 0 {7,S} {9,S}
9 C 0 {8,S} {10,S}
10 C 0 {9,S} {11,S}
```

11 C O {10,S}

For aviation fuel it is possible to chose surrogate species comprising of straight alkanes, iso-alkanes as well as aromatics to try and estimate the behaviour of the fuel. RMG can then be used to generate a detailed mechanism for their behaviour under conditions typical to the environment of an aircraft engine. Whether these surrogates really are representative of the behaviour of fuel will have to established once a model has been drawn up. As the current version of RMG is limited to creating models with at most 1500 species, it is unreasonable to attempt to model the behaviour of a significant proportion of species in aviation fuel. The resulting model size for a given set of reactants will depend on parameters such as the error tolerance as well as pruning.

### 3.3.1.4 Error Tolerance, Pruning - Controlling Mechanism Size

Important closing parameters are the error tolerance and pruning parameters which both affect the size of the final model in two different ways.

**Error Tolerance** The error tolerance influences the size of the species flux in the model core for the model to be considered complete. Hence a lower species flux will lead to a larger model. RMG will calculate a species flux and compare it against the error tolerance criteria, if it is satisfied the model is considered complete, otherwise new species with the highest flux are added from the model edge which covers all possible reactions of the core species and their products. The manual references Susnow et al.<sup>123</sup> from 1997 as the source, which lays out the theory of using a rate based model enlarger. However, the implementation in RMG is different from the published method and relies only on model generated data rather than user supplied information. Originally Susnow et al.<sup>123</sup> suggested using the ratio of the converted reactants to the reaction time as a criteria for the flux of the model core.

$$R_{Char} = \frac{\text{amount of reactant converted}}{\text{reaction time}} \quad (3.3.5)$$

This approach however requires prior knowledge of the reaction time to have an objective criteria at which the model core is evaluated. As this information is not necessarily available prior to setting up a simulation, RMG uses a different approach to calculate a core flux which may be used to evaluate the completeness of the model. RMG calculates the L<sup>2</sup> Norm from the species flux in the core and uses the obtained value for  $R_{Char}$  as shown in Equation (3.3.6).

$$R_{Char} = \sqrt{\frac{\text{number of species}}{\sum_{i=0} (Flux_{Species i})^2}} \quad (3.3.6)$$

The error tolerance is multiplied with  $R_{Char}$  to obtain what is called  $R_{min}$ , which describes the minimum production flux an edge species is required to have to be included

in the model core, shown in Equation (3.3.7).

$$R_{min} = \text{Error Tolerance} \times R_{Char} \quad (3.3.7)$$

A model is considered complete, when no edge species has a flux in excess of  $R_{min}$ . There is no perfect choice for the error tolerance, as all models will eventually complete in some form. However an indication of suitable values is presented by the example input in the RMG manual as well as published papers by Green et al. <sup>124,125</sup> which provide good starting points. Additionally, the amount of RAM available to the user as well as the time available for the computations place additional constraints on the user with respect to the error tolerance. Sometimes, mechanisms appear to work or behave correctly even though RMG believes it has not finished yet. In the case of autoignition, a good test case due to an abundance of published data, this might be related to the fixed temperature simulation that RMG runs. Hence, while the high temperature reactions are all accounted for, the lower temperature reactions prohibit RMG from considering the model complete as their relatively low reaction fluxes lead to an exclusion of required reactions. Thus it is advisable to restrict the temperature range for which a model is generated where possible.

**Pruning** The use of pruning in RMG places constraints on the model edge which allows the user to reduce the complexity of the model generation as well as reduces the computational resources, such as memory, required by RMG. Pruning can help in the creation of a model especially when memory is a finite resource. When a pruning parameter is set, a target size for the number of species is set as well as a threshold at which point the pruning mechanistic comes into effect. The pruning parameter or pruning tolerance acts as a secondary error tolerance which reduces the number of the edge species in the same way that the error tolerance controls the core species. However, while the error tolerance will retain species in the model edge, the pruning parameter leads to removal of species from the model edge.

Lastly, the termination criteria is vital for RMG to allow the code to determine when it has finished and created a valid model. The choice of the termination criteria is explained in Section 3.3.1.5.

### 3.3.1.5 Termination Criteria - Species Conversion or Reaction Time

The termination criteria is to some extent a difficult choice as it ideally requires advance knowledge of the reactions taking place. Two options exist for the termination criteria, one being the reaction time and the other being a specified percentage of conversion for one of the species.

The RMG manual suggests to use the conversion of a specific species as a termination

criteria<sup>122</sup>. This species needs to be chosen carefully, as it has to be a species whose absence needs to signify the end of meaningful reactions taking place. For combustion oxygen was found to be a good choice, mainly because the conversion of oxygen can be predetermined from stoichiometry. At the same time, when modelling autoxidation, it is important to assess whether oxygen is a suitable indicator. Considering that studies have suggested that oxygen is the vital component for autoxidation, oxygen consumption may be a suitable indicator as a termination criteria. Alternatively, a reaction time in excess of the time required for all reactions to complete during an autoxidation process is also a suitable choice.

### 3.3.1.6 Databases

RMG needs to be supplied with a database which contains a number of libraries. The RMG database can be broken down into two components, the libraries supplying elementary rules such as Benson's additivity formulae<sup>122,126</sup> for thermodynamic data or Lennard-Jones sigma and epsilon parameters for species transport<sup>122</sup>, but also libraries supplying validated data for specific species and reactions, such as the GRI-3 Mechanism<sup>94</sup> which is included in RMG.

The underlying rules must be supplied to RMG by the user in the form of the RMG-minimal library and the primary thermodynamics library. Kinetic parameters that constitute the RMG-minimal library typically cover the temperature regime of 300 K upwards for most reaction types. In addition validated libraries may also be supplied by the user. This functionality is offered primarily to enhance the output mechanism and associated thermodynamic as well as transport data by using well tested and validated data.

Libraries can be used to support RMG in the following areas:

- i) thermodynamic data
- ii) species transport data
- iii) seed mechanism
- iv) reaction library

In the case of thermodynamic data and species transport data, RMG will use the values presented in the library instead of using rules to estimate the parameters.

The seed mechanism works by supplying either a set of core species that are added to the mechanism, such as for example the species that make up the GRI-3 Mechanism. The user is given the option of just accepting the reactions in the mechanism or allowing RMG to react the species with each other to add additional reactions to the mechanism.

Finally, there is the reaction library, which the user can use to supply reactions of specific species. However, according to the manual<sup>122</sup>, care must be taken to include all relevant reactions as RMG will not create reactions for a species beyond those included in the reaction library. The GRI-3 Mechanism<sup>94</sup> presents a good seed when testing RMG for autoignition, however in the case of autoxidation reactions, its use as a seed mechanism is limited, being applicable to gas phase only as well as dealing with comparatively small species compared to the bulk process in liquid fuel autoxidation.

Care also needs to be taken where small species are involved, as the group additivity approach employed to estimate species parameters may not be accurate, a point indicated by the developers in the manual<sup>127</sup>. One method of avoiding this issue is to employ a library, such as the included GRI mechanism<sup>94</sup>, as a thermodynamic library which will then be preferred by RMG over estimated values. In contrast, large species do not suffer from any significant inaccuracies in their estimated thermodynamic properties<sup>127</sup>. During the initial testing, no large species was found to behave in any visibly problematic manner such as not reacting fully in the output reaction mechanisms.

### 3.3.2 Influencing Models - Observations

Given that a number of parameters are determined by the problem we aim to model, our scope for varying parameters in RMG is limited to some extent. Nevertheless, there are two settings that can have a profound effect on the results obtained from RMG. These are the error tolerance as well as the database.

#### 3.3.2.1 Effects of the Error Tolerance

The error tolerance has a significant impact on the size of the generated model. However there is no objectively straightforward way of selecting an error tolerance, the same is true for the pruning tolerance. As a result, seeking orientation from papers by Green et al.<sup>124,125,128,129</sup> on suitable error tolerances seems advisable to obtain an initial starting point. Error tolerances mentioned in these publications range from 0.5 to 0.005 for small species, while the examples in the manual often use an error tolerance of 0.1. An example for pruning is only supplied in the manual and suggest a maximum species number of around 10000 species and states that the pruning tolerance should differ by at least a few magnitudes when compared with the error tolerance. With the considerable runtime involved, this can make using RMG a frustrating experience.

#### 3.3.2.2 Effects of the RMG Database

The core component of RMG is its database that contains possible reactions, such as hydrogen abstractions or radical additions as well as rules with respect to the energies involved in such reactions. A database is included with RMG and the latest version of the RMG database can be found in the RMG Github repository<sup>130</sup>. It was for example

found that RMG 3.3 could not create a model for the autoxidation of cyclic alkanes. By moving to the development version of RMG it was possible to obtain an autoxidation scheme for cyclic alkanes. The importance of the database was verified by testing both databases in the same RMG version with the newer database proving to be essential for the creation of an autoxidation scheme incorporating cyclic species. At the time of writing this thesis, RMG does not appear to handle aromatic species correctly, though it no longer fails with an error as it used to under RMG 3.3.

Modifications to the database allow for the addition of new reaction types or the correction of parameters already entered. However care needs to be taken to ensure the data is accurate and in the right format.

### 3.3.3 Computational Requirements

While drawing up preliminary schemes, it was found that RMG requires large amounts of random access memory (RAM) to work effectively while also commanding runtimes of at least several hours. A smaller mechanism was created running with 3500 megabytes of allocated RAM, while some of the more extensive preliminary schemes were drawn up with RMG allocated 9000 megabytes of RAM. Hence it is not unreasonable to expect that creating comprehensive schemes for the autoxidation of aviation fuel will require a significant amount of RAM.

A reduction of the runtime can be achieved by making use of a newer generation processor, however the lack of parallelization does not favour this route. Core RMG modules have been rewritten and parallelized in Python as a Research Project, however the stable release works only in serial and runs on Java<sup>131</sup>.

It is possible to access the log file and check the progress of RMG, but the stated results can be extremely deceptive. RMG can appear to be making great progress towards completing the model, but as it integrates over different time spans, it can at times appear to move away from the termination criteria as well. This leaves the user in an uncomfortable position with little indication if the settings specified lead to a useful model until the model is completed or at least near completion.

### 3.3.4 Potential Difficulties

Another challenge is to efficiently use the generated schemes as RMG is prone to generating extremely large reaction schemes. These can be easily solved using industry standard software such as Chemkin or our in house solver SPRINT, but are difficult to use for example in any fluid dynamics work due to the complexity involved. Reducing the resulting reaction schemes manually will be work intensive and potentially error prone. Alternatively, an automated approach is more likely to lead to more reliable

results.

## 3.4 Computational Chemistry

Computational chemistry aims to describe the interactions of atoms on a molecular level which is described through electron interactions<sup>132</sup>. Quantum mechanics are able to describe both the particle like and wave like behaviour of electrons using the Schrödinger Equation, given as a reference only in (3.4.1)<sup>133</sup>.

$$\left\{ \frac{\hbar}{2} \nabla^2 + \mathbf{V} \right\} \psi(\mathbf{r}, t) = i\hbar \frac{\partial \psi(\mathbf{r}, t)}{\partial t} \quad (3.4.1)$$

Computer codes such as Gaussian<sup>134</sup> aim to approximate a solution to the Schrödinger Equation to a varying degree of accuracy to obtain a description for the energy in a system. In this work, density functional theory (DFT) has been chosen as the primary method for energy calculations as it offers a good balance between computational cost and accuracy when compared to Hartree-Fock theory or higher order methods<sup>132</sup>.

In density functional theory the electronic energy is described through its components, shown in equation (3.4.2)<sup>132</sup>.

$$E = E^T + E^V + E^J + E^{XC} \quad (3.4.2)$$

In equation (3.4.2),  $E$  is the total energy,  $E^T$  the kinetic energy,  $E^V$  describes the potential energy of the nuclear-electron attraction as well as the repulsion between nuclei,  $E^J$  describes the electron-electron repulsion while  $E^{XC}$  describes the “remaining part of electron-electron interactions”<sup>132</sup>.

Each component of the expression is described using functionals in density functional theory, hence giving the method its name. The user is able to chose between a number of different functionals and thus influence both the speed and accuracy of the calculation. One such set is B3LYP, where the name identifies the functionals as being Becke-style three parameter density functional theory with an added Lee-Yang-Parr correlation functional<sup>132</sup>. Other methods follow a similar naming convention.

### 3.4.1 Choosing Appropriate Methods

Two choices are of significant concern when carrying out quantum chemical calculations. First the choice of basis set which contains descriptions for the behaviour and of electrons and secondly the method by which results are calculated.



### 3.4.1.1 Basis Sets

Basis sets contain mathematical approximations for the description of molecular orbitals<sup>132</sup>. Increasing basis sets offer more complete description of the behaviour of molecular orbitals. In a 3-21 basis set, three Gaussian functions are used to describe the behaviour of the wavefunction, while in a 6-31 basis set, six Gaussian functions are employed<sup>135</sup>. A larger basis set is generally required to accurately predict the behaviour of higher order elements or to obtain a higher accuracy result. However, this comes at a computational cost that may make some methods infeasible<sup>132</sup>.

The 6-31G basis set is chosen because it includes a split valence basis set as well as a polarized basis set<sup>132</sup>. In addition, we add the ++ function to include diffusion as well as d and p functions that improve the treatment of heavy atoms (d), such as carbon and the treatment of hydrogen (p). Therefore, the chosen basis set for all calculations is 6-31G++(d,p). This agrees with research by for example Esteves et al.<sup>136</sup> who also employed a 6-31G basis set.

### 3.4.1.2 Computational Method - Level of Theory

The second important choice is the level of theory at which we model the molecules. The simplest and computationally least intensive method is a Hartree-Fock model, however it is also the least accurate. Higher order MPx models can achieve higher accuracy, however carry significant computational costs. Density functional theory based methods have been found to offer reasonable accuracy at an affordable computational cost<sup>132</sup>.

As a result, a density functional theory based approach has been chosen for this investigation, employing the B3LYP set, as it is well established and offers good accuracy at comparatively low cost<sup>132,134,135</sup>. B3LYP has also been employed by other groups, such as Liljenberg et al.<sup>137</sup> or Esteves et al.<sup>136</sup> when describing the behaviour of an aromatic species. In addition, a review by Jenkins<sup>138</sup> suggests that density functional theory has been used extensively to model surface interactions between metals and aromatic hydrocarbon species, however the author also questions the accuracy of density functional theory under such conditions due to a lack of inclusion of Van der Waals interactions in density functional theory<sup>138</sup>.

### 3.4.2 Geometry - Creating Structures

The user needs to supply the geometry of the molecules under investigation to Gaussian 09<sup>134</sup>. This is achieved by building molecules in the supplied secondary software which also offers a general user interface (GUI) for Gaussian 09<sup>134</sup>, called GaussView<sup>139</sup>. The user can build a molecule either by positioning and connecting individual atoms or using molecule fragments. For example, m-toluidine can be built by first picking a benzene ring and then replacing a hydrogen with a nitrogen atom, followed by replacing

an additional hydrogen atom with a carbon atom.

In a second step, this initial structure should be optimized to ensure that bond lengths are appropriate and functional groups orientated in a way that theory would predict.

Provided that the user has chosen an appropriate level of theory, detailed in Section 3.4.1, the user could proceed to start the calculation to obtain a result. If the objective is to obtain and evaluate a transition step, additional steps detailed in Section 3.4.3 are required.

### 3.4.3 Searching For Transition States

In the context of this thesis, Gaussian is used to predict the energy barrier of interactions between two molecules undergoing electrophilic aromatic substitution. The zero point energy difference between the reactants and the transition state will then translate to an activation energy which can be used in a chemical kinetics model<sup>132</sup>.

#### 3.4.3.1 Finding Transition State - QST2

For many cases, the best method in Gaussian 09<sup>134</sup> to obtain a transition state is a QST2 optimization<sup>132,134</sup>. The QST2 method requires the user to produce two input structures, the first one consists of the reactants in a position that makes the reaction likely, while the second one contains the final product or products as they would occur shortly after the reaction. It is of importance that the atoms are numbered identically in both structures, so that Gaussian 09<sup>134</sup> can identify where and how atoms have been displaced.

It is further important that all bonds are included, dashed lines for bonds that will form in the reactants and dashed lines for bonds that were broken in the products.

In addition it is advisable to tweak bonds in molecules to favour an interaction of the atoms. A bond that is expected to break can be lengthened slightly while atoms that are expected to bond together should be moved closer together. One recommendation obtained from Gaussian Support<sup>140</sup> was that the key atoms which bond in a reaction involving the sought transition state should be around 2.5 to 3 Ångström apart.

#### 3.4.3.2 Finding Transition State - QST3

The QST3 method in Gaussian is in many respects identical to the QST2 method introduced in Section 3.4.3.1, the only difference is that the user must supply a third structure which constitutes a guess for the transition state structure<sup>132,134</sup>.

### 3.4.3.3 Finding Transition State - Opt=TS

In some cases, where a transition state calculation has not converged, or the user knows the structure of the transition state in advance, it may be possible to optimize a structure to a transition state immediately rather than a minimum<sup>134</sup>.

### 3.4.3.4 Verifying The Transition State

After a transition state has been found, the user should ideally carry out two verifications to ensure he has indeed found a transition state and found the correct transition state. As a first indication, the user should verify that a frequency calculation shows exactly one negative frequency, an indicator of transition states<sup>132,134</sup>.

In a second step, it is highly recommended to carry out an intrinsic reaction coordinates calculation (IRC), where Gaussian 09<sup>132,134</sup> will follow the reaction path. If an appropriate transition state has been found, the IRC calculation should provide the user with the expected reactant and product structures.

### 3.4.3.5 Solvation

Gaussian will by default calculate energies for gas phase systems. Where solvation chemistry is of interest, a solvation parameter is available to include solvation effects. The implementation of solvation in Gaussian employs a force field only and thus has the largest impact in polar solvents<sup>132,134</sup>.



## Chapter 4

# Reaction Mechanism Generation

### 4.1 Initial Evaluation of RMG Models

The Reaction Mechanism Generator (RMG) was introduced in detail in Section 3.3, including some information on the theoretical aspects and practical implementation of the software. Given that RMG was used successfully in published studies by Green et al.<sup>123–125,128,129,141</sup>, it is not unreasonable to expect the software to work correctly within its limitations with regards to the mechanism generation algorithm.

#### 4.1.1 Criteria for RMG Evaluation

Heptane was chosen for an autoignition model as it is a large enough species for use in RMG but small enough so that the runtime is not prohibitive and also has the benefit of literature data<sup>142</sup> being available for validation purposes. RMG was set up for temperatures ranging from 1000K to 2200K, 650K to 2200K to capture the lower temperature as well as the high temperature behaviour of the alkane. Oxygen consumption was chosen as a termination criteria for RMG, as for combustion the oxygen conversion can be predetermined from stoichiometry.

#### 4.1.2 Heptane Autoignition Delay Times

Initial results for the autoignition times of heptane in the region from 1000 K to 1400 K are extremely promising with respect to the accuracy of the model and match published experimental data from a comprehensive study by Westbrook as well as the Westbrook Heptane Oxidation scheme<sup>142</sup>.

A model with a significantly greater error tolerance spanning 650 K to 1400 K shows the expected behaviour with a systematic shift in the ignition time by roughly one order of magnitude when compared to experimental data as shown in Figure 4.1. During testing, a smaller error tolerance which should improve the accuracy of the model has not lead to an improved model during a runtime of several days. Varying other parameters such

as pruning has also not lead to an improvement in the accuracy of the model and in some cases even had negative effects on the overall model. However given that the models defined for a narrower temperature range were found to be accurate, this is not considered to be a major problem. Ignition times for an RMG derived model as well as published experimental data by Westbrook et al.<sup>142</sup> is shown in Table 4.1b, which indicates the general suitability of RMG models that span 1000 K to 1400 K.

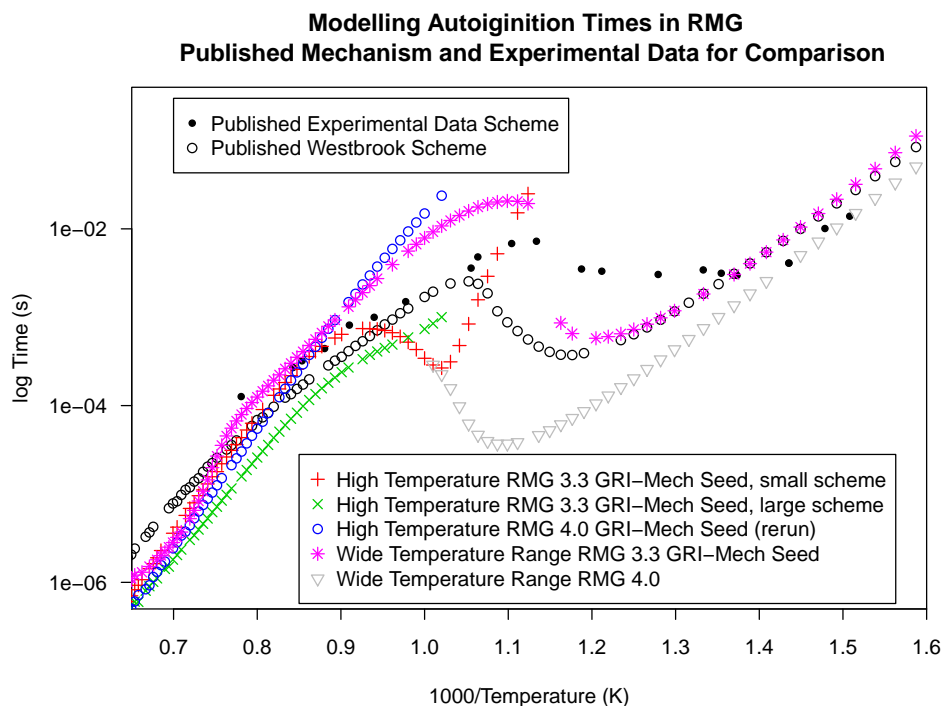


Figure 4.1: Autoignition times from experimental data by Westbrook et al.<sup>142</sup> as well as RMG models for Heptane over a temperature range of 625 K to 1400 K.

The GRI Mechanism is designed to describe the combustion of natural gas at temperatures above 1000 K, hence it deals with the behaviour of the smaller species, which RMG which RMG will have difficulties to estimate the thermodynamic properties off. As the mechanism was created to deal with the autoxidation and then combustion of heptane, RMG will need to simulate the decomposition of the larger alkane into smaller species which are then covered by the GRI Mechanism.

A look at the RMG kinetics database suggests that most entries cover the temperature range of 300-1500 K in RMG 3.3, with RMG 4.x, the number of entries has increased significantly with overall the same temperature distribution but also more high temperature reactions up to 2000 K. In addition the database also contains a number of entries that cover lower temperature reactions below 600 K. The graph suggests that at high temperatures RMG augments the GRI Mechanism<sup>94</sup>, resulting in a good fit. At low temperatures, the high temperature reactions in the GRI Mechanism<sup>94</sup> will be of lesser

significance, while RMG will dominate the lower temperature decomposition reactions. Generating a wide temperature range scheme will most likely result in the inclusion of low temperature reactions which, due to their parameters, such as comparatively low activation energies, will have a significant impact at higher temperatures. The difficulty of RMT to produce a scheme that fails predicts the “middle temperature regime” around 1000 K and less well most likely stems from the the fact that decomposition of the the hydrocarbon species will be too slow for autoignition to occur. The wide temperature regime test in RMG 4.x further indicated that RMG is able to predict the low temperature behaviour comparatively well, while failing in the high temperature regime which is more accurately covered in the GRI Mechanism<sup>94</sup>. This is most likely an artefact of the inability of RMG to predict the thermodynamic parameters of small species well, as stated in Section 3.3.1.6.

#### 4.1.2.1 Comparison of Product Species after Combustion

Considering that the autoignition results for heptane are overall positive, the next step was to look at a few product species to verify that the mechanism has gone to completion. This also indicates whether the thermodynamic data is reasonable as it directly affects species concentrations at the reaction equilibrium. Table 4.1c shows the concentration for select species in two RMG models and the reference heptane model by Westbrook<sup>143</sup> which itself draws from a previous model by Westbrook<sup>144</sup>. Two different error tolerances, 0.5 and 0.1, were set in the RMG set-up file, resulting in differently sized models to be compared against the reference model with initial conditions taken from a review by Westbrook<sup>142</sup>. Comparing the numerical results, it can be seen that the RMG model is very close to the validated scheme.

		Temp K	Experimental	RMG 220	RMG 146
Pressure	13.3 atm	1300	$9.98 \times 10^{-5}$	$2.62 \times 10^{-5}$	$7.95 \times 10^{-5}$
Concentration	$C_7H_{16}$ 0.0197 mol $l^{-1}$	1200	$2.48 \times 10^{-4}$	$1.14 \times 10^{-4}$	$3.75 \times 10^{-4}$
Concentration	$O_2$ 0.2049 mol $l^{-1}$	1100	$8.02 \times 10^{-4}$	$5.00 \times 10^{-4}$	$1.32 \times 10^{-3}$
Concentration	$N_2$ 0.7754 mol $l^{-1}$	1000	$2.11 \times 10^{-3}$	$1.52 \times 10^{-3}$	$1.32 \times 10^{-3}$
	(a) Conditions for autoignition testing.	950	$3.52 \times 10^{-3}$	$3.27 \times 10^{-3}$	$2.45 \times 10^{-3}$
		900	$6.92 \times 10^{-3}$	$1.10 \times 10^{-2}$	$1.76 \times 10^{-2}$

(b) Autoignition delay times.

Species	1200K			1600K		
	Westbrook	RMG 146	RMG 220	Westbrook	RMG 146	RMG 220
$CO_2$	$7.40 \times 10^{-02}$	$7.43 \times 10^{-02}$	$7.42 \times 10^{-02}$	$5.94 \times 10^{-02}$	$6.01 \times 10^{-02}$	$6.00 \times 10^{-02}$
$O_2$	$1.54 \times 10^{-02}$	$1.53 \times 10^{-02}$	$1.54 \times 10^{-02}$	$2.11 \times 10^{-02}$	$2.09 \times 10^{-02}$	$2.10 \times 10^{-02}$
H	$3.55 \times 10^{-03}$	$3.79 \times 10^{-03}$	$3.84 \times 10^{-03}$	$6.82 \times 10^{-03}$	$7.37 \times 10^{-03}$	$7.47 \times 10^{-03}$
CO	$5.11 \times 10^{-02}$	$5.08 \times 10^{-02}$	$5.09 \times 10^{-02}$	$6.39 \times 10^{-02}$	$6.32 \times 10^{-02}$	$6.32 \times 10^{-02}$
$H_2O$	$1.23 \times 10^{-01}$	$1.23 \times 10^{-01}$	$1.23 \times 10^{-01}$	$1.12 \times 10^{-01}$	$1.12 \times 10^{-01}$	$1.11 \times 10^{-01}$
OH	$1.57 \times 10^{-02}$	$1.59 \times 10^{-02}$	$1.59 \times 10^{-02}$	$2.28 \times 10^{-02}$	$2.30 \times 10^{-02}$	$2.31 \times 10^{-02}$
O	$3.28 \times 10^{-03}$	$3.18 \times 10^{-03}$	$3.19 \times 10^{-03}$	$6.69 \times 10^{-03}$	$6.51 \times 10^{-03}$	$6.53 \times 10^{-03}$
$HO_2$	$1.65 \times 10^{-05}$	$1.98 \times 10^{-05}$	$1.97 \times 10^{-05}$	$2.37 \times 10^{-05}$	$2.85 \times 10^{-05}$	$2.83 \times 10^{-05}$
Temp	$3.12 \times 10^{+03}$	$3.12 \times 10^{+03}$	$3.12 \times 10^{+03}$	$3.27 \times 10^{+03}$	$3.27 \times 10^{+03}$	$3.27 \times 10^{+03}$

(c) Species concentrations at equilibrium.

Table 4.1: Table 4.1a shows the initial conditions used in the heptane autoignition model, specifically pressure and concentration. Table 4.1b shows ignition delay times in seconds for Heptane at various temperatures. Data presented is from an experimental study by Westbrook<sup>142</sup> (Figure 9 in the publication) as well as 220 and 146 species RMG models. Table 4.1c shows key species concentrations in the Westbrook model after ignition as well as RMG models drawn up with error tolerances of 0.5 (146 Species) and 0.1 (220 Species). Values of species concentrations are presented for an initial temperature, leading to autoignition and then combustion, of 1200K and 1600K.



This result is indicative of no major problems with the thermodynamic data in the RMG generated models, which is supportive of the methods employed. Only minor differences in the concentrations of key species exist and the final temperature is identical between the Westbrook and RMG model.

### 4.1.3 Initial Conclusion on the Validity of RMG Models

From the results presented in this section, one can conclude that RMG is capable of producing models for specific conditions accurately, such as predicting the behaviour of alkanes over a not too big temperature range. An example would be the autoignition and then combustion of an alkane at temperatures of 1000 K and more. However when one attempts to cover a greater range of conditions, such as a lower initial temperature or a multitude of pressures, RMG does not appear to be able to produce an equally accurate mechanism. The promising results for heptane indicate that the underlying algorithms in RMG are correct and thus support the decision to use the software for the automatic generation of models.

## 4.2 Developing a Good RMG Scheme

Having established that RMG is able to generate reaction schemes which agree reasonably well with published results in the field of combustion and autoignition, work proceeded employing RMG to develop a reaction mechanism which accurately describes autoxidation conditions. This is achieved by first establishing RMG's sensitivity towards key parameters such as the solvation settings, reaction time, temperature and concentration, followed by a closer investigation of the behaviour of different alkane types.

### 4.2.1 RMG Sensitivity

A number of parameters were identified to have a direct influence on model development, namely:

- i) reaction time
- ii) temperature, single vs. multiple
- iii) solvation settings, solvent type and viscosity
- iv) oxygen concentrations

The error tolerance was not looked at further for this study as its primary use is to control mechanism size and the aim was to keep mechanisms small and manageable. As could be seen from the autoxidation testing in Figure 4.1 where schemes were generated for a small temperature range, agreement between large schemes (large tolerance) and small schemes (small tolerance) was good.

#### 4.2.1.1 Termination Criteria - Reaction Time

As the convergence ration for fuel, solvent or oxygen is unknown at the start, the only suitable termination criteria for RMG in the case of autoxidation is the reaction time. It is therefore important to establish whether the RMG scheme will differ for different reaction times, and if they do differ, what the difference is. This is achieved by running RMG for a number of different reactions times, starting at 10 minutes and finishing with 1000 minutes.

The result suggests that RMG will produce very different reaction schemes based on the reaction time. In RMG3, it was found that an increase in reaction time will increase the oxygen consumption rate until a final consumption rate has been reached, shown in Figure 4.2, with a significant change in the oxygen consumption time beyond 20 minutes. This change stems from the fact that beyond a residence time of 20 minutes, between 31 and 32 minutes, the species count more than doubles, which leads to the rather dramatic change in the overall behaviour of the model. This is related to how the rates based enlarger operates, as the addition of a single species can have a “knock on effect” and thus warrant the inclusion of further species, growing the model rapidly. Reaction schemes generated with RMG4 for a reaction time of up to 60 minutes exhibit a slower oxygen consumption rate than reactions generated for a longer reaction time, shown in Figure 4.3, similar to RMG3 and subject to the same knock on effects in the rates based enlarger. However RMG 4.x predicts a faster oxygen consumption at long residence times than RMG 3.3 and a slower oxygen consumption than RMG 3.3 at short residence times. The very peculiar shape of the oxygen depletion curve in the RMG 3.3 model may also be indicative of problems during the model generation for short residence times. In both cases, a longer reaction time will lead to larger reaction schemes with more species, which is to be expected.

As published results from Sicard<sup>59–61,64</sup> as well as experimental observations in the PetroOxy, presented in this thesis, suggest that oxygen consumption is a gradual process, indicated by the gradually increasing rate of the pressure drop in the PetroOxy, one can expect an accelerating reaction rather than an instantaneous reaction. A more gradual oxygen consumption rate in regular fuel has further been reported by Zabarnick<sup>33</sup> as well as Kuprowicz<sup>34</sup>, however it must be noted that the complex mixture of Jet-A may behave very differently from solvents. This would suggest that the best reaction scheme to describe the experimental collected during work for this thesis is obtained by running RMG for a reaction time of about 60 minutes in the case of normal alkanes, which results in a model exhibiting a gradual, accelerating oxygen depletion.

In the case of this thesis, the primary interest lies with dodecane which has been employed as a simple surrogate for more complicated fuel or solvents for small scale experiments.

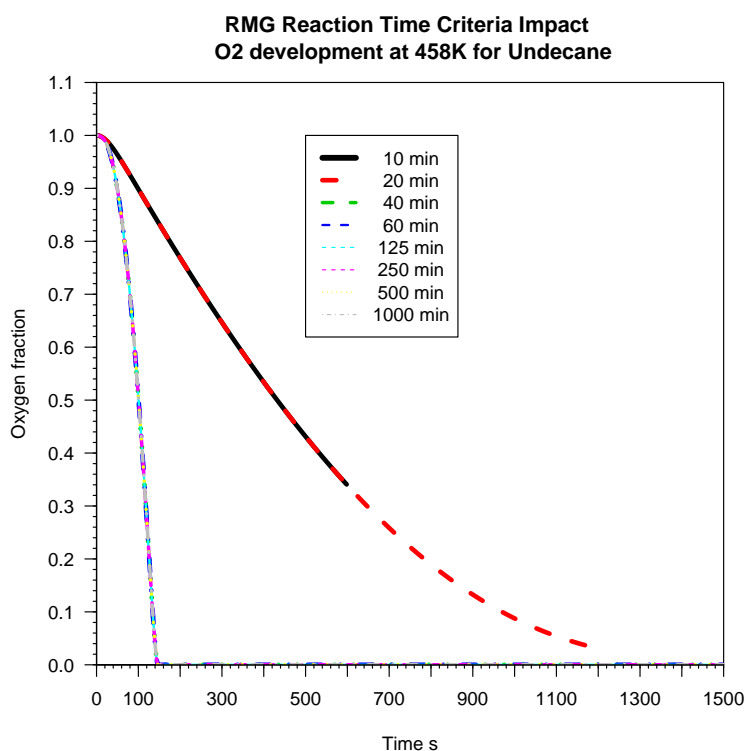


Figure 4.2: Development of the oxygen fraction over time for undecane at 458K for several reaction time termination criteria in the RMG 3.3 model.

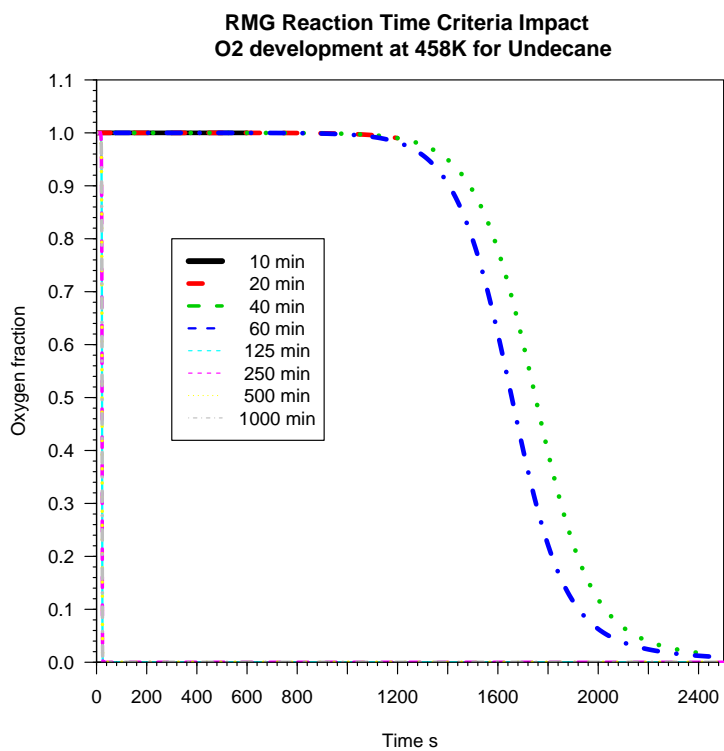


Figure 4.3: Plots of the development of the oxygen concentration in RMG schemes run for varying reaction time termination criteria in RMG4.

We reproduced the undecane methodology of testing variable times and as can be seen from Figure 4.4, use of a reaction scheme with a reaction time criteria of 60 minutes or less is to be preferred over longer reaction times on the basis of the previously presented argument.

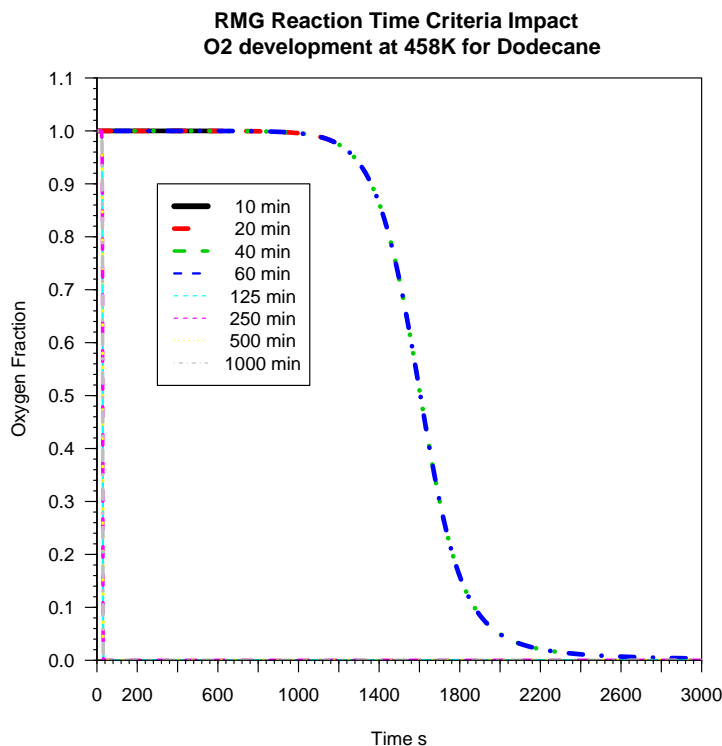


Figure 4.4: Plots of the development of the oxygen concentration in RMG schemes run for varying reaction time termination criteria in RMG4.

It was also noted, that the mechanisms generated by RMG4 were lacking any hydroperoxide decomposition, which lead to a lack of characteristic decomposition products such as alcohols. Therefore, the impact of the reaction time was also assessed in a higher temperature model which would be expected to show decomposition products.

#### 4.2.1.2 Single Reaction Temperature

An attempt was made to include hydroperoxide decomposition products by generating mechanisms for a number of compounds, representative of those tested in the the PetroOxy, by running RMG for an elevated reaction temperature. The compounds investigated are dodecane, 2,2,4-trimethylpentane as well as 2-methylundecane and 3-ethyldecane as representatives of Shellsol T constituents. The observed mechanism behaviour is shown in Figure 4.5. Please note that time for the iso-paraffinic compounds is plotted on a logarithmic scale. As can be seen, the oxygen depletion curves for different reaction times now overlap for dodecane, while reaction mechanisms generated for shorter reaction times of iso-paraffinic compounds were not run to completion by the

solver. Following, the effect of reducing the temperature in the 500 K scheme to 423 K when obtaining the time development of the reaction scheme was assessed, shown in Figure 4.6.

Most compounds behave as expected, with a reduced temperature resulting in a reduced oxygen consumption rate, however interestingly, the dodecane scheme exhibits no effect. This conflicts with both expected behaviour on the basis of chemical kinetics, where elevated temperatures lead to elevated reaction rates, as well described behaviour in the PetroOxy Manual<sup>145</sup> and observed behaviour in the PetroOxy.

#### 4.2.1.3 Single or Multiple Temperatures

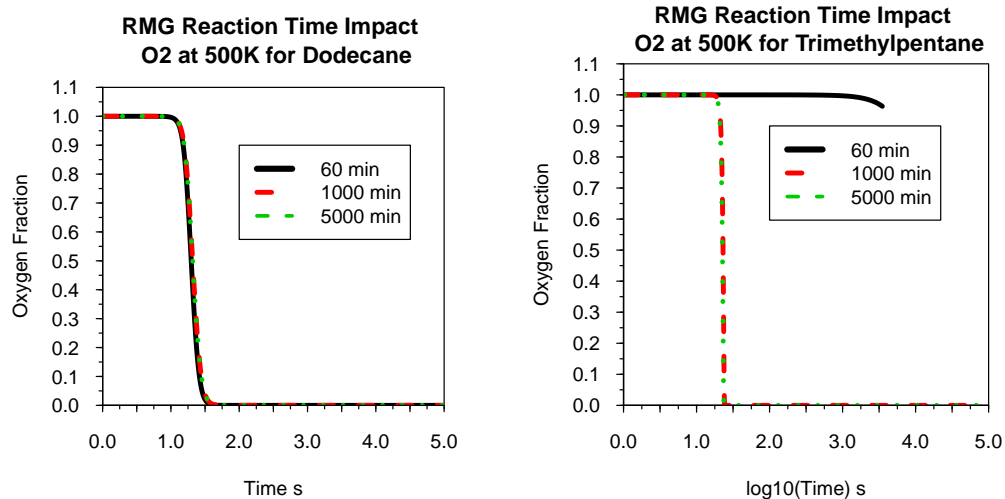
RMG will by default only create reaction mechanisms, for a constant reaction temperature and the RMG solver will evaluate the reaction scheme only at a constant temperature. However the user has the option of specifying multiple temperatures to cover a range of reaction conditions. To identify the impact of the temperature choice, RMG was run for temperatures of 423 K, 438 K, 448 K, 470 K and 560 K to identify whether there is any difference between a single and multiple temperature scheme. While higher temperatures always lead to shorter residence times, the time scale is very different. As can be seen from Figure 4.7b, the onset of oxygen consumption for the single temperature scheme at 458 K starts just after 1000 s. In contrast, the variable scheme suggests that oxygen depletion begins just after 10 s, as can be seen in Figure 4.7a. The solutions for lower temperatures, namely 438 K and 423 K diverge even further, and only the model for 470 K shows minor variation while at 560 K no significant difference can be discerned at the scale of the plot in Figure 4.7a.

This variation in the behaviour of the chemical kinetics scheme depending on the starting temperature is in some respects worrying, as it questions the accuracy of the models produced. Some discrepancy can be explained by the presence of high temperature reactions which also influence low temperature behaviour in a chemical kinetics scheme, but may be unidentified in a low temperature scheme.

#### 4.2.1.4 Solvation - Solvent Type and Viscosity

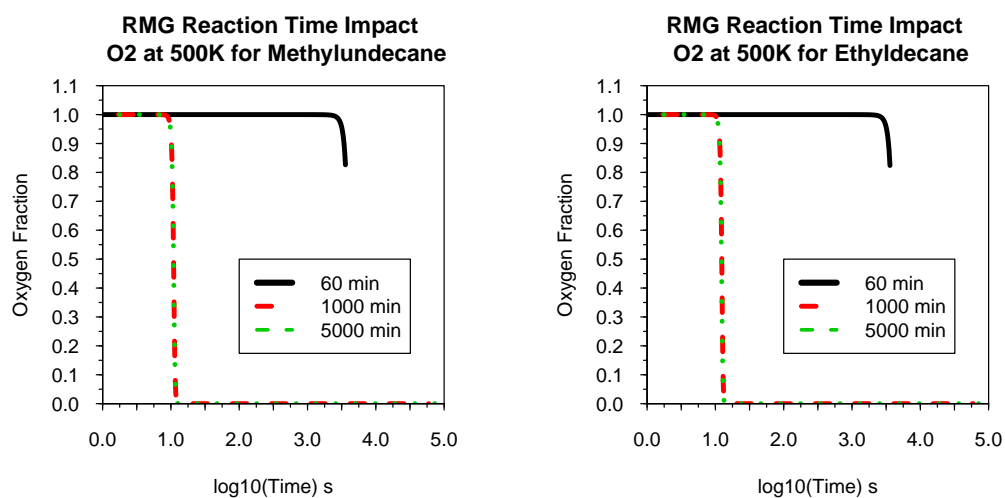
RMG expects the user to supply two parameters to model solvation, the solvent type as well as the viscosity of the solvent under normal conditions. The solvent type lets RMG draw on an internal database which covers the most commonly used solvents, the list of which are implemented in the code being available in the RMG manual<sup>122</sup>.

It was decided to assess the impact of the solvent type for Dodecane and have run RMG with the same Diffusion parameter of  $1 \times 10^{-3}$  Pa s to obtain a comparative result. In addition, two different oxygen concentrations were tested, a typical concentration for air saturated fuel of 0.002 mol/L, shown in Figure 4.8 as well as a large concentration



(a) Dodecane oxygen depletion curve at 500 K

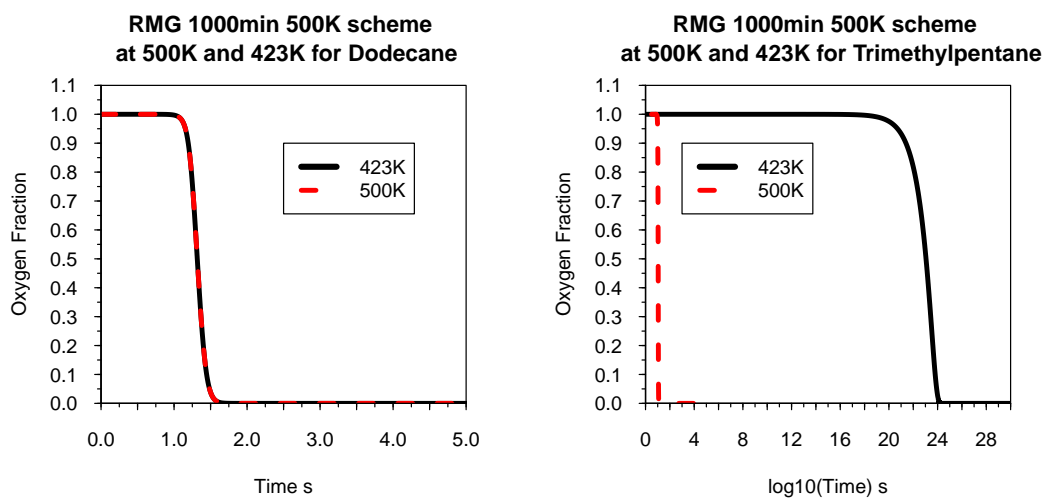
(b) Trimethylpentane oxygen depletion curve at 500 K



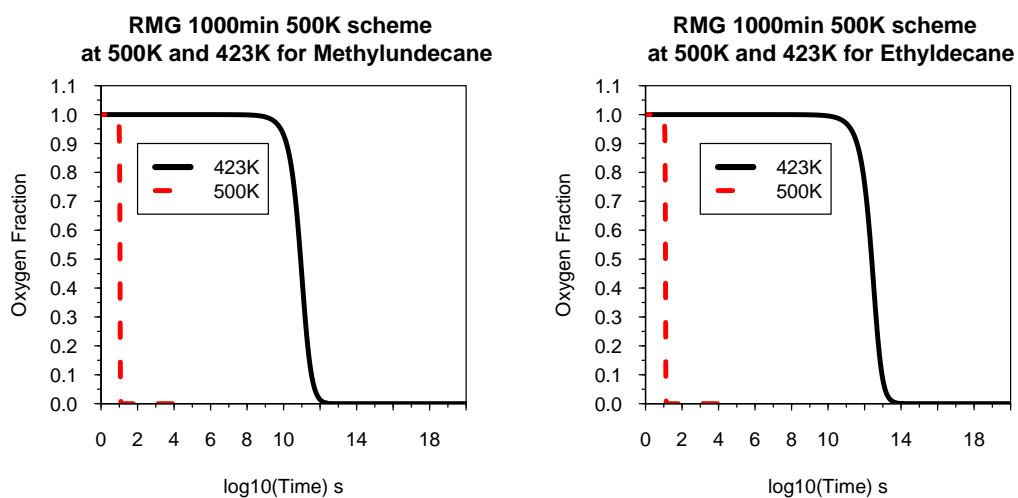
(c) Methylundecane oxygen depletion curve at 500 K

(d) Ethyldecane oxygen depletion curve at 500 K

Figure 4.5: Plots displaying the impact of reaction time on an RMG4 scheme generated and solved at a temperature of 500 K.

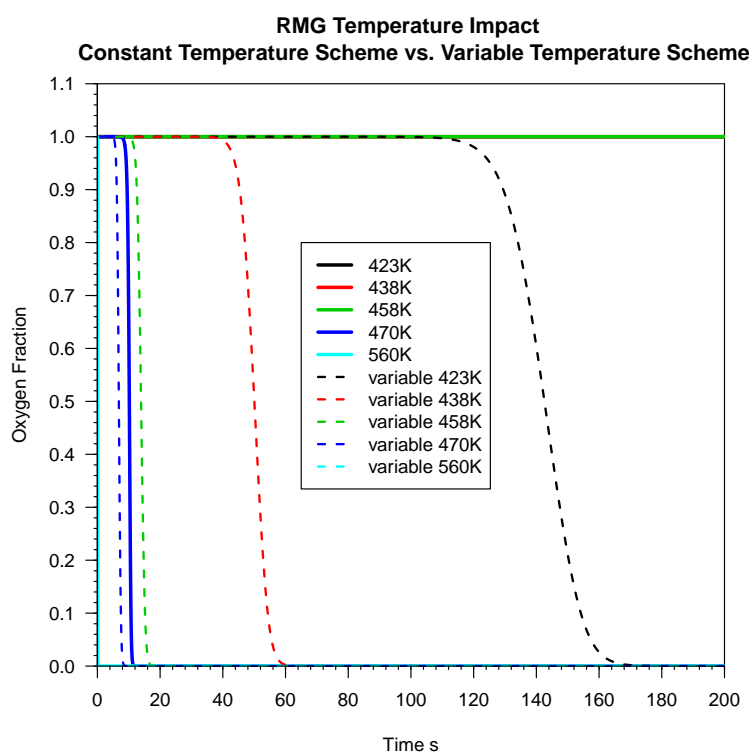


(a) Dodecane oxygen depletion curve at 423 K (b) Trimethylpentane oxygen depletion curve at 423 K

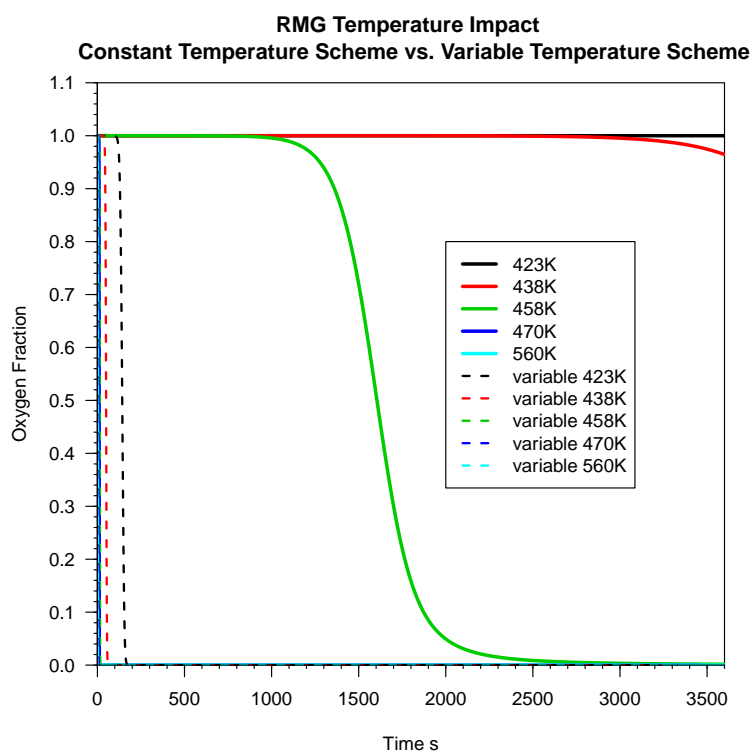


(c) Methylundecane oxygen depletion curve at 423 K (d) Ethyldecane oxygen depletion curve at 423 K

Figure 4.6: Comparative plot of the behaviour of a 1000 minute reaction times 500 K RMG scheme at 500 K and 423 K.



(a) Time range 0-200 s.



(b) Time range 0-3600 s.

Figure 4.7: Comparing a single temperature RMG scheme vs. a multi-temperature RMG scheme.



to approximate the conditions in the PetroOxy more closely of 0.2 mol/L, shown in Figure 4.9.

While for low concentrations of oxygen, the impact of the solvent type is visible but not huge, the results differ significantly for a high oxygen concentration, especially when comparing the octane to the decane model in Figure 4.9.

One can further deduce from comparing Figure 4.8 and Figure 4.9 that an increase in the oxygen concentration leads to an increased consumption rate of oxygen. In this case, a 100-fold increase in the concentration has led to an at most 40-fold increase in the oxygen consumption rate when comparing the worst case octane model.

The second diffusion parameter ensures that reactions do not exceed their diffusion limit, and takes the form of the user providing the viscosity of the solvent in  $\text{Pa} \times \text{s}^{1/2}$ . To identify RMG sensitivity towards viscosity, RMG was run for the same solvent type over a number of viscosities in a high oxygen concentration model. As can be seen from Figure 4.10, variation in the diffusion parameter can have a significant impact on the model accuracy. Especially predicting the solvent to be more viscous than literature data would suggest can slow down the oxygen consumption rate in the mechanism by nearly a factor of three.

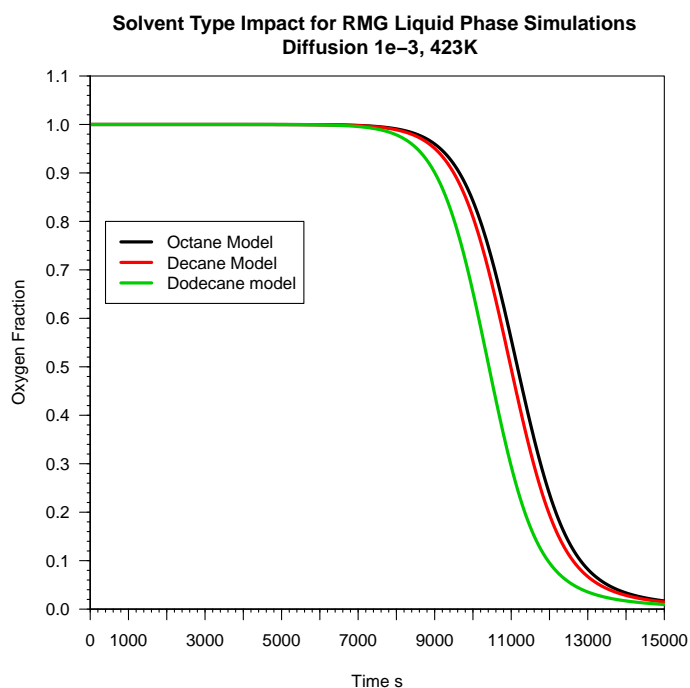


Figure 4.8: Plots of the development of the oxygen concentration in RMG schemes run for dodecane in different solvent types where the initial oxygen concentration is 0.002 mol/L.

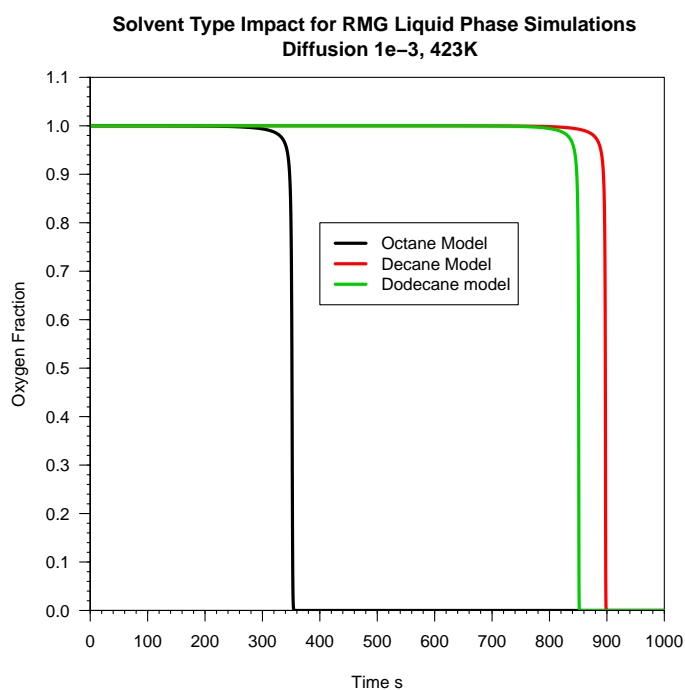


Figure 4.9: Plots of the development of the oxygen concentration in RMG schemes run for dodecane in different solvent types where the initial oxygen concentration is 0.2 mol/L.

Solvent	Viscosity Pas
octane	$5.10 \times 10^{-4}$
decane	$8.59 \times 10^{-4}$
dodecane	$1.34 \times 10^{-3}$

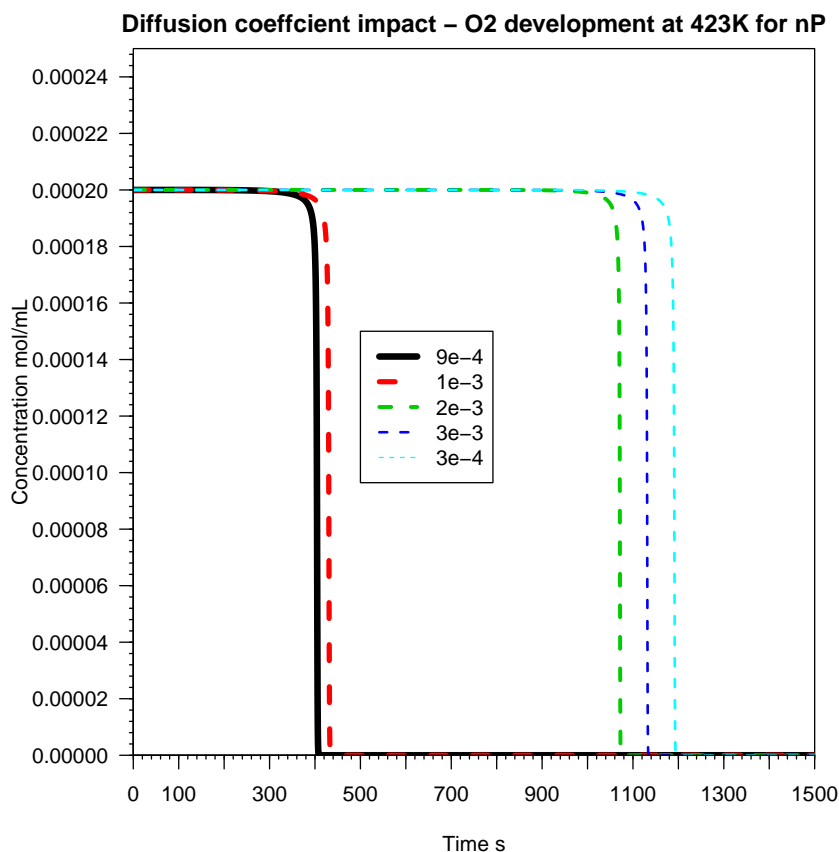
Table 4.2: Typical Values of viscosity of some solvents<sup>146</sup>.

Figure 4.10: Plots of the development of the oxygen concentration in RMG schemes run for dodecane with different viscosity values in Pas.

Viscosity values are available for common single component solvents, however in the case of uncommon hydrocarbons or mixtures, solvation parameters will need to be chosen on a “best guess” basis which leads to additional inaccuracy of the model. Typical values for a number of solvents are shown in Table 4.2.

#### 4.2.2 Chosen Models to Describe Autoxidation Behaviour with RMG

From the assessment of RMG sensitivity, it has been possible to determine that RMG conditions should represent the expected conditions as closely as possible with respect to reaction time, temperature as well as solvent parameters. In addition, while RMG appears to exhibit some problems with low temperatures, it is nevertheless advisable to run RMG for a low temperature to avoid any distortion in the scheme from inaccurate

parameters obtained for higher temperature kinetics. Using a scheme that covers multiple temperatures is also not advisable as again the behaviour of the scheme varies significantly when compared to a single temperature scheme on the lower end of the temperature range.

To be able to assess the chemical kinetics schemes to at least some extent, the difference in the behaviour between normal paraffinic hydrocarbons and iso-paraffinic hydrocarbons under conditions as found in the PetroOxy, a small scale isothermal static thermal stability test device, was investigated. RMG was therefore run for a temperature of 423 K and a pressure of 7.14 atm where the initial hydrocarbon concentration is 4.7 mol/L and the initial oxygen concentration is 0.02 mol/L of oxygen. Dodecane as well as a number of iso-paraffinic compounds were chosen, which are representative of ShellSol T.

To understand the different development of the RMG schemes for both normal and iso alkanes, the development of some of the initially formed species was investigated more closely. Specifically the development of oxygen a commonly used indicator for autoxidation and the alkyl radical,  $R\cdot$ , created by abstraction of a hydrogen atom by the oxygen molecule,  $O_2$  were investigated. The alkyl radical itself can then abstract a hydrogen or react with oxygen to form an  $ROO\cdot$  radical which can then abstract a hydrogen to form a hydroperoxide,  $ROOH$ , which covers the the next two steps in the autoxidative process. These initial steps are vital for the initiation of the autoxidative process, especially in the contest of ideal conditions modelling as is the case with RMG. Thus any difference that is attributable to the molecular structure of the reactants should show in the initial development of the mechanism. As can be seen from Figure 4.11, RMG predicts oxygen to deplete a lot faster in dodecane than in iso-praffinic solvents. While this contradicts PetroOxy measurements of ShellSol T, shown later in Figure 6.3, the rapid oxidation of ShellSol T may be related to unidentified contaminants in the solvent. These can be just about any compound, trace metals, oxidized products from storage or the production process as well as other contaminant species that were not removed in the refinery process. The complex structure of the solvent also means that it would not be possible to identify a definite cause. In contrast to dodecane, 2,2,4-trimethylpentane took ten times as long as dodecane to reach the same pressure drop in the PetroOxy and hence same or similar oxygen consumption. It was attempted to model 2,2,4-trimethylpentane in RMG, however the resulting scheme does not favour any significant oxygen consumption, with a hydrogen abstraction in only one location on the molecule, which suggests RMG may have issues predicting the properties or reactivities of heavily branched iso compounds properly and underpredicts their reactivity.

Therefore focuse lay with only on a number of more simply branched molecules, with their structure illustrated in Figure 4.12. Individual atom positions have been labelled to correspond to the specie identifier assigned by RMG which enables further inspection

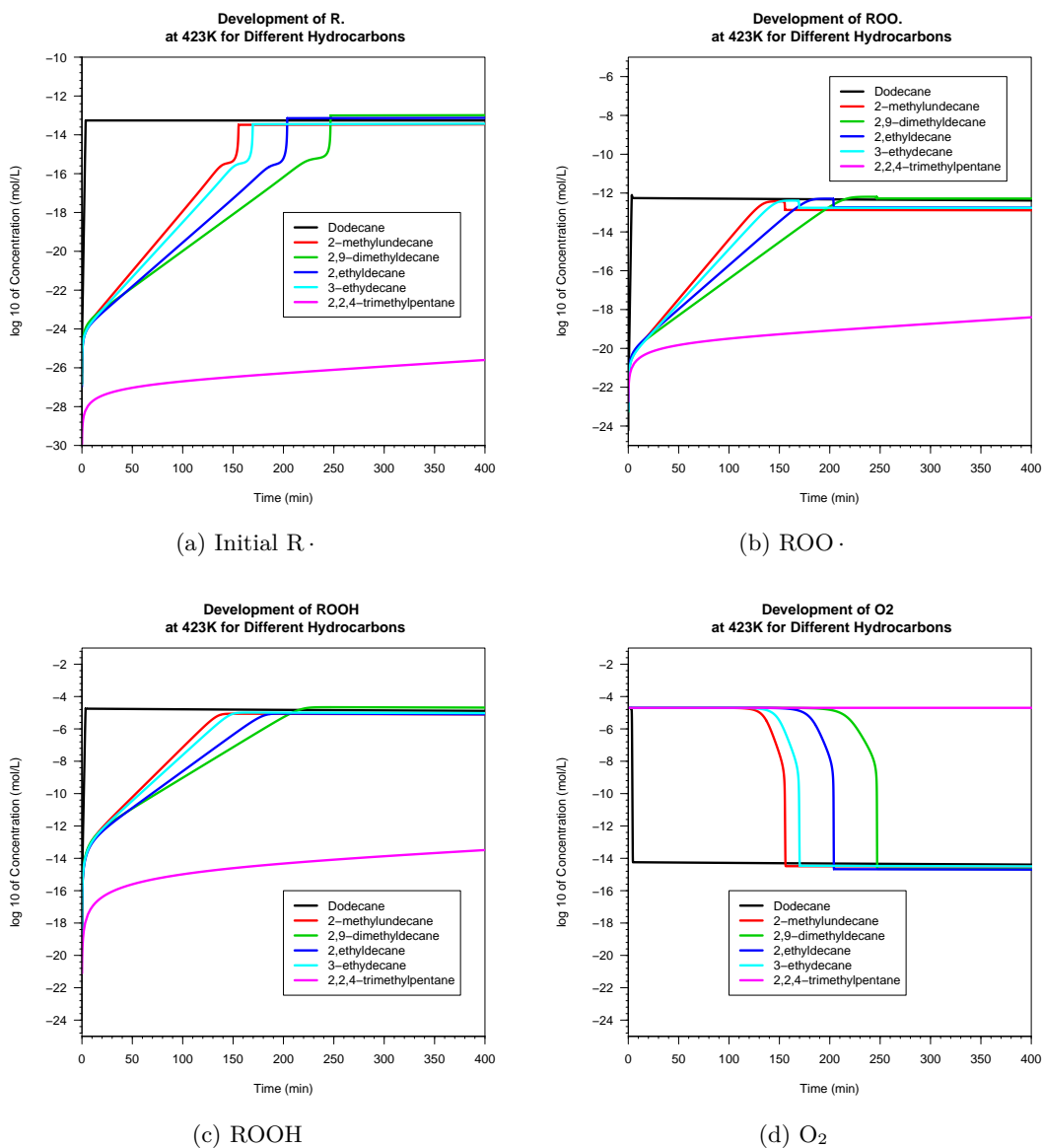


Figure 4.11: Development of a number of initial species in different hydrocarbons in a scheme generated with an O<sub>2</sub> concentration of 0.020 00 mol/L.

of the chemical kinetics scheme.

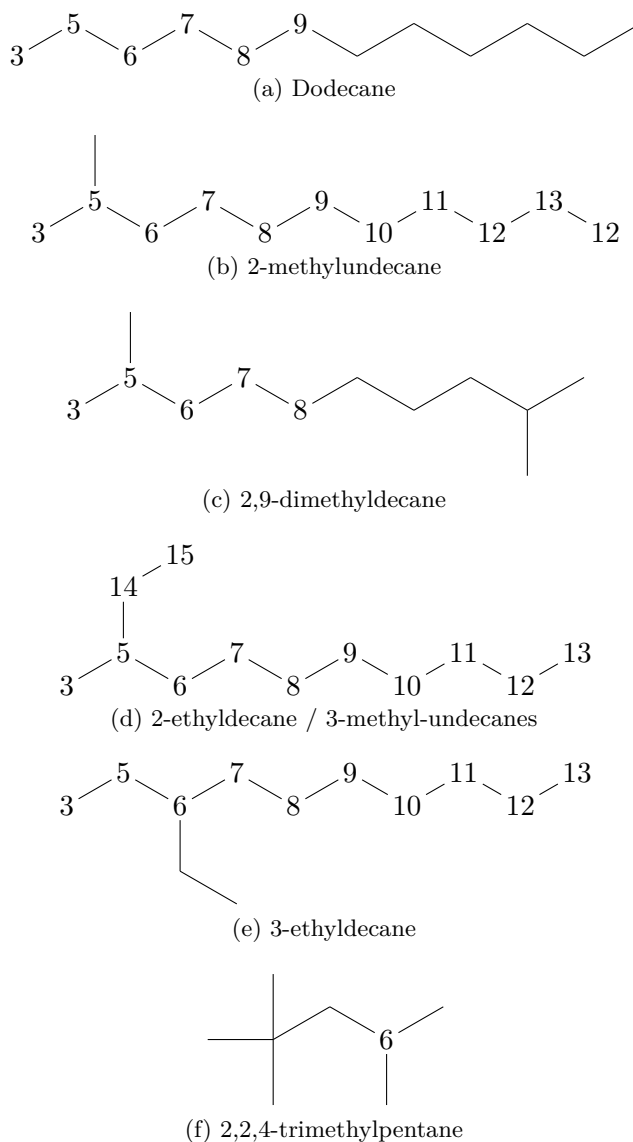


Figure 4.12: Radical Position Identifiers, where positions are left blank, these are covered by symmetry or not included in the final RMG scheme.

Looking at the rate constants for the initial hydrogen abstraction reaction by oxygen in RMG, shown in Table 4.3 and Table 4.4, one can see that reactions rates for initial hydrogen abstraction in dodecane are about one order of magnitude larger than for the iso compounds. It can further be determined that RMG predicts the majority of the abstractions to occur on the “chain part” of dodecane with the final two atoms on the dodecane carbon chain exhibiting reduced rate constants for the hydrogen abstraction reaction by dodecane.

This trend is continued for branched alkanes, where the “tail-part” of the molecule exhibits higher predicted rate constants than the end points or branching points of the molecule. These differences in rate constants are the explanation behind the very different

Species ID	$A$ (moles)	$n$	$Ea$ (K)	$k = At^n e^{(Ea/T)}$
3	5.804E+04	2.701E+00	2.969E+04	2.177E+42
5	7.927E+09	1.181E+00	2.915E+04	8.415E+42
6, 7, 8, 9	1.008E+11	8.139E-01	2.934E+04	1.840E+43

(a) Dodecane

Species ID	$A$ (moles)	$n$	$Ea$ (K)	$k = At^n e^{(Ea/T)}$
6	3.687E+10	7.883E-01	2.851E+04	8.185E+41

(b) 2,2,4-trimethylpentane

Table 4.3: Reaction parameters for different radical positions on dodecane and trimethylpentane. The location of the free radical electron can be determined from Figure 4.12. Values are presented for an RMG scheme created with an initial  $O_2$  concentration of 0.020 mol/L.

initial reaction rates for different compounds in RMG. As can be seen from Figure 4.11, the formation of  $R\cdot$  follows the consumption of oxygen and the following formation of  $ROO\cdot$  and  $ROOH$ . The concentration of  $R\cdot$  builds up gradually, although at insignificant concentrations. Only once the concentration passes  $10 \times 10^{-15}$  mol/L does the rate of formation of  $R\cdot$  accelerate, in line with the accelerated consumption of oxygen. The same is true for the  $ROO\cdot$ , which build up gradually until maintaining a peak concentration, an equilibrium until all oxygen is consumed, when their concentration falls again. The hydroperoxides,  $ROOH$ , as a comparatively stable product only accumulate in the simulation.

Inspection of the RMG scheme suggests that oxygen is predominantly consumed in the initial reactions when the reaction scheme is initiated, which is most visible in the compact dodecane scheme that was obtained by reducing an RMG derived dodecane scheme.

### 4.3 Mechanism Reduction

As RMG schemes are very large, handling them can be cumbersome and both time as well as resource intensive. In addition, their size precludes any closer inspection of the scheme as the most important reactions are effectively drowned out by redundant reactions. Through application of a mechanism reduction algorithm, it is possible to reduce the size and complexity of the mechanism which makes it on the one hand more manageable and on the other hand also offers the opportunity to compare it to published pseudo-detailed schemes.

A simple mechanism reduction algorithm has been implemented, detailed in Section 3.2.3.2, to enable the analysis of RMG generated schemes in greater detail. For this the user is required to supply a list which will group individual species together with

Species ID	$A$ (moles)	$n$	$Ea$ (K)	$k = At^n e^{(Ea/T)}$
3	7.269E+05	2.289E+00	2.994E+04	4.108E+42
5	4.872E+10	7.883E-01	2.851E+04	1.082E+42
6	8.915E+06	1.966E+00	2.871E+04	3.859E+41
7, 8, 9, 10, 11, 12	5.042E+10	8.139E-01	2.934E+04	9.201E+42
13	3.964E+09	1.181E+00	2.915E+04	4.208E+42
14	2.902E+04	2.701E+00	2.969E+04	1.089E+42

(a) 2-Methyl-undecane

Species ID	$A$ (moles)	$n$	$Ea$ (K)	$k = At^n e^{(Ea/T)}$
3	1.454E+06	2.289E+00	2.994E+04	8.216E+42
5	9.743E+10	7.883E-01	2.851E+04	2.163E+42
6	1.783E+07	1.966E+00	2.871E+04	7.718E+41
7, 8	1.008E+11	8.139E-01	2.934E+04	1.840E+43

(b) 2,9-dimethyldecane

Species ID	$A$ (moles)	$n$	$Ea$ (K)	$k = At^n e^{(Ea/T)}$
3	7.269E+05	2.289E+00	2.994E+04	4.108E+42
5	9.743E+10	7.883E-01	2.851E+04	2.163E+42
6, 14	8.915E+06	1.966E+00	2.871E+04	3.859E+41
7, 8, 9, 10, 11	5.042E+10	8.139E-01	2.934E+04	9.201E+42
12	3.964E+09	1.181E+00	2.915E+04	4.208E+42
13, 15	2.902E+04	2.701E+00	2.969E+04	1.089E+42

(c) 3-methylundecane

Species ID	$A$ (moles)	$n$	$Ea$ (K)	$k = At^n e^{(Ea/T)}$
3	2.902E+04	2.701E+00	2.969E+04	1.089E+42
5, 7	8.915E+06	1.966E+00	2.871E+04	3.859E+41
6	4.872E+10	7.883E-01	2.851E+04	1.082E+42
8, 9, 10, 11	5.042E+10	8.139E-01	2.934E+04	9.201E+42
12	3.964E+09	1.181E+00	2.915E+04	4.208E+42
13	2.902E+04	2.701E+00	2.969E+04	1.089E+42

(d) 3-ethyldecane

Table 4.4: Reaction parameters for different radical positions on a number of branched  $C_{12}$  molecules. The location of the free radical electron can be determined from Figure 4.12. Values are presented for an RMG scheme created with an initial  $O_2$  concentration of 0.020 mol/L.



the help of a numeric identifier after the chemkin name, such as shown in Figure 4.13. Species that are not grouped may be left in the species list and comments after an exclamation mark are allowed to improve ease of use with RMG.

```

MAPPING
C12H26(1)
O2(2)
HO2J(4)
C12H25J(5) 1
C12H25J(6) 1
C12H25J(7) 1
C12H25J(8) 1
C12H25J(9) 1
SPC(41) 2 ! C12H25O2J(41)
SPC(42) 3 ! C12H26O2(42)
SPC(92) 2 ! C12H25O2J(92)
END

```

Figure 4.13: Example of species grouping input employed by the chemical kinetics solver presented in this thesis.

One of the species that was grouped together in the mechanism reduction was the initial radical formed by hydrogen abstraction from dodecane, shown in Figure 4.14. Further grouped species are the  $\text{ROO}\cdot$  radials, hydroperoxides and  $\text{R}\cdot\text{OOH}$  radicals.

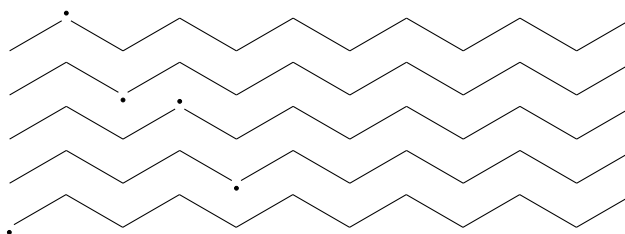


Figure 4.14: Different yet similar dodecane based radical species which can be represented as a single species in a lumped reaction scheme.

This grouping enabled us to reduce the reaction scheme to 1% of its original size, producing a manageable and human readable chemical reaction scheme. The accuracy of the reduced scheme was assessed by looking the normalized behaviour of two different species, oxygen which employed as a general indicator of thermal stability as well as water which is a termination product in a number of RMG-predicted autoxidation reactions at higher temperatures. The excellent agreement between the original unreduced RMG scheme and reduced scheme, shown in Figure 4.15 suggests that the method produces a good reduced scheme for the reaction conditions under which it was created.

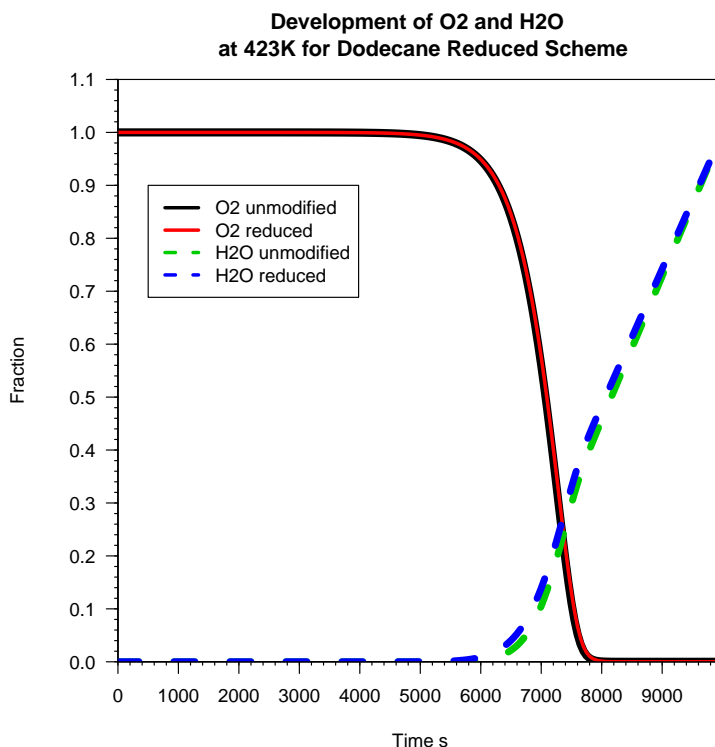


Figure 4.15: Impact of different species grouping on an RMG4 scheme for autoxidation conditions representative of the PetroOxy, 7.14 atm, 423 K

Scheme Type	Reactions	Species	Classes
Original RMG	6410	93	0
All R·	60	16	6

Table 4.5: Reaction and Species counts for original and grouped species chemical kinetics schemes. The class count is included in the species when the scheme is solved.

## 4.4 Modelling the PetroOxy with RMG

An attempt of validating RMG can be made by comparing its performance against a PetroOxy measurement, which is an industry standard static test for biodiesel. The PetroOxy, introduced in depth in Chapter 6 consists of a gold dish which is pressurised with oxygen and kept under isothermal conditions. Dodecane was chosen for this test as it offers a comparatively simple molecule whose behaviour should be predicted well by RMG. In addition, there can be good confident of the accuracy of the dodecane result in the PetroOxy as the solvent was chosen for the PetroOxy repeatability validation work. Another advantage of Banner and Dodecane is that the an industrial solvent oxidised faster, which suggests that diffusion is not a limiting factor for slower oxidising solvents.

Models were drawn up in RMG for 423 K at 7.14 atm which correspond to 700 kPa,

with an initial liquid phase oxygen concentration of 0.020 mol/L and a reaction time of 120 minutes. From the PetroOxy results it is known that the maximum pressure in the experiment was 1015 kPa, which is supplied to the extended chemical kinetics solver, introduced previously in Section 3.2.3, together with the dodecane sample size of 5 mL. The output has been plotted for comparison and is shown in Figure 4.16. The pressure data from the PetroOxy also supplies a good indirect measurement of the oxygen concentration, given that the pressure in the PetroOxy is dominated by the oxygen in the headspace. Using the ideal gas law, it is possible to calculate that a temperature change from 298 K to 423 K corresponds to a pressure increase with a factor of 1.42, assuming both temperature and volume are constant. For an initial pressure of 700 kPa at 298 K, this corresponds to a pressure of 993 kPa at 423 K, which is close to the maximum pressure recorded at the beginning of the test. As a simplification, the

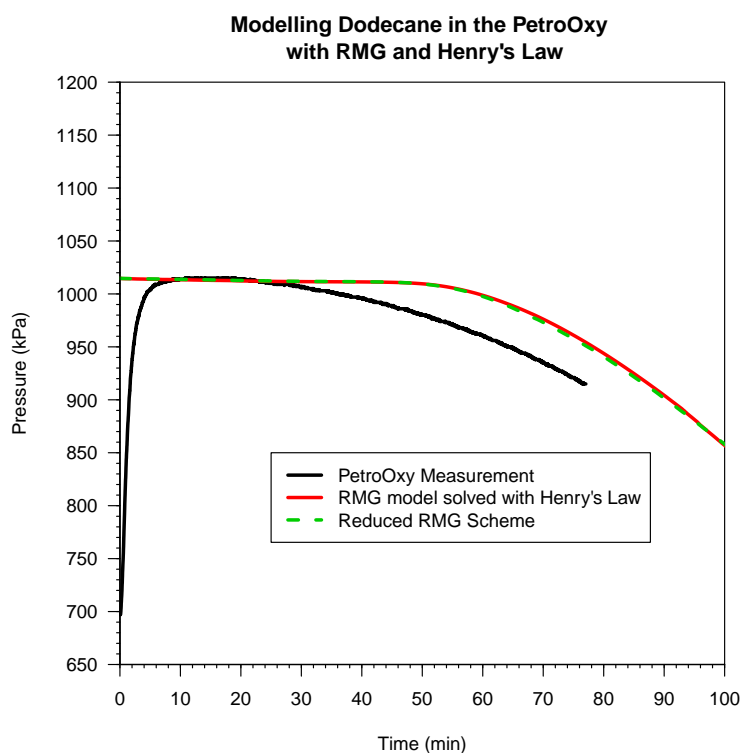


Figure 4.16: Comparison plot for an RMG model of dodecane with Henry's Law applied and PetroOxy data.

model ignores the initial pressure rise in the PetroOxy induced by the temperature rise while the PetroOxy heats up the sample. Hence, the PetroOxy data shows an initial pressure rise towards a maximum pressure after which, in the case of the employed neat solvents, the pressure immediately drops as oxygen is consumed. The model in contrast starts with the maximum pressure which it continues to display until a sufficient amount of alkylperoxy radicals  $\text{ROO}\cdot$  build up which then accelerate the  $\text{O}_2$  consumption in the liquid phase resulting in the observed pressure drop. After sufficient amounts of  $\text{ROO}\cdot$

	Species	Reactions
Decane	15	62
Dodecane	18	92
Banner finite O <sub>2</sub>	25	111
Banner constant O <sub>2</sub>	61	911

Table 4.6: Species and reaction counts in a number of RMG generated autoxidation schemes.

have built up, the model simulates the pressure drop observed in the experimental work fairly well. However while the observed pressure drop curve in the experiment suggests an acceleration in the oxygen consumption rate, over time, the model tends towards a linear pressure drop and is not able to predict the accelerating oxidation rate.

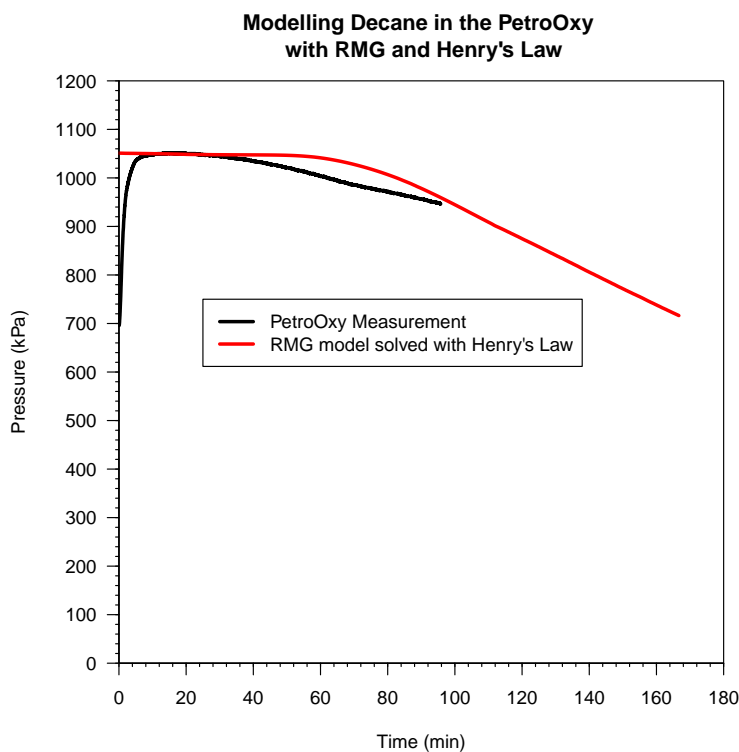


Figure 4.17: Comparison plot for an RMG model of decane with Henry's Law applied and PetroOxy data.

For further evaluation, an RMG model for decane as well as an approximate representation of Banner Solvent np1014 were also obtained. Banner Solvent np1014 is a commercial solvent, consisting primarily of normal paraffinic C<sub>10</sub>–C<sub>13</sub> alkanes as well as a smaller fraction of the normal paraffinic C<sub>14</sub> alkane. Due to its significantly lower cost relative to “pure” solvents, Banner Solvent np1014 is an ideal solvent to carry out more fundamental or in depth studies in a number of small scale thermal stability rigs. While decane is

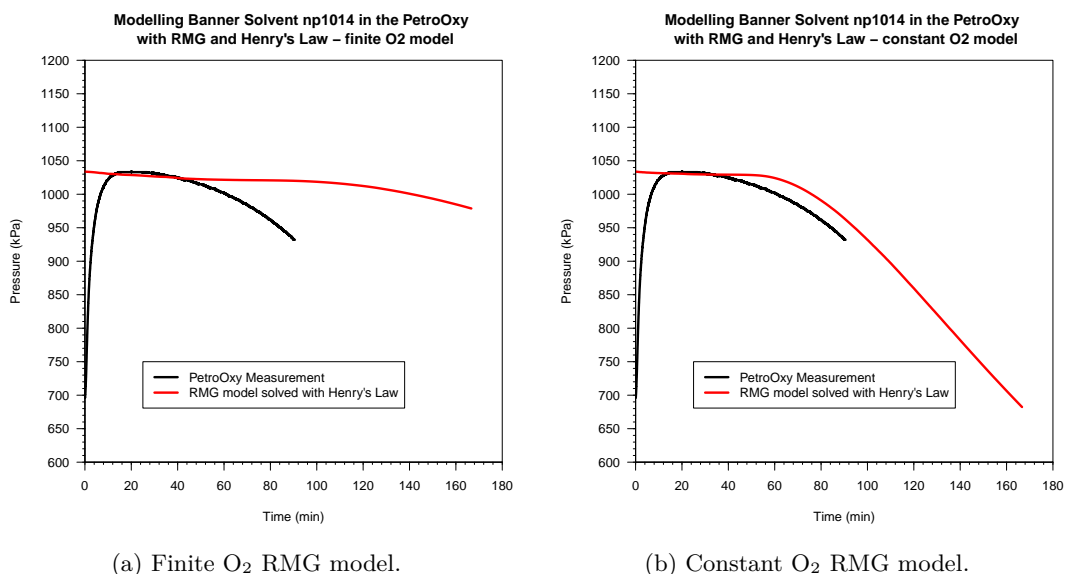


Figure 4.18: Comparison plot for RMG models of Banner Solvent np1014 with Henry's Law applied and PetroOxy data for Banner Solvent in the PTFE dish.

described equally well as dodecane, shown in Figure 4.17. Banner solvent is not by default described well by an RMG generated mechanism, as shown in Figure 4.18a, however the fit of the model can be significantly improved by rerunning RMG with a constant oxygen concentration setting, shown in Figure 4.18b. This improvement in the accuracy of the model is not immediately clear, however a comparison of the generated models using a visualization tool from the RMG developers<sup>127</sup> suggests that the model drawn up with a constant oxygen concentration considers additional initial radical species with a radical electron at additional positions, producing the then appropriate hydroperoxides for those radicals. In terms of species types, both models contain identical species, namely  $R\cdot$ ,  $ROO\cdot$  and  $ROOH$  only. Where reactions overlap, the parameters were found to be identical, hence the accelerated oxygen consumption in the constant  $O_2$  model must be entirely due to the additional reaction paths identified by RMG. However this effect of a larger model with corresponding accelerated  $O_2$  consumption does not occur for single component decane and dodecane models, with model sizes given in Table 4.6. Further testing also revealed that RMG in the version employed (development code from the Master Branch from January 2015) seemingly ignores the viscosity parameter for the Banner multi component mixture.

For a closer look, RMG was run for every individual component using the same conditions as the Banner model to assess the development of every individual component, shown in Figure 4.19. It can be seen that the effect of the more quickly oxidized compounds is present in the mixture, however the slower dodecane dominates. On the other hand, RMG cannot take the different solvation effects of individual components into proper consideration as only one parameter can be supplied. This applies additional constraints

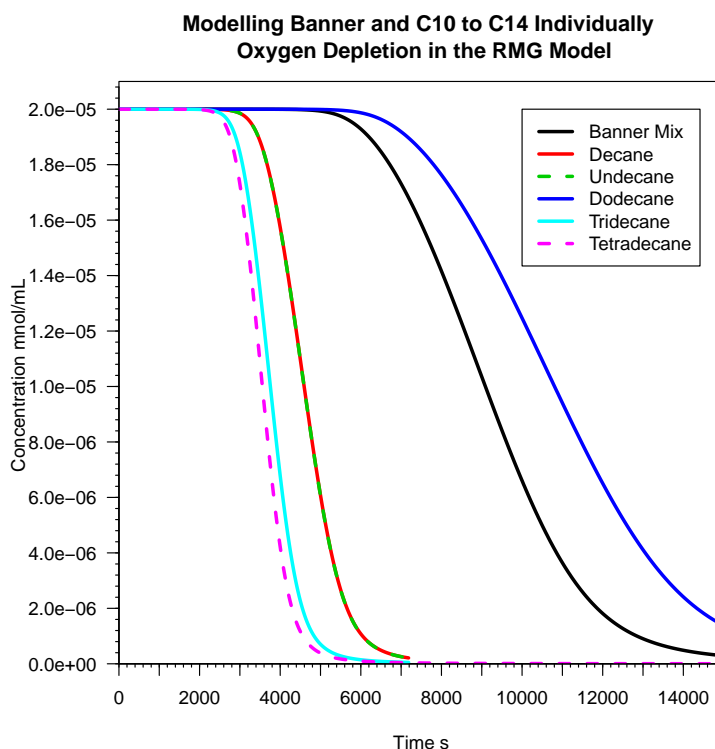


Figure 4.19: Comparison plot for an RMG model of Banner Solvent np1014 and its components under identical conditions.

on the user with respect to producing liquid phase kinetics schemes for non-single-component mixtures which would be a more realistic description or approximation of aviation fuels and surrogate mixtures.

## 4.5 Antioxidant Speculation

In addition, a number of postulated reactions that may describe the slowed oxygen consumption with additives were assessed in connection with the automatically generated mechanism. From the dodecane scheme, presented in Figure 4.23, the only species that participate in the oxygen consumption are the alkyl radical  $R\cdot$ , the alkylperoxy  $ROO\cdot$  or the hydroperoxy  $HOO\cdot$ . Therefore the impact of removing those radical species to inert products was investigated, first by adding a simple reaction and then by including an additive in the mechanism. For simplicity, the only parameter in the Arrhenius expression is  $A$ , the activation energy  $E_a$  is set to zero and the parameters for both  $ROO\cdot$  and  $HOO\cdot$  removal are identical. The values of  $A$  were chosen to be in line with the other pre-exponential factors in the RMG scheme to obtain an overview over the impact of different proposed antioxidant reactions. The resulting development of the oxygen concentration is shown in Figure 4.20, Figure 4.21 and Figure 4.22.

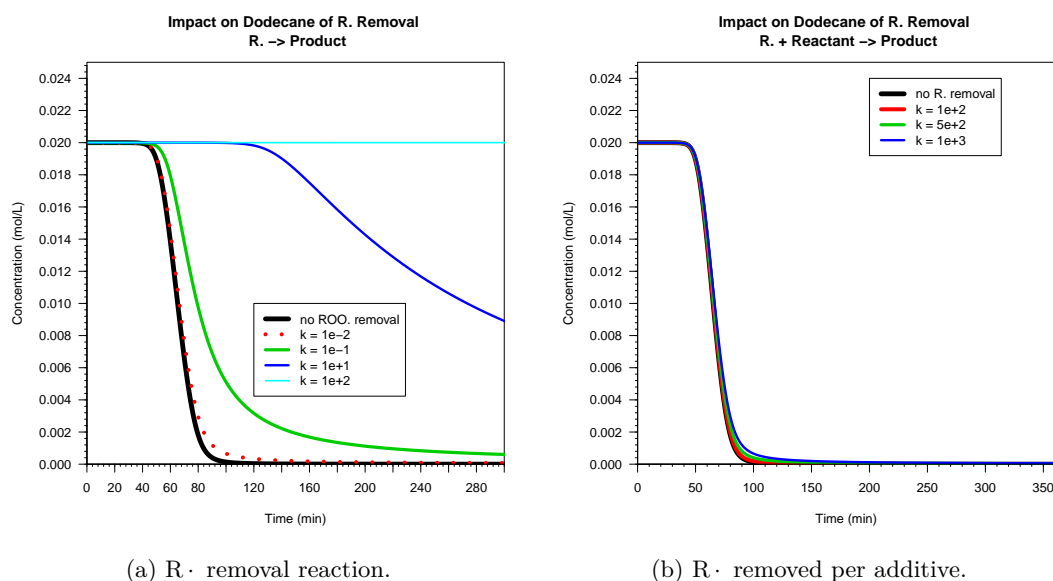
(a)  $R\cdot$  removal reaction.(b)  $R\cdot$  removed per additive.

Figure 4.20: Consumption of  $R\cdot$  in a dodecane mechanism, first by a removal reaction then with an additive.

Removal of  $R\cdot$  shows promise with regards to inhibiting oxygen consumption, shown in Figure 4.20a, however when  $R\cdot$  removal is implemented with an additive, shown in Figure 4.20b, the impact becomes near insignificant. Thus, while removal of  $R\cdot$  is an option for inhibiting the autoxidation process, it is not a feasible route. Removal of  $ROO\cdot$ , shown in Figure 4.21a shows equal promise when compared to  $R\cdot$ , however in contrast, to  $R\cdot$ , use of an additive for removal of  $ROO\cdot$  amplifies the effect over a simple direct removal of  $ROO\cdot$ , shown in Figure 4.21b. Thus the removal of  $ROO\cdot$  offers a very feasible route for the inhibition of the autoxidation process. If it is assumed that additives interact with  $ROO\cdot$ , there is no reason why they could not interact with  $HOO\cdot$  in the same way and thus remove both. Hence the simultaneous removal of  $ROO\cdot$  and  $HOO\cdot$  in the RMG generated mechanism was investigated, shown in Figure 4.22a. Initially encouraging, removal of  $ROO\cdot$  and  $HOO\cdot$  via an additive showed no such reduction in oxygen consumption rate, shown in Figure 4.22b. From the mechanism we presented in Figure 4.23, it can be deduced that  $HOO\cdot$  will release oxygen in conjunction with  $ROO\cdot$  by donating a hydrogen atom, hence if both  $HOO\cdot$  and  $ROO\cdot$  are removed, the oxygen consumption rate remains fast. Oxygen is primarily consumed by alkyl radicals,  $R\cdot$  which are primarily formed by  $ROO\cdot$  as the reaction between alkanes and oxygen is slow. Thus, if  $ROO\cdot$  is removed, fewer  $R\cdot$  are produced slowing the rate of oxygen consumption.

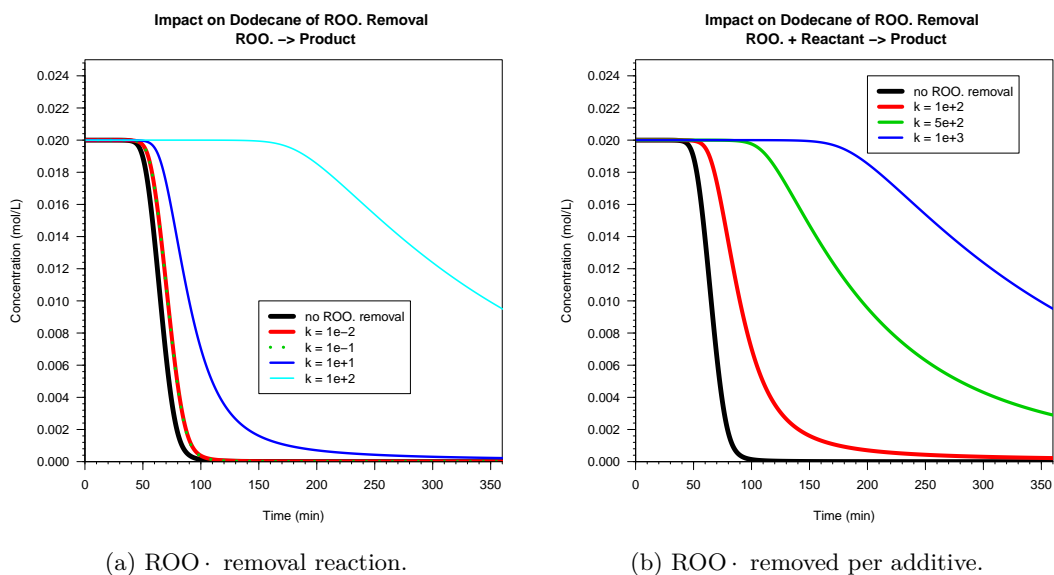


Figure 4.21: Consumption of  $\text{ROO}\cdot$  in a dodecane mechanism, first by a removal reaction then with an additive.

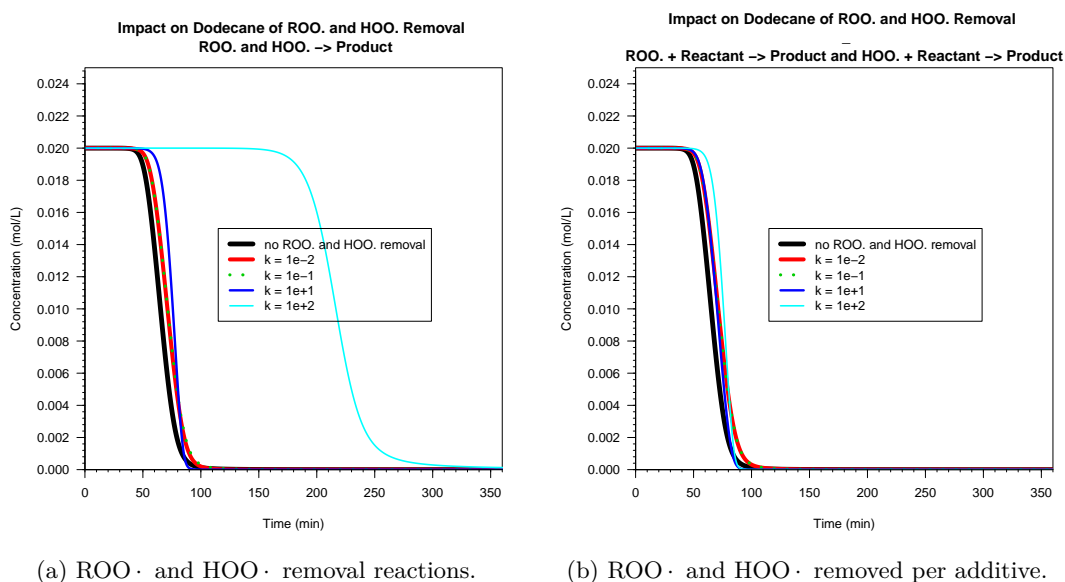


Figure 4.22: Consumption of  $\text{ROO}\cdot$  and  $\text{HOO}\cdot$  in a dodecane mechanism, first by a removal reaction then with an additive.



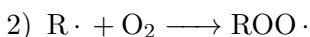
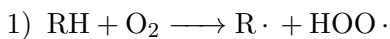
## 4.6 Closer Scheme Inspection

Two aspects of RMG warrant closer inspection, on the one hand the lack of hydroperoxide decomposition as well as the difference between schemes for normal paraffinic hydrocarbons and iso paraffinic hydrocarbons.

### 4.6.1 Difference Between Iso and Normal Paraffinic Scheme

Having established that RMG produces an acceptable model, given its basis in ideal cases, the behaviour of Dodecane was more closely investigated, on the one hand due to the reliability of the available data but also as it offers a simple enough test case. The original RMG scheme was taken, made irreversible and reduced using the rates based mechanism reduction algorithm presented in this thesis. Next species were lumped together to obtain a very small and compact chemical reaction mechanism which is shown in Figure 4.23, where the Arrhenius parameters have been fitted and corrected against  $k$  and thus do not directly represent any real reactions. The reduced scheme continues to model the oxygen depletion well, as was plotted previously in Figure 4.16. For comparison, a 2,9-dimethyldecane scheme generated in RMG was reduced using the same method as for dodecane to obtain the reduced mechanism shown in Figure 4.24. Close comparison of the schemes based on  $k$  reveals that the initiation step for the iso schemes is only marginally slower than for the normal alkane scheme and cannot account for the significant difference in behaviour. The second step of the alkyl radical reaction with oxygen is again of similar speed offering no insight into why the iso scheme behaves as it does. Surprisingly, a reduced scheme does not agree well when the decomposition of  $\text{ROO}\cdot$  to  $\text{R}\cdot$  and  $\text{O}_2$  is removed from the scheme, slowing the consumption of oxygen further. So while there is some difference between the individual kinetics, as would be expected, the difference in overall behaviour cannot be described through the differences in the initial steps but instead are the result of more subtle effects and feedback loops. Thus, as a next step the reaction rates between the different schemes were compared, covering the consumption of oxygen at four key point in the development of the scheme, namely in the buildup phase, just before the consumption of oxygen accelerates, during the highest consumption rate and lastly once the end has been reached. An illustration of the location of the points is shown in Figure 4.26 while the rates of  $\text{O}_2$  consumption are shown in Table 4.7.

Inspection of the reaction rates reveals that in the case of the iso-paraffinic schemes oxygen is consumed one to two orders of magnitude slower than in the normal paraffinic scheme. The reactions consuming oxygen are however the same, and all schemes follow the following pattern:



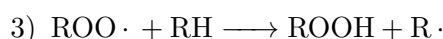
```

SPECIES
Class(1)  ! R·
Class(2)  ! ROO·
Class(3)  ! ROOH
C12H26    ! C12H26, dodecane
O2        ! O2, oxygen
HO2J     ! HO2·, peroxide
C12H25J  ! R·, if lumped, solver hangs
END

REACTIONS KELVINS MOLES
C12H26 + O2      -> HO2J + C12H25J    6.923e+09  1.20  29182
C12H26 + O2      -> Class(1) + HO2J    3.200e-17  0    -70.271
Class(1) + C12H26 -> C12H26 + C12H25J  1.118e+06  0    -13.257
C12H26 + C12H25J -> Class(1) + C12H26    3.916e+06  0    -13.348
Class(1) + C12H26 -> Class(1) + C12H26  5.872e+06  0    -13.257
O2 + C12H25J     -> Class(2)          7.540e+12  0      0
Class(2)         -> O2 + C12H25J     2.616e+28 -3.25  19321
Class(3) + C12H25J -> Class(2) + C12H26    4.237e+11  0     3.469
Class(2) + C12H26 -> Class(3) + C12H25J  4.874e+07  0    -9.033
Class(1) + Class(3) -> Class(2) + C12H26  4.237e+11  0     3.469
Class(2) + C12H26 -> Class(1) + Class(3)  1.707e+08  0    -9.124
Class(2) + HO2J   -> Class(3) + O2     8.745e+11  0     3.899
Class(3) + O2     -> Class(2) + HO2J    1.371e-06  0    -37.208
Class(1) + O2     -> Class(2)          7.540e+12  0   -2.364e-03
Class(2) + Class(3) -> Class(2) + Class(3)  6.751e+06  0    -11.843
END

```

Figure 4.23: Rate Reduced and then Species Lumped RMG Scheme. Minimal irreversible scheme to describe oxygen consumption behaviour in the PetroOxy when solved with the addition of Henry's Law.



The consumption of oxygen closely follows the production of  $\text{ROO}\cdot$  as prior to significant quantities of  $\text{ROO}\cdot$  being produced, the presence of  $\text{R}\cdot$  is fairly negligible and insufficient to initiate the propagation of the reaction chain. Only once significant amounts of  $\text{ROO}\cdot$  form is  $\text{R}\cdot$  formed in sufficient quantities for oxygen to be consumed which then produces  $\text{ROO}\cdot$  which propagates the chain by producing more  $\text{R}\cdot$ . This is explained by the higher reactivity of  $\text{ROO}\cdot$  in comparison to  $\text{O}_2$  with  $\text{RH}$ . This behaviour thus explains the observed delay or induction phase in RMG derived autoxidation schemes.

#### 4.6.2 Hydroperoxide Decomposition Speculation

The second aspect is the hydroperoxide decomposition, a reaction RMG does not include normally in a reaction. By raising the temperature criteria in RMG as well as covering a temperature range from 423 K to 560 K one can enforce the inclusion of a hydroperoxide decomposition while a small enough error tolerance can enforce the production of lighter

```

SPECIES
Class(1)  R·
Class(2)  ROO·
Class(3)  ROOH
C12H26   C12H26
O2       O2
HO2J     HO2·
C12H25J  R·
SPC(36)  ROO·
H2O2     H2O2
SPC(37)  ROOH
HOJ      HO·
H2O      H2O
END

REACTIONS KELVINS MOLES
C12H26 + O2      -> HO2J + C12H25J    9.743e+10  0.79    28514
O2(2) + C12H25J -> SPC(36)                1.410e+13  0         0
SPC(36)          -> O2 + C12H25J    1.148e+31 -3.77    21403
C12H26 + HO2J   -> C12H25J + H2O2    3.174e+07  1.60     6331
C12H26 + O2     -> Class(1) + HO2J    2.529e-017  0    -70.092
C12H26 + HO2J   -> Class(1) + H2O2    45249.3    0    -17.863
Class(1) + C12H26 -> C12H26 + C12H25J    879849    0    -10.503
C12H26 + C12H25J -> Class(1) + C12H26    348232    0    -12.581
Class(1)         -> C12H25J        1046.88    0    -15.938
C12H25J          -> Class(1)        698.69    0    -17.939
Class(1) + O2    -> Class(2)        5.655e+12  0    -2.364e-03
Class(2)         -> Class(1) + O2    4.14911    0    -42.416
Class(3) + C12H25J -> Class(2) + C12H26    2.255e+08  0     -2.759
Class(2) + C12H26 -> Class(3) + C12H25J    136071    0    -13.351
Class(1) + Class(3) -> Class(2) + C12H26    4.237e+11  0     3.469
Class(2) + C12H26 -> Class(1) + Class(3)    1.223e+08  0     -9.047
Class(3) + O2     -> Class(2) + HO2J    1.371e-06  0    -37.209
Class(1) + C12H26 -> Class(1) + C12H26    367083    0    -12.979
Class(1)          -> Class(1)        19.877    0    -16.376
Class(2) + Class(3) -> Class(2) + Class(3)    562626    0    -11.843
C12H25J + SPC(37) -> C12H26 + SPC(36)    5.042e-07  5.18    -1021
C12H26 + SPC(36) -> C12H25J + SPC(37)    1.149e-3   4.54     5190
Class(1) + SPC(37) -> C12H26 + SPC(36)    9.748e+07  0     -4.341
C12H26 + SPC(36) -> Class(1) + SPC(37)    746.378    0    -20.311
O2(2) + SPC(37) -> HO2J + SPC(36)    1.344e+14 -1.24    14804
Class(2) + SPC(37) -> Class(3) + SPC(36)    843939    0    -11.843
Class(3) + SPC(36) -> Class(2) + SPC(37)    26574.4    0    -15.292
END

```

Figure 4.24: Reduced chemical reaction scheme from RMG for 2,8-dimethyldecane.

```

SPECIES
Class(1)  R·
Class(2)  ROO·
Class(3)  ROOH
C12H26    C12H26
O2(2)     O2
HO2J(4)   HO2·
C12H25J   R·
SPC(52)   ROO·
H2O2(38)  H2O2
SPC(118)  R·OOH
SPC(186)  ROO·OOH
SPC(187)  R(OOH)2
END

REACTIONS KELVINS MOLES
C12H26 + O2      -> HO2J + C12H25J      4.255e+10  0.808  28549.9
C12H26 + O2      -> Class(1) + HO2J      3.193e-17  0      -70.222
Class(1) + C12H26(1) -> C12H26 + C12H25J      361393    0      -10.64
C12H26 + C12H25J -> Class(1) + 1C12H26      481394    0      -12.591
O2 + 1C12H25J(5) -> SPC(52)      1.410e+13  0      0
SPC(52)          -> 1O2 + C12H25J(5)    1.148e+31 -3.768  21403
Class(1) + O2     -> Class(2)      7.540e+12  0     -2.364e-03
Class(3) + C12H25J -> Class(2) + C12H26      2.25e+08  0     -2.759
Class(2) + C12H26 -> Class(3) + C12H25J      68040.1   0     -13.351
Class(1) + Class(3) -> Class(2) + C12H26      4.237e+11  0      3.469
Class(2) + C12H26 -> Class(1) + Class(3)    1.703e+08  0     -9.074
Class(3) + O2(2)  -> Class(2) + HO2J      1.371e-06  0     -37.209
C12H26 + HO2J     -> C12H25J + H2O2      1.587e+07  1.599  6331.86
C12H26 + HO2J     -> Class(1) + H2O2      9661.01   0     -18.983
SPC(52)           -> SPC(118)      6.760e+10  0.21  9310.1
SPC(118)          -> SPC(52)      5.731e+07  0.827  2262.77
O2 + SPC(118)     -> SPC(186)      7.540e+12  0      0
C12H25J + SPC(187) -> C12H26 + SPC(186)      5.04e-07  5.18  -1021.59
C12H26 + SPC(186) -> C12H25J + SPC(187)      5.746e-04  4.538  3730.82
Class(1) + SPC(187) -> C12H26 + SPC(186)      4.237e+11  0      3.469
C12H26 + SPC(186) -> Class(1) + SPC(187)      1.703e+08  0     -9.0744
Class(1) + C12H26 -> Class(1) + C12H26      482593    0     -13.236
Class(2) + Class(3) -> Class(2) + Class(3)      738446    0     -11.843
END

```

Figure 4.25: Reduced chemical reaction scheme from RMG for 2-methylundecane.

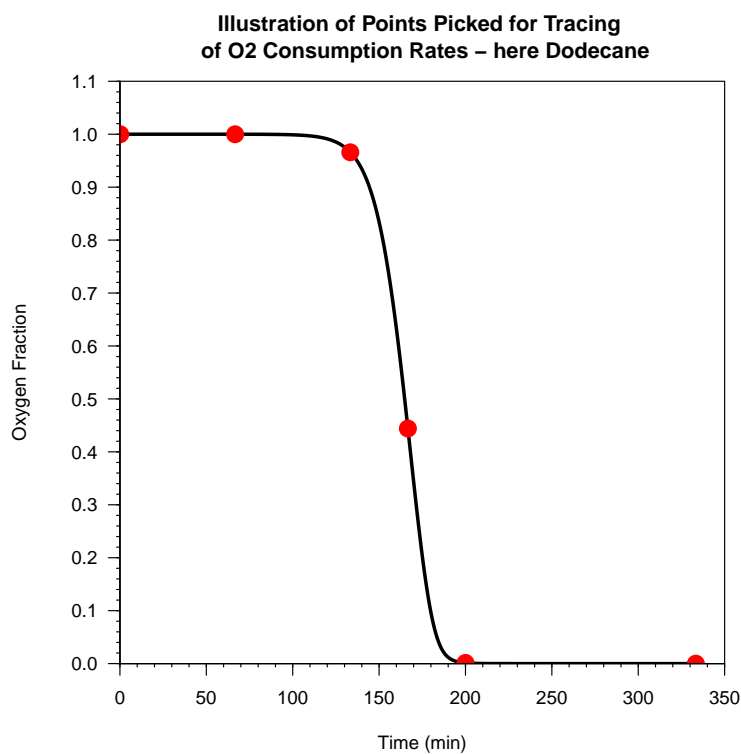


Figure 4.26: Illustration of points picked for a closer inspection of the O<sub>2</sub> consumption rates. For the iso-schemes points at similar locations were chosen.

Phase	Dodecane	2-methylundecane	2,9-dimethyldecane
Buildup	1.258e-10	7.160e-13	1.568e-11
“cliff edge”	1.133e-07	2.726e-09	1.529e-08
rapid consumption	1.004e-06	1.380e-08	8.045e-08
O <sub>2</sub> nearly gone	9.210e-09	6.744e-09	2.791e-08
O <sub>2</sub> consumed	3.454e-15	5.046e-13	9.043e-14
Max O <sub>2</sub> consumption	7.847e-07	1.988e-08	2.045e-09

Table 4.7: Overview of O<sub>2</sub> consumption rates, in mol L s<sup>-1</sup> in a normal paraffinic as well as iso paraffinic RMG scheme.

hydrocarbon products. The resulting plot is shown in Figure 4.27 which suggests that in a liquid phase scheme the half life of the hydroperoxides is about 1000 minutes, well in excess of any residence time in a standard flowing system or a regular solvent test in the PetroOxy without additives.

While Kuprowicz<sup>34</sup> suggests that the decomposition of hydroperoxides leads to the formation of radical products which propagate the reaction chain, RMG predicts no hydroperoxide decomposition, as shown in Figure 4.23. RMG can be forced to decompose hydroperoxides by generating a mechanism for multiple temperatures, including significantly elevated temperatures and in this case the decomposition is faster in the liquid phase scheme than in the gas phase scheme, shown in Figure 4.27 for a temperature of 423 K. This agrees with literature, especially Denisov<sup>147</sup> who suggests that the O–O bond in a hydroperoxide has a bond strength of 38 kcal/mol with a slightly lower bond strength in some liquids. At such a large activation energy, the reaction rate of the decomposition of the hydroperoxides would be comparatively slow, thus it is unlikely to occur in an ideal environment which agrees with the mechanism predicted by RMG which uses a rate based enlarger to determine reaction paths. However, Denisov<sup>147</sup> further suggests that species such as sulfur as well as metal complexes will catalyse or accelerate the decomposition reaction which would apply for regular fuel or even most experimental setups and thus does not contradict RMG which does not predict it.

Another question that arises is what impact a potential hydroperoxide decomposition would have on the rate of oxygen consumption. It is possible to extend a reduced reaction mechanism manually by adding in the reactions and Arrhenius parameters for the hydroperoxide decomposition as published for example by Kuprowicz et al.<sup>34</sup>, as well as adjusting the parameters to evaluate their impact on the reaction mechanism, shown in Figure 4.29. To achieve this, the reduced Dodecane model with fitted Arrhenius parameters was taken and extended with a hydroperoxide decomposition reaction as well as an interaction of the resulting radicals with the bulk fuel, shown in Figure 4.28. A number of adjustments were then evaluated, such as slowing the rate of hydroperoxide decomposition as well as inhibiting the reactions of the decomposition products, with the choices shown in Table 4.8, where the last adjustment was to include a trace hydroperoxide “contamination” in the model to obtain an improved fit when compared to experimental data.

The results show that inclusion of the hydroperoxy decomposition significantly accelerates the oxygen consumption rate over the original model. However by reducing the pre-exponential factor of the decomposition reaction by one order of magnitude to  $1 \times 10^{11} \text{ molL}^{-1}\text{s}^{-1}$ , the agreement of the model with observed data can be improved significantly. In contrast, the model is pretty insensitive to changes in the secondary step of the reaction in which the hydroperoxide decomposition products produce new radicals from a fuel. Raising the activation energy for that reaction to 13 kcal/mol from 0 kcal/mol results in only a minor shift of the oxygen depletion time relative to

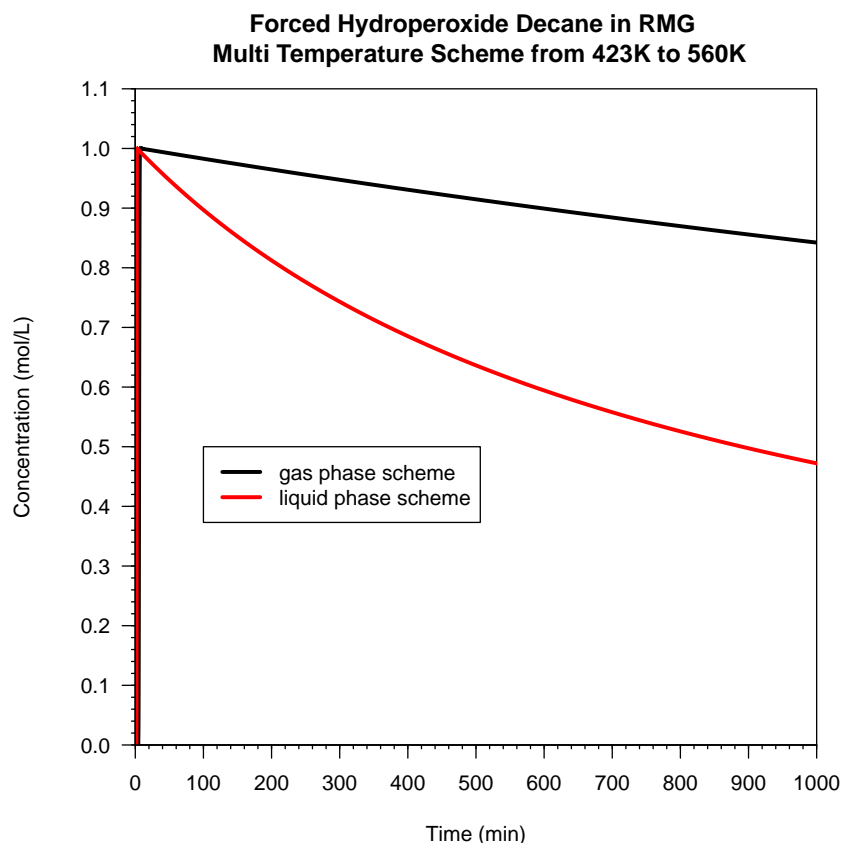


Figure 4.27: Plots of hydroperoxide decomposition in an elevated temperature RMG scheme, solved at 423K.

the very unrealistic parameter change for a radical reaction. Improved agreement of the model can however be achieved by including a trace amount of  $1 \times 10^{-7}$  mol/L of hydroperoxides and raising the activation energy for the decomposition reaction to 45 kcal/mol or higher. However this activation energy appears unreasonably large when compared to literature<sup>147</sup>.

## 4.7 RMG Conclusions

The authors of RMG<sup>127</sup> have created a most interesting tool for in depth studies into the fundamental behaviour of hydrocarbon compounds. The rate based enlarger which investigates all possible reaction paths and picks the most dominant offers us the ability to consider the kinetics of hydrocarbon autoxidation from a fundamental first principles approach. The major benefit of this approach lies in its independence of a priori knowledge about the expected specific kinetics. On the other hand, to produce good schemes, RMG requires a sufficient complete reaction kinetics database which describes the possible interactions between molecules.

$C_{12}H_{26} + O_2$	$\longrightarrow R\cdot + HO_2\cdot$	$4.11 \times 10^{-17}$	0	$-1.40 \times 10^{-1}$
$R\cdot + C_{12}H_{26}$	$\longrightarrow R\cdot + C_{12}H_{26}$	$6.38 \times 10^5$	0	$-2.64 \times 10^{-2}$
$R\cdot + O_2$	$\longrightarrow ROO\cdot$	$7.54 \times 10^{12}$	0	$-4.70 \times 10^{-6}$
$R\cdot + ROOH$	$\longrightarrow ROO\cdot + C_{12}H_{26}$	$4.24 \times 10^{11}$	0	$6.89 \times 10^{-3}$
$ROO\cdot + C_{12}H_{26}$	$\longrightarrow R\cdot + ROOH$	$2.19 \times 10^8$	0	$-1.81 \times 10^{-2}$
$ROO\cdot + HO_2\cdot$	$\longrightarrow ROOH + O_2$	$8.75 \times 10^{11}$	0	$7.75 \times 10^{-3}$
$ROOH + O_2$	$\longrightarrow ROO\cdot + HO_2\cdot$	$1.37 \times 10^{-6}$	0	$-7.40 \times 10^{-2}$
$ROO\cdot + \text{Class}$	$\longrightarrow ROO\cdot + ROOH$	$6.75 \times 10^5$	0	$-2.36 \times 10^{-2}$
$ROOH$	$\longrightarrow RO\cdot + HO\cdot$	$A$	$n$	$E_a$
$C_{12}H_{26} + HO\cdot$	$\longrightarrow R\cdot + H_2O$	$A$	$n$	$E_a$
$C_{12}H_{26} + RO\cdot$	$\longrightarrow ROH + R\cdot$	$A$	$n$	$E_a$

Figure 4.28: Modified reduced mechanism with added hydroperoxide decomposition.

	$A \text{ molL}^{-1}\text{s}^{-1}$	$n$	$E_a \text{ kcal/mol}$
Kuprowicz <sup>34</sup> - Green Line			
$ROOH \longrightarrow RO\cdot + HO\cdot$	$1 \times 10^{12}$	0	39
$C_{12}H_{26} + HO\cdot \longrightarrow R\cdot + H_2O$	$3 \times 10^6$	0	0
$C_{12}H_{26} + RO\cdot \longrightarrow ROH + R\cdot$	$3 \times 10^6$	0	0
Modification 1 - Blue Line			
$ROOH \longrightarrow RO\cdot + HO\cdot$	$1 \times 10^{11}$	0	39
Modification 2 - Turquoise Line			
$ROOH \longrightarrow RO\cdot + HO\cdot$	$1 \times 10^{12}$	0	39
$C_{12}H_{26} + HO\cdot \longrightarrow R\cdot + H_2O$	$3 \times 10^6$	0	13
$C_{12}H_{26} + RO\cdot \longrightarrow ROH + R\cdot$	$3 \times 10^6$	0	13
Modification 3 - Pink Line			
Initial ROOH at $1 \times 10^7 \text{ mol/L}$			
$ROOH \longrightarrow RO\cdot + HO\cdot$	$1 \times 10^{12}$	0	45
$C_{12}H_{26} + HO\cdot \longrightarrow R\cdot + H_2O$	$3 \times 10^6$	0	0
$C_{12}H_{26} + RO\cdot \longrightarrow ROH + R\cdot$	$3 \times 10^6$	0	0

Table 4.8: Tabulated overview of modifications of the Arrhenius Parameters for Figure 4.29.



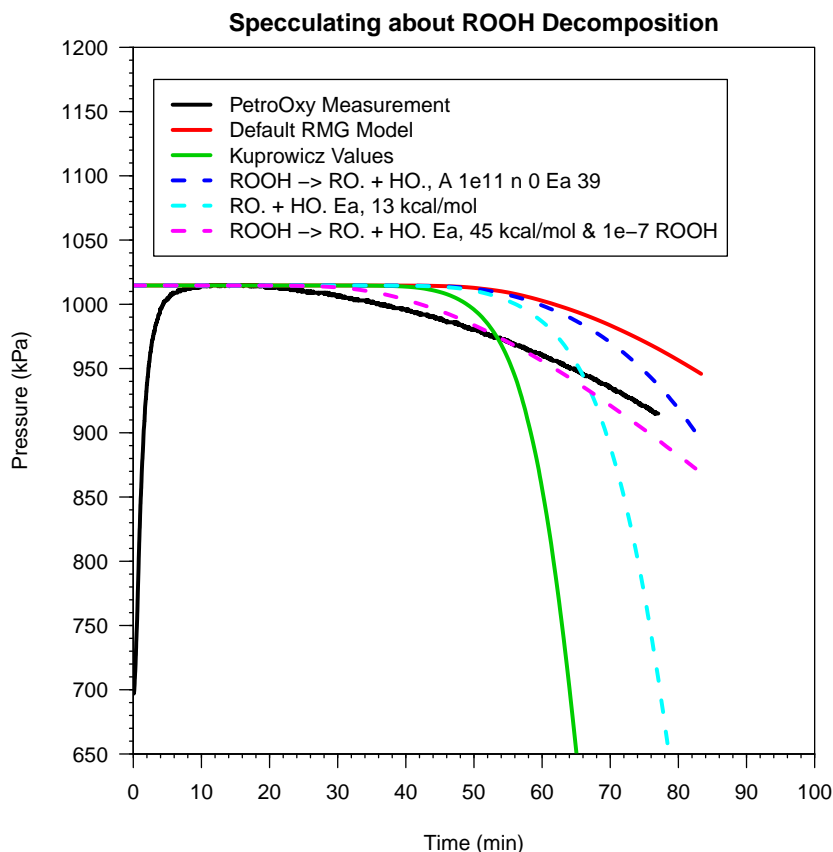


Figure 4.29: Plots of artificially added hydroperoxide decomposition in an RMG scheme, solved at 423K.

Comparing RMG generated mechanisms to published data suggests that RMG produces schemes which exhibit a good agreement with published data in combustion, encouraging further work on thermal stability with RMG and comparisons to thermal stability data. Making a simplifying approximation about the gas to liquid phase transfer in the experimental rig, the PetroOxy, it was found that RMG produces a remarkably good description of the observed behaviour. RMG was able to describe the oxygen depletion rate well for decane, dodecane as well as the commercial  $C_{10}$  to  $C_{14}$  solvent. However, the same cannot be said for iso-alkanes where RMG does not produce a model which represents observations from the PetroOxy. For simple iso structures, RMG produces schemes which upon inspection look reasonable, however for a more complex iso structure like 2,2,4-trimethylpentane RMG fails to produce a suitable looking autoxidation scheme and can only be forced with effort to produce more than just a most basic scheme which does not reproduce the PetroOxy results. This may indicate that the kinetics library in RMG does not contain all of the reactions types needed to simulate autoxidation properly.

Another issue, which is also a benefit, which was identified during this work, is the

continued development of RMG. While issues are fixed in newer releases, it was also found that some previously predicted reactions and products no longer form. For example, initially RMG 3.3 would crash with cyclic species and aromatics, a development build would work with aromatics while RMG 4.1 once again fails with aromatic species.

There is also some inconsistency in the RMG prediction of chemical interactions under similar conditions. RMG can be forced to decompose hydroperoxides if a scheme is drawn up covering a number of temperatures from 423-560 K, however no decomposition is predicted if RMG is run for the same temperatures individually, including the comparatively high 560 K. At the same time, the behaviour of the multi temperature scheme differs remarkably from the single temperature scheme, specifically in that O<sub>2</sub> consumption is significantly more rapid compared to single temperature schemes. However this may be accurate as Denisov<sup>147</sup> suggests a comparatively large activation energy for the hydroperoxide decomposition. On the other hand, elevating the reaction temperature should lead to the inclusion of the decomposition reaction and does not. A further issue in some ways is the reaction time dependence of RMG when generating schemes. Setting a reaction time well in excess of what is needed should not produce a scheme which is significantly different with regards to the initial behaviour of the scheme. However it was found that to obtain a suitable RMG scheme to describe the observed behaviour in the PetroOxy, it is necessary to chose a reaction time representative of the reaction time in the PetroOxy.

## Chapter 5

# Deposits and Precursors in the HiReTS

Blakey and Wilson<sup>148</sup> at the University of Sheffield have identified the chemical compound m-toluidine (m-tol) as being implicated in having a significant detrimental effect on the thermal stability of a synthetic jet fuel. Through collaboration with Blakey and Wilson<sup>148</sup> we have received access to data for a High Reynolds Number Thermal Stability (HiReTS)<sup>149</sup> test rig where they have shown that aromatics such as toluene or naphtalene in significantly larger concentrations than m-toluidine do not have a significant impact on the thermal stability of the same fuel .

This suggested that investigating possible reaction paths of m-toluidine and investigating the difference between it and aromatic species could offer a potential explanation for its hugely detrimental impact on the thermal stability in both a conventional as well as a synthetic fuel. The reported significant and different impact that Blakey and Wilson<sup>148</sup> reported for m-toluidine over aromatic species or neat fuel, further suggested that it should be comparatively easy to identify in any postulated reactions as any differences in the behaviour of these species can be expected to be large. Hence the information provided by Blakey and Wilson<sup>148</sup> offered a very tangible basis for the speculative ab initio investigation of possible interactions between fuel and m-toluidine as well as aromatic species that could lead to deposits.

Testing with a simpler test liquid, such as an industrial solvent, reduces the uncertainty caused by potential trace contaminants in a product as complex as Jet-A and provide a clearer picture of the impact m-toluidine has on the thermal stability of hydrocarbons. Tests with Banner solvents, a normal paraffinic solvent as well as ShellSol T, an iso paraffinic solvent, were carried out to experimentally investigate whether the reported results for conventional fuel as well as synthetic fuel could be reproduced under more controlled conditions.

## 5.1 The HiReTS

The HiReTS is a small scale experimental test rig, designed to enable rapid assessment of the thermal stability of Jet-A aviation fuel in a production environment, such as refineries and airports. As a result, primary focus in the HiReTS lay not so much with research capabilities but with simplicity and automation. An image of the original development prototype nowadays owned and used by the University of Sheffield is shown in Figure 5.1



Figure 5.1: Photograph of the HiReTS Thermal Stability Test Rig.

### 5.1.1 Specifications

When working with the recommended specifications of ASTM D6811<sup>150–152</sup>, the parameters are as follows:

- i)  $<300\ \mu\text{m}$  diameter capillary pipe
- ii) 153 mm length of pipe
- iii)  $>20\ \text{mL}/\text{min}$  flow rate,  $35\ \text{mL}/\text{min}$  flow rate in this work
- iv) 563 K exit temperature,  $\pm 3\ \text{K}$
- v) 65 or 125 minutes test duration
- vi) in a test this mandates 3 L or 5 L of sample fuel

In a test, the pyrometer samples the initial external temperature of the capillary pipe and then continuously cycles over a set section of the capillary pipe throughout the test, recording the external temperature. In the initial design, this covered nine positions which was later expanded to twelve positions, with the initial position to be defined 1 mm below the top bus bar<sup>153</sup>. The measurement positions on the capillary tube are 2.5 mm apart, and a single measurement cycle from the top to the bottom point takes 300 s to complete<sup>154,155</sup>. For a test duration of 125 min this would translate to 25 cycles of pyrometer measurements across the measurement section on the capillary pipe. Figure 5.3 shows a schematic of the capillary mounted between the bus bars.

After the test is complete, the “HiReTS Number” is calculated by summing the observed temperature difference between the recorded minimum temperature over the whole test run and the final temperature, shown in equation (5.1.1).

$$\text{HiReTS Number} = \sum_{n=1}^{12} (T_{final} - T_{min}) \quad (5.1.1)$$

The schematic sketch of the HiReTS is presented in Figure 5.2, while a more detailed outline of the active test section consisting of the mounted capillary pipe is shown in Figure 5.3. During the test, the operator is presented with a plot of the temperature measurements relative to the first measurement cycle. A graph for an unstable jet fuel as well as a solvent test are shown in Figure 5.4. The specifications for the HiReTS states that a HiReTS number of less than 1000 constitutes a pass of the fuel with regards to its thermal stability while a HiReTS number of greater than 1000 constitutes a fail<sup>154</sup>. While not a quantitative measurement, carbon burnoff data suggests that the HiReTS number correlates with the amount of carbon deposited in the capillary pipe, where a larger HiReTS number equates to a larger amount of carbon in the pipe<sup>155</sup>.

### 5.1.2 Test Methodology

When a sample is tested in a standard HiReTS test, in this test series employing a test time of 125 minutes, 5 L of fuel need to be prepared and made available in a suitable fuel drum. To ensure that the sample is saturated with oxygen, air is bubbled through it for about 15 minutes prior to testing. In the HiReTS, a new capillary tube is securely mounted between two bus bars prior to every test. The operator is then required to align the top and bottom position of the pyrometer to ensure that temperature readings are taken from the centre of the capillary pipe. Next, the unpressurised system is flushed with heptane, following which, the system is pressurised, and flushed with heptane again, so to allow the operator to check whether any leaks can be observed around the capillary pipe. If no leaks are observed, the device is ready for testing and the inlet pipe may be placed in the drum containing the fuel sample. After the test the device is flushed with heptane again, ready for another test cycle. Parameters such as flow

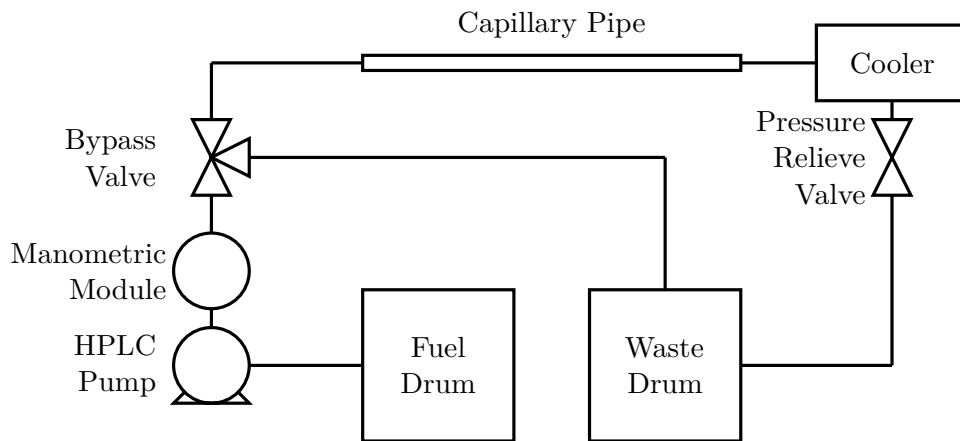


Figure 5.2: Schematic Outline of the key elements of the HiReTS thermal stability tester.

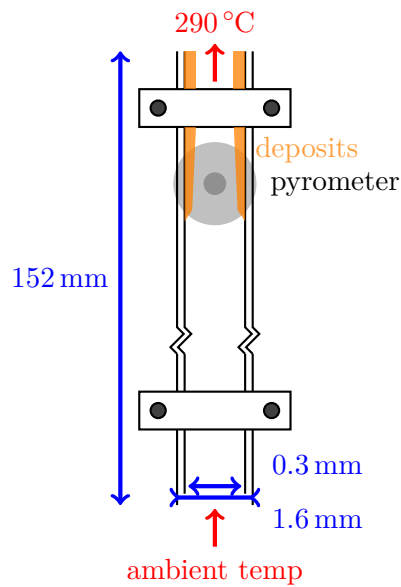


Figure 5.3: Schematic sketch of the capillary pipe test section in a HiReTS test device.

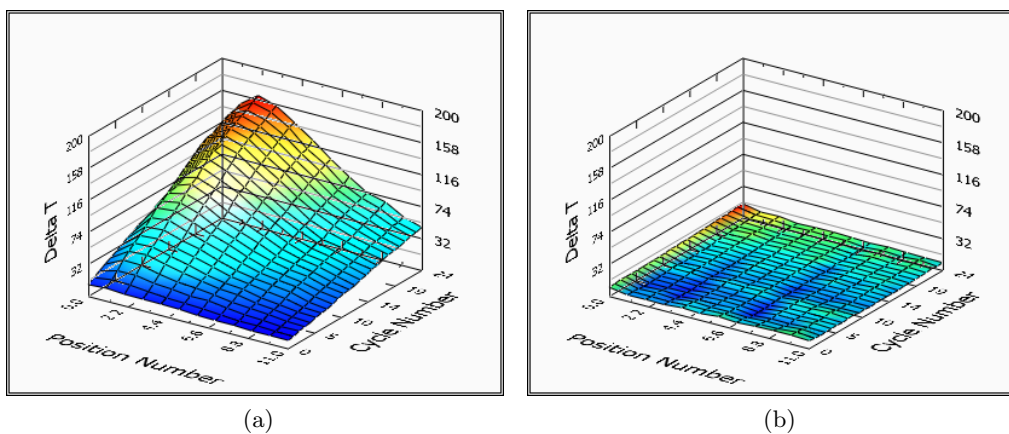


Figure 5.4: Original plots for both a Jet-A and GTL blend showing a peak in Figure 5.4a as well as Banner Solvent showing a flat surface in Figure 5.4b, as generated by the HiReTS interface during a run.

rates and pressure are pre-set and not changed in a standard test and follow the ASTM D6811<sup>150–152</sup> recommendation. A schematic of the key elements of the HiReTS is shown in Figure 5.2.

### 5.1.3 Known Issues

Sheratt et al.<sup>155</sup> have addressed four aspects that are considered potential issues in the HiReTS as well as their resolution:

- i) pressure effects on result  
resolved by using a sufficiently accurate pressure regulator
- ii) aeration of sample, especially when treated with nitrogen for storage  
resolved by mandating 10 minutes of bubbling of air through test sample
- iii) heptane cleaning of equipment  
has not lead to any observed effects
- iv) exit temperature control  
resolved using a platinum resistance thermometer with the widest possible diameter for robustness

In addition, the pyrometer samples every point with a time delay, hence it does not obtain a momentary assessment of the pipe test section temperature during the experiment. The user does not obtain a “running log” of temperature data but rather a set of twelve regularly sampled datasets. However over the course of a 125 minutes experiment this is of no significance. Sheratt et al.<sup>155</sup> have analysed the pipes employed in the HiReTS and found them to be appropriately manufactured (no contamination, similar surface structure), however there is some uncertainty over the interior structure of the pipe as well as interior diameters. It was further noted by Sheratt et al.<sup>155</sup> that a wider bore will result in a higher HiReTS number.

No fluid dynamics studies were found which describe the flow through the HiReTS, however Reynolds numbers of “more than 5000” or  $\gg 10000$ <sup>156</sup> as well as 15000<sup>157</sup> are stated. If one estimates the Reynolds number for the HiReTS employing standard condition data for decane one obtains a value of around 1380 for the Reynolds number in the HiReTS with a flow rate of 35 mL/min on a capillary pipe with a 300  $\mu\text{m}$  diameter, a smaller capillary pipe would increase the value. In addition, hydrocarbons are known to exhibit a significantly lower viscosity and also lower density at elevated temperatures, while elevated pressure increases the viscosity. According to Dymond et al.<sup>158</sup>, a temperature of 373 K would reduce the viscosity from 1.355 mPa s at 1 atm to 0.671 mPa s at 24.1 MPa, which would more than double the calculated Reynolds number to 2770 or 2630 when including the change in density.

Finally, one can question whether the presence of electric current, applied for heating to the capillary tube, may not have an effect on the deposition behaviour. It was also pointed out in personal communication with Blakey<sup>159</sup> that the force with which the nuts on the bus bars are tightened will influence the obtained result leading to further loss of accuracy.

## 5.2 Precursor Concentration and Deposit Formation in HiReTS

Based on the data received from Blakey and Wilson<sup>148</sup>, an attempt is made to identify possible speculative routes to deposit formation. As the reported impact of m-toluidine is large, any postulated reactions should exhibit comparatively large rate to be a viable candidate for explainign the observed behaviour. The HiReTS works by pumping five litres of fuel through a metal pipe which is heated via induction. The exit temperature of the fuel is held constant at 560 K and the surface temperature of the pipe is monitored externally using a pyrometer. Deposits have been shown to have a detrimental effect on the heat transport from the pipe to the fuel and are therefore indirectly measurable through monitoring of the outer surface temperature of the pipe, evident through a rise in the surface temperature of the pipe. Once the experiment has been concluded, the test result is summarized to describe the stability of the fuel. Deposits occur primarily in the last 10-20 mm of the pipe where they will form a deposition layer of between 10-20  $\mu\text{m}$  thickness<sup>148</sup>. This would translate to an approximate volume of deposits of:

- for 20 mm length at 10  $\mu\text{m}$  thickness  
 $20 \times (0.15^2 - 0.14^2) \pi \text{ mm}^3 = 0.18221 \text{ mm}^3$
- for 20 mm length at 20  $\mu\text{m}$  thickness  
 $20 \times (0.15^2 - 0.13^2) \pi \text{ mm}^3 = 0.35186 \text{ mm}^3$

As Blakey and Wilson<sup>148</sup> have shown that in HiReTS tests m-toluidine is of significant importance when it comes to detrimental effects on thermal stability, it is reasonable to assume that the species is involved in the formation of deposits. Therefore, the properties of m-toluidine can be used to obtain an initial estimate for limits in a chemical kinetics simulation that describe the production of deposits, provided that m-toluidine is the dominant contributor of deposits. The specification of m-toluidine is as follows:

- density: 0.999 g/mL
- molar mass: 107.153 g/mol
- this translates to:  $9.3231 \times 10^{-3} \text{ mol/mL}$

Over a fuel sample size of 5 L, this translates to minimum required concentrations of:



- for 20 mm length at 10  $\mu\text{m}$  thickness  
 $0.18221 \times 10^{-3} \text{ mL} \times 9.3231 \times 10^{-3} \text{ mol/mL} \div 5 \text{ L} \approx 3.40 \times 10^{-7} \text{ mol/L}$
- for 20 mm length at 20  $\mu\text{m}$  thickness  
 $0.35186 \times 10^{-3} \text{ mL} \times 9.3231 \times 10^{-3} \text{ mol/mL} \div 5 \text{ L} \approx 6.56 \times 10^{-7} \text{ mol/L}$

These two concentrations form an initial estimate for the required minimum concentrations of precursor species and provide a quantitative value that can be used for a preliminary assessment of the feasibility of any proposed mechanism.

### 5.3 Application - Electrophilic Aromatic Substitution

The SMORS hypothesis suggests that aromatic species in fuel undergo substitution reactions to produce large insoluble molecules<sup>16,38,42</sup>. While Blakey and Wilson<sup>148</sup> have shown that not all aromatics are universally reactive, m-toluidine is a suitable candidate for electrophilic aromatic substitution reactions, given that the amine and methyl groups have a favourable impact on reactivity<sup>160</sup>. Therefore, the activation energies for the reaction of a number of aromatic compounds are investigated using computational chemistry methods to assess the feasibility of a liquid phase interaction between m-toluidine, other aromatics and a suitable reactant.

Electrophilic aromatic substitution reactions require a polar species that is susceptible to attack by the aromatic. The primary candidates for substitution reactions in m-toluidine doped synthetic fuel are oxygenated species such as aldehydes, ketones or carboxylic acids. Figure 5.5 shows a proposed electrophilic aromatic substitution reaction between m-toluidine and propionaldehyde.

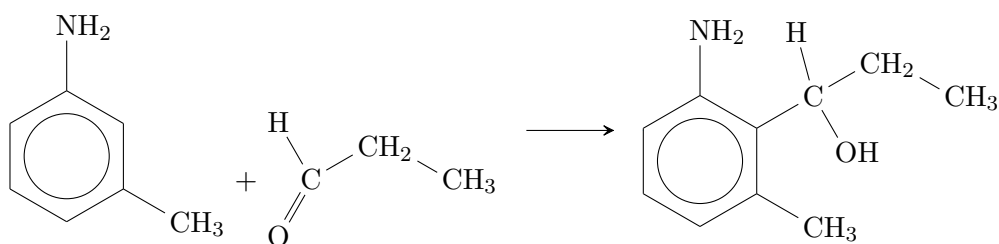


Figure 5.5: Electrophilic addition reaction between m-toluidine and propionaldehyde.

To test this hypothesis, the reaction path and corresponding energies of postulated electrophilic aromatic substitution reactions between m-toluidine as well as m-xylene, toluene and benzene, under solvation in decane, were investigated using Gaussian 09<sup>134</sup>. These estimates enable us to assess the feasibility of a liquid phase reaction leading to the formation of sufficient deposition precursors. Another species suspected of affecting thermal stability are hydroperoxides, however these were found to not exhibit significant polarity in a Gaussian 09<sup>134</sup> calculation and therefore do not constitute a suitable candidate for substitution reactions despite their prevalence in thermally stressed fuel.

Results are obtained by first building the reactants in Gaussian 09<sup>134</sup> and optimizing them. In a second step, the optimized structures are arranged in a manner such that a molecular interaction is favourable. The bonds to be broken are lengthened by about 20% while the atoms due to react were moved closer together to around 120% of a typical bond length when bonded. Specifically, for electrophilic aromatic substitution, the C=O bond was lengthened while the O-H distance was reduced. The main carbon atoms that would bond together were positioned so that their distance was about 2 Å apart while taking care to ensure that no atoms would be positioned too closely together so that their interaction would lead to a calculation error. Where appropriate this could involve reorientating alkyl groups or atoms, for example by rotation. The structure was next duplicated and rebonded to form the product and a QST2 calculation was employed to obtain a transition state.

A frequency calculation was used to verify that a transition state has been found, identifiable by the presence of a single imaginary (negative) frequency and an intrinsic reaction co-ordinates (IRC) calculation was used to verify that the obtained transition state corresponds to the transition state in the desired reaction path. The energies of the reactants, the transition state as well as the product are calculated in Gaussian 09<sup>134</sup> and were extracted from the finished calculation to obtain the energy gap between reactants and the transition state, an estimate for the activation energy in a chemical reaction scheme. A number of calculated energies are given in Table 5.1 for both direct addition reactions as well as a number of reactions that proceed via a reasonably stable intermediary, an example of which is shown in Figure 5.6.

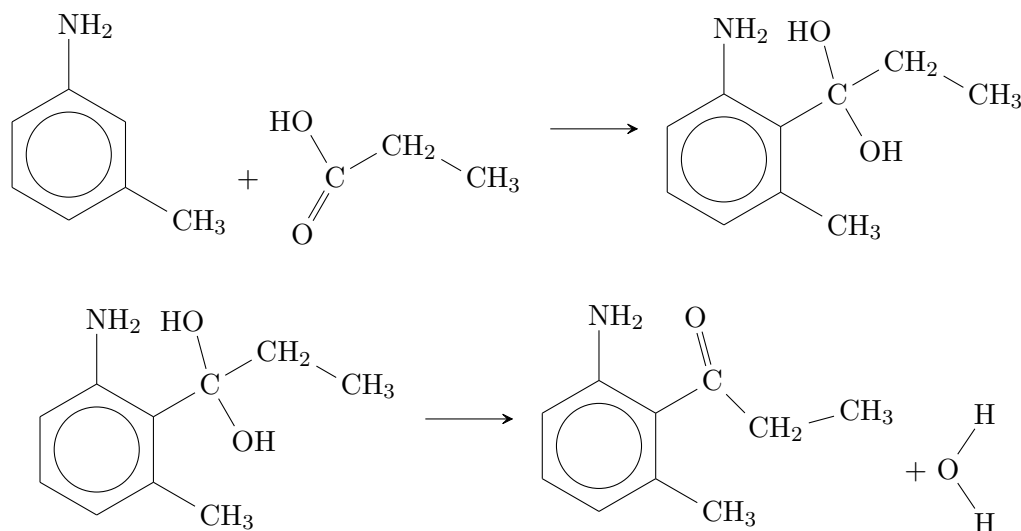


Figure 5.6: Two step Electrophilic addition reaction between m-toluidine and propanoic acid in which water is released.

The calculated activation energies for electrophilic aromatic substitution reactions were found to be comparatively and unexpectedly large. As can be seen in Table 5.1, the

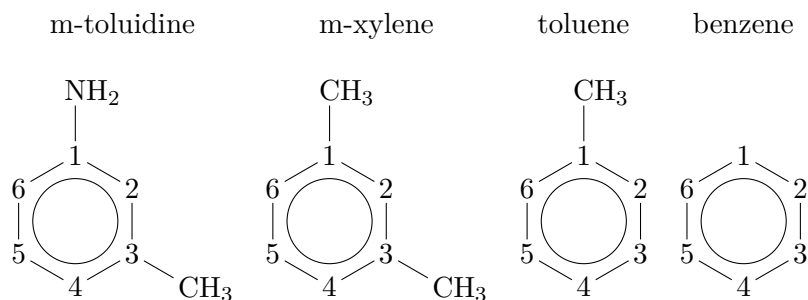


Figure 5.7: Numbering scheme to identify the position at which an aromatic substitution reaction takes place in connection with Table 5.1

energies required for the reaction to proceed are relatively similar across m-toluidine, m-xylene, toluene and benzene with an overall activation energy of around 300-360 kJ/mol for both single and two step reactions. It was expected that m-toluidine would exhibit a significantly lower activation energy to explain its propensity to form deposits in contrast to other aromatic compounds, to explain the effect shown by Blakey and Wilson<sup>148</sup>. The calculated activation energies however show no evidence of m-toluidine being sufficiently more reactive to explain its behaviour in the HiReTS tests.

For analysis purposes, a very fast reaction between aldehydes and m-toluidine, with a pre-exponential factor,  $A$ , set to  $1 \times 10^{13} \text{ L mol}^{-1} \text{ s}^{-1}$ , was added to an RMG-generated autoxidation scheme. The calculated activation energy is approximated at 60 kcal/mol, the lower bound for the calculated activation energy,  $\pm 10$  kcal/mol and 0 kcal/mol are included as a reference and then solved in a time dependant chemical kinetics simulation. A logarithmic plot of the concentration development of the product over time appropriate for modelling a HiReTS<sup>149</sup> test is shown in Figure 5.8.

Assuming a 100% deposition rate of any precursors with properties similar to m-toluidine, using the estimate from Section 5.2 which specifies a minimum concentration of  $3.40 \times 10^{-7} \text{ mol/L}$ , it can be seen from Figure 5.8 that a purely non-catalytic liquid phase mechanism is insufficient to describe the process by which deposits form. The variation of around 18 orders of magnitude between the required precursor concentration and the predicted precursor concentration is too significant as to be an artefact of modelling inaccuracies. Only the reference reaction with an activation energy of 0 kcal/mol produces a concentration of deposit precursors that is sufficient to explain the observed deposition assuming all or nearly all precursors deposit. This suggests that the postulated mechanism to deposit formation is not a feasible route and alternative paths should be explored.

Reactants		Position & Note	Energy kJ/mol
m-tol	propionaldehyde	2 step 1	139.915
m-tol	propionaldehyde	2 step 2	149.047
m-tol	propionaldehyde	4	269.274
m-tol	propionaldehyde	6	269.908
m-tol	propionaldehyde	6 step 1	148.420
m-tol	propionaldehyde	6 step 2	239.546
m-tol	propanoic acid	2 path 1	360.082
m-tol	propanoic acid	2 path 2	327.951
m-tol	propanoic acid	4	334.367
m-tol	propanoic acid	6 step 1 H <sub>2</sub> O released	199.801
m-tol	propanoic acid	6 step 2 H <sub>2</sub> O released	131.302
m-tol	propanoic acid	step 1, imine product	162.762
m-tol	propanoic acid	step 2, imine product	191.165
m-xylene	acetone	4	335.370
m-xylene	acetone	4	335.309
m-xylene	propionaldehyde	2	315.307
m-xylene	propionaldehyde	4	316.916
toluene	acetone	2	339.794
toluene	acetone	4	326.152
toluene	propionaldehyde	2	311.996
toluene	propionaldehyde	2	308.339
toluene	propionaldehyde	4	305.176
benzene	acetone		331.073
benzene	propionaldehyde	1	307.915
benzene	propanoic acid	1 path 1	337.396
benzene	propanoic acid	1 path 2 H <sub>2</sub> O released	314.832

Table 5.1: Energy gaps between reactants and the transition state as calculated by Gaussian 09 for a number of reactant combinations. Steps one and two denote a reaction with a predicted relatively stable intermediary step. The number denotes the position in the aromatic ring at which the substitution takes place based on the numbering in Figure 5.7.

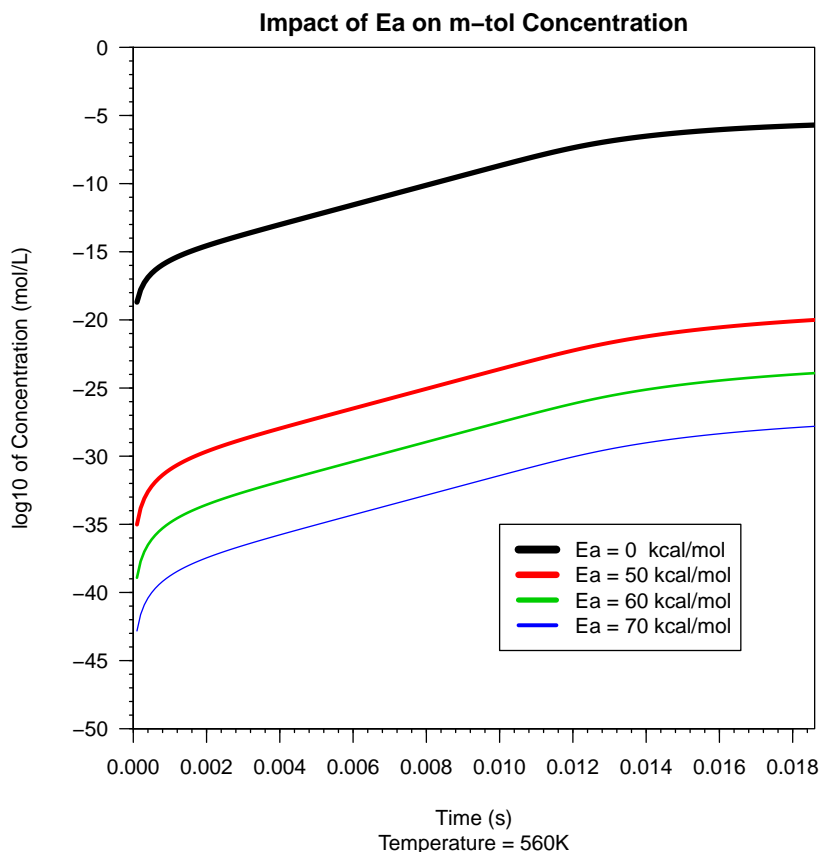


Figure 5.8: Logarithmic plot of the concentration development over time for the reaction  $m\text{-toluidine} + \text{aldehyde} \longrightarrow \text{product}$

A question that arises from this result is how large the activation energy can get before the concentration of deposit precursors becomes too low assuming a 100% deposition rate. This was resolved by running a chemical kinetics simulation for varying activation energies using the same high pre-exponential factor of  $1 \times 10^{13} \text{ L mol}^{-1} \text{ s}^{-1}$ . The output suggests that the maximum activation energy would lie around 20 kcal/mol before the product concentrations becomes too low to be of significance in the deposition process. While this is not a particularly low activation energy, in relation to the estimates obtained from the Gaussian 09<sup>134</sup> calculation, it is equivalent to roughly 30% of the predicted activation energy of all deposit precursors.

This significant discrepancy between the theoretical model and the observed results suggests that the process cannot be explained solely through a liquid phase reaction but depends on surface catalytic effects in the pipe.

## 5.4 Amine Alkene Reaction

Amines are known to undergo polymerisation reactions, both in the form of addition as well as condensation reactions. The initial step of a polymerisation of an amine with an alkene is illustrated in Figure 5.9. The polymerisation of amines with an alkene was investigated using Gaussian. The alkene double bond can be exposed or more central, the amine can also attach to either of the carbons involved in the carbon-carbon double bond.

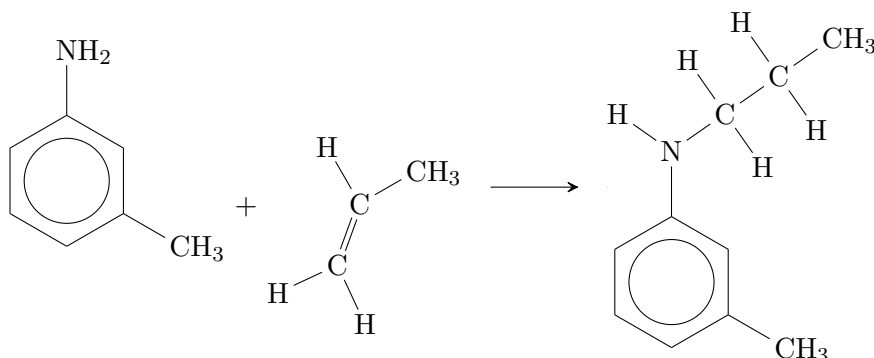


Figure 5.9: Schematic polymerisation between m-toluidine and an alkene.

Activation energies were calculated for such reactions and found to be equally high as for electrophilic aromatic substitution with values shown in Table 5.2.

## 5.5 Surface Effects

As it was shown in Section 5.3 that a purely liquid phase process can be ruled out, surface effects are the most probable explanation for the observed phenomena. To estimate the effect of a postulated surface effect, it is necessary to either determine or estimate the collision rate with the pipe surface.

For gases, the work of Baldwin and Howarth<sup>161</sup> provides an estimate for the surface collision rate of gas molecules in a cylinder under static conditions on the basis of the kinetic theory of gases<sup>88</sup>. As the HiReTS exhibits a turbulently mixed flow, the simplifying assumption that the kinetic theory of gases can be used to approximate the relevant parameters to describe the postulated chemical reactions in the liquid phase is made. Given the assumption that the surface is very efficient, hence that all molecules that collide with the surface terminate at the surface, Baldwin and Howarth<sup>161</sup> provide a limit for the surface termination rate under static conditions in a cylindrical pipe, given in equation (5.5.1), where  $D$  is the diffusion coefficient and  $r$  the radius of a cylindrical pipe.

$$k_s = 8D/r^2 \quad (5.5.1)$$

Reactants		Activation Energy kJ/mol
pentene-1	butylamine	255
pentene-1	aniline	264
pentene-1	butylamine	254
pentene-2	butylamine	235
pentene-2	butylamine	220
pentene-2	m-toludine	252
pentene-2	aniline	254
hexene	butylamine	249
hexene	m-toludine	281
hexene	aniline	284
hexene	butylamine	264
benzene	butylamine	289
benzene	m-toludine	316
benzene	aniline	319
toluene	aniline	316
toluene	aniline	332
toluene	butylamine	295
toluene	butylamine	287
toluene	m-toludine	327

Table 5.2: Activation energies for the polymerisation/addition of an amine and an alkene as well as an aromatic ring. Calculations were carried out to consider various positions and hence varying accessibility of the carbon-carbon double bond.

Literature suggests methods to estimate the diffusion coefficient for liquids, such as the work by Wilke and Chang<sup>121,162</sup> shown in Equation (5.5.2) or Hayduk and Minhas<sup>121,163</sup> shown in Equation (5.5.3) who derived a diffusion estimate for paraffinic liquids only.

$$D_{AB}^0 = \frac{7.4 \times 10^{-8} (\phi M_B)^{1/2} T}{\eta_B V_A^{0.6}} \quad (5.5.2)$$

$$D_{AB}^0 = 13.3 \times 10^{-8} \frac{T^{1.47} \eta_B^\epsilon}{V_A^{0.71}}, \quad \epsilon = \frac{10.2}{V_A} - 0.791 \quad (5.5.3)$$

In Equations (5.5.2) and (5.5.3),  $D_{AB}^0$  denotes the diffusion coefficient for a low concentration of solute A in solvent B. The properties of the solvent are included through  $M_B$  denoting the molecular weight of solvent B in g/mol,  $\eta_B$  the viscosity of solvent B in cP, and  $V_A$  the molar volume in cm<sup>3</sup>/mol of solute A at its normal boiling temperature<sup>121</sup>.

To employ Baldwin and Howarth's<sup>161</sup> equation, a diffusion coefficient is required that includes the mixing effect as a result of the turbulent flow in the HiReTS test pipe and not only the inherent diffusion through liquids. Taylor<sup>164</sup> published a study that aims to provide an estimate for what he calls a "virtual coefficient of diffusion" to incorporate the effects of mixing that would occur in a turbulent flow, shown in Equation (5.5.4).

$$K = 10.1r \left( \frac{\tau_0}{\rho} \right)^{1/2} \quad (5.5.4)$$

In Taylor's<sup>164</sup> expression,  $\tau_0$  is the "friction stress" or "shear stress" in the fluid while  $r$  is the radius of the pipe. As some parameters are not available in published literature, it is unavoidable that their values are approximated. The molar volume of solute A at its normal boiling temperature,  $V_A$ , is not available for m-toludine, therefore the value for toluene was chosen instead. For Taylor's<sup>164</sup> expression, the shear stress had to be approximated and was set to  $\tau_0 = 800\text{Pa}$  from a simple smooth surface two dimensional Fluent<sup>46</sup> simulation. If the appropriate parameters are inserted into Equations (5.5.2), (5.5.3) and (5.5.4), the following diffusion coefficients are obtained.

- 1955, Wilke & Chang:  $D_{AB}^0 = 4.328 \times 10^{-6}\text{cm}^2\text{s}^{-1}$
- 1982, Hayduk & Minhas:  $D_{AB}^0 = 2.863 \times 10^{-6}\text{cm}^2\text{s}^{-1}$
- 1954, Taylor:  $K = 1.5364 \times 10^3\text{cm}^2\text{s}^{-1}$

Next Baldwin and Howarth's<sup>161</sup> formula for an efficient surface is applied, shown in Equation (5.5.1) to give the following rate constant estimates:

- 1955, Wilke & Chang:  $A = 1.539 \times 10^{-1}\text{cm}^2\text{s}^{-1}$
- 1982, Hayduk & Minhas:  $A = 1.018 \times 10^{-1}\text{cm}^2\text{s}^{-1}$
- 1954, Taylor:  $A = 5.455 \times 10^5\text{cm}^2\text{s}^{-1}$

These values are then tested in a simple postulated reaction, m-toluidine  $\xrightarrow{\text{surface}}$  deposit. Assuming an initial activation energy of zero results in the concentration time development of the product shown in the graph in Figure 5.10. As can be clearly seen, the diffusion terms from Wilke and Chang<sup>162</sup> as well as Hayduk and Minhas<sup>163</sup>, applicable to diffusion under static conditions would not lead to the production of a sufficient concentration of deposit, given the limit estimated in Section 5.2, of at least  $3.40 \times 10^{-7}\text{mol/L}$ . The formula from Taylor<sup>164</sup> however leads to an estimate in excess of the estimated minimum concentration of depositing species required, which is ideal as the estimate from employing Baldwin and Howarth's<sup>161</sup> method presents an upper limit for efficient surface termination.

Further testing on this basis reveals, that a combination of Taylor's<sup>164</sup> virtual diffusion coefficient as well as Baldwin and Howarth's<sup>161</sup> estimate for the surface collision rate would allow for a maximum activation energy of around 13kcal/mol before the concentration drops below the minimum requirement of  $3.40 \times 10^{-7}\text{mol/L}$  estimated in Section 5.2.

These results would suggest that the postulated catalytic surface effect in the deposition process provides a feasible route that results in sufficient product for deposition in a chemical kinetics simulation.



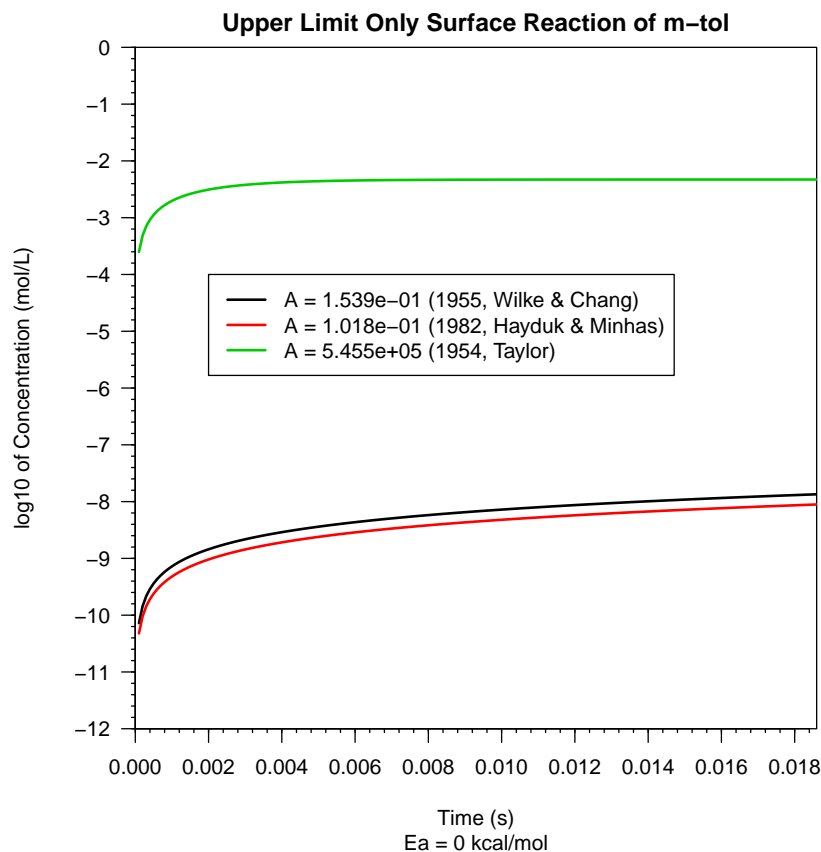


Figure 5.10: Plot of the effect of estimated ideal case limits for the pre-exponential factor  $A$  given an activation energy of zero.

## 5.6 Deposition Process - Initial Conclusion

The results presented in Section 5.3 suggest that a mechanism towards deposit formation cannot be described by a purely liquid phase process. The energy barriers to the reactions are found to be too high to lead to any measurable concentration of product, even for a fast pre-exponential Arrhenius coefficient.

This result strongly suggests that the mechanism by which deposits form includes either catalytic effects of trace metals or catalytic surface effects from the heated pipe. Given that Blakey and Wilson<sup>148</sup> have shown that a synthetic fuel exhibits significantly reduced thermal stability after the addition of m-toluidine, influence from dissolved metals may be ruled out in the HiReTS results. In regular aviation fuel however, trace metals may be a significant contributing factor to deposit formation. Hence the only practical explanation of the surface deposits phenomena needs to consider the effect of surface interactions between m-toluidine as well as other hydrocarbon components in the fuel.

The results presented in Section 5.5 suggest that a surface reaction of just m-toluidine in

a chemical reaction mechanism may produce sufficient product to explain the deposition layer in the HiReTS test rig, even when a small activation energy is included in the reaction. However, the nature of the HiReTS does not allow for any direct validation of any proposed mechanisms and can only enable a speculative assessment of proposed mechanisms.

## 5.7 HiReTS Experimental Work

As the High Reynolds Thermal Stability (HiReTS) tester is a small scale experimental test rig, designed around comparatively small fuel samples and short test durations, it offered an enticing test platform following the theoretical investigation of deposit formation which offered no definite route to deposit formation. As Wilson and Blakey<sup>148</sup> provided results obtained from a GTL fuel that consists of normal paraffinic and iso paraffinic hydrocarbons, which suggested that m-toluidine exhibited a significant negative behaviour on thermal stability, it was decided to investigate this further by simplifying the test conditions. Solvents with components representative of the major constituents of a GTL fuel were purchased, from which it was hoped to evaluate the behaviour of the individual fuel components to obtain a better understanding of the behaviour of m-toluidine in the HiReTS.

These solvents are Banner Solvent np1014 which consists primarily of normal alkanes from C10 to C14, and ShellSol T which is an iso-paraffinic solvent of similar molecular weight. A 50/50 blend of the normal and iso paraffinic solvents was also evaluated, in all cases with and without m-toluidine. HiReTS repeatability was evaluated by running a Jet-A and GTL blend through the HiReTS as well as by running the same normal paraffinic solvent through the HiReTS in a neat condition. The results that were obtained from the test series are shown in Table 5.3.

## 5.8 HiReTS Conclusion

As can be seen from the data gathered, shown in Table 5.3, m-toluidine did not exhibit any negative impact on the HiReTS number for both Banner solvent as well as Shellsol T. This is in contrast to the results provided to us by Wilson and Blakey<sup>148</sup> with GTL as well as Jet fuel which showed a propensity to exhibit elevated HiReTS numbers when doped with m-toluidine. In the tests m-toluidine may even be considered to have improved thermal stability in some cases. At the same time, the observed HiReTS numbers of around 50 mean that any variation is primarily attributable to both noise and experimental variation in the HiReTS rather than observed chemical effects. While this does agree with the prior theoretical study that offered no definite route to deposits, it leaves the behaviour of GTL unexplained.

Date	HiReTS Number		Pipe Batch	Fuel	Additives m-Tol
	Total	Peak			
16/12/13	760.21	126.76		80% Jet-A 20% GTL <sup>a</sup>	
16/01/14	63.10	8.53	3504	Banner Sol	
20/01/14	25.58	4.29	3504	Banner Sol	
11/02/14	25.08	2.86	3504	Banner Sol	5 mL
11/02/14	52.21	6.83	4604	Banner Sol	5 mL
20/01/14	15.53	2.22		Banner Sol	5 mL
16/12/13	17.49	3.40	0803C	Tsol	
16/01/14	16.70	3.11	3504	Tsol	5 mL
17/02/14	13.58	2.40	3504	50% Banner 50% Tsol	
17/02/14	9.85	2.65	3504	50% Banner 50% Tsol	25 mL
18/02/14	47.45	5.19	3504	Banner Sol <sup>b</sup>	
19/02/14	1243.17	162.99	3504	80% Jet-A 20% GTL	
19/02/14	1393.86	169.67	3504	80% Jet-A 20% GTL	

<sup>a</sup> The last two cycles missing - final result would be around 850.

<sup>b</sup> A long term run of 15L over 6h. Values after 125 minutes are 10.80 and 1.85.

Table 5.3: Results of HiReTS runs for various solvent and fuel combinations.

The test to test variation with a GTL Jet-A blend, both which failed the pass criteria for aviation fuel, is also cause for further concern as relative accuracy improves with higher HiReTS numbers and raises additional questions about the suitability of the HiReTS as a thermal stability test device. In the context of this investigation, the HiReTS was found to not be reliable and suitable for further investigations into the thermal stability of hydrocarbon compounds. Such problems with the HiReTS may very well explain the lack of wide adoption and the eventual withdrawal of the HiReTS as an ASTM test method in 2013

As a research tool the HiReTS also offers only limited scope for fundamental work. Post test sampling is subject to considerable uncertainty as cross contamination between tests can occur when the sample has passed the test section and enters the cooler where residue builds up over time. In addition, analysis of the deposits formed in the capillary is not possible as the pipe surface cannot be accessed easily. As a result, validation attempts of any postulated model in the HiReTS are rather speculative and the HiReTS can only provide vague limits for postulated reactions.



## Chapter 6

# Assessing Thermal Stability with the PetroOxy

### 6.1 The PetroOxy - A Look at the Device

The PetroOxy, shown in Figure 6.1, is an industry standard small scale, static, thermal stability test device designed to offer industry a fast and reliable method of establishing the thermal stability and thus suitability of fuel. Anton Paar have established the suitability of the PetroOxy for regular petrol, diesel, biodiesel and grease which thus are preprogrammed in the machine<sup>145</sup>. The PetroOxy has previously been used by Sicard et al.<sup>59-61,64</sup> who used it to evaluate the behaviour of both jet fuel and a number of solvents under autoxidation conditions. Due to its small scale and well controlled environment, the PetroOxy offers an excellent opportunity to study the chemistry of autoxidation in fuels as well as the impact of various additive compounds in a comparatively reproducible manner. The PetroOxy further allows the user to retain the sample at the end of the test without the possibility of contamination from other sources, such as the cooler on a larger scale rig.

### 6.2 Experimental Methodology

#### 6.2.1 Sample Preparation

A standard PetroOxy test employs a 5 mL sample of test liquid<sup>145</sup> which must hence be available or prepared. For neat tests, a sample can be measured out directly into the PetroOxy using a suitable measuring device such as a pipette or pipettor. Where blends are employed, the mixing must take place before the sample is placed in the PetroOxy to ensure an accurate measurement of the test sample volume. In this thesis, 10 mL of test fuel or solvent were added to a glass container to which the dopant was then added, to cover any losses such as coating the surface of the pipettor as well as glass vessel used for mixing. For ease of use, ratios are employed as opposed to volume percentages, thus to

10 mL of dodecane, 200  $\mu$ L of the dopant would be added to achieve a 50:1 ratio. 5 mL of the blended sample can then be accurately measured out for testing in the PetroOxy.

### 6.2.2 PetroOxy Usage

The PetroOxy consists of a gold dish for 5-10 mL of sample, with a schematic cross section provided in Figure 6.2. The seal is a viton ring, PTFE coated while the lid for the dish is gold as well. The user is required to attach the seal to the dish as well as to place or add the sample to the dish. Following, the lid is screwed on and the insulating hood closed. When the program is started, the PetroOxy adjusts the temperature to 25 °C. Next it is automatically pressurized to the target pressure through the gas inlet, then if desired, vented once (or more often) followed by a final pressurization after which it is ready to start. The temperature is raised to the desired test temperature and the current pressure as well as temperature are recorded throughout the test. If the user opts for logging the data on a PC, a higher sampling rate may be used and power input as a percentage of maximum power is recorded as well.

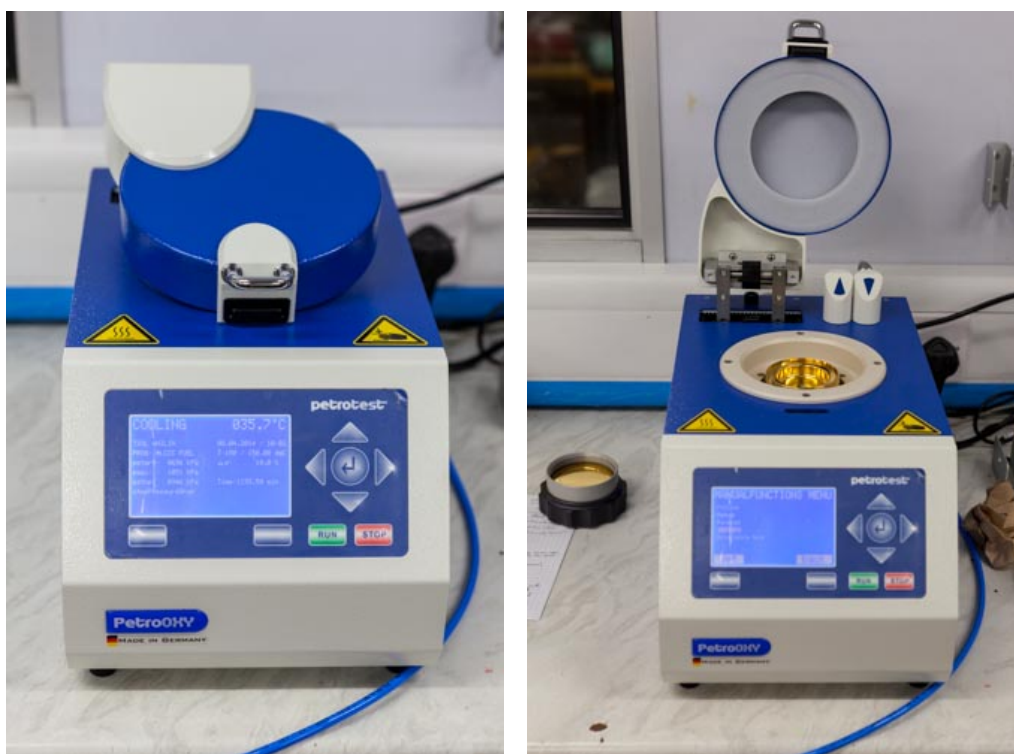


Figure 6.1: The PetroOxy, in operation and ready for use.

The PetroOxy will maintain the temperature, making minor corrections where necessary until the termination criteria is reached. This is defined as either a percentage pressure drop below the maximum pressure (10% for a standard test) or alternatively a test time or combination of both, whichever occurs first. When this point is reached, the time taken is recorded and the PetroOxy will cool the sample to 20 °C, after which it

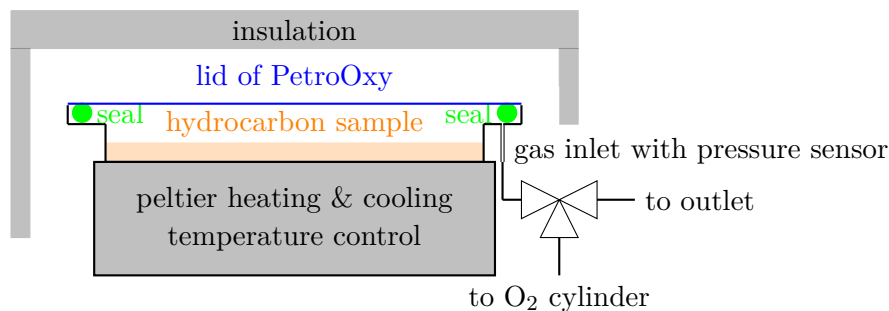


Figure 6.2: Schematic side view of the PetroOxy.

vents the dish. The sample may be retained for further analysis or disposed of, the gold dish is cleaned with a tissue, optionally acetone or ethanol, and the gas inlet is purged automatically to remove any residue liquid. The PetroOxy is further supplied with a PTFE dish as an unreactive vessel for tests of grease or other very viscous samples, however it can also be employed to avoid liquid phase contact between the test sample and the gold dish. This work follows the test regime employed for diesel, which is also the regime chosen by Sicard<sup>61,62</sup> in his investigation. This uses a 5 mL sample, vents the PetroOxy once and re-pressurizes it to 700 kPa with a thermal stress temperature of 150 °C and a 10% pressure drop in the headspace as a test termination criteria.

### 6.3 Test Series

The test series investigated the behavioural differences under thermal stress of a jet fuel blend, a synthetic jet fuel as well as solvents representative of aviation fuel components. In this case this is a 20% GTL 80% Jet-A blend, a synthetic GTL fuel as well as ShellSol T, an industrial solvent of iso alkanes, Banner Solvent np1014, an industrial solvent of C<sub>10</sub> to C<sub>14</sub> normal alkanes as well as dodecane and trimethylpentane from Sigma Aldrich, with the known specifications shown in Table 6.1.

	aromatics % weight	benzene	sulfur	purity
Banner nP1014	< 0.030	< 1 ppm	< 1 ppm	
ShellSol T	< 0.01	< 30 mg/kg	< 1 mg/kg	
dodecane (Sigma Aldrich)				> 99%
decane (Merck)				94%
2,2,4-trimethylpentane				> 99%

Table 6.1: Specification for fuel/solvents employed in the test series.

Initially the difference between the behaviour of the individual compounds in a PetroOxy test was established. Following that it was established whether the gold dish or a 4 cm<sup>2</sup> 316 stainless steel metal foil would exhibit any influence on the behaviour of the compounds. Lastly tests were carried out with additive components which consisted of

amines which are suspected of being present in fuels and aromatic compounds which are present in regular jet fuel as well as sulfur compounds which are known to produce deposits and generally considered to be undesirable<sup>42,165,166</sup>. Both the suppliers and stated purities of the additives are shown in Table 6.2 while a tabulated overview of the tests is given in Table 6.3.

compound	supplier	purity
butylamine	Sigma Aldrich	99.5%
aniline	Sigma Aldrich	99%
m-toluidine	Alfa Aesar	99%
p-xylene	VWR International	100%
toluene	VWR International	100%
benzene	Sigma Aldrich	99%
1,4-diaminobutane	Sigma Aldrich	99%
m-phenylenediamine	Sigma Aldrich	99%
dibutylsulfide	Sigma Aldrich	99%
dibutyldisulfide	Sigma Aldrich	97%

Table 6.2: Specification for additives employed in the test series.

test compound	ratio	additive	extras
Banner np1014	50:1	amine, aromatics	PTFE dish, metal foil
ShellSol T	50:1	amine, aromatics	PTFE dish, metal foil
GTL	50:1	amine	
GTL with Jet-A	50:1	amine	PTFE dish, metal foil
Dodecane	500:1	sulfide, disulfide	metal foil
Trimethylpentane	500:1	sulfide, disulfide	metal foil

Table 6.3: Overview of tests carried out in the PetroOxy.

In addition, gas chromatography mass spectrometry was employed to attempt to qualitatively identify compounds in both the solvent and jet fuel blend, however due to the complexity of the solution only major compounds can be identified with any certainty. Where metal foils were employed, a number of samples were investigated more closely using SEM EDX to determine the morphology of any deposits and to assess the elemental composition of the deposits. In addition, high resolution images were obtained, some of which are reproduced here, using a Canon 5D MK II with a 100mm f2.8 IS USM L macro lens, recording raw files and post processing these in Capture One Pro 7.2.3.



## 6.4 Experimental Results and Observations

### 6.4.1 Repeatability of the PetroOxy

The repeatability of the PetroOxy tests was investigated and found to be excellent for laboratory grade dodecane, with times shown in Table 6.4. The outlier from the 4<sup>th</sup> test in the repeatability series most likely stems from contamination from a prior amine test as the tissue stained yellow, which was not the case in the other neat dodecane tests. Normally dodecane is found to be perfectly clear and the tissue used to clean the dish is found to be visibly clean too. However in this one case it stained from residue not removed from the previous test.

	Test Date	Time (min)
1)	17/03/14	75.30
2)	25/06/14	79.01
3)	25/06/14	75.38
4)	26/06/14	69.70
5)	26/06/14	77.05

Table 6.4: Repeatability of tests in the PetroOxy using Dodecane - test 4 suffered from a contaminated dish from the previous test.

This suggests that the PetroOxy is very sensitive to minor changes in the chemical composition of the test sample. To verify this conclusion, Shellsol T, a commercial solvent which had been stored undisturbed for a number of days was sampled from the top, middle and bottom of the bottle followed by a well mixed sample for the final run. In this test series it was observed that the bottom sample exhibited visible “bubbles” of a separate liquid phase at the bottom of the gold dish which suggests a separation of the components had occurred. The test results are shown in Table 6.5.

sampling location	Time (min)
top	24.38
middle	25.23
bottom	32.15
well mixed	27.31

Table 6.5: Sampling from different locations in the bottle of Shellsol T, a commercial solvent.

Thus it may be concluded that storage of complex solvents can lead to a compositional change in the solvent that influences the test results. In addition, in the initial series of tests a month earlier, Shellsol T was found to have a residence time of 18.55 min which suggests that other changes have also occurred over time in the liquid.

### 6.4.2 Neat Fuels

The initial tests evaluated performance of the neat fuels in the gold dish which found the order of reactivity from high to low being ShellSol T, Banner, Dodecane, GTL, GTL with Jet. Dodecane and GTL oxidise slightly slower than Banner solvent, however in a similar overall time-scale which is to be expected for similar compounds. The time development of pressure for neat solvents in the gold dish is presented in Figure 6.3, with time measurements given in Table 6.6 and is representative of the behaviour of pure hydrocarbons in the PetroOxy. Use of a PTFE dish increased oxidation time slightly which may be explained by the reduced surface area of the liquid when the dish is used. Use of a 316 stainless steel metal foil in the PTFE dish has no significant impact on the residence time for neat solvent.

solvent	neat	PTFE dish	PTFE dish & foil
Shellsol T	18.55	23.26	23.48
Banner	64.01	90.58	88.71
Dodecane	75.30	82.53	
GTL	103.78		
GTL with Jet	625.01	652.78	647.43

Table 6.6: Residence time in the PetroOxy in minutes.

### 6.4.3 Addition of Amines

The next test series investigated the impact of amine species on the oxygen consumption rate in the PetroOxy. Tests were carried out with butylamine, aniline and m-toluidine with the residence time results given in Table 6.7.

solvent	butylamine	aniline	m-toluidine
Shellsol T	49.85	1193.50	1021.46
Banner	103.58	862.05	1188.45
Dodecane	104.21		
GTL with Jet			1112.48

Table 6.7: Residence time in minutes in the PetroOxy with amine species additives at a ratio of 50:1.

1,4-diaminobutane as well as m-phenylenediamine were further tested to obtain a better understanding of the impact of the amine group, with residence times given in Table 6.8. However the very hard to remove varnish-like coating formed on the dish and lid of the PetroOxy when testing diamines, shown in Figure 6.6b, suggests that an alternative test method is required to avoid damage to the gold dish.

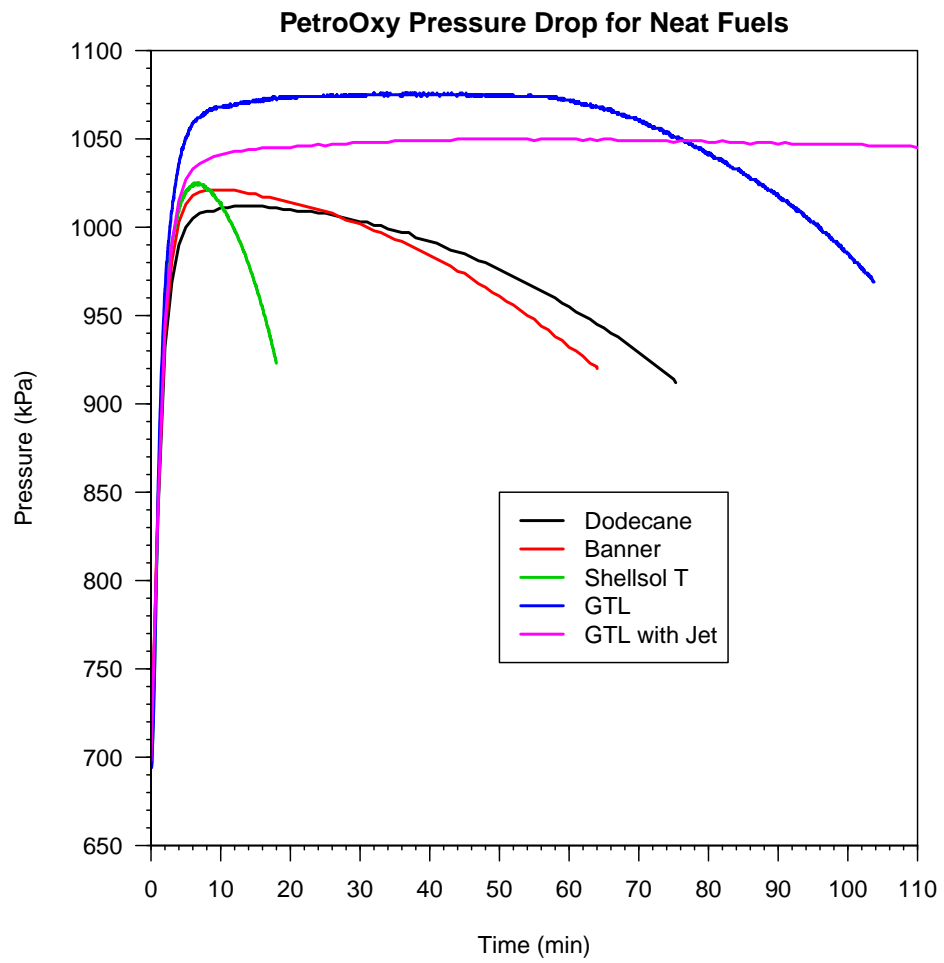


Figure 6.3: Pressure development in the PetroOxy using a gold dish for neat fuels.

solvent	1,4-diaminobutane	m-phenylenediamine
Banner np1014	303.06	620.98

Table 6.8: Residence in the PetroOxy with diamine species additives at a ratio of 50:1.

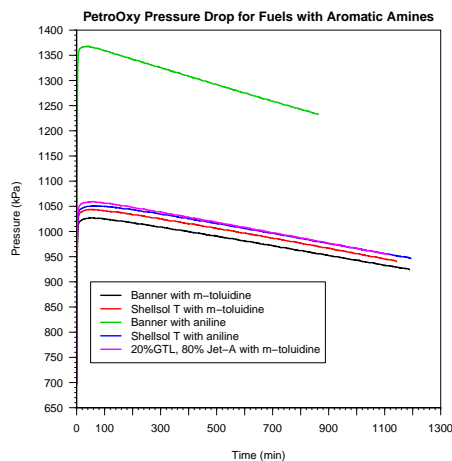


Figure 6.4: Pressure development in the PetroOxy with the addition of aromatic amines.

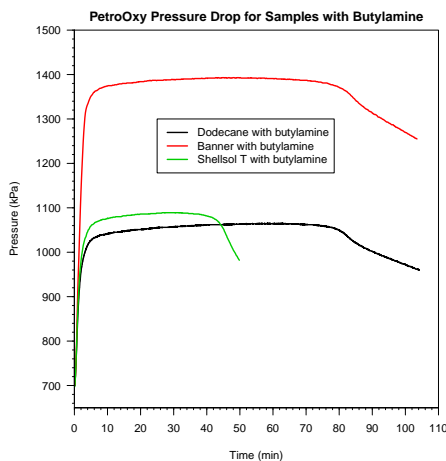
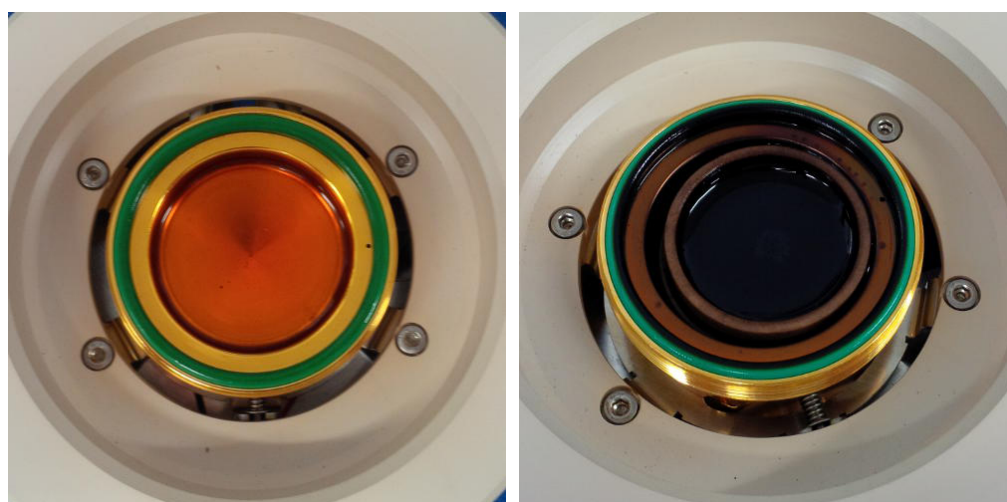


Figure 6.5: Pressure development in the PetroOxy with the addition of butylamine.

In addition to changes in reactivity, evident in the different residence time, the tests showed that inclusion of an amine compound leads to the solution discolouring or darkening as well as the production of deposits. In the case of butylamine, the solution had yellowed visibly and the tissue stained yellow when cleaning the gold dish, suggesting that some material had deposited. It was further found that particulates formed in the sample vial post test during storage which may be indicative of a polymerization reaction occurring. A longer stress test of 150 minutes with butylamine and Shellsol T was carried out, in which it was found that the butylamine formed a dark brownish oily liquid at the bottom of the dish as well as dark brown deposits on the lid which were difficult to remove. In the case of aniline and m-toluidine the solution darkened significantly and deposits could be observed on the dish, further confirmed by residue on the tissue when cleaning the PetroOxy. While both the Shellsol T and Banner solvent remained clear, albeit darker, after the stress test with m-toluidine, the GTL and Jet-A blend with m-toluidine appeared to be effectively black after the stress test and inspection of the post test solution in a vial with a light source suggests that no visible particulates formed in the liquid phase. A further unexplained phenomena is the significantly higher pressure with Banner solvent and aniline as well as butylamine, shown in Figure 6.4 as well as Figure 6.5. Given that Banner solvent did not exhibit any unexpected behaviour in the neat test shown in Figure 6.3, this behaviour is very much unexpected.



(a) Darkening of solution which contained m-toluidine.

(b) Coating from Phenylenediamine.

Figure 6.6: Photos of the different look of two samples post stressing in the PetroOxy.

The darkening of an m-toluidine solution as well as the coating developed during the test with phenylenediamine are shown in Figure 6.6. Especially the addition of phenylenediamine has led to a comprehensive coating of the interior of the PetroOxy.

For further analysis, a metal foil was placed in a 50:1 blend of Banner Solvent np1014 with m-toluidine and run through a standard 10% pressure drop PetroOxy test, which enabled the retention of any deposits formed for further analysis. Upon initial inspection, the foil exhibited a uniform brown coating, shown in Figure 6.7.



(a) Uniform brown coating on foil with a part unsplit for SEM and EDX analysis.

(b) Magnified view, showing the "spotty" nature of the coating.

Figure 6.7: Macro photographs of deposits formed on a metal foil during a PetroOxy thermal exposure test with Banner Solvent np1014 doped with m-toluidine.

In addition, m-toluidine was added to a 20% GTL with 80% Jet-A blend of which a sample was filtered through a 0.2  $\mu\text{m}$  filter before stressing and a second sample was filtered post stressing. Photos of the filters are shown in Figure 6.8.

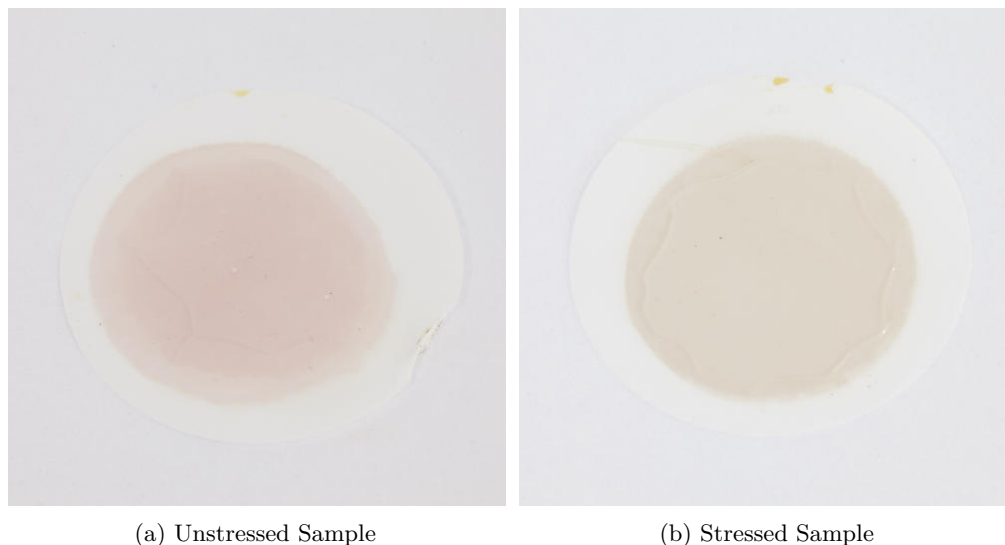


Figure 6.8: Macro photographs of 0.2  $\mu\text{m}$  pore size filters through which stressed and unstressed 20% GTL with 80% Jet-A with a 50:1 addition on m-toluidine were passed.

Both filters were discoloured or stained as a result of the filtration process. As can be seen clearly from Figure 6.8, the filter through which the unstressed sample was passed, shown in Figure 6.8a has a distinct red hue while the filter through which the stressed sample was passed exhibits a more brownish discolouration lacking the red hue, shown in Figure 6.8b. Given the short stressing time of 120 minutes, this suggests that the process which leads to the discolouration of the sample and the formation of the deposits must start comparatively quickly with the exposure to thermal stress, irrespective of the rate of oxygen consumption.

#### 6.4.4 Addition of Aromatic Species

Further tests aimed to establish the impact of addition of an aromatic compound to the test sample. Tests with benzene, toluene and p-xylene were carried out with both Shellsol T and Banner np1014, with the residence times given in Table 6.9.

solvent	neat	benzene	toluene	p-xylene
Shellsol T	18.55	31.93	33.10	29.88
Banner np1014	64.01	879.96	464.43	178.61
Dodecane	75.30			82.78

Table 6.9: Residence times in minutes in the PetroOxy with aromatic species additives at a volume based ratio of 50:1. The different ShellSol times are a result of ShellSol behaviour changing during the test period.

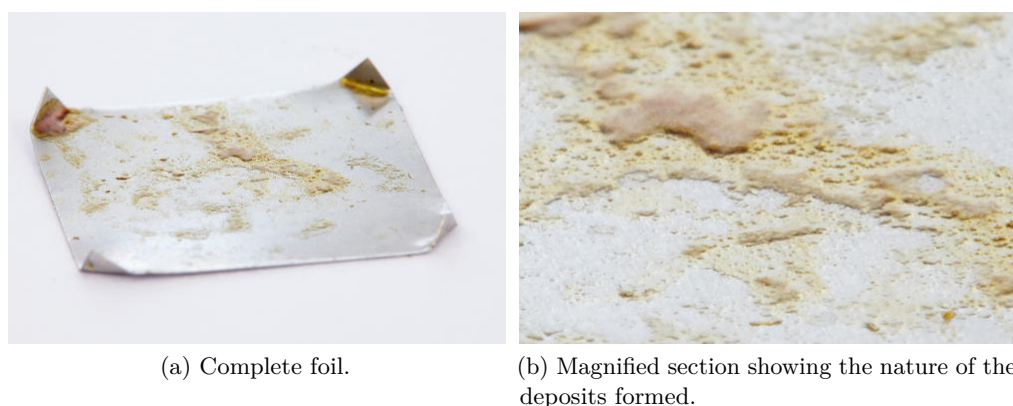


Figure 6.9: Macro photographs of a metal foil placed in a 50:1:1 blend of Banner Solvent np1014 with both butylamine and p-xylene.

Addition of an aromatic species (benzene/toluene/p-xylene) to Shellsol T has led to a 50% increase in the residence time of the solution. In contrast, in Banner Solvent, benzene has increased the residence time from 64 minutes to 880 minutes after which the solution was still perfectly clear.

#### 6.4.5 Addition of Aromatic Species and Butylamine

Because fuels tend to be a complex multicomponent mixture, it was decided to evaluate the behaviour of mixing aromatic and butylamine additives. In addition, tests with a 316 stainless steel foil were carried out to assess whether the presence of stainless steel will have an influence on the residence time in the PetroOxy.

	Shellsol T	Banner	Dodecane
Series 1			
solvent only	18.55	64.01	75.3
p-xylene	29.88	178.61	82.78
butylamine	49.85	103.58	104.21
Series 2			
butylamine metal foil	48.05	56.63	95.96
p-xylene, butylamine	50.96	50.08	108.53
p-xylene, butylamine, metal foil	26.68	82.13	87.15

Table 6.10: Residence times for additive combinations from two test series.

As there has been a break of two months between the test series, the industrial solvents Shellsol T and Banner Solvent may have changed, as was shown for Shellsol T in Table 6.5, introducing some uncertainty into the results. However, from the dodecane tests, run with reagent grade dodecane, it can be concluded that in the presence of an amine additive a metal foil will slightly accelerate the oxygen consumption rate, based on the

data collected over two test series, shown in Table 6.10.

The only outlier is the test with Banner Solvent with both the amine and p-xylene additives where a metal foil had an opposite effect. This is most likely attributable to contaminants in the solvent which could have lead to a different reaction path. The lack of a clearly observable effect on the ShellSol T tests with butylamine suggests that the solvent may already contain a metal contaminant.

#### 6.4.6 Addition of Sulphurous Species

To obtain a more complete picture, the effects of a sulfide as well as disulfide additive were also investigated. The additives chosen were dibutylsulfide and dibutyldisulfide which were added at a ratio of 500:1 by volume to two reagent grade solvents, dodecane and 2,2,4-trimethylpentane. An additional combination included two additives, p-xylene as well as a sulfurous component. The measured PetroOxy residence times are given in Table 6.11. During the test, it was observed that the dodecane sample with dibutylsulfide

	Dodecane	vs. neat	Isooctane	vs. neat
no additive	75.38	$\pm 0\%$	776.25	$\pm 0\%$
dibutylsulfide	101.08	+43%	655.11	-16%
dibutyldisulfide 500:1	316.26	+320%	645.35	-17%
dibutylsulfide, p-xylene 500:1:10	146.28	+94%	1213.10	+56%
dibutyldisulfide, p-xylene 500:1:10	384.80	(10 mL)	875.40	+13%

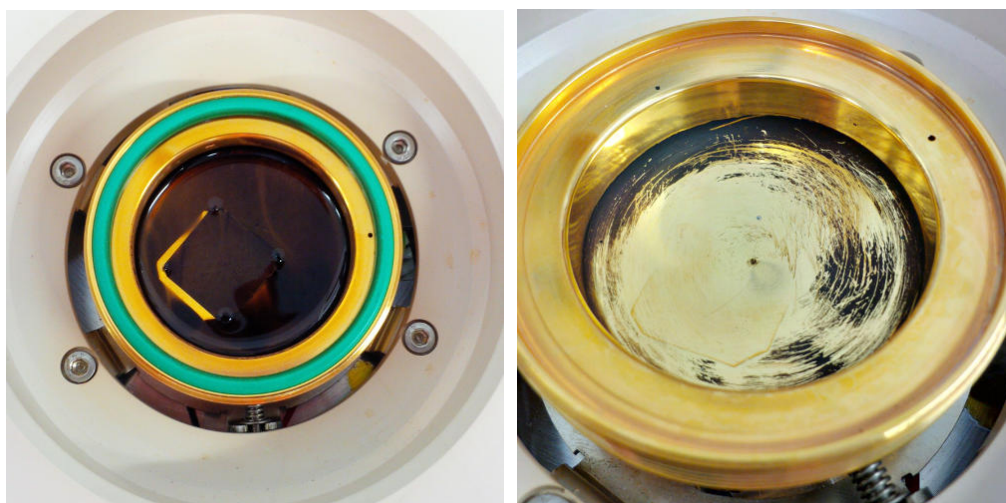
Table 6.11: Residence times in the PetroOxy for a blend of dodecane or 2,2,4-trimethylpentane (Isooctane) with additives consisting of p-xylene as well as dibutylsulfide and dibutyldisulfide. A metal foil was also added to retain potential deposits. One test, as indicated was carried out with a larger sample.

only exhibited slight yellowing at best and was otherwise clear. Deposits formed in all other tests involving sulfur, where the test with 2,2,4-trimethylpentane suggests that deposits form as a result of the long residence time when compared to dodecane. What is most interesting is that the liquid component of the products formed in the sulphur tests is clear and pretty much colourless with potentially faint traces of yellow. This may be indicative of reactions occurring just at the surface rather than in the bulk liquid.

Figure 6.10 shows clearly how deposits have only formed exclusively at the liquid solid interface during the test. The gold surface above the liquid as well as the lid of the PetroOxy were found to be perfectly clean. The deposits were also found to be extremely hard to remove and impervious to acetone, isopropanol and ethanol so that vigorous scrubbing with a paper tissue was the only method which aided in the removal of deposits.

Close inspection of the foils further suggests that the nature of deposits formed is very different between dibutylsulfide and dibutyldisulfide. While the former results in filamentous deposits, the latter produces spherical particulates and deposits illustrated





(a) Deposits formed during a sulfur test. (b) Deposits from sulfur tests are hard to remove.

Figure 6.10: Deposits from a sulfur test; post test and during the cleaning phase.

in Figure 6.11. Photographs for metal foils placed in dodecane are shown in Figure 6.12. The visual inspection of the foils, seen in Figure 6.11 and Figure 6.12 suggests that deposit formation in the case of sulfur compounds is primarily an effect of time, though all samples exhibit some onset of deposits. The longer the exposure time, the more severe the deposit coating. Given that that oxygen consumption is similar in all tests, due to the 10% pressure drop stop criteria in the PetroOxy, oxygen cannot be a major factor in the deposits themselves and can only feature in the chemical processes that initiate the formation of deposits.

Further, from the data collected, shown in Table 6.11 it appears that the antioxidant effect of both dibutylsulfide and dibutyldisulfide is reduced or even negated in a solvent which exhibits inhibition to oxidation. In relative terms, the impact of sulphurous additives to 2,2,4-trimethylpentane is significantly reduced when compared to the dodecane tests which suggests that the sulfurous species will inhibit oxidation only up to a point after which their effect is lost and they may even accelerate oxygen consumption.

## 6.5 Gas Chromatography

Gas chromatography mass spectrometry was used to attempt to identify some of the components in both the neat and stressed solvent. The gas chromatograph was a Perkin Elmer Turbo Mass Spectrometer, the column was made by Phenomenex, a Zebron ZB-5 Capillary GC column, specified to have low bleed, to be 30 m in length, with an internal diameter of 0.25 mm and a film thickness of 0.25  $\mu\text{m}$ .

A surrogate product was used to establish a detection limit for the gas chromatograph



(a) Tiny filamentous deposits with a “powder-like looking coating” on a metal foil placed in 2,2,4-trimethylpentane and dibutylsulfide. (b) Tiny particulate deposits on a metal foil placed in 2,2,4-trimethylpentane with p-xylene and dibutylsulfide.



(c) Tiny spherical deposits on a metal foil placed in 2,2,4-trimethylpentane with dibutylsulfide with a dark carbon like coating. (d) Tiny filamentous deposits on a dark coating on a metal foil placed in 2,2,4-trimethylpentane with p-xylene and dibutylsulfide.

Figure 6.11: Macro photographs of deposits formed on metal foils during PetroOxy thermal exposure tests.



(a) Tiny filamentous deposits between yellowish spots on a metal foil placed in dodecane and dibutylsulfide. (b) A small amount of tiny particulates on what is a liquid film coating on a metal foil placed in dodecane with p-xylene and dibutylsulfide.



(c) Tiny spherical looking deposits on a metal foil with spiderweb cracks as well as a dark carbon like coating placed in dodecane with dibutylsulfide. (d) Tiny particulate deposits on a metal foil placed in dodecane with p-xylene and dibutylsulfide.

Figure 6.12: Macro photographs of deposits formed on metal foils during PetroOxy thermal exposure tests.

mass spectrometer, which provides a rough estimate of the minimum concentration that can be detected. The surrogate was blended from hexanoic acid, 2-octanol, 4-dodecanol, 2-dodecanone and dodecane which was diluted in both acetone and chloroform, with an initial test employing ethanol as well. The surrogate tests suggest that components are lost in noise between a concentration of 0.01% and 0.001% by volume.

To avoid overloading of the detector, samples in a gas chromatograph mass spectrometer are diluted, in this case to 0.1% by volume which would place the detection limit for any components at about 10% concentration by volume in the undiluted solution. Gas chromatography mass spectrometry has been applied to stressed samples and it was found that any differences between the neat and stressed sample cannot be detected using standard gas chromatography methods as the concentrations of products is too low to be detected. It is possible to analyse undiluted samples in the gas chromatograph mass spectrometer which was done for stressed dodecane without any additives, however this overloads the mass spectrometer. It could be attempted to filter out the solvent with a solvent delay, however this is met with a number of issues. The solvent delay is designed to filter out an initial light solvent in which the sample is diluted. It is possible to include more than one solvent delays, however outside of Banner solvent, for which an insufficient number of delays is available, it would be impossible to identify appropriate times during which the detector should be switched off.

Where gas chromatography mass spectrometry analysis was carried out, a temperature range from 40-200 °C, at a ramp rate of 5 °C per minute was employed, holding for 10 minutes at the end with an initial solvent delay of 3 minutes. The detector was set to detect ions with a molecular mass of 50-450 g/mol. Blanks were not employed in this study.

Gas chromatography mass spectrometry established that dodecane contains minute traces of contaminants, mainly undecane and some tridecane. Banner solvent is relatively clean and well specified given that it is a commercial industrial solvent and consists predominantly of C<sub>10</sub> to C<sub>14</sub> hydrocarbons with some minor contaminants. Shellsol T, the 20% GTL with 80% Jet-A blend as well as neat GTL both produce a very complex chromatogram in which a smaller number of compounds dominate but nevertheless a significant number of additional compounds are present. Banner solvent, Shellsol T as well as the 20% GTL with 80% Jet-A mixture were diluted to establish if the dominant compounds can be identified. The chromatograms for 0.1% diluted solvent are shown in Figure 6.13, where the solvent has been omitted by applying an appropriate solvent delay. As can be seen, the number of compounds detected has reduced dramatically, however both Shellsol T and the 20% GTL with 80% Jet-A blend contain a large number of different compounds. In addition, it is well known that trace compounds have a significant impact on the behaviour of fuel with respect to thermal stability<sup>6,167</sup>, the presence of

which, at tiny quantities, can be deduced from the neat Dodecane chromatogram shown in Figure 6.14.

Except in the case of Banner solvent and Dodecane where the constituents of the solvent are well defined, analysis of the composition of both the ShellSol as well as 20% GTL with 80% Jet-A blend is problematic. A number of larger peaks may be identified using automated methods. The composition of Banner Solvent is shown in Table 6.12, tetradecane is not listed as its mass spectrum did not agree well enough with mass spectra samples in the database in the dilute sample. An automated analysis of the ShellSol T composition is shown in Table 6.14. Because of the similarity of iso-compounds, a large number of peaks can be attributed to a variation of similar iso-compounds. The reported composition for 20% GTL with 80% Jet-A is shown in Table 6.13. Hence it is only possible to establish that in an overall picture, dominant compounds in Shellsol T are predominantly in the C<sub>9</sub>–C<sub>12</sub> range, while dominant compounds in the GTL with Jet fuel blend are in the C<sub>9</sub>–C<sub>10</sub> range.

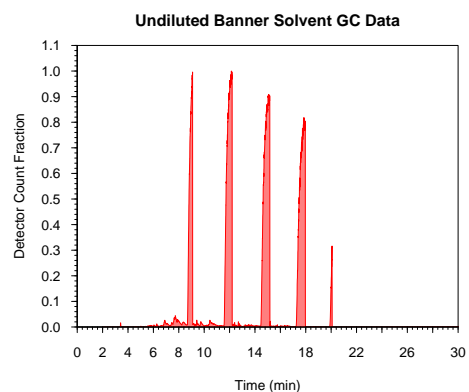
Name	CAS	Match Factor	Reverse Match
Decane	124-18-5	88,3	88,3
Undecane	1120-21-4	90,0	90,5
Dodecane	112-40-3	93,1	93,1
Tridecane	629-50-5	89,2	89,2

Table 6.12: Output of automated identification of compounds in 0.1% diluted Banner solvent.

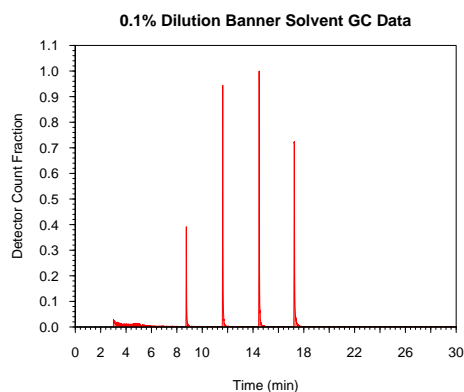
Name	CAS	Match Factor	Reverse Match
Nonane	111-84-2	88,1	88,4
Decane	124-18-5	85,3	86,2
Pentane, 2,3,4-trimethyl-	565-75-3	80,4	84,1
Octane, 2,3,6-trimethyl-	62016-33-5	83,9	84,8
Pentane, 2,2,3,4-tetramethyl-	1186-53-4	80,6	84,8

Table 6.13: Output of automated identification of compounds in 0.1% diluted 20% GTL with 80% Jet-A solvent.

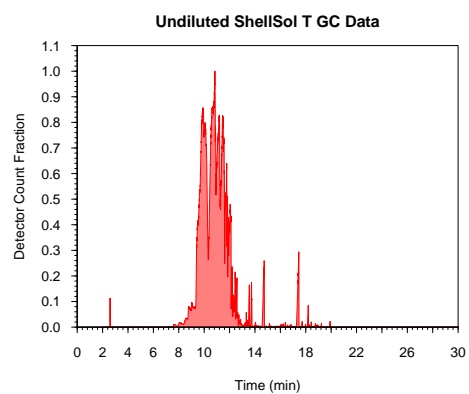
In conclusion, the gas chromatography results proved inconclusive with respect to product formation. This can be attributed to operator inexperience and hence for future work, the assistance of a significantly more experienced operator would be required in an effort to obtain better qualitative data with regards to products which could not be identified in this work.



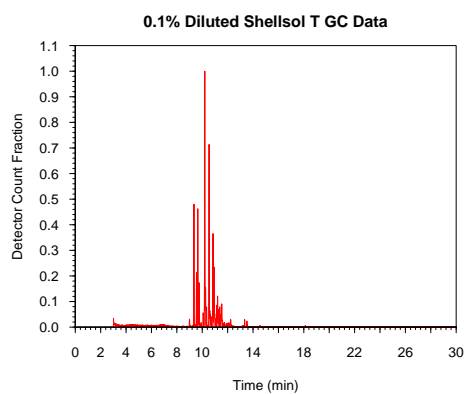
(a) Banner solvent, no dilution.



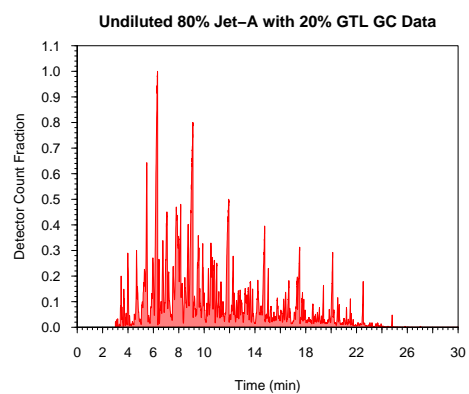
(b) Banner solvent, 0.1% dilution.



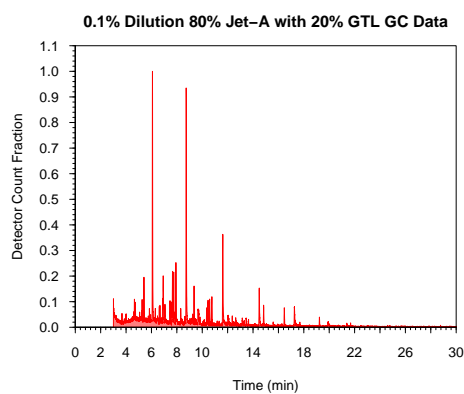
(c) Shellsol T, no dilution.



(d) Shellsol T, 0.1% dilution.



(e) 20%GTL with 80% Jet-A, no dilution.



(f) 20%GTL with 80% Jet-A, 0.1% dilution.

Figure 6.13: Chromatograms of samples of Banner Solvent, Shellsol T and 20% GTL with Jet-A.

Name	CAS	Match Factor	Reverse Match
Heptane, 2,2,4,6,6-pentamethyl-	13475-82-6	88,2	88,3
Undecane, 2,2-dimethyl-	17312-64-0	88,3	89,4
Decane, 3,7-dimethyl-	17312-54-8	83,9	83,9
Octane, 6-ethyl-2-methyl-	62016-19-7	84,3	84,3
Undecane, 4,7-dimethyl-	17301-32-5	83,7	85,0
Decane, 2,5,9-trimethyl-	62108-22-9	84,7	85,0
Heptane, 2,2,4,6,6-pentamethyl-	13475-82-6	82,6	83,0
Octane, 2,6-dimethyl-	2051-30-1	82,8	82,8
Hexane, 2,2,4-trimethyl-	16747-26-5	84,4	86,9
Hexane, 2,2,4-trimethyl-	16747-26-5	85,0	85,5
Heptane, 2,2-dimethyl-	1071-26-7	85,6	89,3
Decane, 2,5,9-trimethyl-	62108-22-9	83,7	84,5
Heptane, 4-ethyl-2,2,6,6-tetramethyl-	62108-31-0	84,4	85,2
Pentane, 3-ethyl-2,2-dimethyl-	16747-32-3	82,8	86,4
Pentane, 3-ethyl-2,2-dimethyl-	16747-32-3	82,8	82,8
Hexane, 2,2,3-trimethyl-	6747-25-4	82,9	82,9
Pentane, 2,2,3,4-tetramethyl-	1186-53-4	83,2	84,9
Octane, 2,6,6-trimethyl-	54166-32-4	81,0	81,1
Undecane, 2,8-dimethyl-	17301-25-6	81,7	81,8
Undecane, 4,8-dimethyl-	17301-33-6	81,3	81,3
Heptane, 2,2,4,6,6-pentamethyl-	13475-82-6	85,4	85,7
Pentane, 2,2,3,4-tetramethyl-	1186-53-4	87,7	90,0
Pentane, 2,2,3,4-tetramethyl-	1186-53-4	87,4	88,7
Octane, 3,3-dimethyl-	4110-44-5	83,6	84,1
Nonane, 2,6-dimethyl-	17302-28-2	83,0	83,5
Heptane, 2,5,5-trimethyl-	1189-99-7	84,3	84,8
Octane, 6-ethyl-2-methyl-	62016-19-7	83,7	83,9
Undecane, 4-methyl-	2980-69-0	81,8	81,8
Hexane, 3,3-dimethyl-	563-16-6	80,0	81,0
Octane, 2,6,6-trimethyl-	54166-32-4	84,3	84,9
Heptane, 2,5,5-trimethyl-	1189-99-7	81,0	81,9
Octane, 2,6,6-trimethyl-	54166-32-4	84,3	84,3
Undecane, 4-methyl-	2980-69-0	84,7	84,7
Octane, 2,3,6,7-tetramethyl-	52670-34-5	84,3	84,3
Hexane, 2,2,5,5-tetramethyl-	1071-81-4	80,4	81,0
Heptane, 4-ethyl-2,2,6,6-tetramethyl-	62108-31-0	81,0	81,2
Heptane, 2,5,5-trimethyl-	1189-99-7	82,2	82,2
Heptane, 2,5,5-trimethyl-	1189-99-7	80,1	80,1

Table 6.14: Output of automated identification of compounds in 0.1% diluted ShellSol T solvent.

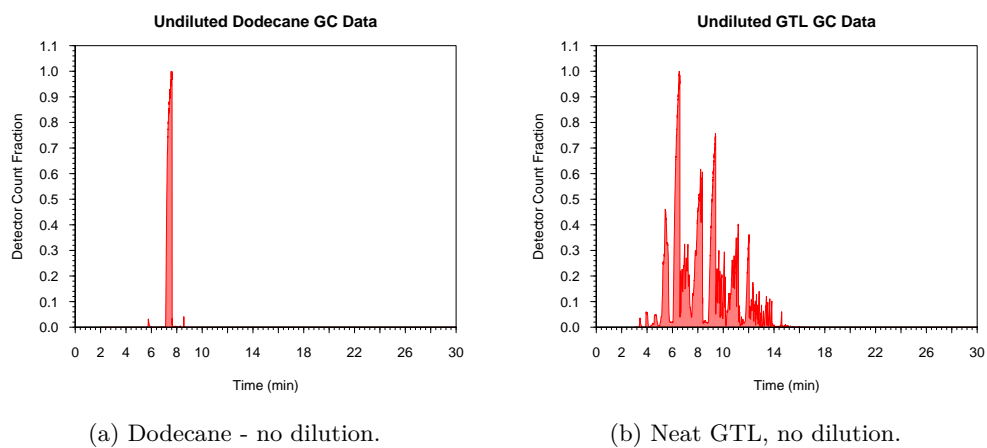
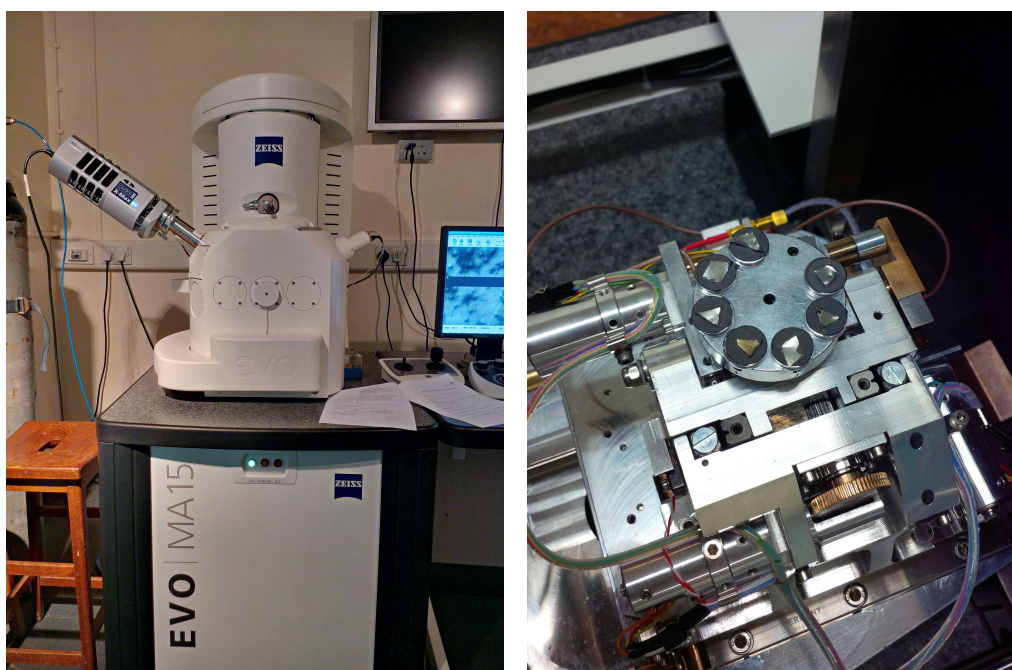


Figure 6.14: Chromatograms of undiluted samples of Dodecane and GTL.



## 6.6 SEM EDX

A number of tests involved metal foils which enabled the investigation whether these catalyse autoxidation reactions as well as to retain any deposits that have formed during the test. Some foils were analysed with a Carl Zeiss EVO MA15 scanning electron microscope which employs tungsten as an electron source. This is coupled with an Oxford Instruments XMax 80 mm<sup>2</sup> EDX analyser. A photograph of the SEM EDX is shown in Figure 6.15a while a number of foils (cut from the test foil) mounted on the sample holder are shown in Figure 6.15b. As the samples consisted of a metal foil, foil pieces were mounted directly on the sample holder with the edges painted over using a carbon paint to provide grounding and no metal coating applied as electrostatic charging would not be a major issue.



(a) Carl Zeiss EVO 15 SEM with Oxford Instruments XMax 80 mm<sup>2</sup>. (b) Samples of metal foils on sample holder.

Figure 6.15: SEM EDX equipment.

Because the SEM EDX only samples a small areas at a time, due to time constraints during its usage, investigated sites were chosen based on how interesting they appeared. This was achieved by obtaining a “general picture” and then focussing on potential points of interest. Hence attention was given to sites that exhibited visible defects or visible deposits or alternatively very different deposit morphologies and are thus of a comparative interest, such as is the case with butylamine and p-xylene in Figure 6.22. In addition, it was advised that the EDX should complete at least seven passes, which was adhered to, in order to obtain reliable results with regards to the elemental distribution.

### 6.6.1 Clean Foil

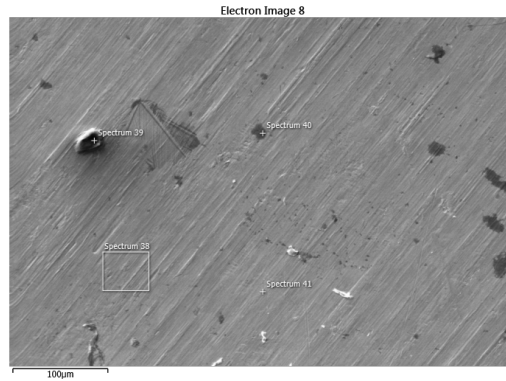
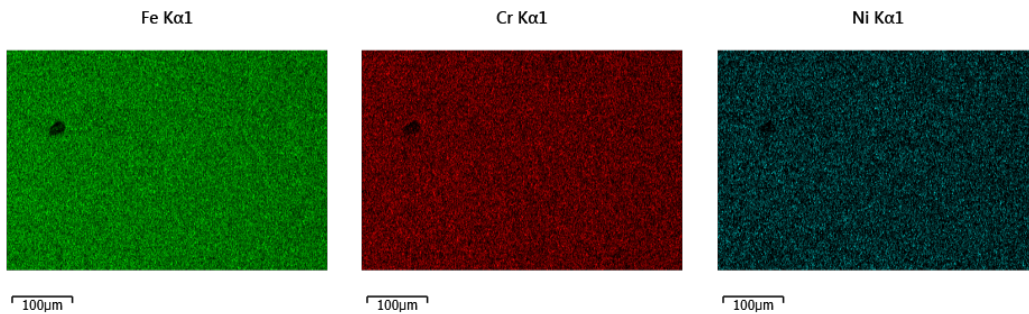
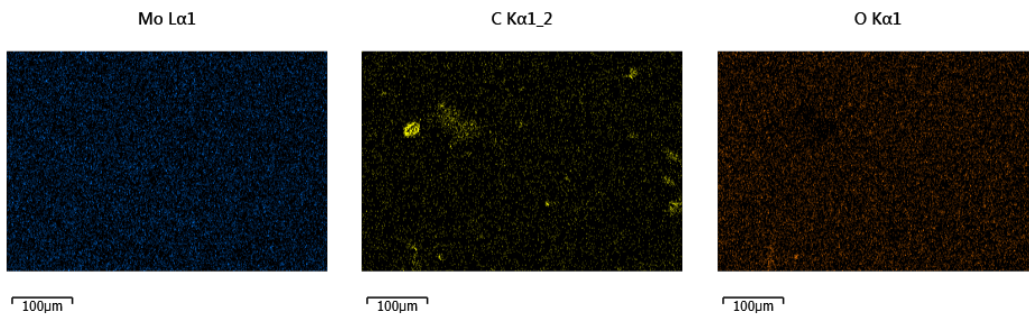


Figure 6.16: SEM image of a clean foil which had been stored in heptane after cutting to clean it.

Elemental analysis of the surface with EDX provides an overview over the elements which can be identified on the surface of the foil. An image of what can be considered a clean foil is shown in Figure 6.16, with the corresponding elemental distribution shown in Figure 6.17.



(a) Elemental analysis map of iron. (b) Elemental analysis map of chromium. (c) Elemental analysis map of nickel.



(d) Elemental analysis map of molybdenum. (e) Elemental analysis map of carbon. (f) Elemental analysis map of oxygen.

Figure 6.17: Selected element distributions from a clean 316 stainless steel metal foil.

As can be seen from Figure 6.17, the constituents of the metal foil itself, iron, chromium,

nickel and molybdenum are very much randomly distributed with no observable hotspots. Some surface contamination is visible in the form of carbonaceous particulates, seen both on the carbon map in Figure 6.17 as well as the scanning electron microscope image in Figure 6.16.

### 6.6.2 Banner Solvent Only Foil

The surface of a foil placed in Banner solvent during the stress test is shown in Figure 6.18. A particle can be observed, however this may be an artefact of the solvent production process or the metal foil preparation process.

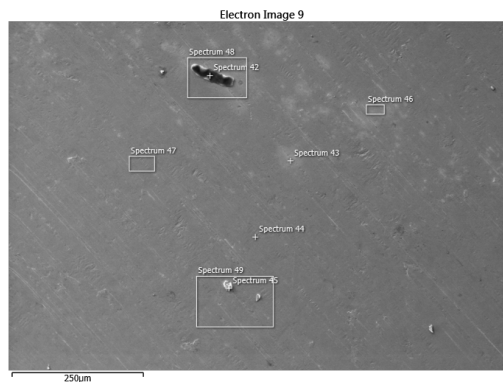


Figure 6.18: SEM image of a foil with deposits from a test in neat Banner Solvent.

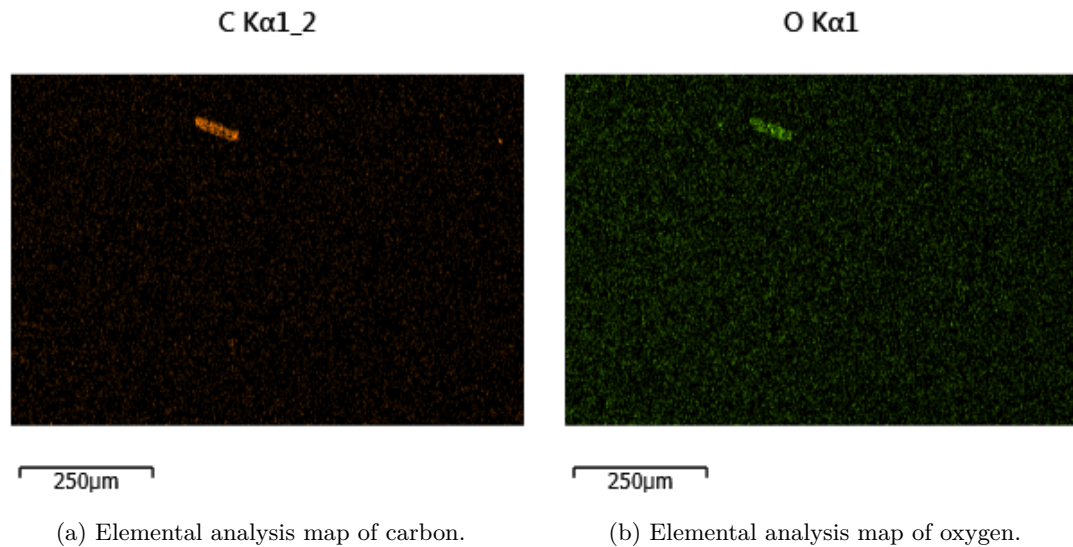


Figure 6.19: Selected element distributions from a 316 stainless steel metal foil placed in Banner Solvent.

Inspection of the foil suggest that some faintly visible coating has formed, evidence of which can be found in the elevated oxygen levels identified on the surface of the foil using EDX, shown in Figure 6.19b. However, outside of the particle, no accumulation of carbon can be determined on the foil, evident from Figure 6.19a.

### 6.6.3 Banner Solvent with 50:1 Butylamine

An image of the metal foil stressed with butylamine is provided in Figure 6.20. It is of interest that the deposits, which to the naked eye look like yellowish gums, apparently consist of spherical particulates. It is very interesting to observe that these deposits appear to be aligned with the grain of the metal which suggests tiny surface defects play a role in the formation or accumulation of these deposits.

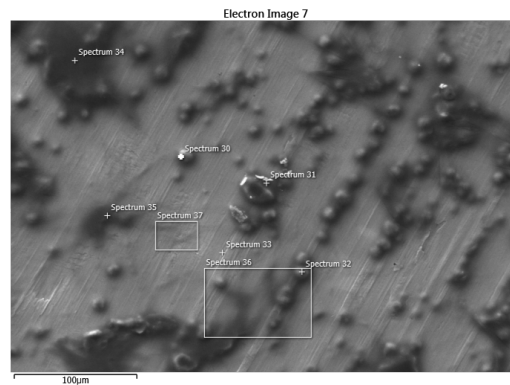


Figure 6.20: SEM image of a foil with deposits from a test Banner Solvent with 50:1 butylamine added.

Elemental analysis, shown in Figure 6.21 suggests that these deposits are rich in carbon but do not offer any clear oxygen hotspots, however in correspondence with carbon hotspots, oxygen levels are slightly elevated where carbon levels are elevated. Unfortunately, EDX is not sensitive toward nitrogen, therefore its presence cannot be determined with any reliability.

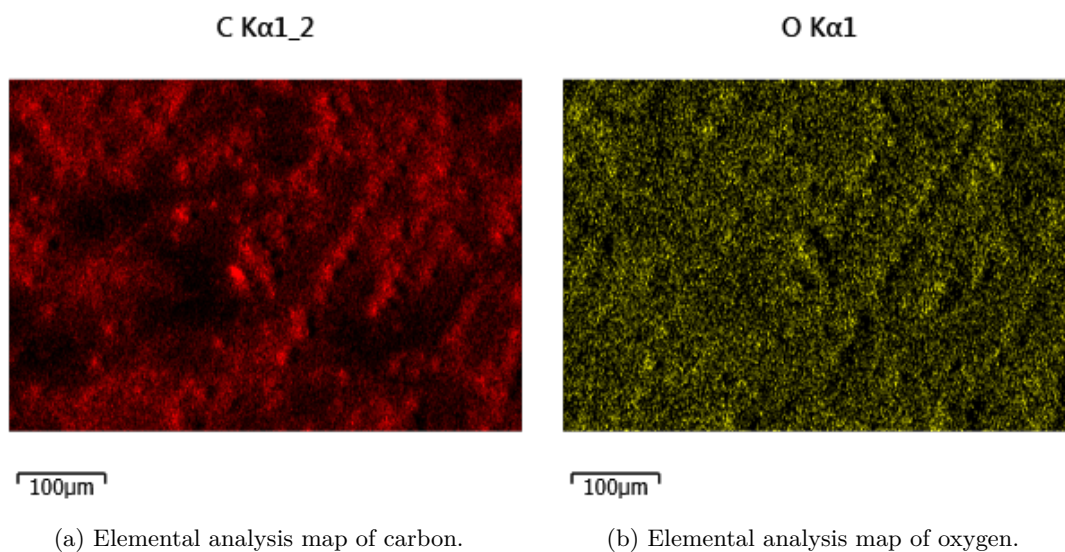


Figure 6.21: Selected element distributions from a 316 stainless steel metal foil placed in Banner Solvent with 50:1 butylamine added.

#### 6.6.4 Banner Solvent with 50:1:1 Butylamine and p-Xylene

Banner solvent with a 50:1:1 addition of butylamine and p-xylene produced an extensive deposition coating, as was shown in Figure 6.9. Under the scanning electron microscope, it was possible to discern distinctively different deposition patterns between the apparently clear foil and the brown coating, shown in Figure 6.22.

Sections which, to visual inspection appear clear, contain some spherical deposits, shown in Figure 6.22a, which are similar to those observed with only butylamine, shown previously in Figure 6.20, but lack arrangement with the metal “grain”. In contrast, the clearly visible thick brownish coating appears to consist of a more diverse grouping of particulates, from spherical particles, to agglomerated microspheres to thread-like objects with no distinctive deposition pattern, shown in Figure 6.22b.

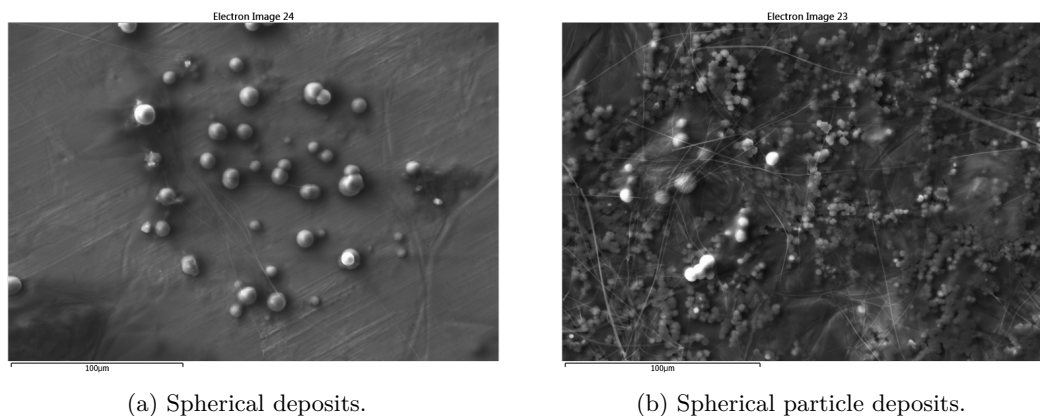


Figure 6.22: SEM image of deposits from Banner Solvent with butylamine and p-xylene.

Elemental analysis of the deposits reveals increases in carbon as well as oxygen in deposits, with hotspots on the map corresponding to observed larger particles, shown in Figure 6.23 and Figure 6.24. It is of interest that in Figure 6.24c the particles block the detection of iron, while in Figure 6.23c a uniform iron distribution may be observed. This would suggest that the particles visible in Figure 6.22a are both denser and thicker than the particles or the coating observed in Figure 6.22b. However, it is not possible to quantify this difference using the available data.

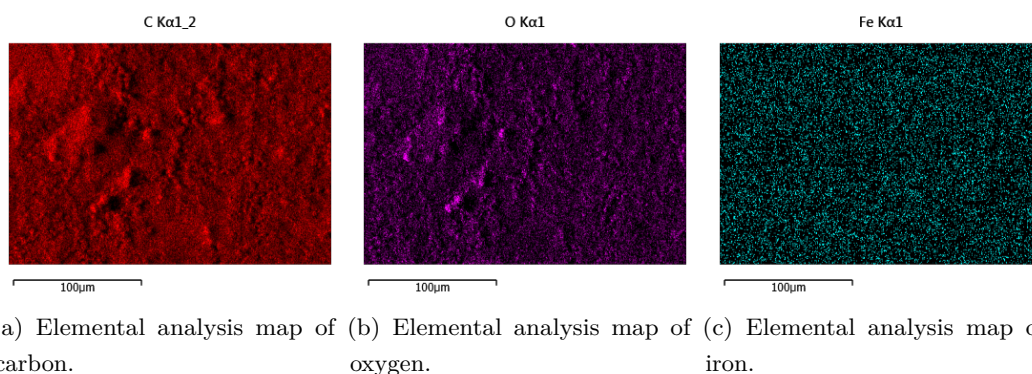


Figure 6.23: Elemental maps of the deposits from Banner Solvent with butylamine and p-xylene.

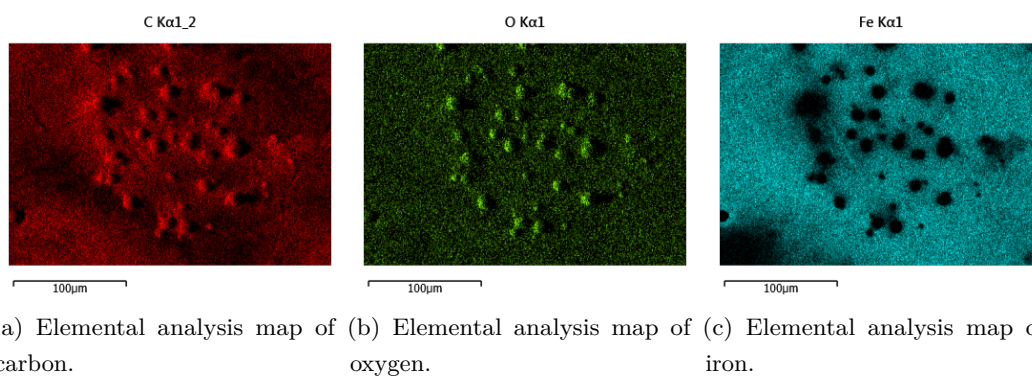


Figure 6.24: Elemental maps of the spherical particle deposits from Banner Solvent with butylamine and p-xylene.

It is further of interest that gold was detected on the foil in a uniform coating, which suggests the solvents and additives have interacted with the gold dish of the PetroOxy and dissolved some of it. Gold was not detected in any other samples analysed with SEM EDX.

### 6.6.5 Banner Solvent with 50:1 m-Toluidine

The foil which was placed in 5 mL of Banner Solvent with a 50:1 m-toluidine sample showed a uniform brown coating upon removal from the PetroOxy. A SEM image of the foil is shown in Figure 6.25. As can be clearly seen, the apparently uniform coating consists of local hotspots of deposited material. EDX analysis of the area identifies these as being rich in carbon, Figure 6.26a, but not oxygen, Figure 6.26b. In contrast, the small number of particles that can be observed are rich in both carbon and oxygen. It should be noted, that the deposits observed with m-toluidine, see Figure 6.25 are very different in their structure when compared to the deposits observed in the presence of butylamine, see Figure 6.20.

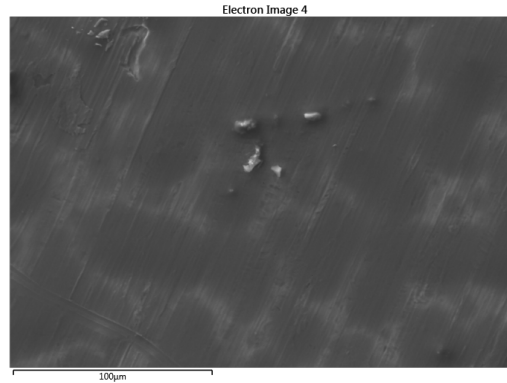


Figure 6.25: SEM image of a foil with deposits from a test in Banner Solvent with 50:1 m-toluidine.

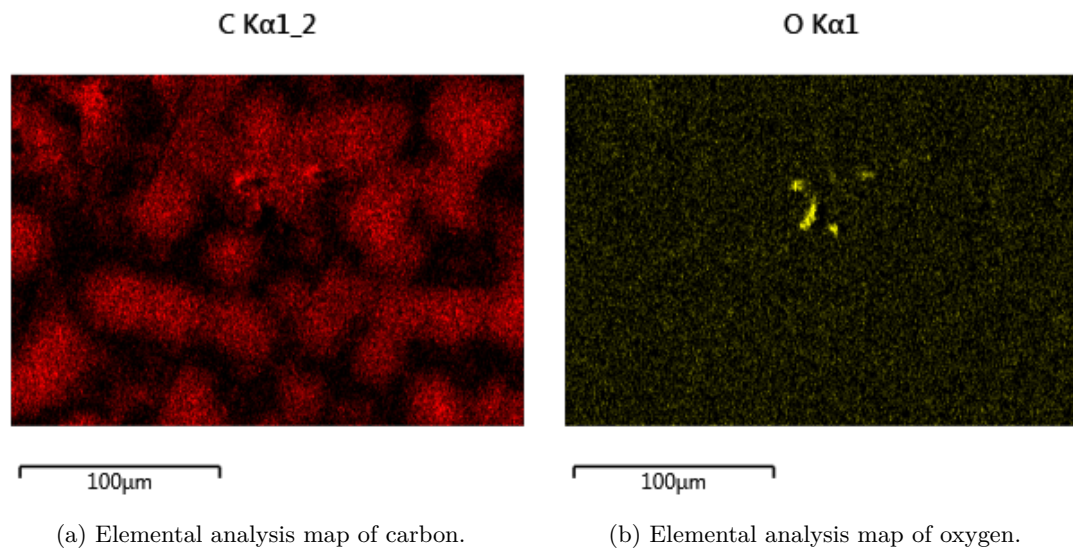


Figure 6.26: Selected element distributions from a 316 stainless steel metal foil placed in Banner Solvent with a 50:1 additive ratio of m-toluidine for the duration of thermal stressing.

### 6.6.6 20% GTL 80% Jet-A

The foil which was placed in 5 mL of 20% GTL 80% Jet-A showed a slightly brownish deposit which exhibited a rainbow colour reflection. Inspection of a sample from the foil in the electron microscope shows that the foil has been uniformly coated with a transparent compound, evident by the difficulty of focussing on the metal surface below, shown in Figure 6.27, with no distinct particles found on the foil. Elemental analysis of the surface with EDX was more insightful as it suggests the presence of interesting hotspots, shown in Figure 6.28.

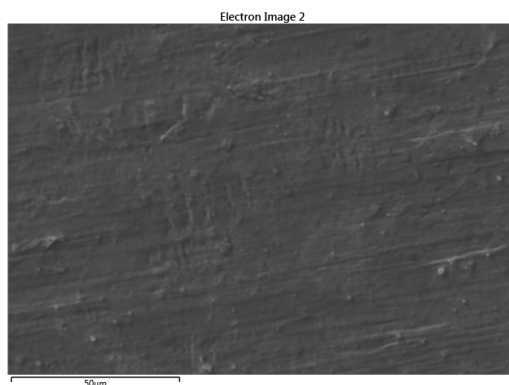
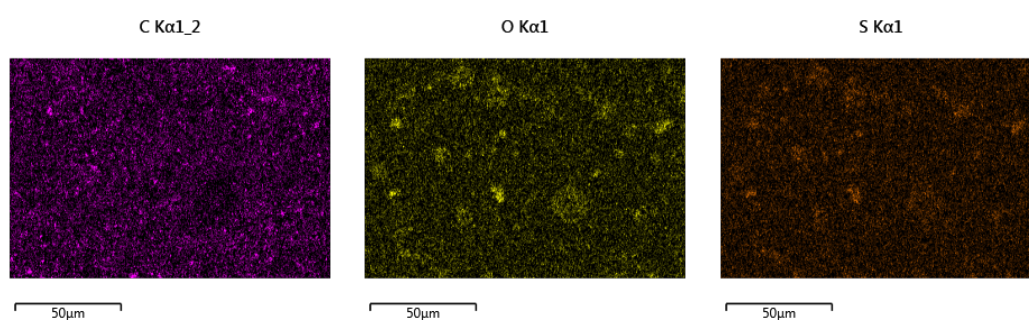


Figure 6.27: SEM image of a foil with deposits from a test in 20% GTL 80% Jet-A.



(a) Elemental analysis map of carbon. (b) Elemental analysis map of oxygen. (c) Elemental analysis map of sulfur.

Figure 6.28: Selected element distributions from a 316 stainless steel metal foil placed in a 20% GTL with 80% Jet-A fuel mixture for the duration of thermal stressing.

It is of interest that the sulfur has apparently clustered in select locations. However it cannot be determined whether this is due to the structure of the underlying metal foil or whether sulphurous deposits will agglomerate where initial deposits have formed. Analysis of a clean foil would suggest that elements are distributed randomly on the foil, as would be expected, shown in Figure 6.17. Nevertheless, even the clean foil contained some carbon contamination which cannot be ruled out as a possible nucleation point for deposits.

### 6.6.7 Filtered Unstressed Blend 20% GTL 80% Jet-A with 50:1 m-Tol

10 mL of a 20% GTL with 80% Jet-A blend that had been doped with a 50:1 ratio of m-toluidine were filtered through a 0.2 µm pore size polycarbonate filter to determine whether any particulate matter is formed in the liquid phase during a thermal stress test. The volume of 10 mL was chosen to improve the chance of detecting any particulates in unstressed fuel should these be present, even though only 5 mL are stressed in the PetroOxy. Figure 6.29 suggests that the solution is effectively free from particulates. While some tiny particulates are visible, these may very well be the result of post test contamination of the filter with atmospheric dust or soot.



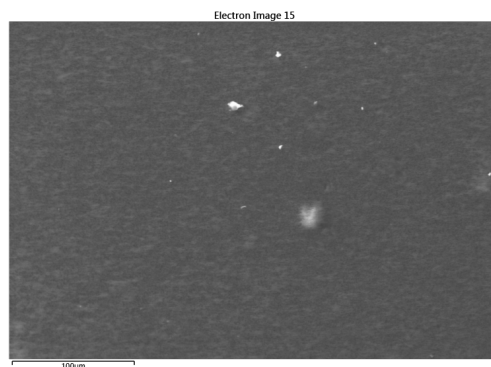


Figure 6.29: SEM image of filter through which an unstressed 20% GTL with 80% Jet-A blend doped with m-toluidine was passed.

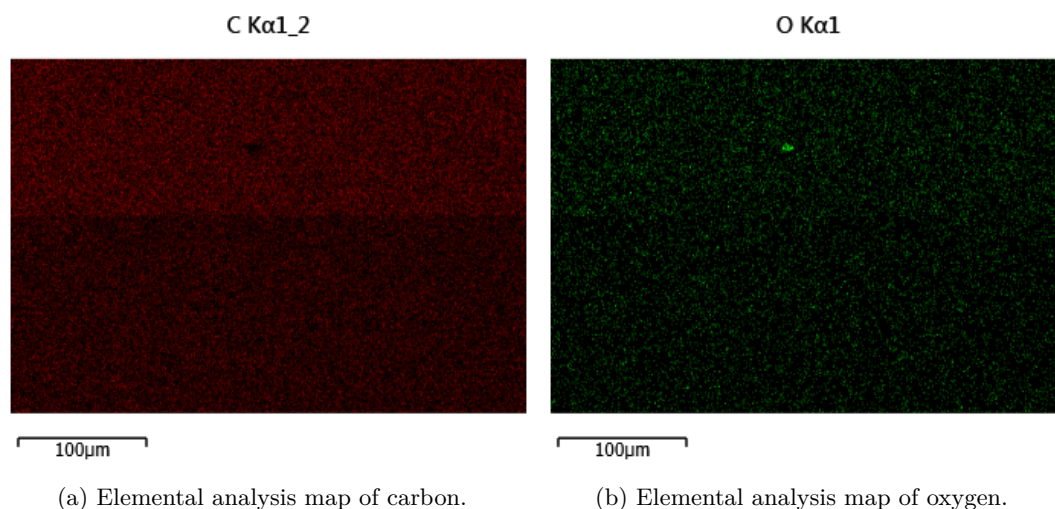


Figure 6.30: Elemental analysis of a polycarbonate filter through which 10 mL of an unstressed blend of 20% GTL with 80% Jet-A doped with 50:1 m-toluidine was passed.

Elemental analysis of the filter, shown in Figure 6.30 offers no unexpected results. The filter background, being a polymer exhibits a uniform presence of carbon. The particle shows an oxygen hotspot, however this does not offer any further insight as they may be dust deposited on the filter post test during photographing and preparation for the SEM EDX analysis. Otherwise no other elements were identified by the EDX analysis.

### 6.6.8 Filtered 120 min Stressed Blend 20% GTL 80% Jet with 50:1 m-Tol

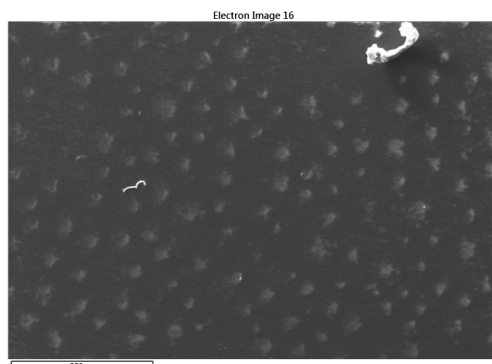
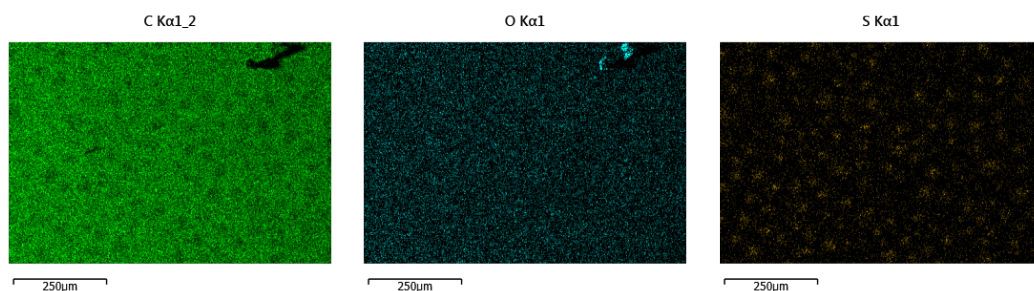


Figure 6.31: SEM image of filter through which a stressed 20% GTL with 80% Jet-A blend doped with m-toluidine was passed.

Following the filtration of an unstressed sample, 5 mL of a 20% GTL with 80% Jet-A blend that had been doped with a 50:1 ratio of m-toluidine were filtered after stressing it in a standard PetroOxy test for 120 minutes. Figure 6.31 suggests that the solution is effectively free from particulates. While some tiny particulates are visible, these may very well be the result of post test contamination of the filter with atmospheric dust or soot as well as cellulose fibres from the tissues employed when cleaning the PetroOxy.



(a) Elemental analysis map of carbon. (b) Elemental analysis map of oxygen. (c) Elemental analysis map of sulfur.

Figure 6.32: Elemental analysis of a polycarbonate filter through which approximately 5 mL of a stressed blend of 20% GTL with 80% Jet-A doped with 50:1 m-toluidine was passed.

Figure 6.32c shows that the filter pores exhibit increased levels of sulfur, an observation that was not made with the unstressed sample. This would suggest that trace sulphur species in the fuel have formed some sort of sticky material that adhered to the filter pores.

### 6.6.9 Addition of Sulfides and Disulfides

A set of systematic tests was carried out, covering the addition of sulfides and disulfides in solvents, both with and without the presence of an aromatic, introduced in Section 6.4.6. After initial evaluation at the macro scale, a number of samples were selected for further analysis under a scanning electron microscope with the capability of EDX based elemental analysis.

#### 6.6.9.1 Trimethylpentane with 500:1 Dibutylsulfide

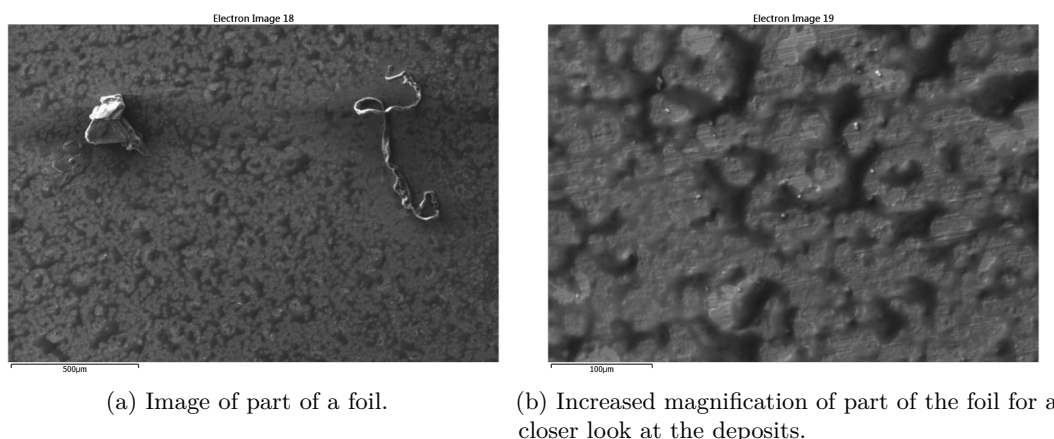


Figure 6.33: SEM image of part of a foil placed in trimethylpentane with dibutylsulfide.

Figure 6.33a shows part of a foil placed in trimethylpentane with 500:1 dibutylsulfide. While the filamentous object may be cellulose from the tissues used to clean the PetroOxy, the particle provides an object of greater interest. EDX analysis of the particle visible

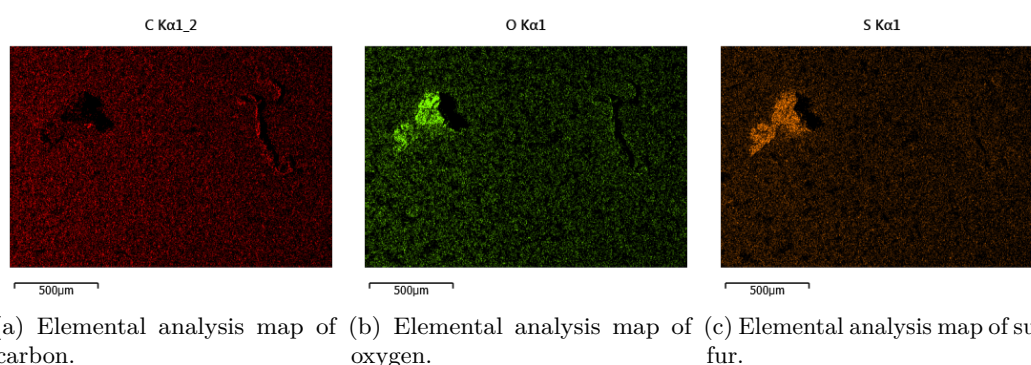


Figure 6.34: Elemental analysis of the surface and detected particle.

in Figure 6.33a suggests that the particle is rich in both in oxygen and sulfur, shown in Figure 6.34. This is unusual as most deposits tend to be rich in carbon, which may indicate that the particle was present in the solvent pre stressing. Closer analysis of the deposits from dibutylsulfide in trimethylpentane under a scanning electron microscope,



## 6.6.9.2 2,2,4-Trimethylpentane with 500:1:10 Dibutylsulfide and p-Xylene

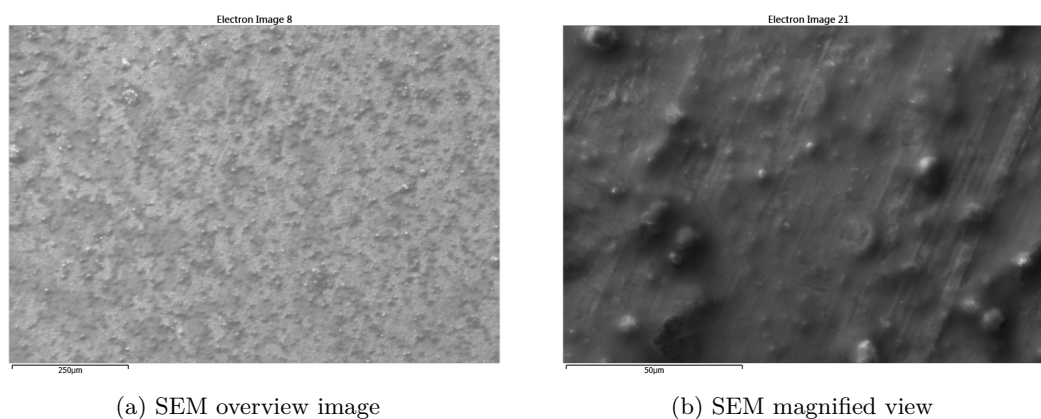


Figure 6.36: SEM images of the surface of a foil placed in trimethylpentane with 500:1:10 dibutylsulfide and p-xylene.

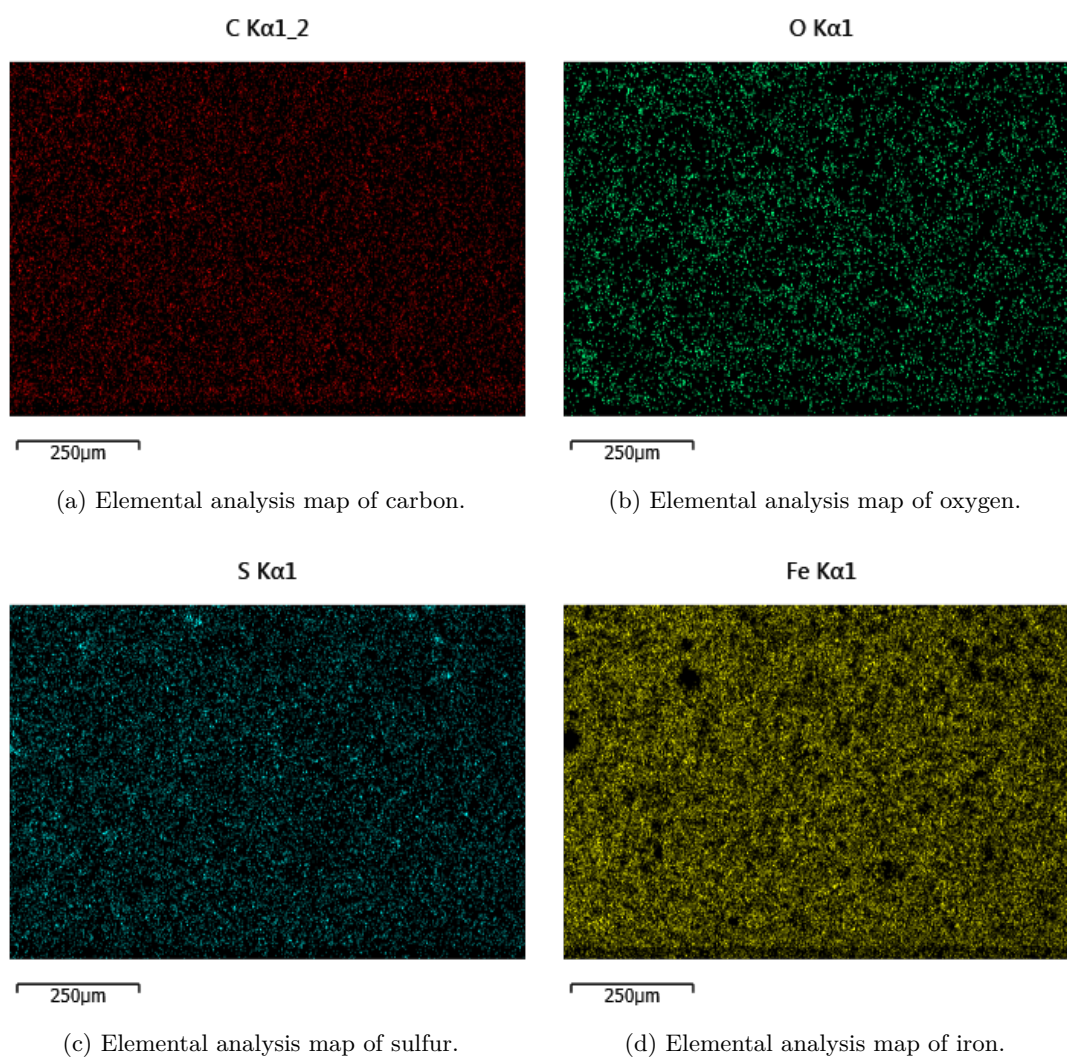


Figure 6.37: EDX analysis of the surface area shown in Figure 6.36a

The combination of 2,2,4-trimethylpentane with dibutylsulfide and p-xylene at a ratio of 500:1:10 lead to a comparatively uniform coating of the foil. Figure 6.36a suggests that the coating has no distinct pattern and consists of a mix of particle like deposits and polymeric coatings. A closer look, shown in Figure 6.36b suggests the presence of a uniform coating encapsulating spherical-particle-like deposits.

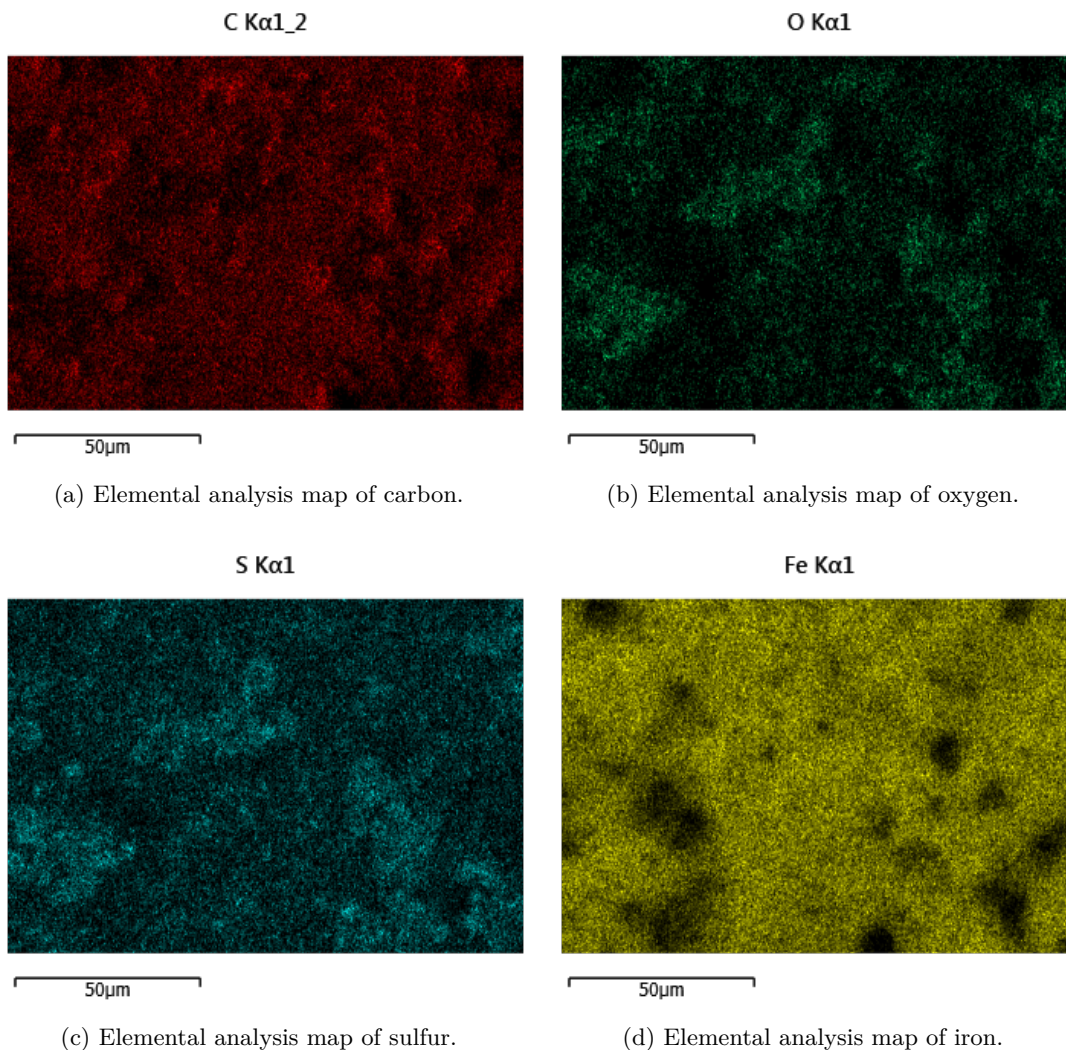


Figure 6.38: EDX analysis of the surface area shown in Figure 6.36b

EDX analysis suggests that the deposits contain carbon, oxygen and sulfur, evident from Figure 6.37, while detection of the underlying iron from the foil indicates varying thickness, corresponding to the visible larger agglomerations of deposits. Overall, EDX analysis suggests that the deposit coating is very thin. Closer analysis of the deposits suggests that the visible spheres are predominantly rich in carbon, shown in Figure 6.38a, while not corresponding to both oxygen and sulphur hotspots, shown in Figure 6.38b and Figure 6.38c. From the presented maps, it appears that sulphur and oxygen form one type of deposit, while carbon leads to another with sulphur and oxygen presenting

hotspots in the same location and the presence of carbon being slightly reduced in areas where the concentration of oxygen and sulphur is high. A look at the iron distribution shown in Figure 6.38d suggests that deposits are thicker where carbon hotspots occur. However, there is no correlation between the elemental distribution of sulphur and oxygen versus iron suggesting that these deposits are very thin.

### 6.6.9.3 Trimethylpentane with 500:1 Dibutyldisulfide

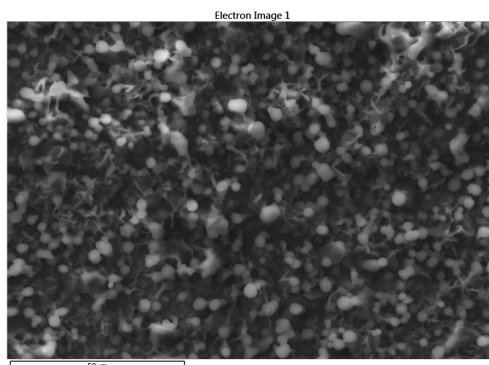
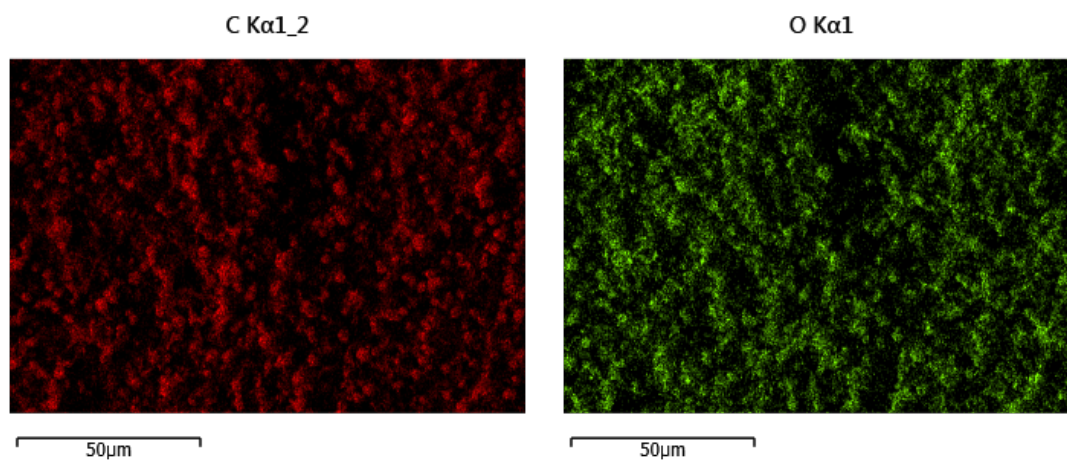


Figure 6.39: SEM image of the surface of a foil placed in trimethylpentane with dibutyldisulfide.

Close inspection of the coating on the foil, shown in Figure 6.39, shows once again spherical particulates that have agglomerated to form a uniform looking coating. EDX analysis of the coating suggests that it consists, as would be expected, of carbon, oxygen and sulphur, shown in Figure 6.40. A look at the iron distribution, contained in the foil forming the base layer, shown in Figure 6.40d suggests that the coating is not uniform but exhibits hotspots where more material has deposited, thus blocking the EDX from detecting the underlying iron layer.



(a) Elemental analysis map of carbon.

(b) Elemental analysis map of oxygen.

Figure 6.40: EDX analysis of the surface area shown in Figure 6.39

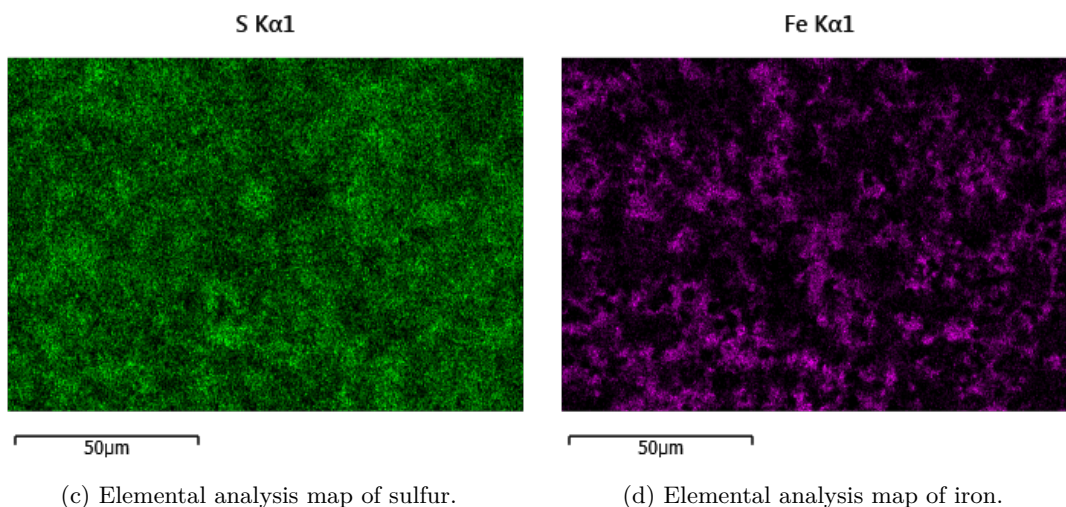


Figure 6.40: EDX analysis of the surface area shown in Figure 6.39

#### 6.6.9.4 Trimethylpentane with 500:1:10 Dibutyldisulfide and p-Xylene

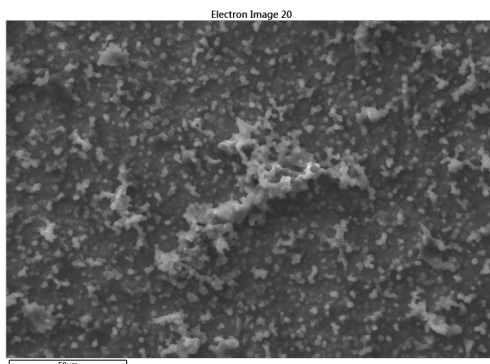


Figure 6.41: SEM image

Trimethylpentane with 500:1:10 dibutyldisulfide and p-xylene produces similar deposits to trimethylpentane with 500:1 dibutyldisulfide, shown in Figure 6.39 and Figure 6.41, consisting of tiny spherical particles. However, the deposits formed after addition of p-xylene appear to be less dense and also exhibit a greater propensity to sticking together forming larger particulates rather than a uniform looking coating.

The elemental distribution, shown in Figure 6.42 suggests that deposits from trimethylpentane with 500:1:10 dibutyldisulfide and p-xylene do not exhibit sulfur hotspots, shown in Figure 6.42c. Instead, deposits present some small carbon and oxygen hotspots, shown in Figure 6.42a and Figure 6.42b. A look at the iron distribution, shown in Figure 6.42d confirms the earlier observation that deposits are comparatively thin, with the metal foil base layer very visible to the EDX.



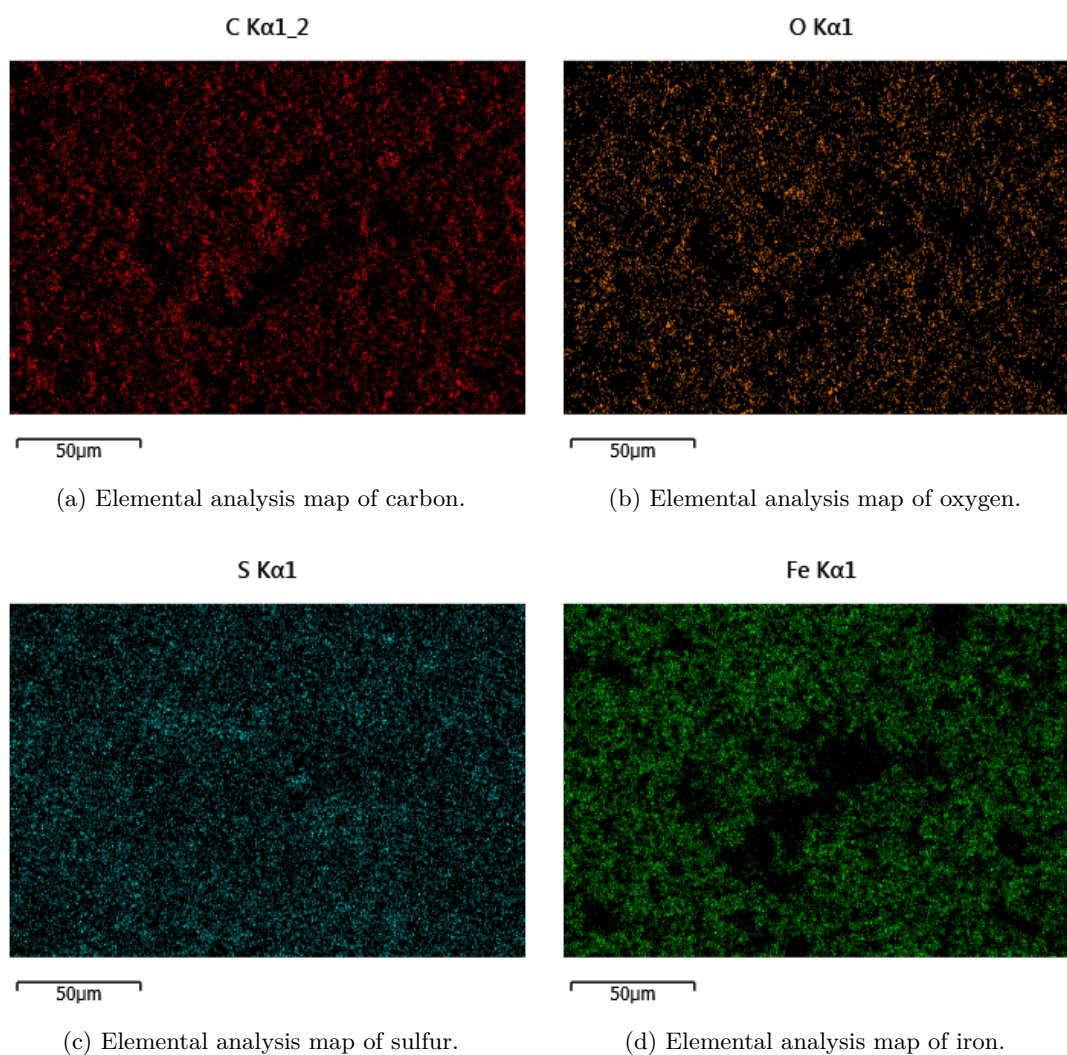


Figure 6.42: EDX analysis of the area shown in the image Figure 6.41.

#### 6.6.9.5 Dodecane with 500:1 Dibutyldisulfide

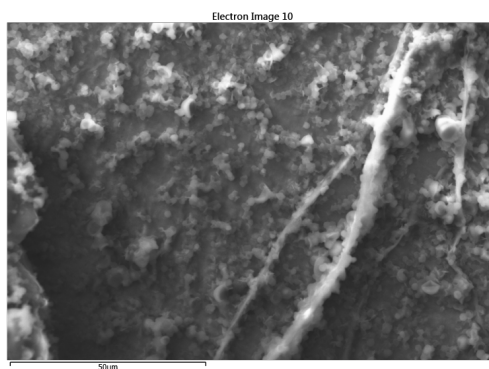


Figure 6.43: SEM image of one of the “arms” reaching outwards from a bubble, such as was shown in Figure 6.12c.

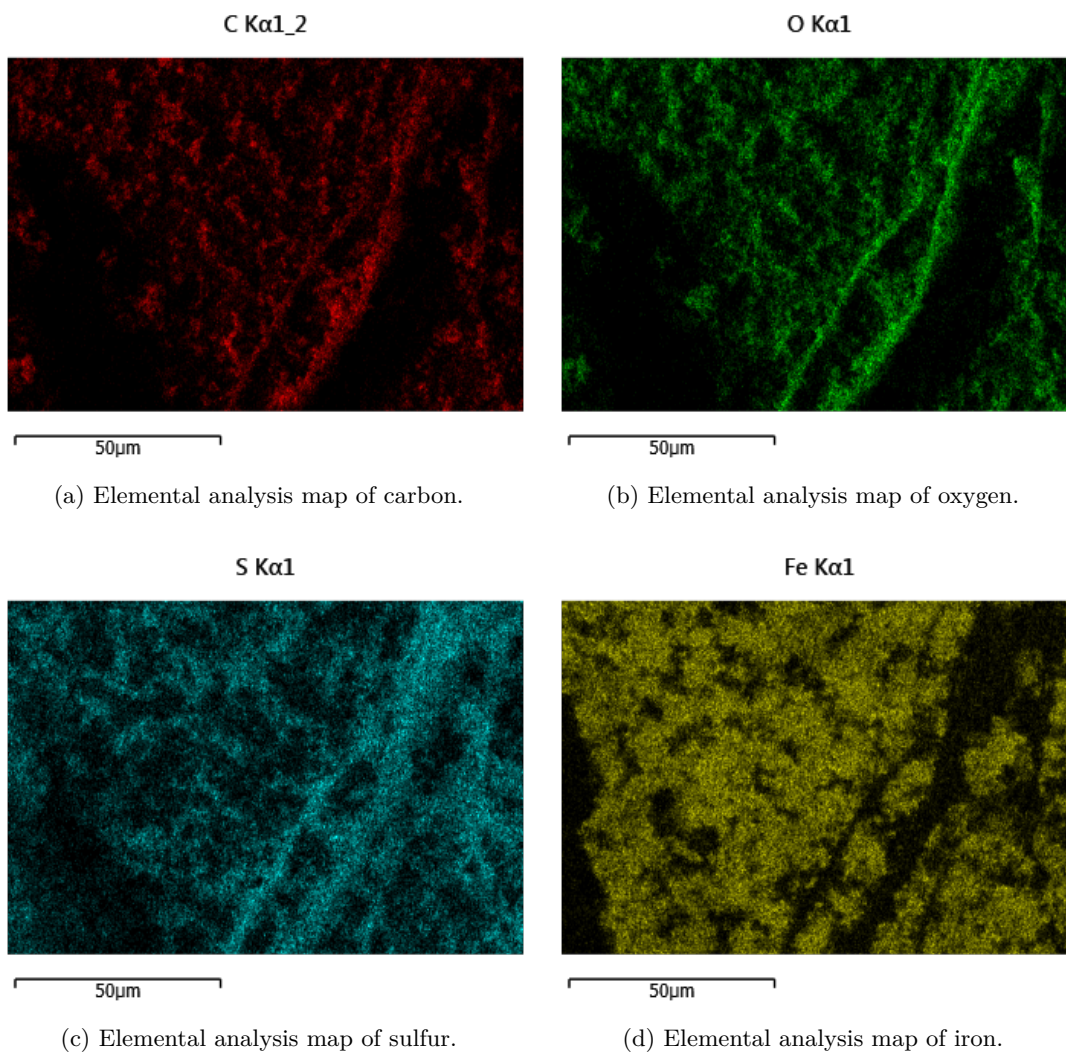


Figure 6.44: EDX analysis of the area shown in the image Figure 6.43.

In Figure 6.12c the macro scale differences between different additives were shown. As the bubbles with the “cracks” were of interest, one such site was analysed more closely using a scanning electron microscope with EDX. Figure 6.43 provides an image of one of the “cracks” or arms, which rather than being a “defect” of some sort in the surface are apparently a structure on top. EDX analysis, shown in Figure 6.44 suggests that these deposits are rich in carbon, oxygen and sulfur with clearly identifiable elemental hotspots agreeing with the observed surface structure.

Interestingly, on a particle level, the particles produced resemble those that were obtained from mixing trimethylpentane with both dibutyldisulfide and p-xylene, shown previously in Figure 6.41, namely stuck together particles based on apparently spherical sub-particles.

## 6.6.9.6 Dodecane with 500:1:10 Dibutyldisulfide and p-Xylene

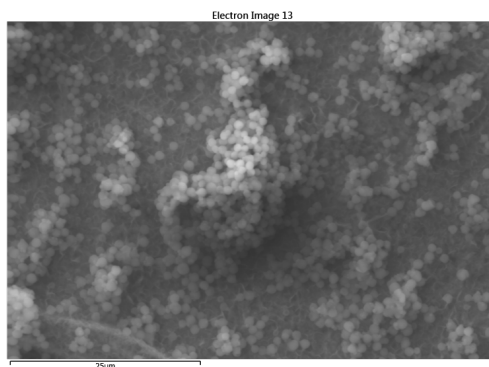
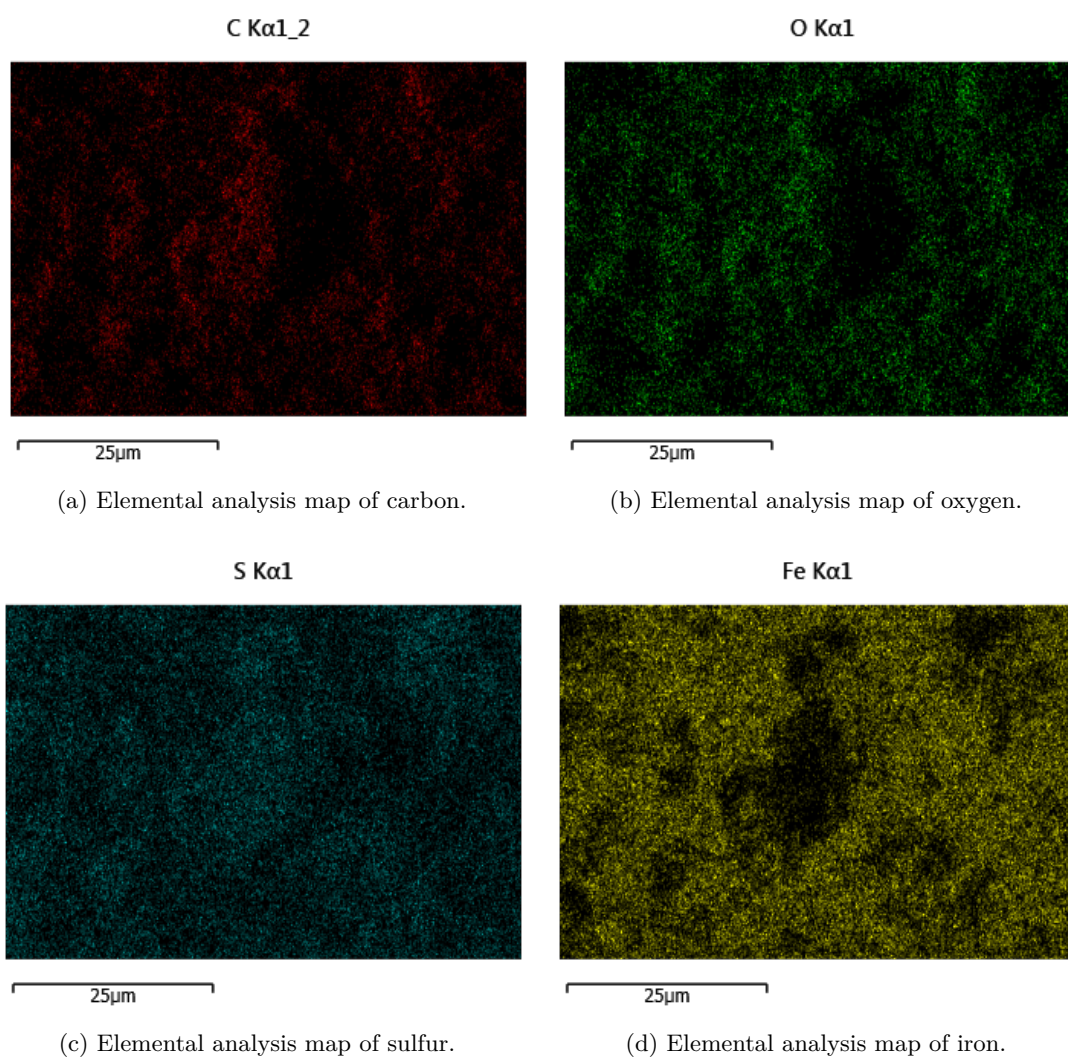


Figure 6.45: SEM image of a particle found on the foil placed in Dodecane with dibutyldisulfide and p-xylene.



(a) Elemental analysis map of carbon.

(b) Elemental analysis map of oxygen.

(c) Elemental analysis map of sulfur.

(d) Elemental analysis map of iron.

Figure 6.46: EDX analysis of the area shown in the image Figure 6.45.

The deposits formed from dodecane with 500:1:10 dibutylsulfide and p-xylene are of a similar appearance to those observed from sulfur induced deposits, consisting of microspheres which may agglomerate to form larger particles and are shown in Figure 6.45. Analysis of the elemental distribution suggests that the deposits consists of carbon, oxygen and sulfur, shown in Figure 6.46. an investigation of the iron distribution from the metal foil indicates that in agreement with the SEM image, shown in Figure 6.45, the deposits are very thin, evident from Figure 6.46d and even in the more visible agglomeration, the iron background is clearly visible in the EDX analysis.

### 6.6.9.7 Sulfide species Summary

Addition of sulfides has lead to the formation of similar coatings on metal foils, from brown to black. Placing the samples under an electron scanning microscope reveals that most, but not all, samples that contained either dibutylsulfide or dibutyldisulfide formed deposits that consist of agglomerations of tiny spherical particulates.

The smaller variations between the deposits suggest that the bulk solvent also has some impact on the structure of deposits formed. For example, while deposits consist of spherical looking particles, the particles formed from dodecane exhibit a more perfect spherical shape than those formed from trimethylpentane.

From the limited number of tests carried out, it also appears that p-xylene acts as an inhibitor to particle or deposit growth in combination with dibutyldisulfide, leading to thinner deposits and lesser agglomeration of microparticles. However, given the individual tests carried out, this would require further experimental research and analysis before a conclusion can be drawn with any certainty.

### 6.6.10 SEM EDX Summary

As can be seen, the structure of deposits generated from the the thermal stressing of hydrocarbon compounds is very different, dependent on the additive which affects the formation of deposits. While some additives have lead to varnish like coatings, both butylamine as well as most sulfur compounds have lead to spherical deposits at the micro scale. Interestingly, the size of these spheres is significantly different, with individual butylamine spheres on the 10  $\mu\text{m}$  scale while spheres in sulfur deposits are smaller than 5  $\mu\text{m}$ , however both can agglomerate to form larger structures. The difference between butylamine and m-toluidine is possibly the most striking, with the former leading to spherical deposits rich in carbon while the latter leads to “splotches” of carbon deposits, devoid of oxygen hotspots with no obviously discernible 3D structure. Sulfurous species also form their own very specific deposition type, which appears to be a uniform coating, but can be found to consists of microspheres that agglomerate to form a more uniform deposition layer, but may also lump together to form larger particles.

This would suggest that inspection of the structure of deposits might allow the researcher to draw conclusions about the nature of the contaminant responsible for deposition, provided a library of different deposit structures by additive is available. The obvious lack of a significant presence of carbonaceous particles comes as a surprise. While beyond the scope of data obtained, it can be speculated that the similarity of the few carbonaceous particles observed may indicate that these are not so much formed during stressing but rather an artefact of foil and solvent preparation and already present before the test, as indicated in the filtration of an unstressed GTL Jet-A blend. However it would require further experimental and analytical data to ascertain this with any reliability.

## 6.7 PetroOxy Conclusion

The PetroOxy offers us a controlled oxidation test device requiring very small quantities of fuel, with very few variables when compared to larger thermal stability test rigs such as the HiReTS. The mechanics of the PetroOxy also allow us to collect samples of the product for further analysis with no issue of cross contamination from previous runs as the sample does not pass through any pipework or other hard to clean components. Thus the observed behaviour in the PetroOxy must be dominated by the presence of the chemical species in the test sample, allowing us to draw a number of conclusions from the observed results.

Pure solvents oxidise more rapidly than a jet fuel blend, as is evident by the eightfold increase in residence time exhibited by the GTL Jet-A blend over dodecane or Banner Solvent, but also do not exhibit a propensity to form deposit when stressed neatly. The Shellsol T exhibited the fastest oxidation rate, suggesting that iso alkanes are more reactive than normal alkanes, assuming no contamination of the solvent is to blame. The recorded pressure drop from the stressing of neat samples suggests that the oxygen consuming reactions in the samples are accelerating during the test.

None of the neat samples tested show any significant differences in the oxygen consumption rate due to the presence of a metal surface in the form of either a stainless steel foil or the gold which strongly suggests that the consumption of oxygen in a hydrocarbon sample is not influenced by surface interactions with either gold or stainless steel 316.

It was shown that the addition of aromatic species has no negative impact on thermal stability in that the solution has remained perfectly clear and free from visible deposits. Of interest is the discrepancy between the impact of aromatic species on the residence time between Shellsol T and Banner np1014 which was significantly different. While Banner np1014 showed a significant and varied response to the addition of aromatic species, the residence time of ShellSol T was affected less and identically by all aromatic additives.

It was observed that amine species will form deposits and also inhibit the rate at which oxygen is consumed. The mechanism by which this occurs warrants further investigation. The huge impact of amine species is evident in the observation that the pressure drop recorded is linear as opposed to an ever steeper curve in a neat sample, indicative of a constant oxygen consumption rate. The impact of *m*-toluidine on the oxygen consumption rate is in so far remarkable as Shellsol T was shown to not respond as strongly as Banner np1014 to the addition of an aromatic or a more simple amine such as butylamine.

The longer tests with butylamine suggest that at least two mechanisms are involved in the formation of deposits. In a regular stress test, which stressed the sample until the pressure has dropped by 10%, deposits offer little resistance to removal by cleaning with a paper tissue. In contrast, the longer test with butylamine produced a hard to remove coating that offered resistance to both traditional cleaning solvents such as acetone or ethanol as well as mechanical cleaning with a tissue. Thus it may be concluded that, in the case of amine additives, precursors to the deposition process initially accumulate and only bond weakly through intermolecular interaction. Varnish like deposits then form from those compounds, most likely through a polymerization reaction.

Sulfur, as expected, lead to the formation of deposits, where interestingly the liquid phase has remained nearly colourless and clear. In addition, deposits from sulphur only coat the dish where in contact with the liquid while amines lead to coatings on the entire internal surface of the PetroOxy dish. This suggests that sulfur interactions predominantly take place at the metal surface in the liquid phase while amine reactions occur in both the liquid as well as the gas phase.

From the observed data it appears that, with the exception of pure solvent grade aromatics, benzene, toluene and *p*-xylene, any additives that lead to deposits act as antioxidants. In the tests, every additive has slowed the rate at which the pressure in the PetroOxy dropped, which indicates that the additives must interfere very efficiently with the autoxidation process. While oxygen has been identified in high atom counts in some deposits, other deposits have been found to be oxygen deprived. This leads to the question whether oxygen is an active contributor to the formation of deposits or rather just an initiator for the reaction chain that ultimately leads to the formation of deposits. In the case of 2,2,4-trimethylpentane, sulfide additives alone did not exhibit an antioxidant behaviour, acting potentially as an accelerator instead while retaining their antioxidant behaviour in conjunction with dodecane. The major difference between both dodecane and trimethylpentane is the neat solvent residence time, which is significantly longer for trimethylpentane than for dodecane. Thus, it appears that compounds or rather products of compounds that initially act as antioxidants may become accelerators once a critical point in the reaction has been reached at which the oxygen consumption

continues and the autoxidation propagates irrespectively of the additive.

The SEM EDX analysis has revealed some surprising results, such as the lack of oxygen hotspots in m-toluidine induced deposits, as well as the alignment of spherical particulates with the “metal grain” in the neat butylamine test, a structure that was lost in the presence of p-xylene. The similarity of the sulfur deposits under a scanning electron microscope is also remarkable, especially given that on a macro scale these look significantly different, from black over brown to faintly yellow. This diversity in the deposit morphology as well as their, in the case of m-toluidine, unexpected composition establish that employing foils in the PetroOxy is a good method for analysing the deposits that formed as a result of the thermal exposure of a hydrocarbon solution. More sophisticated analysis may be able to provide greater insight into further aspects of the deposit morphology, such as thickness, as well as better information about the type of compounds formed, for example by identifying atomic and molecular bonds.





## Chapter 7

# Conclusion and Future Work

### 7.1 Conclusion

The scope of this thesis covered two aspects of thermal stability research. First the suitability of an automated mechanism generator to develop chemical kinetics schemes for autoxidation processes where only the prior composition is known was assessed. Secondly a systematic investigation of the behaviour of a number of solvents and additives in a small scale thermal stability test rig was carried out.

Due to the complexity of aviation fuel, current mechanisms are preferably fitted to experimental data to obtain an accurate description of the observed behaviour. To develop a more fundamental approach to mechanism development, MIT's Reaction Mechanism Generator has been employed which derives chemical reaction mechanisms from the initial reactants through the use of a kinetics library and Benson Group Additivity for property estimation. As synthetic paraffinic kerosene forms one of the options for more environmentally friendly fuels when compared to conventional aviation fuel, as well as offers the potential for higher performance engines. A number of representative solvents whose composition is more closely defined than that of jet fuel or synthetic fuel, covering normal paraffinic hydrocarbons as well as iso paraffinic hydrocarbons were investigated. The work presented in this thesis shows that RMG appears to be able to accurately predict the behaviour of normal paraffinic hydrocarbons while it appears to struggle with producing accurate descriptions of iso paraffinic hydrocarbons, at least in so far that RMG struggles to produce a comprehensive mechanism for a strongly branched species, while the predicted mechanism for simpler iso-species does not agree with expectations. This may be related to the fact that RMG only produces mechanisms for ideal cases in which catalytic interactions are not considered which thus leads to reaction paths that occur in experiments being ignored by RMG, such as for example the decomposition of hydroperoxides. In addition, closer work with RMG mechanisms requires the ability to compact and reduce the generated reaction scheme into a more human readable and manageable format. Our work has shown that employing a species lumping mechanism

combined with a rates based reduction offers a suitable method to obtain significantly size-reduced reaction mechanisms. As a result, in its current form, RMG offers a very interesting, but limited tool for the investigation of autoxidation behaviour of solvents.

A problem encountered when employing RMG for autoxidation processes is the topic of validation which is dependent on reliable data. The inherent complexity of real world fuels makes validation of RMG schemes impossible, which leaves the focus on more closely defined solvents. In addition, the use of very controlled conditions with minimal outside influences is essential when validation attempts are made. The PetroOxy employed in this thesis presents a sufficiently simple test device that validation of an RMG scheme with a laboratory grade solvent may be attempted. However it should be pointed out that with no data on the autoxidation products found in the PetroOxy, only an indirect comparison with the headspace pressure is possible. Simulating the headspace pressure by describing the gas solvation in the liquid phase through Henry's law while employing a very fast headspace to liquid gas transfer rate resulted in a very good initial model given the lack of any fitting. This result should encourage further work employing a simple model for the gas to liquid transfer with zero dimensional chemical kinetics modelling as the PetroOxy can be easily employed to test a number of compounds in very controlled conditions.

Some experimental work with solvents was carried out in a HiReTS test rig which was an accepted ASTM test method until it was withdrawn in 2013. Unfortunately while the comparatively high test temperature promises accelerated processes, the tests proved inconclusive. Technical problems with the test apparatus as well as the inability to obtain post test samples meant that work was discontinued on the HiReTS after a number of tests in favour of a, for research purposes, more suitable method.

As a result of the limitations of the HiReTS, the evaluation of the impact of a number of postulated bimolecular reactions, for which the activation energies were calculated in Gaussian is highly speculative as a direct comparison between observed and predicted results is impossible. The inability to reproduce the reported impact of *m*-toluidine with a commercial solvent in the HiReTS also suggests that the observed effects are not generally applicable to solvents. What may be concluded from the Gaussian calculations is that any uncatalysed interaction between an aromatic species or amine and an oxygenated species or alkene is unlikely due to the large energy barrier.

The PetroOxy was employed to carry out an experimental investigations into the thermal stability of solvents as its small scale experiments and static conditions mean that test conditions are well described and known, the retention of samples with little or no cross contamination is possible and solvents may be used as surrogates to carry out a study into their fundamental behaviour. In connection with the reasonable test time, the

PetroOxy enabled us to carry out an experimental investigation that would be more difficult to carry out in larger scale test rigs. The ability to place metal foils in the sample also meant that it was possible to investigate the potential for catalytic effects of a stainless steel foil and to retain the deposits for further analysis.

The tests in the PetroOxy presented us with a number of expected as well as unexpected results. Most tests were carried out using a standard 10% pressure drop termination criteria, which means that a broadly similar quantity of oxygen was consumed before the test terminated. Tests in the PetroOxy demonstrated that regular solvents, such as decane, dodecane but also industrial Banner Solvent np1014 are not prone to form deposits under thermally stressed conditions. Further, there appears to be no clearly discernible effect on neat solvents from the gold dish or metal foil when compared to a PTFE dish. This suggests that the autoxidation of suitably pure normal paraffinic hydrocarbons is not catalysed by solid metal surfaces. The slow oxidation rate of 2,2,4-trimethylpentane and fast oxidation of ShellSol T, a commercial iso paraffinic solvent contradict each other, however it is possible that ShellSol T was contaminated or aged or that 2,2,4-trimethylpentane through its compact structure is more stable than would be expected due to hindrance effects. The vastly different impact of aromatics on the residence time and hence oxidation rate of Banner Solvent and ShellSol T is also of interest and may suggest that the ShellSol suffered from a problem of some sort. On the other hand, neither sample exhibited any form of deposit formation as a result of the addition of reagent grade aromatics which is especially remarkable in the context of the 800 minutes residence time observed with Banner Solvent and benzene, a more than tenfold increase in the residence time, which saw no visible deposits or discolouration of the sample. The conclusion that can be drawn from this is that reagent grade aromatics do not harm the thermal stability of hydrocarbon solvents, however their impact in connection with other additives or contaminants may differ.

Amines exhibit a small antioxidant effect when added as butylamine and a significant, in many ways remarkable impact when added as either aniline or m-toluidine. At the same time, the tests showed that amines are prone to deposit formation of varying severity with diamines having the worst impact. Final deposit layers from amines are varnish like and extremely hard to remove, thus it seems prudent to suggest that no amines should be present in commercial fuels as their propensity to form deposits would place components at elevated risk of failure. The filter test carried out with m-toluidine in a blend of 80% Jet-A and 20% GTL shows that a comparatively short residence time of 120 minutes already results in visible changes of the hydrocarbon solution. The tests with a combination of butylamine, metal foils and p-xylene suggest that amine interactions may be catalysed or enhanced by both metals as well as aromatics, however further work is needed to confirm and clarify this observation.

The sulfur tests lead to an expected formation of deposits whose nature differed depending on the involved hydrocarbon combination and possibly residence time too, given that it differs significantly between the tests. The observations suggest that the addition of aromatics to a sample which contains a sulfide additive leads to a reduction in deposits as well as an antioxidant effect in the solution. Inspection of the samples on the macro scale also shows a different deposit morphology between filamentous and spherical particulates, however this distinction does not hold true when analysing the deposits under a scanning electron microscope. The observation that deposits only formed at the liquid surface interface in the sulfur tests and other parts of the PetroOxy dish remaining uncoated further suggests that the chemistry involving sulfur only occurred in the liquid phase. In contrast, amines also coated the lid of the PetroOxy dish which suggests that a gas phase interaction was also a part of the chemical interactions during the test.

While the contribution of heteroatomic species is well established, their impact on the autoxidation process itself is often neglected. The work in this thesis clearly shows that the autoxidation process, namely the consumption of oxygen by the “test fuel” is strongly related to the presence of heteroatomic compounds in the fuel or solvent. Due to the significant impact of some compounds as well as the manifold interactions between different species, more fundamental work is required. For example the tests of sulfur compounds in neat dodecane would suggest that the sulfides and disulfides act as antioxidant species, while in contrast the same sulfides in isooctane acted as a weak accelerator while the disulfides continued to act as antioxidants. Any study hence investigating the autoxidation behaviour of fuels will thus suffer from distortions introduced by the presence of heteroatomic species. In connection with the potential for catalytic interactions between heteroatomic species and metal surfaces in pipes, their presence introduces significant uncertainty into any experimental data outside of very well controlled test conditions. The observation that both heteroatomic species as well as aromatics exhibited antioxidant properties in solvents further suggests that the topics of thermal stability and autoxidation must be considered independently. The presence of neat oxygen in pure hydrocarbon mixtures will only lead to the production of oxygenated products. In contrast, in the presence of heteroatomic species, oxygen will initiate the reactions that lead to the formation of deposits, as it is well established that de-oxygenation of fuels can improve the thermal stability of test fuels<sup>166</sup>.

The last part of the experimental investigation covered analysis of select foils under a scanning electron microscope with x-ray diffraction elemental analysis to obtain a better understanding of the morphology as well as the composition of the deposits. SEM imaging enabled us to identify comparatively distinct deposition patterns based on the type of additive employed. Butylamine formed spherical particulate deposits that are orientated with the grain of the metal indicating a potential surface catalytic effect in their formation. The addition of p-xylene led to spherical deposits that were no

longer orientated, as well as a comparatively thin coating of the foil where deposits are predominantly rich in carbon but also show a presence of oxygen. M-toluidine produced very atypical deposits which were only rich in carbon but devoid of oxygen suggesting that it is probable that very different mechanisms were at work in the formation of both types of amine deposits. Whether deposits would form in an m-toluidine doped sample would hence also form under de-oxygenated conditions would thus be a potential question for future work.

The sulfur samples presented the most consistent candidates under the scanning electron microscope. The two investigated samples of sulfide deposits present a potentially polymeric deposit, while the disulfide samples consist of microspheres which agglomerated to form the observed deposits. The elemental analysis map also reveals varying agreement between elemental hotspots of carbon, oxygen and sulfur suggesting that despite the similarity of solvents and additives, the mechanisms as well as products are very different. However, it can be concluded that sulfur species interact, either in the liquid phase or on the surface, with oxygen, exhibiting a clearly discernible oxygen presence which in some cases shows good agreement with sulfur hotspots and observable deposits.

In conclusion, it can be said that the PetroOxy has proven to be a very valuable tool for investigating the thermal stability in greater detail with the flexibility and controllability of the test method offering many opportunities to seek an enhanced understanding into the behaviour of hydrocarbons under thermal stress offering many ideas for future investigations. The analysis of deposits under a scanning electron microscope lead to the observation that the morphology of deposits is related to the nature of the heteroatomic compounds present in the test solvent. This observation may offer the potential for future modelling in which the morphology of deposits can be taken into account when investigating potential surface deposition reactions.

## 7.2 Suggestions for Future Work

We have shown that an investigation into the fundamentals of thermal stability using idealised conditions in the form of simple static test methods and solvents can lead to increased insights into the thermal degradation of aviation fuels. Such data can be used to develop more realistic models of thermal degradation behaviour as well as to obtain initial predictions as to the source of thermal deposits from their very different structure and composition.

We therefore recommend that future work should aim to expand on the idea developed in this thesis, which is to investigate the behaviour of surrogate compounds in connection with additive combinations under a large number of test conditions, covering additive concentration, temperature and exposure time. The behaviour of individual fuel compo-

ment compounds has been investigated previously, most recently by Sicard et al.<sup>61</sup>, but does not include any additives or contaminants which can have significant impact on the behaviour of a tested fuel or solvent. Previous work<sup>168</sup> as well as our current study has shown that most of the behaviour of thermally stressed aviation fuel is attributed to the presence of trace compounds. These compounds exhibit reasonably predictable patterns, allowing them to be correlated to the observed effect in specific fuels. However, due to the complexity of fuel, interactions with unidentified trace species cannot be ruled out which in itself may influence the behaviour of known contaminants. Our work shows that the addition of some additives such as amines and aromatic compounds can have a significant impact on the chemical behaviour of the fuel which is again distinct when comparing individual additives to additive combinations. Therefore a systematic evaluation and systematic mapping the behaviour of a number of surrogate and additive compounds will improve our understanding of thermal stability. Especially the assessment of multiple additive tests will offer valuable insight into the behaviour of fuels under autoxidation conditions. While our work did not show any clear impact of metal foils on the autoxidation behaviour outside of the butylamine-doped samples, future work should also consider more thoroughly investigating the impact of different metals on the autoxidation process, especially in doped samples which are more likely to respond to the presence of a metal foils than neat solvents.

Future work should look at establishing a comprehensive relational database of additive behaviour under varying conditions. Such a resource would allow us to both improve our understanding of thermal stability as well as to predict the behaviour of compounds by querying and studying behavioural patterns between additives.

Detailed analysis of any products formed can be used to postulate possible reaction paths leading to the formation of products in the liquid phase and deposits. This could involve not only an improved investigation of the morphology, but also quantitative data about the elemental composition as well as information about the atomic and molecular bonds in the deposits. Information about the molecular weight of deposits would be advantageous to obtain estimates of how many species from the test fuel are required to form individual particulates and would aid with the postulation of possible reactions for deposit formation. In addition, an understanding of how the oxygen is included or bonded in the deposits would aid in the identification of precursor species to deposit formation. For example, if an alcohol group,  $-OH$  were identified, a test with an alcohol can establish whether the alcohol has any direct impact. If no impact from the presence of an alcohol is observed, the most likely route for alcohol formation is hydrogen abstraction by an  $-RO\cdot$  group which can form as a result of a hydroperoxide decomposition as well as also the less likely termination of an alkyl radical,  $R\cdot$  with a hydroxyl group  $\cdot OH$ . In conjunction with both an automated mechanism generation tool, model reduction and quantum chemistry calculations, improved models to describe

the chemical kinetic processes may be developed for further application.

RMG also shows great promise as a research tool for the investigation of hydrocarbons under thermal stress. We suggest that future work should look at extending the database and potentially at enabling catalytic reactions, even if the kinetics data has to be specified by the user in the input file to obtain an improved description of the autoxidation behaviour of hydrocarbons under more realistic conditions.

The work on employing an extended zero-dimensional chemical kinetics simulation has shown promising results. Hence a further recommendation would be to improve on the proposed model as well as to employ more complete autoxidation models to obtain an improved model of the autoxidation behaviour of test samples in the PetroOxy. Expansion of the work presented in this thesis may also be able to explain the mechanisms through which any heteroatomic species interact with the autoxidation process as well as explain the very different impact different compounds have on the oxygen consumption behaviour of test samples with different heteroatomic dopants.

In connection with a more experienced operator as well as quicker access to a gas chromatograph, future work may also be able to offer a more direct validation method for proposed autoxidation mechanisms in conjunction with the PetroOxy.





## Appendix A

# Full List of Options “initial.inp”

### Essential

```
Temperature 423      ! initial temperature/K
EndTime 5e4 1.0e0! second entry is time step
O2(2)      0.02 ! concentrations of initial species, assumes mol/
            L
C12H26(1)   4.7

Threshold 1.0e-13
RTOL 1.0e-7
```

or

```
Tolerance 1.0e-7      1.0e-13 ! relative tolerance and threshold
```

### Optional

```
IRREV ! flag to make scheme irreversible, set automatically when
      necessary
PrintReac ! prints reaction rates
RatesMaxAnalysis ! find the maximum rates for every reaction
RatesAnalysisAtTime x y z ! print rates at timex xyz
ReduceReactions 7 ! Mechanism Reduction, based on magnitude of
      rate
hm 1.e-12 ! minimum timestep if other is desired
initialh 1.e-3 ! initial timestep for solver if other is desired
Jacobian ! to use the analytical Jacobian

PetroOxy Solvent Sample=5
PetroOxy Initial Pressure=700
PetroOxy Maximum Pressure=1015
PetroOxy Gas Species=O2(2)
PetroOxy Gas Solubility=0.002
```



# Appendix B

## Excel VBA Code

### B.1 The VBA Menu Addition

```
Private Sub Workbook_Open()  
    If ActiveWorkbook Is Nothing Then CreateCommandBar  
End Sub  
  
Sub CreateCommandBar()  
    CreateMenuItem "Senkin Species Profile Import v3", "SenkinImport.  
        GetFileLocation"  
End Sub  
  
Private Sub CreateMenuItem(ByVal Caption As String, ByVal Action As String)  
    Dim ctl As CommandBarControl  
    Dim i As Long  
    Dim ControlCollection As New Collection  
    Dim myMenuBar As CommandBar, toolsMenu As CommandBarPopup, newMenuItem As  
        CommandBarControl, newButton As CommandBarControl  
  
    'First Create Menu Item  
    Set myMenuBar = Application.CommandBars.ActiveMenuBar  
    Set toolsMenu = myMenuBar.Controls(6)  
    Set newMenuItem = myMenuBar.FindControl(Tag:=Action, recursive:=True)  
    If Not newMenuItem Is Nothing Then newMenuItem.Delete  
    Set newMenuItem = toolsMenu.Controls.Add(Type:=msoControlButton, Before:=3)  
    newMenuItem.Tag = Action  
  
    ' Versions before Office 2007 only (=> ribbons!)  
    If CLng(Split(Application.Version, ".")(0)) < 12 Then  
        'Now create tool bar  
        Dim myToolBar As CommandBar  
        On Error Resume Next  
        Set myToolBar = Application.CommandBars(Action)  
        On Error GoTo 0  
        If myToolBar Is Nothing Then  
            Set myToolBar = Application.CommandBars.Add(Name:=Action)  
        End If  
        If myToolBar.Controls.Count > 0 Then myToolBar.Controls(1).Delete  
  
        myToolBar.Position = msoBarTop  
        myToolBar.Visible = True  
        Set newButton = myToolBar.Controls.Add(msoControlButton)  
    End If  
  
    If Not newButton Is Nothing Then  
        ControlCollection.Add newButton  
    End If  
    If Not newMenuItem Is Nothing Then  
        ControlCollection.Add newMenuItem
```

```

End If

For Each ctl In ControlCollection
    ctl.OnAction = Action
    ctl.FaceId = 107
    ctl.TooltipText = Caption
    ctl.Caption = Caption
Next
End Sub

```

## B.2 The VBA Data handling Module

```

Dim EndCount As Integer
Dim FilePath As String

Sub GetFileLocation()

Dim UserFileSelect As String
Dim UserInput As String

UserFileSelect = Application.GetOpenFilename(, , "Select Last Input File")

FilePath = Left(UserFileSelect, Len(UserFileSelect) - 2)

If FilePath <> "" Then

    'http://support.microsoft.com/kb/213646
    UserInput = Right(UserFileSelect, 2)

    If UserInput <> "" Then
        EndCount = UserInput
        Call Import
    End If

Else
    MsgBox ("You have not Selected a File Path - Aborting!")
End If

End Sub

Sub Import()
,
' Import Macro
' Will Import ALL Secies Concentration Profiles from the provided set of files
,
Dim i, j As Integer
Dim Filename, ConnectionSetup As String

For i = 11 To EndCount

'FilePath = "C:\Users\pmdcm\Desktop\RMG-97\All Species Profiles\Contain
Interesting Species\fort." & i
ConnectionSetup = "TEXT;" & FilePath & i

'With ActiveSheet.QueryTables.Add(Connection:= _
"TEXT;C:\Users\pmdcm\Desktop\RMG-97\All Species Profiles\Contain Interesting
Species\fort.11" _
, Destination:=Range("$A$1"))

With ActiveSheet.QueryTables.Add(Connection:= _
ConnectionSetup _
, Destination:=Range("$A$1"))
'Filename = "fort." & i
'.Name = "fort.11"
.Name = Filename
.FieldNames = True

```

```

        .RowNumbers = False
        .FillAdjacentFormulas = False
        .PreserveFormatting = True
        .RefreshOnFileOpen = False
        .RefreshStyle = xlInsertDeleteCells
        .SavePassword = False
        .SaveData = True
        .AdjustColumnWidth = True
        .RefreshPeriod = 0
        .TextFilePromptOnRefresh = False
        .TextFilePlatform = 850
        .TextFileStartRow = 1
        .TextFileParseType = xlDelimited
        .TextFileTextQualifier = xlTextQualifierDoubleQuote
        .TextFileConsecutiveDelimiter = True
        .TextFileTabDelimiter = True
        .TextFileSemicolonDelimiter = False
        .TextFileCommaDelimiter = False
        .TextFileSpaceDelimiter = True
        .TextFileColumnDataTypes = Array(1, 1, 1, 1, 1, 1)
        .TextFileTrailingMinusNumbers = True
        .Refresh 'BackgroundQuery:=False
    End With

    'ActiveWorkbook.RefreshAll

    ' http://msdn.microsoft.com/en-us/library/office/aa221563%28v=office.11%29.
    ' aspx
    Dim myColumnsUnion As Range
    Dim PasteColumn As Integer

    If i = 11 Then
        ' Copy All 5 columns to new sheet
        'Set myColumnsUnion = Union(Columns(2), Columns(3), Columns(4), Columns
        ' (5), Columns(6))
        ' 2 Columns in new Design
        Set myColumnsUnion = Union(Columns(2), Columns(3))
        'Columns(2).Select
        myColumnsUnion.Select
        Selection.Copy
        Sheets("Sheet3").Select
        Columns(2).Select
        ActiveSheet.Paste
    Else
        'Columns("D:F").Select
        'Set myColumnsUnion = Union(Columns(4), Columns(5), Columns(6))
        ' Species now fill the file
        Set myColumnsUnion = Union(Columns(2), Columns(3), Columns(4), Columns
        (5))
        myColumnsUnion.Select
        Selection.Copy
        'Columns(2).Select
        Sheets("Sheet3").Select
        'PasteColumn = 3 * (i - 10) + 1
        ' Steping in steps of 4
        PasteColumn = 4 * (i - 11) '+ 3
        Columns(PasteColumn).Select
        ActiveSheet.Paste
    End If

    Sheets("Sheet2").Select
    Columns("B:F").Clear

    Call Display_Delete_All_QueryTables_In_Sheet

Next i

```

```

End Sub

' From: http://www.officekb.com/Uwe/Forum.aspx/excel-prog/142846/how-delete-old-querytables

Sub Display_Delete_All_QueryTables_In_Sheet()

'THIS PROGRAM DISPLAYS A COUNT OF ALL QUERYTABLES IN THE ACTIVESHEET
'WITH THEIR NAMES; THEN DISPLAYS A COUNT OF ALL QUERYTABLES IN THE
'ACTIVE FILE WITH THEIR NAMES; THEN DISPLAYS AN OPTION TO DELETE ALL
'QTS IN THE ACTIVESHEET OR ALL QTS IN THE ACTIVE FILE OR QUIT.

'Ignore errors
On Error Resume Next

'Display QTs in sheet
xQTCCount = ActiveSheet.QueryTables.Count
For x = 1 To xQTCCount
    sMsg = sMsg & ActiveSheet.QueryTables(x).Name & vbCr
Next
'MsgBox "Sheet QueryTables (" & ActiveSheet.QueryTables.Count & "):" & vbCr &
    sMsg

'Display Qts in file
xSheetCount = ActiveWorkbook.Sheets.Count
For s = 1 To xSheetCount
    xQTCCount = Sheets(s).QueryTables.Count
    q = q + xQTCCount
    For f = 1 To xQTCCount
        fMsg = fMsg & Sheets(s).Name & "!" & Sheets(s).QueryTables(f).Name & vbCr
    Next f
Next s
'MsgBox "File QueryTables (" & q & "):" & vbCr & fMsg

'Skip if none are found
If q > 0 Then

'Display option for deletion
'dMsg = "Yes = Delete ALL querytables in the active sheet" & vbCr
'dMsg = dMsg & "No = Delete ALL querytables in the file" & vbCr
'dMsg = dMsg & "Cancel = Quit program"
'xResponse = MsgBox(dMsg, vbYesNoCancel)

'Cancel
'If xResponse = vbCancel Then End

'Yes - delete sheet QTs
xQTCCount = ActiveSheet.QueryTables.Count
For x = 1 To xQTCCount
    ActiveSheet.QueryTables(x - n).Delete
    n = n + 1
Next x

'No - delete file QTs
xSheetCount = ActiveWorkbook.Sheets.Count
For s = 1 To xSheetCount
    xQTCCount = Sheets(s).QueryTables.Count
    For q = 1 To xQTCCount
        Sheets(s).QueryTables(q - n).Delete
        n = n + 1
    Next q
Next s
End If

End Sub

```

## Appendix C

# Automated Ignition Time Plot in R

```
## Simple function to do the data analysis

CollectData <- function(filename)
{
  Time <- NULL
  Temp <- NULL

  files <- list.files(path=filename, pattern=".txt", all.files=T,
    full.names=T)
  for (file in files) {
    Data <- read.table(file, sep=" ", header=FALSE)

    IsSet = FALSE

    for (i in 1:length(Data$V1)){
      check <- ( Data$V2[i+1]-Data$V2[i] ) / ( Data$V1[i+1]-Data$V1
        [i] )

      if(!is.na(check) && !IsSet)
      {
        if(check >= 10000)
        {
          Time <- c(Time,Data$V1[i])
          Temp <- c(Temp,as.numeric(gsub("[A-z \\\\.\\(\\) \\/]", "",
            gsub("^.*?/", "",file))))
          IsSet = TRUE
        }
      }
    }
  }

  Set <- data.frame(Time,Temp)

  return(Set)
}
```

```

Expe <- read.table("./Experimental/Data.txt", sep="", header=TRUE
)
Set1 <- CollectData("Westbrook/")
Set2 <- CollectData("Old-RMG-30/") # RMG 146 in thesis draft
Set3 <- CollectData("Old-RMG-30 Rerun/")
Set4 <- CollectData("Heptane 1/")
Set5 <- CollectData("Old-RMG-34/") # very good data set
Set6 <- CollectData("Old-RMG-28/") # RMG 220 in thesis draft

Set2 <- subset(Set2, Temp > 885, select=c(Time,Temp))
Set3 <- subset(Set3, Temp > 975, select=c(Time,Temp))
Set6 <- subset(Set6, Temp > 975, select=c(Time,Temp))

pdf("plot-of-different-autignition-models.pdf",width=8,height=6)

## colouring points? http://www.statmethods.net/advgraphs/parameters.html

par(mar=c(5,6,4,2))
plot(Expe$InvTemp, Expe$Time,
log="y",
type="p", col=1,
pch=20,
tck=-0.02, lab=c(10,10,4), las=1,
xaxs="i", xlab="1000/Temperature K",
xlim=c(0.65,1.6),
yaxs="i", ylab="log Time s\n",
ylim=c(5e-7,4e-1)
)

lines((1000/Set1$Temp), Set1$Time, type="p", col=1, pch=21) #
  Westbrook

lines((1000/Set2$Temp), Set2$Time, type="p", col=2, pch=3) # High
  temperature range RMG 3.3
lines((1000/Set6$Temp), Set6$Time, type="p", col=3, pch=4)
lines((1000/Set3$Temp), Set3$Time, type="p", col=4, pch=1) # High
  temperature range RMG 4.0 - rerun
lines((1000/Set5$Temp), Set5$Time, type="p", col=6, pch=8) # Wide
  temperature range RMG 3.3
lines((1000/Set4$Temp), Set4$Time, type="p", col=8, pch=6) # Wide
  temperature range RMG 4.0 - new conditions

title("Modelling Autoignition Times in RMG \n Published
  Mechanism and Experimental Data for Comparison")

legend(0.85, 2.8e-5,
c(
"High Temperature RMG 3.3 GRI-Mech Seed, small scheme",
"High Temperature RMG 3.3 GRI-Mech Seed, large scheme",
"High Temperature RMG 4.0 GRI-Mech Seed (rerun)",
"Wide Temperature Range RMG 3.3 GRI-Mech Seed",
"Wide Temperature Range RMG 4.0"
),

```



```
pch=c(3,4,1,8,6),  
col=c(2,3,4,6,8)  
)  
  
legend(0.7,3e-1,  
c(  
"Published Experimental Data Scheme",  
"Published Westbrook Scheme"  
),  
  
pch=c(20,21),  
col=c(1,1)  
)  
  
dev.off()
```



# Bibliography

- [1] J. Conti, P. Holtberg, L. E. Doman, K. A. Smith, J. O’Sullivan, K. R. Vincent, P. D. Martin, J. L. Barden, P. Budzik, A. F. Coal, M. L. Mellish, D. R. Kearney, B. T. Murphy, N. Slater-Thompson, P. Gross, V. V. Zaretskaya, G. Jacobs, D. R. Kearney, D. Gaul, A. Geagla, P. Lindstrom, L. Mayne, B. McLeod, C. L. Smith, P. Wells, E. M. Yucel, and T. Tatum., “International energy outlook 2011,” tech. rep., U.S. Energy Information Administration, Sept. 2011.
- [2] BP, “BP Statistical Review of World Energy June 2012,” tech. rep., BP, June 2012.
- [3] S. Scalla, A. Ott, and G. Welslau, “Umwelt und Luftverkehr,” Tech. Rep. 2, Europäisches Parlament, Generaldirektion Wissenschaft, Abteilung für Umwelt, Energie und Forschung, STOA, 1998.
- [4] J. Sieber, “Langfristige Sicherung des Luftverkehrs durch neue Antriebstechnologien und alternative Brennstoffe,” tech. rep., MTU Aero Engines, München, 2008.
- [5] U. Schumann, “Klimawirkungen des Luftverkehrs,” tech. rep., Deutsches Zentrum für Luft- und Raumfahrt, 2007.
- [6] T. Edwards, “Advancements in gas turbine fuels from 1943 to 2005,” *Journal of Engineering for Gas Turbines and Power*, vol. 129, no. 1, p. 13, 2007.
- [7] G. Hemighaus, T. Boval, J. Bacha, F. Barnes, M. Franklin, L. Gibbs, N. Hogue, J. Jones, D. Lesnini, J. Lind, and J. Morris, “Aviation fuels technical review,” tech. rep., Chevron Global Aviation, Chevron Products Company 1500 Louisiana Street Houston, TX 77002, 2004.
- [8] A. H. Lefebvre and D. R. Ballal, *Gas Turbine Combustion Alternative Fuels and Emissions*. CRC Press, third ed., 2010.
- [9] H. Huang, L. J. Spadaccini, and D. R. Sobel, “Fuel-cooled thermal management for advanced aeroengines,” *Journal of Engineering for Gas Turbines and Power*, vol. 126, no. 2, p. 284, 2004.
- [10] J. I. Hileman, H. M. Wong, I. A. Waitz, D. S. Ortiz, J. T. Bartis, M. A. Weiss, and P. E. Donohoo, “Near-Term Feasibility of Alternative Jet Fuels,” tech. rep., Partnership for AiR Transportation Noise and Emission Reduction, 2009.
- [11] S. Blakey, L. Rye, and C. W. Wilson, “Aviation gas turbine alternative fuels: A review,” *Proceedings of the Combustion Institute*, vol. 33, pp. 2863–2885, Jan. 2011.

- [12] D. Daggett, O. Hadaller, R. Hendricks, and R. Walther, "Alternative Fuels and Their Potential Impact on Aviation," tech. rep., NASA, Oct. 2006.
- [13] L. Rye, S. Blakey, and C. W. Wilson, "Sustainability of supply or the planet: a review of potential drop-in alternative aviation fuels," *Energy Environmental Science*, vol. 3, no. 1, p. 17, 2010.
- [14] G. Hemighaus, T. Boval, C. Bosley, R. Organ, J. Lind, R. Brouette, T. Thompson, J. Lynch, and J. Jones, "Alternative jet fuels," tech. rep., Chevron Global Aviation, Chevron Products Company 1500 Louisiana Street Houston, TX 77002, 2006.
- [15] M. Vera-Morales and A. Schaefer, "Fuel-cycle assessment of alternative aviation fuels draft final report," tech. rep., University of Cambridge Institute for Aviation and the Environment, Apr. 2009.
- [16] M. Sobkowiak, J. M. Griffith, B. Wang, and B. Beaver, "Insight into the Mechanisms of Middle Distillate Fuel Oxidative Degradation . Part 1 : On the Role of Phenol , Indole , and Carbazole Derivatives in the Thermal Oxidative Stability of Fischer-Tropsch / Petroleum Jet Fuel Blends," *Energy & Fuels*, vol. 23, no. 4, pp. 2041–2046, 2009.
- [17] I. Uryga-Bugajska, M. Pourkashanian, D. Borman, E. Catalanotti, and C. W. Wilson, "Theoretical investigation of the performance of alternative aviation fuels in an aero-engine combustion chamber," *Proceedings of the Institution of Mechanical Engineers Part G Journal of Aerospace Engineering*, vol. 225, pp. 1–9, Oct. 2009.
- [18] D. L. Daggett, R. C. Hendricks, R. Walther, and E. Corporan, "Alternate fuels for use in commercial aircraft," tech. rep., NASA, Apr. 2008.
- [19] E. Catalanotti, K. J. Hughes, M. Pourkashanian, and C. W. Wilson, "Development of a chemical reaction mechanism for alternative aviation fuels," *Energy & Fuels*, 2011.
- [20] H. Schulz, "Short history and present trends of Fischer-Tropsch synthesis," *Applied Catalysis A: General*, vol. 186, pp. 3–12, 1999.
- [21] M. E. Dry, "The Fischer-Tropsch process: 1950-2000," *Catalysis Today*, vol. 71, pp. 227–241, 2002.
- [22] J. T. Wolan and F. L. Prado, "American institute of chemical engineers central florida section annual meeting," tech. rep., American Institute of Chemical Engineers, Clearwater, 2008.
- [23] B. L. Smith and T. J. Bruno, "Composition-explicit distillation curves of aviation fuel jp-8 and a coal-based jet fuel," *Energy & Fuels*, vol. 21, no. 9, pp. 2853–2862, 2007.
- [24] D. Lamprecht, "Fischer-tropsch fuel for use by the u.s. military as battlefield-use fuel of the future," *Energy & Fuels*, vol. 21, no. 3, pp. 1448–1453, 2007.
- [25] M. L. Huber, E. W. Lemmon, V. Diky, B. L. Smith, and T. J. Bruno, "Chemically Authentic Surrogate Mixture Model for the Thermophysical Properties of a Coal-Derived Liquid Fuel," *Energy & Fuels*, vol. 22, pp. 3249–3257, Sept. 2008.

- [26] NNFCC, “The Potential for Renewable Aviation Fuels,” tech. rep., National Non-Food Crops Centre, The National Non-Food Crops Centre Biocentre, York Science Park Innovation Way, Heslington York YO10 5DG, UK, Feb. 2007.
- [27] M. E. Dry, “Practical and theoretical aspects of the catalytic Fischer-Tropsch process,” *Applied Catalysis A: General*, vol. 138, pp. 319–344, 1996.
- [28] G. Marsh, “Biofuels: aviation alternative?,” *renewable energy focus*, pp. 48–51, August 2008.
- [29] E. Corporan, T. Edwards, L. Shafer, M. J. Dewitt, C. Klingshirn, S. Zabarnick, Z. West, R. Striebich, J. Graham, and J. Klein, “Chemical , Thermal Stability , Seal Swell , and Emissions Studies of Alternative Jet Fuels,” *Energy & Fuels*, vol. 25, pp. 955–966, 2011.
- [30] W. F. Taylor, “Kinetics of deposit formation from hydrocarbons III. heterogeneous and homogeneous metal effects,” *Journal of Applied Chemistry*, vol. 18, 1968.
- [31] W. F. Taylor, “Kinetics of Desposit Formation From Hydrocarbons,” *Industrial & Engineering Chemistry Product Research*, vol. 8, no. 4, pp. 375–380, 1969.
- [32] A. S. Wade, *A Theoretical Inverstigation into Thermal Oxidation and Deposition Processes in Aviation Fuels Using Genetic Algorithms*. PhD thesis, University of Leeds, January 2005.
- [33] J. S. Ervin and S. Zabarnick, “Computational fluid dynamics simulations of jet fuel oxidation incorporating pseudo-detailed chemical kinetics,” *Energy & fuels*, vol. 12, no. 2, pp. 344–352, 1998.
- [34] N. J. Kuprowicz, S. Zabarnick, Z. J. West, and J. S. Ervin, “Use of Measured Species Class Concentrations with Chemical Kinetic Modeling for the Prediction of Autoxidation and Deposition of Jet Fuels,” *Energy & Fuels*, vol. 21, no. 7, pp. 530–544, 2007.
- [35] V. R. Katta, E. G. Jones, and W. M. Roquemore, “Modeling of Deposition Process in Liquid Fuels,” *Combustion Science and Technology*, vol. 139, no. 1, pp. 75–111, 1998.
- [36] Z. J. West, *Studies of Jet Fuel Autoxidation Chemistry: Catalytic Hydroperoxide Decomposition & High Heat Flux Effects*. Phdthesis, University of Dayton, 2011.
- [37] Ö. Gül, R. Cetiner, J. M. Griffith, B. Wang, M. Sobkowiak, D. a. Fonseca, P. Aksoy, B. G. Miller, and B. Beaver, “Insight into the Mechanisms of Middle Distillate Fuel Oxidative Degradation. Part 3: Hydrocarbon Stabilizers to Improve Jet Fuel Thermal Oxidative Stability,” *Energy & Fuels*, vol. 23, pp. 2052–2055, Apr. 2009.
- [38] P. Aksoy, O. Guül, R. Cetiner, D. a. Fonseca, M. Sobkowiak, S. Falcone-Miller, B. G. Miller, and B. Beaver, “Insight into the Mechanisms of Middle Distillate Fuel Oxidative Degradation. Part 2: On the Relationship between Jet Fuel Thermal Oxidative Deposit, Soluble Macromolecular Oxidatively Reactive Species, and Smoke Point,” *Energy & Fuels*, vol. 23, pp. 2047–2051, Apr. 2009.
- [39] R. C. Striebich, J. Contreras, L. M. Balster, Z. West, L. M. Shafer, and S. Zabarnick, “Identification of Polar Species in Aviation Fuels using Multidimensional Gas

- Chromatography-Time of Flight Mass Spectrometry,” *Energy & Fuels*, vol. 23, pp. 5474–5482, 2009.
- [40] M. Commodo, O. Wong, I. Fabris, and C. P. T. Groth, “Spectroscopic Study of Aviation Jet Fuel Thermal Oxidative Stability,” *Energy & Fuels*, vol. 24, no. 2, pp. 6437–6441, 2010.
- [41] M. Commodo, I. Fabris, and C. P. T. Groth, “Analysis of Aviation Fuel Thermal Oxidative Stability by Electrospray Ionization Mass Spectrometry ( ESI-MS ),” *Energy & Fuels*, pp. 2142–2150, 2011.
- [42] B. D. Beaver, L. Gao, C. Burgess-Clifford, and M. Sobkowiak, “On the mechanisms of formation of thermal oxidative deposits in jet fuels. Are unified mechanisms possible for both storage and thermal oxidative deposit formation for middle distillate fuels?,” *Energy & fuels*, vol. 19, no. 4, pp. 1574–1579, 2005.
- [43] E. T. Denisov and I. B. Afanas’ev, *Oxidation and Antioxidants in Organic Chemistry and Biology*. Taylor & Francis, 2005.
- [44] M. J. Dewitt and T. Edwards, “Effect of Aviation Fuel Type on Pyrolytic Reactivity and Deposition Propensity under Supercritical Conditions,” *Industrial & Engineering Chemistry Research*, vol. 50, pp. 10434–10451, 2011.
- [45] Z. J. West, R. K. Adams, and S. Zabarnick, “Homogeneous Catalysis of Liquid-Phase Hydroperoxide Decomposition in Hydrocarbons,” *Energy & Fuels*, vol. 25, pp. 897–904, Mar. 2011.
- [46] “ANSYS Fluent 13.0.” [www.ansys.com](http://www.ansys.com). Accessed July 2012.
- [47] E. Catalanotti, M. Pourkashanian, K. J. Hughes, I. Uiyga-bugajska, I. Shafagh, A. Williams, and C. W. Wilson, “Development of a detailed reaction mechanism for the oxidation of bio-aviation fuel,” in *Proceedings of the 16th European Biomass Conference*, (Valencia), 2008.
- [48] E. G. Jones, L. M. Balster, and W. J. Balster, “Autoxidation of Neat and Blended Aviation Fuels,” *Energy & Fuels*, vol. 12, no. 8, pp. 990–995, 1998.
- [49] J. S. Ervin, S. Zabarnick, and T. F. Williams, “One-Dimensional Simulations of Jet Fuel Thermal-Oxidative Degradation and Deposit Formation Within Cylindrical,” *Journal of Energy Resources Technology*, vol. 122, no. December, pp. 229–238, 2000.
- [50] N. J. Kuprowicz, J. S. Ervin, and S. Zabarnick, “Modeling the liquid-phase oxidation of hydrocarbons over a range of temperatures and dissolved oxygen concentrations with pseudo-detailed chemical kinetics,” *Fuel*, vol. 83, pp. 1795–1801, Sept. 2004.
- [51] I. Shafagh, K. J. Hughes, E. Catalanotti, Z. Liu, M. Pourkashanian, and C. W. Wilson, “Experimental and Modeling Studies of the Oxidation of Surrogate Bio-Aviation Fuels,” *Journal of Engineering for Gas Turbines and Power*, vol. 134, no. 4, p. 041501, 2012.
- [52] X. You, F. Egolfopoulos, and H. Wang, “Detailed and simplified kinetic models of n-dodecane oxidation: The role of fuel cracking in aliphatic hydrocarbon combustion,” *Proceedings of the Combustion Institute*, vol. 32, no. 1, pp. 403–410, 2009.

- [53] S. Dooley, S. H. Won, M. Chaos, J. S. Heyne, Y. Ju, F. L. Dryer, K. Kumar, C.-J. Sung, H. Wang, M. a. Oehlschlaeger, R. J. Santoro, and T. a. Litzinger, "A jet fuel surrogate formulated by real fuel properties," *Combustion and Flame*, vol. 157, pp. 2333–2339, Dec. 2010.
- [54] M. L. Huber, E. W. Lemmon, and T. J. Bruno, "Surrogate Mixture Models for the Thermophysical Properties of Aviation Fuel Jet-A," *Energy & Fuels*, vol. 24, pp. 3565–3571, June 2010.
- [55] J. a. Widegren and T. J. Bruno, "Thermal Decomposition Kinetics of the Aviation Turbine Fuel Jet A," *Industrial & Engineering Chemistry Research*, vol. 47, pp. 4342–4348, July 2008.
- [56] J. a. Widegren and T. J. Bruno, "Thermal Decomposition Kinetics of Propylcyclohexane," *Industrial & Engineering Chemistry Research*, vol. 48, pp. 654–659, Jan. 2009.
- [57] G. Liu, Y. Han, L. Wang, X. Zhang, and Z. Mi, "Solid Deposits from Thermal Stressing of n -Dodecane and Chinese RP-3 Jet Fuel in the Presence of Several Initiators," *Energy & Fuels*, vol. 23, pp. 356–365, Jan. 2009.
- [58] J. S. Heyne, A. L. Boehman, and S. Kirby, "Autoignition Studies of trans - and cis -Decalin in an Ignition Quality Tester (IQT) and the Development of a High Thermal Stability Unifuel/Single Battlefield Fuel," *Energy & Fuels*, vol. 23, pp. 5879–5885, Dec. 2009.
- [59] M. Sicard, J. Boulicault, B. Raepsaet, J. Ancelle, and F. Ser, "OXIDATION STABILITY OF JET FUEL MODEL MOLECULES EVALUATED BY RAPID SMALL SCALE OXIDATION TESTS," in *13th International Conference on Stability, Handling and Use of Liquid Fuels*, (Rhodes, Greece), 2013.
- [60] M. Sicard, B. Raepsaet, J. Ancelle, L. Starck, and N. Jeuland, "Thermal stability of alternative jet fuels," in *IASH 2009, the 11th International Conference on Stability, Handling and User of Liquid Fuels*, (Prague, Czech Republic), 2009.
- [61] M. Sicard, L. Starck, S. Blakey, J. Ancelle, N. Jeuland, A. Piperel, B. Raepsaet, S. Frederic, T. Spalton, and C. W. Wilson, "Evaluation of the alternative fuel oxidation stability within the european swafea program," in *IASH 2011, the 12th International Conference On Stability, Handling And Use Of Liquid Fuels*, (Sarasota, Florida), 2011.
- [62] M. Sicard, L. Starck, S. Blakey, J. Anelle, N. Jeuland, A. Piperel, B. Raepsaet, F. Ser, T. Spalton, and C. W. Wilson, "Evaluation of the Alternative Fuel Thermal-Oxidation Stability Within The European Swafea Program," in *IASH 2011 the 12th International COnference on Stability, Handling and Use of Liquid Fuels*, (Sarasota, Florida), pp. 1–16, 2011.
- [63] L. Starck, N. Jeuland, M. Sicard, and F. Ser, "Potential of alternative fuels for aircraft : Focus on thermal and oxidation stability," in *IASH 2009, the 11th International Conference on Stability, Handling and User of Liquid Fuels*, (Prague, Czech Republic), 2009.

- [64] M. Sicard, C. Hein, S. Gernigon, F. Ser, D. Brodzki, and G. Djega-mariadassou, "Study of the oxidation of the main hydrocarbon families contained in the kerosene jet a-1," in *10th International Conference on Stability, Handling and Use of Liquid Fuels*, (Tuscon, Arizona), pp. 1–20, 2007.
- [65] S. Gernigon, A. Aubourg, M. Sicard, F. Ser, and F. Bonzon-Verduraz, "Hydrocarbon Liquid Fuels Thermal Stability, Antioxydant Influence and Behaviour," in *IASH 2007, the 10th International Conference on Stability, Handling and Use of Liquid Fuels*, (Tuscon, Arizona), p. 2007, 2007.
- [66] S. Gernigon, M. Sicard, F. Ser, and F. Bozon-Verduraz, "Hydrocaron Liquid Fuels Thermal Stability, Antioxidant Influence and Behaviour," in *IASH 2007, the 10th International Conference on Stability, Handling and Use of Liquid Fuels*, (Tuscon, Arizona), 2007.
- [67] M. J. DeWitt, Z. West, S. Zabarnick, L. Shafer, R. Striebich, A. Higgins, and T. Edwards, "Effect of aromatics on the thermal-oxidative stability of synthetic paraffinic kerosene," *Energy & Fuels*, 2014.
- [68] R. K. Adams, S. Zabarnick, Z. J. West, R. C. Striebich, and D. W. Johnson, "Chemical Analysis of Jet Fuel Polar, Heteroatomic Species via High-Performance Liquid Chromatography with Electrospray Ionization "Mass Spectrometric Detection," *Energy & Fuels*, vol. 27, pp. 2390–2398, May 2013.
- [69] M. Colket, T. Edwards, S. Williams, N. P. Cernansky, D. L. Miller, P. Lindstedt, F. L. Dryer, C. K. Law, D. Friend, D. B. Lenhert, A. Sarofim, and M. Smooke, "Development of an experimental database and kinetic models for surrogate jet fuels," tech. rep., American Institute of Aeronautics and Astronautics, 2007.
- [70] B. D. Beaver, L. Gao, M. G. Fedak, M. M. Coleman, and M. Sobkowiak, "Model studies examining the use of dicyclohexylphenylphosphine to enhance the oxidative and thermal stability of future jet fuels," *Energy & Fuels*, vol. 16, no. 96, pp. 1134–1140, 2002.
- [71] B. D. Beaver, C. B. Clifford, M. G. Fedak, L. Gao, P. S. Iyer, and M. Sobkowiak, "High Heat Sink Jet Fuels. Part 1. Development of Potential Oxidative and Pyrolytic Additives for JP-8," *Energy & Fuels*, vol. 20, pp. 1639–1646, July 2006.
- [72] M. Sobkowiak, C. B. Clifford, and B. Beaver, "High Heat Sink Jet Fuels . 2 . Stabilization of a JP-8 with Model Refined Chemical Oil/Light Cycle Oil (RCO/LCO)-Derived Stabilizers," *Energy & Fuels*, vol. 21, no. 23, pp. 982–986, 2007.
- [73] B. Beaver, M. Sobkowiak, C. B. Clifford, Y. Wei, and M. Fedek, "High Heat Sink Jet Fuels . 3 . On the Mechanisms of Action of Model Refined Chemical Oil/Light Cycle Oil (RCO/LCO)-Derived Stabilizers for JP-8," *Energy & Fuels*, vol. 21, pp. 987–991, 2007.
- [74] T. J. Bruno, A. Wolk, and A. Naydich, "Stabilization of biodiesel fuel at elevated temperature with hydrogen donors: Evaluation with the advanced distillation curve method," *Energy & Fuels*, vol. 23, pp. 1015–1023, Feb. 2009.
- [75] I. Uryga-Bugajska, M. Pourkashanian, D. Borman, E. Catalanotti, and C. W. Wilson, "Theoretical investigation of the performance of alternative aviation fuels in



- an aero-engine combustion chamber,” *Proceedings of the Institution of Mechanical Engineers, Part G: Journal of Aerospace Engineering*, vol. 225, pp. 874–885, June 2011.
- [76] I. Uryga-Bugajska, M. Pourkashanian, D. Borman, E. Catalanotti, and L. Ma, “Draft: Assessment of the Performance of Alternative Aviation Fuel in a Modern Air-Spray Combustor (MAC),” in *2008 ASME International Mechanical Engineering Congress and Exposition*, (Boston), pp. 1–9, 2008.
- [77] D. K. Hughes, “Personal communication,” 2012.
- [78] L. J. Spadaccini, D. R. Sobel, and H. Huang, “Deposit Formation and Mitigation in Aircraft Fuels,” *Journal of Engineering for Gas Turbines and Power*, vol. 123, no. 4, p. 741, 2001.
- [79] T. I. M. Edwards, “Cracking and deposition behaviour of supercritical hydrocarbon aviation fuels,” *Combustion Science and Technology*, pp. 307–334, 2006.
- [80] L. Q. Maurice, H. Lander, T. Edwards, and W. E. Harrison, “Advanced aviation fuels: a look ahead via a historical perspective,” *Fuel*, vol. 80, no. 5, pp. 747–756, 2001.
- [81] M. Commodo, C. P. T. Groth, and O. L. Gülder, “Experimental Investigation of Aviation Fuel Thermal Oxidative Stability,” in *34th Meeting of the Italian Section of the Combustion Institute*, pp. 1–6, 2012.
- [82] M. Commodo, I. Fabris, O. Wong, C. P. T. Groth, and O. L. Gu, “Three-Dimensional Fluorescence Spectra of Thermally Stressed Commercial Jet A-1 Aviation Fuel in the Autoxidative Regime,” *Energy & Fuels*, vol. 26, pp. 2191–2197, 2012.
- [83] S. R. Turns, *An Introduction to Combustion: Concepts and Applications*. McGraw-Hill, 1993.
- [84] J. Clark, “Orders of reaction and rate equations.” <http://www.chemguide.co.uk/physical/basicrates/orders.html>, 2002. Accessed July 2012.
- [85] U. Fries, “Reaktionskinetik.” [www.iup.uni-heidelberg.de/institut/studium/lehre/Atmosphaerenphysik/script2/Reaktionskinetik.pdf](http://www.iup.uni-heidelberg.de/institut/studium/lehre/Atmosphaerenphysik/script2/Reaktionskinetik.pdf).
- [86] R. Tuckermann, “Chemische reaktionen.” [www.pci.tu-bs.de/aggericke/PC5-Atmos/Reaktionskinetik.pdf](http://www.pci.tu-bs.de/aggericke/PC5-Atmos/Reaktionskinetik.pdf), 2005.
- [87] R. J. Kee, F. M. Rupley, and E. Meeks, “CHEMKIN-III: A FORTRAN chemical kinetics package for the analysis of gas-phase chemical and plasma kinetics,” tech. rep., Sandia National Laboratories, Livermore, May 1996.
- [88] P. Atkins and J. de Paula, *Physical Chemistry*. W. H. Freeman and Company, eight ed., 2011.
- [89] J. Clark, “rate constants and the arrhenius equation.” <http://www.chemguide.co.uk/physical/basicrates/arrhenius.html>, 2002. Accessed July 2012.

- [90] R. M. Panoff, R. R. Gotwals, S. Thomas, V. D. Crockett, C. Novotny, L. Mauro, F. Drickamer, A. Thissen, B. O'Neill, J. Pahl, W. Jones, N. Nafissi, H. A. Patrick, and M. Evans. <http://www.shodor.org/unchem/advanced/kin/arrhenius.html>. Accessed July 2012.
- [91] K.-H. Gericke. [http://www.pci.tu-bs.de/aggericke/PC5/Kap\\_III/Arrhenius-Gleichung.htm](http://www.pci.tu-bs.de/aggericke/PC5/Kap_III/Arrhenius-Gleichung.htm). Accessed July 2012.
- [92] V. Großmann, "Fundamental constants - a short introduction." <http://www.ptb.de/cms/en/themenrundgaenge/wegweiser/naturkonstanten/zahlenwertewichtignaturkonst.html>, 2006. Accessed July 2012.
- [93] A. Burcat and B. Ruscic, "Third millenium ideal gas and condensed phase thermochemical database for combustion with updates from active thermochemical tables," tech. rep., Faculty of Aerospace Engineering, Technion Israel Institute of Technology, Chemistry Division, Argonne National Laboratory, Sept. 2005.
- [94] G. P. Smith, D. M. Golden, M. Frenklach, N. W. Moriarty, B. Eiteneer, M. Goldenberg, C. T. Bowman, R. K. Hanson, S. Song, W. C. Gardiner, Jr., V. V. Lissianski, and Z. Qin, "Gri mech 3.0." [http://www.me.berkeley.edu/gri\\_mech/](http://www.me.berkeley.edu/gri_mech/).
- [95] I. Flyagina, "Personal communication," June 2012.
- [96] [http://www.me.berkeley.edu/gri\\_mech/data/nasa\\_plnm.html](http://www.me.berkeley.edu/gri_mech/data/nasa_plnm.html). Accessed 13th June 2012.
- [97] C. R. Nave. <http://hyperphysics.phy-astr.gsu.edu/hbase/thermo/firlaw.html>. Accessed July 2012.
- [98] C. R. Nave. <http://hyperphysics.phy-astr.gsu.edu/hbase/therm/entrop.html>. Accessed July 2012.
- [99] E. W. Weisstein, "Ideal gas law." <http://scienceworld.wolfram.com/physics/IdealGasLaw.html>. Accessed 12th October 2012.
- [100] D. C. Brennan, "Computation and simulation ee317." [http://elm.eeng.dcu.ie/~ee317/Course\\_Notes/handout1.pdf](http://elm.eeng.dcu.ie/~ee317/Course_Notes/handout1.pdf). School of Electronic Engineering, Dublin City University.
- [101] E. W. Weisstein, "Forward differencing." <http://mathworld.wolfram.com/ForwardDifference.html>. Accessed 8th June 2015.
- [102] E. W. Weisstein, "Backward differencing." <http://mathworld.wolfram.com/BackwardDifference.html>. Accessed 8th June 2015.
- [103] E. W. Weisstein, "Central differencing." <http://mathworld.wolfram.com/CentralDifference.html>. Accessed 8th June 2015.
- [104] E. W. Weisstein, "Finite difference." <http://mathworld.wolfram.com/FiniteDifference.html>. Accessed 8th June 2015.
- [105] L. F. Shampine and C. W. Gear, "A user's view of solving stiff ordinary differential equations," *Society for Industrial and Applied Mathematics*, vol. 21, no. 1, 1979.

- [106] M. Berzins, P. Dew, and R. Furzeland, "Software for time-dependent problems," in *P.D.E. Software: Modules, Interfaces and Systems. proc. of 1983 IFIPS Conference*, North Holland, 1983. School of Computer Studies, The University of Leeds.
- [107] L. R. Petzold, "A Description of DASSL : A Differential/Algebraic System Solver," tech. rep., Sandia National Laboratories, Livermore, 1982.
- [108] E. Hairer, S. Nørsett, and G. Wanner, *Solving Ordinary Differential Equations: Stiff and differential-algebraic problems*. Springer Series in Computational Mathematics, Springer-Verlag, 1993.
- [109] A. E. Lutz, R. J. Kee, and J. A. Miller, "Senkin: A fortran program for predicting homogeneous gas phase chemical kinetics with sensitivity analysis," tech. rep., Sandia National Laboratories, Livermore, Nov. 1997.
- [110] A. E. Lutz, R. J. Kee, and J. A. Miller, "Senkin: A fortran program for predicting homogeneous gas phase chemical kinetics with sensitivity analysis," tech. rep., Sandia National Laboratories, Livermore, Dec. 1993.
- [111] P. Glarborg, R. J. Kee, J. F. Grcar, and J. A. Miller, "PSR: A fortran program for modelling well-stirred reactors," tech. rep., Sandia National Laboratories, Livermore, 1982.
- [112] Shell Research Limited, Thornton Research Centre, Chester, UK, *A user's manual for SPRINT - a versatile software package for solving systems of algebraic, ordinary and partial differential equations*, 1989. Report No. TNER 85.058.
- [113] T. Turányi, "Mechmod." <http://garfield.chem.elte.hu/Combustion/mechmod.htm>. Accessed 20th July 2012.
- [114] T. Turányi, "Kinalc." <http://garfield.chem.elte.hu/Combustion/kinalc.htm>. Accessed 20th July 2012.
- [115] D. C. Mielczarek, "chemical kinetics solver." <http://dx.doi.org/10.5281/zenodo.19293>, <https://github.com/DetlevCM/chemical-kinetics-solver>.
- [116] Intel Corporation. <http://software.intel.com/en-us/articles/intel-ordinary-differential-equations-solver-library>, 2011.
- [117] S. Rolland and J. M. Simmie, "The comparison of detailed chemical kinetic mechanisms; forward versus reverse rates with CHEMRev," *International Journal of Chemical Kinetics*, vol. 37, pp. 119–125, Mar. 2005.
- [118] G. D. Byrne and A. M. Dean, "The numerical solution of some kinetics models with VODE and CHEMKIN II," *Computers & Chemistry*, vol. 17, no. 3, pp. 297–302, 1993.
- [119] W. H. Green, J. W. Allen, B. A. Buesser, R. W. Ashcraft, G. J. Beran, C. A. Class, C. Gao, C. F. Goldsmith, M. R. Harper, A. Jalan, M. Keceli, G. R. Magoon, D. M. Matheu, S. S. Merchant, J. D. Mo, S. Petway, S. Raman, S. Sharma, J. Song, Y. Suleymanov, K. M. V. Geem, J. Wen, R. H. West, Andrew Wong, Hsi-Wu Wong, P. E. Yelvington, N. Yee, and J. Yu, "RMG - Reaction Mechanism Generator v4.0," tech. rep., Massachusetts Institute of Technology, 2013.

- [120] “Rmg py user guide - liquid phase systems.” <http://greengroup.github.io/RMG-Py/users/rmg/liquids.html>.
- [121] B. E. Poling, J. M. Prausnitz, and J. P. O’Connell, *The properties of gases and liquids*. McGraw-Hill, fifth ed., 1987.
- [122] W. H. Green, J. W. Allen, R. W. Ashcraft, G. J. Beran, C. A. Class, C. Gao, C. F. Goldsmith, M. R. Harper, A. Jalan, G. R. Magoon, D. M. Matheu, S. S. Merchant, J. D. Mo, S. Petway, S. Raman, S. Sharma, J. Song, K. M. V. Geem, J. Wen, R. H. West, A. Wong, H.-W. Wong, P. E. Yelvington, and J. Yu, *RMG Manual*, 2011.
- [123] R. G. Susnow, A. M. Dean, W. H. Green, P. Peczak, and L. J. Broadbelt, “Rate-based construction of kinetic models for complex systems,” *Journal of Physical Chemistry*, vol. 5639, no. 96, pp. 3731–3740, 1997.
- [124] M. R. Harper, K. M. Van Geem, S. P. Pyl, G. B. Marin, and W. H. Green, “Comprehensive reaction mechanism for n-butanol pyrolysis and combustion,” *Combustion and Flame*, vol. 158, pp. 16–41, Jan. 2011.
- [125] K. M. Van Geem, M.-F. Reyniers, G. B. Marin, J. Song, W. H. Green, and D. M. Matheu, “Automatic reaction network generation using RMG for steam cracking of n-hexane,” *AIChE Journal*, vol. 52, pp. 718–730, Feb. 2006.
- [126] S. Benson, F. Cruickshank, and D. Golden, “Additivity rules for the estimation of thermochemical properties,” *Chemical*, 1969.
- [127] W. H. Green, J. W. Allen, R. W. Ashcraft, G. J. Beran, C. A. Class, C. Gao, C. F. Goldsmith, M. R. Harper, A. Jalan, G. R. Magoon, D. M. Matheu, S. S. Merchant, J. D. Mo, S. Petway, S. Raman, S. Sharma, J. Song, K. M. V. Geem, J. Wen, R. H. West, A. Wong, H.-W. Wong, P. E. Yelvington, and J. Yu, “RMG - reaction mechanism generator v3.3.” <http://rmg.sourceforge.net/>, 2011.
- [128] S. Sharma, M. R. Harper, and W. H. Green, “Modeling of 1,3-hexadiene, 2,4-hexadiene and 1,4-hexadiene-doped methane flames: Flame modeling, benzene and styrene formation,” *Combustion and Flame*, vol. 157, pp. 1331–1345, July 2010.
- [129] G. R. Magoon, J. Aguilera-iparraguirre, W. H. Green, J. J. Lutz, P. Piecuch, H.-w. Wong, and O. O. Oluwole, “Modeling of jp-10 (exo-tetrahydrodicyclopentadi-ene) high-temperature oxidation : Exploring the role of biradical species in initial decomposition steps,” *International Journal of Chemical Kinetics*, vol. 10, 2012.
- [130] W. H. Green, J. W. Allen, R. W. Ashcraft, G. J. Beran, C. A. Class, C. Gao, C. F. Goldsmith, M. R. Harper, A. Jalan, G. R. Magoon, D. M. Matheu, S. S. Merchant, J. D. Mo, S. Petway, S. Raman, S. Sharma, J. Song, K. M. V. Geem, J. Wen, R. H. West, A. Wong, H.-W. Wong, P. E. Yelvington, and J. Yu, “Rmg github repository.” <https://github.com/GreenGroup/RMG-Java>.
- [131] G. M. Oxberry, “Parallelizing the graph isomorphism portion of an automatic reaction mechanism generation algorithm,” tech. rep., Massachusetts Institute of Technology, 2009.
- [132] J. Foresman, A. Frisch, and I. Gaussian, “Exploring Chemistry With Electronic Structure Methods.pdf,” 1996.

- [133] E. W. Weisstein, "Schrödinger equation." <http://mathworld.wolfram.com/SchroedingerEquation.html>. Accessed 29th July 2013.
- [134] M. J. Frisch, G. W. Trucks, H. B. Schlegel, G. E. Scuseria, M. A. Robb, J. R. Cheeseman, G. Scalmani, V. Barone, B. Mennucci, G. A. Petersson, H. Nakatsuji, M. Caricato, X. Li, H. P. Hratchian, A. F. Izmaylov, J. Bloino, G. Zheng, J. L. Sonnenberg, M. Hada, M. Ehara, K. Toyota, R. Fukuda, J. Hasegawa, M. Ishida, T. Nakajima, Y. Honda, O. Kitao, H. Nakai, T. Vreven, J. A. Montgomery, Jr., J. E. Peralta, F. Ogliaro, M. Bearpark, J. J. Heyd, E. Brothers, K. N. Kudin, V. N. Staroverov, R. Kobayashi, J. Normand, K. Raghavachari, A. Rendell, J. C. Burant, S. S. Iyengar, J. Tomasi, M. Cossi, N. Rega, J. M. Millam, M. Klene, J. E. Knox, J. B. Cross, V. Bakken, C. Adamo, J. Jaramillo, R. Gomperts, R. E. Stratmann, O. Yazyev, A. J. Austin, R. Cammi, C. Pomelli, J. W. Ochterski, R. L. Martin, K. Morokuma, V. G. Zakrzewski, G. A. Voth, P. Salvador, J. J. Dannenberg, S. Dapprich, A. D. Daniels, . Farkas, J. B. Foresman, J. V. Ortiz, J. Cioslowski, and D. J. Fox, "Gaussian 09 Revision C.01." Gaussian Inc. Wallingford CT 2009.
- [135] J. Foresman, H. P. Hrnt, D. J. Fox, M. Bearpark, and G. A. Petersson. Gaussian Workshop 2013, Wrocław, Poland, 2013.
- [136] P. M. Esteves, J. W. De M Carneiro, S. P. Cardoso, A. G. H. Barbosa, K. K. Laali, G. Rasul, G. K. S. Prakash, and G. a. Olah, "Unified mechanistic concept of electrophilic aromatic nitration: convergence of computational results and experimental data.," *Journal of the American Chemical Society*, vol. 125, pp. 4836–49, Apr. 2003.
- [137] M. Liljenberg, T. Brinck, B. Herschend, T. Rein, G. Rockwell, and M. Svensson, "Validation of a computational model for predicting the site for electrophilic substitution in aromatic systems.," *The Journal of organic chemistry*, vol. 75, pp. 4696–705, July 2010.
- [138] S. J. Jenkins, "Aromatic adsorption on metals via first-principles density functional theory," *Proceedings of the Royal Society A: Mathematical, Physical and Engineering Sciences*, vol. 465, pp. 2949–2976, July 2009.
- [139] R. Dennington, T. Keith, and J. Millam, "Gaussview Version 5." Semichem Inc. Shawnee Mission KS 2009.
- [140] D. J. Fox, "Contact with gaussian tech support, 3rd may 2013." Personal Communication.
- [141] R. H. West and W. H. Green, "Reaction Mechanism Generator : Cheminformatics for Kinetic Modeling," 2010.
- [142] C. K. Westbrook, W. J. Pitz, O. Herbinet, H. J. Curran, and E. J. Silke, "A comprehensive detailed chemical kinetic reaction mechanism for combustion of n-alkane hydrocarbons from n-octane to n-hexadecane," *Combustion and Flame*, vol. 156, pp. 181–199, Jan. 2009.
- [143] R. Seiser, H. Pitsch, K. Seshadri, W. J. Pitz, and H. J. Curran, "Extinction and Autoignition of n-Heptane in Counterflow Configuration," *Combustion*, vol. 28, pp. 2029–2037, 2000.

- [144] H. J. Curran, P. Gaffuri, W. J. Pitz, and C. K. Westbrook, "A Comprehensive Modeling Study of n-Heptane Oxidation," *Combustion and Flame*, vol. 2180, no. 97, 1998.
- [145] Anton Paar GmbH, *PetroOxy Manual*, 7 2013.
- [146] [http://www.engineeringtoolbox.com/absolute-viscosity-liquids-d\\_1259.html](http://www.engineeringtoolbox.com/absolute-viscosity-liquids-d_1259.html). [http://www.engineeringtoolbox.com/absolute-viscosity-liquids-d\\_1259.html](http://www.engineeringtoolbox.com/absolute-viscosity-liquids-d_1259.html). Accessed last 28th July 2014.
- [147] E. Denisov, O. M. Sarkisov, and G. Likhtenshtein, *Chemical Kinetics: Fundamentals and New Developments*. Elsevier Science B.V., 2003.
- [148] C. W. Wilson and S. Blakey, nov 2012. internal meeting presentation.
- [149] C. W. Wilson, S. Blakey, and T. Spalton, "Quantitative thermal stability testing." [http://www.shef.ac.uk/polopoly\\_fs/1.25999!/file/HiReTS-Information.pdf](http://www.shef.ac.uk/polopoly_fs/1.25999!/file/HiReTS-Information.pdf).
- [150] S. J. Rand, "Methods for Assessing Stability and Cleanliness of Liquid Fuels," in *Significance of Tests for Petroleum Products*, ASTM International, 2003.
- [151] S. J. Rand, "Methods for Assessing Stability and Cleanliness of Liquid Fuels," in *Significance of Tests for Petroleum Products*, pp. 151–163, ASTM International, 2010.
- [152] R. A. K. Nadkarni, "Thermal Stability of Aviation Turbine Fuels by HiReTS Method: D 6811," in *Guide to ASTM Test Methods for the Analysis of Petroleum Products and Lubricant*, pp. 254–261, ASTM International, second ed., 2007.
- [153] B. J. Wright, "C-JFTOT Jet Fuel Tester, No. 1 Operating Manual," tech. rep., Blue Chip Technology, 1996.
- [154] E. Jessica M., B. Sarah P., R. A. J. Frederick, and A. J. Wood, "High reynolds number thermal stability experiments," in *40th AIAA/ASME/SAE/ASEE Joint Propulsion Conference and Exhibit*, pp. 1–7, 2004.
- [155] M. Sherratt, J. Wood, J. Bauldreay, and R. Heins, "Factors influencing the results obtained by the high reynolds number thermal stability test instrument (hirets)," in *7th International Conference on Stability and Handling of Liquid Fuels*, 2000.
- [156] J. Bauldreay, R. J. Heins, G. —Houlbrook, and J. Smith, "High reynolds number thermal stability (hirets) rig for realistic, rapid evaluation of distillate fuel thermal oxidative stability," in *6th International Conference on Stability and Handling of Liquid Fuels*, 1997.
- [157] S. G. Pande, D. R. Hardy, R. A. Kamin, C. J. Nowack, J. E. Colbert, R. E. Morris, and L. Salvucci, "Quest for a reliable method for determining aviation fuel thermal stability: Comparison of turbulent and laminar flow test devices," *Energy & Fuels*, vol. 15, pp. 224–235, 2001.
- [158] J. H. Dymond, J. Robertson, and J. D. Isdale, "Transport Properties of Nonelectrolyte Liquid Mixtures - III. Viscosity Coefficients for the n-Octane + n-Dodecane and Equimolar Mixtures of n-Octane + n-Dodecane and n-Hexane + n-Dodecane from 25 to 100 °C at Pressures up to the Freezing Pressure or 500 M," *International Journal of Thermophysics*, vol. 2, no. 2, pp. 133–154, 1981.

- [159] S. Blakey. Personal Communication.
- [160] M. Clugston and R. Flemming, *Advanced Chemistry*. Oxford University Press, 2000.
- [161] R. R. Baldwin and J. A. Howarth, "Surface Termination in Chain Reactions and the Interaction with Homogeneous Termination," *Journal of the Chemical Society, Faraday Transactions*, pp. 451–464, 1982.
- [162] C. R. Wilke and P. Chang, "Correlation of diffusion coefficients in dilute solutions," *AIChE Journal*, vol. 1, pp. 264–270, June 1955.
- [163] W. Hayduk and B. Minhas, "Correlations for prediction of molecular diffusivities in liquids," *The Canadian Journal of Chemical Engineering*, vol. 60, pp. 295–299, april 1982.
- [164] G. Taylor, "The Dispersion of Matter in Turbulent Flow through a Pipe," *Proceedings of the Royal Society A: Mathematical, Physical and Engineering Sciences*, vol. 223, pp. 446–468, May 1954.
- [165] P. Rawson, "Evaluation of a Jet Fuel Thermal Stability Rig," tech. rep., Air Vehicles Division Platforms Sciences Laboratory, Australian Ministry of Defence, 2004.
- [166] W. F. Taylor, "Deposit Formation from Deoxygenated Hydrocarbons. II. Effect of Trace Sulfur Compounds," *Industrial & Engineering Chemistry Product Research and Development*, vol. 15, pp. 64–68, Mar. 1976.
- [167] J. S. Ervin, T. a. Ward, T. F. Williams, and J. Bento, "Surface Deposition within Treated and Untreated Stainless Steel Tubes Resulting from Thermal-Oxidative and Pyrolytic Degradation of Jet Fuel," *Energy & Fuels*, vol. 17, pp. 577–586, May 2003.
- [168] L. M. Balster, S. Zabarnick, R. C. Striebich, L. M. Shafer, and Z. J. West, "Analysis of polar species in jet fuel and determination of their role in autoxidative deposit formation," *Energy and Fuels*, vol. 20, no. 14, pp. 2564–2571, 2006.